Walking on Weed: Predicting THC-induced motor impairment reveals disrupted cortical activity

Anthony English

A dissertation

submitted in partial fulfillment of the

requirements for the degree of

Doctor of Philosophy

University of Washington

2025

Reading Committee:

Nephi Stella, Chair

Susan Ferguson

Larry Zweifel

Program Authorized to Offer Degree:

Pharmacology

University of Washington

Abstract

Walking on Weed: Predicting THC-induced motor impairment reveals disrupted cortical activity

Anthony English

Chair of the Supervisory Committee:
Nephi Stella
Department of Pharmacology

Cannabis has been used by humans for thousands of years for its multi-faceted properties as industrial tools, medicinal effects, and recreational value. And in the past several hundred years, international prohibition movements have been in a struggle with scientists investigating its effects on the human body. Despite this, scientists have persisted to isolate the primary psychoactive compound THC and use it as a basis to uncover an entire neurotransmitter system in humans: the endocannabinoid system. This system plays a critical role in modulating behavior, neurological development, and general brain activity. Further research into the endocannabinoid system and the Cannabis plant lags behind other similar fields despite its importance. The research and

findings presented here show another step towards expanding our understanding and functional applications with THC and the endocannabinoid system.

Cannabinoid compounds such as THC are notoriously difficult to work with due to their high lipophilicity and, in in vivo rodent studies, their high taste avoidance. Therefore, to counter the potent smells and flavors of raw THC, in an effort to uncover its in vivo behavioral effects. To address this gap, we developed a novel gelatin-based method for THC delivery that enhances palatability and voluntary intake in mice. By incorporating THC into a chocolate-flavored nutritional shake (Ensure™) and gelatinizing the mixture, we formulated an E-gel matrix. In mice, we enhanced voluntary consumption of high-dose THC compared to standard gelatin and succeeded in promoting the mice to consume enough to reach highly psychoactive behavioral effects. The use of Cannabis products containing high concentrations of THC is rapidly increasing, with a growing body of evidence links high-THC Cannabis use with increased psychotic and affective symptoms and Cannabis-associated vehicular accidents. The need for tools to investigate the mechanistic insight into how high-potency THC influences the brain is increasingly relevant. The E-gel model thus provides a translationally relevant, voluntary oral intake paradigm for characterizing THC's pharmacokinetics and behavioral impacts in rodents, offering an essential tool for investigating the consequences of high-dose THC exposure.

The endogenous cannabinoid receptor CB1 plays a key role in brain development, but the long-term effects of adolescent THC exposure remain poorly understood. To explore its impact on addiction vulnerability, I exposed mice to THC during adolescence and assessed morphine-related behaviors in adulthood, finding no significant alterations in analgesia or drug-seeking. However, female mice showed THC-dependent

impairments in memory recall, suggesting a sex-specific effect on learning. Preliminary behavioral analyses using pose estimation also revealed a unique exploratory behavior in THC-exposed animals, warranting further investigation into the neural circuits underlying these effects.

Emerging technologies in other fields provide a pathway to overcome technical and political limitations to enable more sophisticated analyses. In recent years, computer vision tools like DeepLabCut and SLEAP have transformed behavioral research by allowing detailed tracking of individual points on animals during experiments, improving our ability to analyze animal behavior with greater precision than the human eye. Here, we utilized the SLEAP pose estimation algorithm within a linear track system that enables high-resolution and high-frame rate visualization of mice side and bottom-up profiles. Then, animal poses were used to calculate key features that to train dose prediction models capable of identifying the dose of THC animals were treated with solely based on their general or specifically locomotor behavior. These models were then utilized, along with the unsupervised identification of nuanced behaviors, to investigate the effects of THC on excitatory/inhibitory balance of cortical neurons in the mPFC. Inhibitory GABAergic neurons and excitatory glutamatergic neurons of the mPFC were observed to be modified in their activity during THC-impaired motor behavior. Manipulation of CB_1R expression and activation of specific neurons time locked to movement with a closed-loop optogenetic model revealed the enhanced GABAergic activity correlates with worsened motor behavior, suggesting the E/I balances criticality in modifying THC-impairment. This effect also greatly modified native endocannabinoid signaling as identified by the novel $GRAB_{eCB2.0}$ senor. These findings marked a novel application of behavioral identification

utilized to identify a novel THC-dependent modification in E/I balance of the cortical neurons during motor behavior.

Together, the research displayed in this thesis combines advanced computational applications and cutting-edge biosensor technologies to address a pressing challenge in cannabinoid research: quantifying the multi-faceted signatures of THC’s effects in vivo.

TABLE OF CONTENTS

LIST OF FIGURES

ACKNOWLEDGEMENTS

I want to start by thanking Nephi Stella and Michael Bruchas for being excellent mentors. Starting from the time he interviewed me as a prospective graduate student, I greatly appreciated and admired both of their excitement about scientific research. And I appreciate how both can approach science in their own unique style while working in harmony with each other. It's clear they have placed significant trust in my abilities over the course of my degree, which has given me confidence as I explored new ideas and techniques, which I am truly grateful for.

I also want to acknowledge the rest of the Stella and Bruchas Labs, both past and present members, for their support and friendship throughout this process. In particular, I want to thank Simar Singh, Dennis Sarroza, and Kainat Khan from the Stella lab. And, David Marcus, Raaj Gowrishankar, Jingyi Chen, Sean Piantadosi, Kasey Girven, Erich Zhang, Avi Matarraso, Carrie Stine, Kaylin Ellioff, Cat Zamorano, Madison, Elena, and Azra Suko of the Bruchas lab. I also want to thank a key member of the UW Cannabinoid Network (Dr. Benjamin Land) who has functioned as a third mentor for my degree, my cohort (Maddy and Evan), volunteers (Victoria Corbit and Allan Levy) my committee and the Department of Pharmacology and University of Washington at large. I finally want to thank all the undergraduates I have mentored for their incredible contributions to my work. They have all shown incredible perseverance and intelligence beyond the expectations for an undergraduate: Anna Slaven, Fleur Uittenbogaard, Rayna Simons, Khushi Yadav, Yassin Elkhouly, Maddy Ask, Anika Svedburg, Ben Anger, Jordan Poces-Ball, and Gunn Chen. I have thoroughly enjoyed working with all of you and this experience would not have been as fulfilling or fun without the experiences, both scientific and otherwise, that I've shared with all of you.

Next, I want to thank all my friends who have been pillars of support through all times of my life, whether that be graduate school or not. I'm fortunate to have always been surrounded by intelligent, emotionally mature, creative, fun, and impressive friends that care so much for others. I am proud to call you my friends and I hope we can spend many more decades together!

Finally, I want to thank my entire family for their unwavering support. To my parents: thank you for your sacrifices that have allowed me to follow any path I wanted to and for modeling the importance of primarily being a kind and loving person over all else. To my siblings and extended family: thank you for being understanding of my situation as I maintained a student status into my late 20s and always being ready and okay to support me. Thank you.

To sum up my acknowledgements to the people that have supported me, the people we surround ourselves with make us who we are. "Associate with people who are likely to improve you." I am fortunate and overjoyed at the opportunities I have had to live around and learn from those around me "Welcome those whom you yourself can improve. The process is mutual; for men learn while they teach."

Seneca

Chapter 1. INTRODUCTION

Forward

The year is 2025 as I sit here writing my PhD dissertation at the University of Washington, Seattle, USA. The current climate of research, biological or otherwise, is uncertain in the face of the newly appointed political Trump administration. The atmosphere at the academic level is grim at best, with most friends and colleagues seeking opportunities in an industry market swamped with highly skilled and intelligent scientists desperately hunting for income. In the past, there have been "brain drains" that caused great minds to flock to other countries willing to support their work. Inevitably, these great minds performed great feats. But now, the United States seems to be dumping their great minds, and it's unclear if any existing country will welcome them or if corporations will flourish into even greater governing bodies. The uncertainty around us has become an addictive drug, pervasively filling our heads endlessly while slowly tearing our souls and drive for scientific intrigue away. Luckily, humanity has shown throughout history that intrigue for the world around us is an inevitability. Humans will never cease to invest their hearts and souls in creating and discovering everything. And, much like the history of humanity, there has always been ignorant power attempting to suppress this intrigue.

My curiosity for science, particularly in the realm of cannabis research, began during my undergraduate years when I first encountered the rich history of cannabis legislation and its scientific exploration in the United States. This early exposure spiked my interest, guiding me toward a path that would eventually lead to my PhD. It seems only appropriate,

then, that I begin my thesis by summarizing the intricate relationship of scientific intrigue in cannabis throughout human history. As I, a 28-year-old graduate student about to defend my thesis, prepare for the scientific and rapidly advancing world, I fear for the world I enter, but I also yearn for the opportunity to build upon the scientific intrigue of my past and that of humanity's ancestors. My thesis work, like every other PhD thesis, marks a small step toward understanding our world and, in part, understanding the human condition's unyielding drive to strive for answers.

History of the Human-Cannabis Relationship

"It is a plant that reveals to you the things of your own soul," attributed to an ancient Sufi mystic from around the 12th century, reflects writings on hashish and Islamic mysticism in the *Ilāhī-Nāma*, believed to reference Cannabis[1]. The Cannabis plant is estimated to have ecologically existed around 12,000 years ago[2]. At this time, human ancestors were still primarily hunter-gatherers, beginning to discover agriculture as the Neolithic Revolution was beginning. As humans evolved, so too did Cannabis and humanity's relationship with the natural world, advancing from simple survival to mastery of agricultural techniques and creative applications of plants beyond food. As the human mind expanded, so did our innovations: trees were cut for construction, leaves bound for clothing, and stems woven into tools. With the invention of fire, humans discovered that chemical manipulation of plants yielded new substances—smoke, oils, and more. Among these evolving interactions, the Cannabis plant stands out as a consistent presence across ancient societies worldwide, a silent witness to our development.

Ancient use of specific plants like Cannabis is difficult to confirm, obscured by the rise and fall of empires and the natural evolution of language and record-keeping. Currently, it is believed that Cannabis was utilized by ancient humans in regions corresponding to modern-day India[3], China[3], Egypt[4], Syria[5], and Greece[6]. In these records, Cannabis—technically hemp in most cases—was applied in diverse and creative ways. Notably, ancient Egyptians referred to it as *Shemshemet* and used it in eye treatments around 1700 BCE[7]. In ancient China, the plant known as *Ma* (specifically hemp seeds) was believed to induce hallucinations when consumed in high quantities[8]. These early uses suggest not only practical value but enduring human curiosity for the deeper potentials of the natural world.

The Cannabis plant likely remained in human use for centuries until methods were developed to concentrate its stalked resin glands, known as trichomes, into what is now recognized as hashish. Hashish was first recorded in Islamic nations around the 10th century, and shortly thereafter in what is now modern-day India[9,10]. The popularity of hashish notably spread to European regions from tales of the Islamic leader Hasan I-Sabah and his Hashshashin, translated as “smokers of hashish”, who’s tales of their exploits helped popularize the substance through the writings of Marco Polo[11]. Hashish became a prized formulation for its ability to deliver Cannabis’ medicinal, recreational, and ritualistic effects in a potent form, inducing states of deep relief or altered consciousness. Still in use today, hashish played a significant cultural role, influencing native tribes in 14th-century Africa (e.g., the Bantu people) and inspiring 18th-century French literary figures such as Alexandre Dumas[12]. These uses illustrate humanity’s

enduring fascination with unlocking the mind's hidden dimensions through the Cannabis plant.

In contrast to the psychoactive potency of hashish, hemp represents another major branch in Cannabis' historical significance; one centered on industrial utility. "Hemp" refers to cultivars of the Cannabis plant bred to produce less than 0.3% of the primary psychoactive compound Δ^9-Tetrahydrocannabinol (THC)[13]. Valued for its strong fibrous stalks, hemp became an essential resource for making textiles and ropes. This practical value extended across the Atlantic: early North American colonies such as Jamestown in Virginia cultivated hemp, and U.S. founding father George Washington grew it on his Mount Vernon plantation[14]. By the late 18th century, the medicinal uses of Cannabis saw renewed interest in Europe and America. Dr. William O'Shaughnessy notably reintroduced Cannabis preparations into Western medicine, reporting benefits for managing symptoms of rabies, cholera, and tetanus[15]. These developments underscore Cannabis' dual legacy as both a utilitarian crop and a pharmacological tool, woven into the fabric of human advancement.

The dynamic history of humanity's relationship with Cannabis has evolved across cultural, medicinal, and economic dimensions; marked by periods of both enthusiastic support and intense opposition. Throughout different regions and time periods, the Cannabis plant has faced legal restriction. However, it wasn't until the 19th century that Cannabis prohibition began to gain significant international traction. Napoleon Bonaparte banned hashish use among his troops following the French invasion of Egypt[16,17]. By the late 19th century, several powers including the Ottoman Empire, Morocco, Greece, and Britain had enacted laws restricting the cultivation, sale, or consumption of Cannabis[18-21]. Yet amid this

growing caution, some took a more scientific approach. In British-ruled India, a formal commission was established to investigate the use of hemp drugs. Their conclusion: “moderate use practically produces no ill effects,” and “injury from habitual moderate use is not appreciable.” This moment stands as an early example of careful investigators attempting to objectively assess Cannabis use amid a rising tide of prohibition.

Despite these findings, humanity continued down a path of restriction. By the early 20th century, countries such as Jamaica (1913), Mexico (1920), Canada (1923), and Italy (1923) had all implemented bans on the cultivation, sale, or use of Cannabis[22-24]. A pivotal moment came in 1925, when the League of Nations introduced international control over Cannabis extracts during the Opium Convention, placing them under the same regulatory framework as opiates[25,26]. This decision marked the beginning of a broader trend: one that increasingly equated Cannabis with other high-risk illicit substances such as opioids, amphetamines, and cocaine. Unlike scientific or biological evidence, these prohibitions were often driven by political, racial, or religious motivations. For instance, Jamaica’s early Ganja Law was strongly backed by colonial leaders aiming to suppress local cultural practices[23,27,28]. Over the course of the 20th century, laws such as the UK Dangerous Drugs Act of 1920 and Ireland’s Dangerous Drugs Act of 1934[29-31] helped reshape public opinion, embedding the idea of Cannabis as a “dangerous drug” in global consciousness, rarely with a semplence of scientific justification.

In the United States, this prohibition fervor was reflected in restrictive state laws passed during the 1910s and 1920s, alongside the Pure Food and Drug Act of 1906, which began regulating patent medicines containing Cannabis[32]. Then, in 1930, Henry Anslinger, a man already known for his role in the Federal Narcotics Board, was appointed

commissioner of the Treasury's newly formed Federal Bureau of Narcotics, where he was given significant funding and flexibility. It was here that Anslinger ignited the public and institutional "war on Cannabis." He promoted obscure and extreme anecdotes linking Cannabis to violent crime, drawing on racism and sensationalism to shift the opinions of politicians and the public[33]. Anslinger spread alarmist rhetoric through mass media, describing the rise of dangerous "marihuana" (a Mexican slang term gaining popularity at the time) coming over the border to stoke fear and xenophobia[33,34]. He notoriously leaned on racist narratives, portraying Black Americans as drug-using criminals, and even stating, "Reefer makes darkies think they're as good as white men" [34-37]. One of his most targeted public campaigns was against the iconic jazz singer Billie Holiday, who was known to use Cannabis and other narcotics[38]. As she lay dying of liver cirrhosis, Anslinger's agents handcuffed her to her hospital bed, likely staged to serve his broader agenda[39]. Supported by powerful religious groups such as those behind *Tell Your Children*, Anslinger's campaign helped cement a perception of Cannabis as a dangerous substance. His influence expanded the War on Drugs and helped entrench anti-Cannabis sentiment in American culture, despite limited scientific support for such views[40].

The following decades through Anslinger's reign and on marked a slow growing counter movement in the United States against the notion of Cannabis' touted dangers. Medical practitioners attempted to communicate research findings and clinical observations. The American Medical Association released a discussion of 30 pharmacists, 29 of which opposed federal bans, despite Anslinger using the single dissenter's story for the Bureau's use[41]. In 1937, Dr. William C. Woodward of the AMA testified before Congress, criticizing the Marihuana Tax Act for its lack of scientific justification and warning that it

would obstruct future medical research[42]. A few years later, the LaGuardia Committee, backed by the New York Academy of Medicine, published a landmark 1944 report finding no evidence that cannabis use incited violence or insanity, directly challenging the federal narrative[43]. Meanwhile, psychiatrists such as Dr. Samuel Allentuck and Dr. Karl Bowman published clinical data in the early 1940s suggesting cannabis had therapeutic promise and posed less risk of dependence than substances like alcohol or tobacco[44].

Around the mid-20th century, scientists intrigued by the Cannabis plant became equipped with advancing biological investigative technologies. With these tools, they began isolating and characterizing the chemical compounds responsible for the plant's effects. This led to the first isolation of a cannabinoid (a compound derived from Cannabis or active within the endogenous cannabinoid system), cannabidiol (CBD), in 1940 by the Adams lab[45]. Then, in 1963 and 1964, Israeli chemist Raphael Mechoulam and colleagues identified and described the chemical structures of both CBD and the psychoactive compound tetrahydrocannabinol (THC), sparking the formal beginning of cannabinoid research[46,47]. These early studies catalyzed a cascade of critical discoveries: the synthesis of THC/CBD enantiomers (1965)[48], foundational investigations into their pharmacological effects (1969)[49], and insights into THC's metabolism and pharmacokinetics in humans (1983)[50]. These breakthroughs laid the groundwork for understanding how Cannabis compounds interact with the human body and mind.

At the same time, the political landscape around Cannabis in the U.S. was becoming increasingly convoluted. In 1969, the Marihuana Tax Act, long used to criminalize possession and distribution, was ruled unconstitutional[51]. But rather than marking progress, the following year the Nixon administration introduced the Controlled

Substances Act, which created the American drug scheduling system to classify substances based on their medical value and potential for abuse[52]. While the framework had some administrative value, the scheduling decisions were widely criticized as being politically motivated. Cannabis was classified as a Schedule I drug, the most restrictive category, despite being less addictive and dangerous than many Schedule II drugs, such as cocaine[52]. This designation claimed that Cannabis had a high potential for abuse and no accepted medical use, making it federally illegal to possess, sell, or study without a difficult-to-obtain Schedule I research license. This move aligned with Nixon's broader campaign against what he saw as political enemies, including anti-war activists and the counterculture; many of whom openly used Cannabis[53]. In 1972, the Shafer Commission, which Nixon himself had appointed, released a report after extensive review of Cannabis and its societal impact. Contrary to expectations, the commission concluded that Cannabis did not pose a significant threat to public health or safety[54]. It even recommended decriminalization and proposed social interventions over punitive measures. The administration ignored the findings entirely, choosing instead to double down on criminalization.

Though largely driven by political agendas, these decisions had sweeping and long-lasting consequences. They contributed to widespread economic and racial disparities, increased incarceration rates, and created a chilling effect on scientific research. The ability, and often the will, of researchers to explore Cannabis's potential benefits and risks was stalled for decades. It wasn't until 18 years later, in 1988, that another major discovery transformed the field: Devane et al. published the groundbreaking identification of the first cannabinoid receptor, cannabinoid type 1 receptor (CB_1R), found in the rat

brain[55]. This receptor was revealed to be a G protein-coupled receptor (GPCR) that is abundantly expressed throughout many regions of the brain[56]. The identification of a specific protein target for cannabinoid compounds sparked a race among scientists to uncover the receptor's physiological role and, crucially, to identify its endogenous ligand.

Cannabinoid compounds presented a unique challenge for researchers: their chemistry. Cannabinoids are lipophilic molecules, fundamentally different from most other small molecules, whether endogenous ligands like neurotransmitters or exogenous drugs. THC, for instance, has a LogP of ~5.94, meaning it is nearly a million times more soluble in fats than in water, dramatically higher than morphine (0.8–2) or dopamine (-0.98–0.03)[57-59]. This high lipophilicity makes even basic lab procedures more difficult: separating compounds during purification, storing them in stable formulations, or even simply transferring them without leaving behind residue on standard lab surfaces, many of which are designed for water-soluble compounds. Cannabinoid scientists thus faced a triple burden: political stigma, public skepticism, and unique chemical hurdles. Still, research pushed forward to uncover the fundamental biology connecting Cannabis and the human body. The presence of a receptor strongly suggested the existence of an endogenous ligand designed to act at it.

In 1992, Mechoulam and collaborators made another breakthrough by identifying the first endogenous ligand for CB_1R: Anandamide (N-arachidonoylethanolamine, or AEA)[55]. This finding marked a pivotal shift from studying external compounds like THC to understanding the body's own cannabinoid signaling system. Anandamide's structure was itself a surprise: not a compact molecule like traditional neurotransmitters or even THC, but a long, flexible lipid chain. With both a receptor and a native ligand identified, it

became clear that a novel biological communication system existed within the body: the Endocannabinoid (eCB) System. This new framework allowed researchers to investigate how Cannabis affects physiology without relying solely on plant-derived compounds. As a result, the pace of discovery accelerated dramatically.

Just a year later, in 1993, scientists identified a second cannabinoid receptor, CB2R, predominantly expressed on immune cells such as microglia and macrophages[60]. Unlike CB_1R, CB2R is not generally associated with the classic cannabimimetic effects of Cannabis, but its presence in immune tissues suggested a biological explanation for the plant's long-observed anti-inflammatory properties. As researchers dug deeper, an important discrepancy arose: CB_1R was found to be the most abundantly expressed GPCR in the brain, but levels of anandamide were relatively low, too low to justify such high receptor expression from an evolutionary perspective[61,62]. This led to a new question: what other ligands might be activating CB_1R? In 1997, the second endogenous cannabinoid ligand, 2-arachidonoyl glycerol (2-AG), was discovered[63]. It was found in the brain at levels 100–1000 times greater than AEA, offering a compelling explanation for the high CB_1R expression[63]. With this discovery, the biological architecture of the eCB system became more complete, opening the door for a deeper understanding of how it regulates everything from mood and pain to immune function and memory. Over the next ~28 years, cannabinoid researchers have worked to define the molecular, cellular, and behavioral roles of this intricate signaling system.

In the next four paragraphs, I will move beyond the historical narrative to break down our current understanding of the eCB system, focusing on four key areas: 1) THC metabolism and its metabolites, 2) the biology of 2-AG and AEA, 3) core functional roles of the eCB

system, 4) how Cannabis exposure during adolescence alters this system, and 5) the broader ways in which Cannabis interacts with and modifies eCB signaling.

THC metabolism and its metabolites:

Tetrahydrocannabinol (THC), the main psychoactive compound in cannabis, undergoes significant metabolism in the human liver, primarily via the cytochrome P450 enzyme system, particularly the enzyme CYP2C9. THC metabolism first introduces a hydroxy (-OH) group onto the 11th Carbon creating 11-hydroxy-THC (11-OH-THC), as the primary metabolite. 11-OH-THC is capable of passing the blood brain barrier and acts much like THC, including it's capability to bind to, and activate, the CB_1R to elicit psychoactive effects[64]. The activity of the primary metabolite contributes to the long half-life of Cannabis' effects compared to many other illicit substances[65,66] (Meier et al., 2017). Further metabolism of 11-OH-THC through oxidation by the enzyme CYP3A4 leads to the formation of 11-nor-9-carboxy-THC (11-COOH-THC), which is pharmacologically inactive where it is then excreted[67] (Karschner et al., 2009). While 11-OH-THC remains bioactive at the CB1 receptor, 11-COOH-THC does not produce significant psychoactive effects due to its inability to effectively bind the CB1 receptor. THC and its metabolites are primarily eliminated through urine (with 11-COOH-THC excreted more readily). However, due to the high lipophilic nature of the compounds, they can also be readily excreted in feces and stored in adipose tissue[68]. Single use exposure to Cannabis will take hours to be effectively eliminated from the body. This is an additional contributing factor to capability to build a strong tolerance to cannabis as it can stay circulating without inducing robust impairing effects[65].

2-AG and AEA biology:

As the two primary endocannabinoid (eCB) ligands, 2-AG and anandamide (AEA) have overlapping targets but serve distinct roles within the eCB system. 2-AG is a low-affinity, full agonist at both CB_1R and CB_2R, whereas AEA is a high-affinity, partial agonist, with even lower activity at CB_2R[69-71]. 2-AG is synthesized from diacylglycerol (DAG) by the enzyme diacylglycerol lipase (DAGL) and is primarily hydrolyzed into arachidonic acid and glycerol by monoacylglycerol lipase (MAGL), with additional hydrolysis performed by enzymes such as ABHD6 and ABHD12[72-74]. AEA is synthesized from N-arachidonoyl phosphatidylethanolamine (NAPE) via the enzyme NAPE-phospholipase D (NAPE-PLD) and is hydrolyzed by fatty acid amide hydrolase (FAAH) into arachidonic acid and ethanolamine[75,76]. Given its higher abundance in the brain, 2-AG is considered the primary endocannabinoid involved in central nervous system signaling.

The synthesis of 2-AG occurs post-synaptically and is typically triggered by neuronal depolarization, consistent with its “on-demand” signaling role. This mechanism relies on the influx of calcium ions during depolarization, as 2-AG production is calcium-dependent[63,77,78]. In addition, protein-mediated mechanisms, such as the activation of Group I metabotropic glutamate receptors (mGluR1/5), can also initiate 2-AG synthesis, providing an upstream trigger that similarly depends on intracellular calcium dynamics[79]. Due to the structural and metabolic nature of these endocannabinoids, it has been believed that their synthesis occurs directly on the lipid bilayer where they are then released to the synaptic cleft where fatty acid binding proteins like carry them presynaptically[80]. Then, their binding at the CB_1R allows them to be readily integrated with the membrane where they can then be metabolized further. Due to the nature of the lipids, investigation of these basic biological functions has been severely limited.

eCB System Functionality:

Shortly after the discovery of 2-AG, researchers confirmed that CB_1R is primarily expressed on presynaptic terminals, where it modulates the release of neurotransmitters such as GABA[81,82]. The enzymes responsible for synthesizing 2-AG and AEA are localized postsynaptically, while their hydrolyzing enzymes are presynaptic—further supporting the functional localization of CB_1R on the presynaptic neuron. Consistent with other retrograde signaling systems, endocannabinoids are produced *on demand* at the postsynaptic membrane, then travel backward across the synaptic cleft to bind CB1R and suppress neurotransmitter release[83].

CB_1R is a Gi-coupled GPCR, and its activation leads to the inhibition of adenylyl cyclase, resulting in decreased levels of the second messenger cAMP. In addition, CB_1R can couple to Gβγ subunits to inhibit voltage-gated calcium channels and activate G-protein–regulated inwardly rectifying potassium (GIRK) channels, which together reduce neuronal excitability. One of the primary downstream mechanisms of CB_1R-mediated inhibition is the suppression of synaptic vesicle release[84]. Beyond these immediate effects, CB_1R activation can also engage the β-arrestin pathway, which facilitates receptor internalization and contributes to tolerance when CB_1R is repeatedly activated by exogenous cannabinoids[85]. This tolerance is robustly observed in chronic Cannabis users, who may become completely unresponsive to otherwise moderate doses.

The functional effects of CB_1R are complex, and its expression levels do not always correlate directly with its signaling output. For instance, cell-specific CB_1R knockout studies in the hippocampus revealed that only ~20% of CB_1R is expressed on

glutamatergic neurons, yet these neurons contribute roughly 50% of the receptor's G-protein–mediated activity[86]. Conversely, while GABAergic neurons express about 80% of total hippocampal CB_1R, they account for only ~20% of G-protein signaling. These findings highlight the importance of cell-type specificity and local circuitry in regulating CB_1R function. In the cortex and other regions, CB_1R expression is delicately balanced across neuronal subtypes, reflecting its nuanced role in neural circuit modulation.

Experimental evidence from electrophysiology has helped define this signaling mechanism. In one study, post-synaptic stimulation of hippocampal neurons induced the release of endocannabinoids, leading to a suppression of inhibitory postsynaptic currents (IPSCs). This suppression of GABA release was reversed by a CB_1R antagonist, confirming a CB_1R-dependent mechanism[87-89]. These findings demonstrate how activity-dependent, retrograde endocannabinoid signaling dynamically regulates synaptic transmission.

Cannabis and eCB modifications after adolescent exposure:

eCB signaling plays a crucial role in the regulation of brain development, particularly during early stages of embryonic and adolescent development. This signaling system, which starts by influencing cell fate determination, transitions during adolescence to regulate metabolic pathways and synaptic transmission in the mature central nervous system (CNS)[90]. However, the adolescent brain undergoes significant structural remodeling, making it vulnerable to external influences like THC, which can disrupt essential cellular processes such as cell proliferation, migration, and differentiation[91,92]. Activation of CB_1R during development can impair these processes, impacting neuronal

differentiation and the connectivity of key brain regions, including the hippocampus and cerebral cortex[93,94]. Activation of CB_1R by THC, influences neuronal and glial progenitor differentiation, axon growth, and cell migration, which is critical for the formation of complex brain structures[95-97].

The prefrontal cortex (PFC) is another region that undergoes significant developmental changes during adolescence, making it particularly vulnerable to the impacts of bioactive agents like THC. The PFC is critical for high-level cognitive functions and executive functions, and its proper development requires the intricate coordination of synaptic pruning, myelination, and interneuron migration. Disruption of these processes due to THC exposure during adolescence can lead to long-term functional impairments, including an increased risk for psychiatric disorders[98]. The dysfunction of microRNA-mediated maturation in the PFC has been associated with such disorders, further supporting the idea that cannabis use during this critical developmental window may lead to lasting neurocognitive deficits[99,100]. THC interferes with key molecular mechanisms in the PFC, affecting neurotransmitter balance and receptor expression, ultimately compromising the maturation of synaptic functions crucial for executive functioning[101]. This disruption is accompanied by changes in excitatory/inhibitory balance, receptor expression, and synaptic signaling, which can result in impairments in learning, memory, and other executive functions[102-105].

Cannabis' Effects within the eCB System:

Cannabis contains over 75 different phytocannabinoid compounds, all defined by their lipophilic, 21-carbon polyketide structure. Among these, Δ^9-tetrahydrocannabinol (THC)

is the most abundant and is primarily responsible for the plant's psychoactive effects through its action at the CB_1R. Like anandamide (AEA), THC is a high-affinity partial agonist at CB_1R. However, due to the widespread expression of CB_1R throughout the brain, systemic administration of THC leads to broad, activity-independent activation of the receptor.

This exogenous, activity-independent activation contrasts with the endogenous, activity-dependent retrograde signaling that defines normal endocannabinoid function. The result is widespread disruption of synaptic transmission, producing altered neuronal activity that manifests as changes in consciousness and behavior. In preclinical behavioral research, these effects have been standardized using a tetrad of cannabimimetic assays in rodents. These include:

- **Analgesia** (measured via tail-flick or hot plate tests)
- **Hypolocomotion** (open field assay)
- **Hypothermia** (rectal body temperature measurement)
- **Catalepsy** (bar test)

These behaviors are tightly linked to CB_1R activity within specific brain regions. For instance, THC's hypolocomotive and hypothermic effects have been shown to depend on its activation of CB_1R on glutamatergic neurons within the Hippocampus, a region typically rich in CB_1R expression on GABAergic neurons[106,107]. Furthermore, recent studies indicate that under strong neuronal depolarization, THC can compete with and even antagonize 2-AG at CB_1R, interfering with endogenous signaling[108]. Over the past five years—coinciding with the duration of my PhD—the cannabinoid research field has

made significant strides in unraveling both the eCB system and the pharmacology of Cannabis. A particularly transformative advancement came in 2020, when Yulong Li's lab introduced a genetically encoded sensor known as $GRAB_{eCB2.0}$ (GPCR-Activation-Based eCB sensor). This biosensor is built on a modified CB_1R scaffold, with a circularly permuted enhanced green fluorescent protein (EGFP) fused to the third intracellular loop. Rather than activating G-protein signaling, the sensor undergoes a conformational change upon agonist binding, inducing a measurable fluorescence shift[109].

The $GRAB_{eCB2.0}$ sensor has significantly expanded our capacity to monitor eCB signaling dynamics across in vivo, ex vivo, and in vitro platforms. With this tool, research groups have revealed previously unknown mechanisms of endocannabinoid signaling[110]. For example, the Stella lab identified a novel pathway in which neuronal 2-AG production is triggered via $P2X_7$ receptor activation[111]. They also used the sensor to uncover ABHD6-dependent modifications in metabotropic endocannabinoid signaling[112]. The Lovinger lab further uncovered alternate modes of 2-AG mobilization in the dorsolateral striatum, diverging from canonical cortical-projecting neuron circuits, and linked this signaling to ethanol's effects on synaptic transmission[113,114]. Perhaps most paradigm-shifting was the discovery that 2-AG can be packaged within extracellular vesicles, allowing for its rapid release—challenging the long-standing view that 2-AG is synthesized and released directly at the plasma membrane[115].

THC self-administration by adolescent rodents: Few preclinical approaches are available to study the health impact of voluntary consumption *Cannabis*-based products in rodents. The primary route of administration of such products by humans is inhalation through smoking and more recently vaporizing and dabbing; however, consumption of

edibles infused with *Cannabis* extracts and cannabinoids is rapidly increasing[116]. Of particular concern, human adolescents classified as frequent users of THC-infused edibles report both a younger age of first use compared to users who never consumed edibles and increased likelihood to have recently used *Cannabis*-based products[117]. Adolescents are particularly drawn to such products over traditional methods of using *Cannabis* given their strong appealing cues and packaging (e.g., brownies, lollipops, gummies, etc.), inconspicuous appearance, and perceived lower risk[118,119]. Given the increased prevalence of adolescents being exposed and consuming THC-containing edibles, research on the short-term and long-term consequences of this behavior is urgently needed.

The bioactivity of THC in preclinical rodent models has been studied using various routes of administration, including i.p., intravenous, subcutaneous, inhalation, solution drinking and oral gavage [116,120,121]. However, a limitation of these approaches is that they do not study the effects of THC self-administration at doses that trigger cannabimimetic responses and often require food and/or water-deprived conditions. In a recent effort to translationally represent oral self-administration of phyto-CBs by rodents, both gelatin- and dough-based formulations have been designed for behavioral analysis (**Figure 6**). For example, voluntary oral consumption of THC-containing gelatin by rodents can be measured second-by-second using high-resolution, piezoelectric scales, and the amount of THC consumed by rodents over 1-2 h trigger reliable cannabimimetic responses [122,123]. Specifically, we found that adolescent rats self-administer 2–3 mg/kg of THC-gelatin over 1 h that results in 2–3 ng/ml THC in plasma THC levels measured at the end of the intake period, and significant cannabimimetic responses [122]. THC consumption by adolescent

male rats and not female rats leads to impaired Pavlovian reward-predictive cue behaviors in adulthood consistent with a male-specific reduction in CB_1R expression by vGlut-1 synaptic terminals in the VTA [122]. Thus, THC-gelatin consumption by adolescent rats (PND 25–58) is associated with sex-dependent behavioral impairment in adulthood [122]. Consumption of THC-dough by adolescent mice (PND 26-38) impairs drug-free rotarod performance and reduces THC-triggered hypothermic responses at the end of consummatory exposure [124]. An important observation made with both of the gelatin and dough paradigms is that rodents consume less THC at higher doses, raising the possibility that there might be an avoidance to the taste/odor of THC and/or to the unwanted cannabimimetic behaviors experienced by the animal (suggesting self-titration) [122,124]. Furthermore, adolescent rodents learn to consume THC gelatin faster if access is reduced over time, thus reaching similar consumption in less time and suggesting that they learn to eat faster [122].

It is important to acknowledge that inhaled THC methods have also been implemented preclinically, providing a second ingestion method with human relevance (**Figure 6C**). Typically, this involves either burning *Cannabis* cigarettes or vaporizing THC extract in an airtight environment similar to an operant chamber [125-127]. Several labs have used involuntary THC vapor exposure to elicit cannabimimetic responses in adult rodents, including effects on anxiety and locomotor behaviors [128]. Through continued exposure, THC dependence has also been shown [129]. More relevant to this section, reliable self-administration of THC vapor has also been demonstrated [126]. Rats were trained to nose poke for THC vapor and showed high rates of responding, as well as motivation to take vapor by measuring progressive ratio and extinction responses. In contrast to i.p.

injection, inhaled cannabinoids show behavioral responses more consistent with human behavior, such as increased food intake [125]. Thus, preclinical models are beginning to both represent human consumption patterns more accurately and provide relevant PK and PD profiles of cannabis exposure and consumption patterns, and how this triggers cannabimimetic effects.

Cannabis in the current political climate: Since the passage of the Controlled Substances Act, public perception of Cannabis has shifted significantly. In 1970, only about 15% of Americans supported legalization—even for medical purposes. By 2020, that number had climbed to nearly 70%[130]. Over time, individual states began to follow a consistent pattern: decriminalization, followed by medical legalization, and eventually, full recreational legalization. This movement began with Oregon in 1973—just three years after federal prohibition—when the state decriminalized Cannabis, reducing possession penalties to a simple fine. Decriminalization spread through the following decades until 1996, when California became the first state to legalize medical Cannabis. Then, in 2012, Colorado and Washington became the first to legalize recreational use, sparking both overwhelming support and equally intense opposition from a wide range of voices. As of 2025, 24 U.S. states have legalized recreational Cannabis, and an additional 15 states have legalized it for medical use.

Resulting effects of U.S. state legalization: From the 1970s to the mid-2010s, Cannabis itself has evolved alongside the changing legal landscape. Growers and enthusiasts have selectively bred the plant to maximize THC content, pushing average concentrations from around 3% in the 1970s to approximately 12% by 2013[131]. These numbers have only continued to rise with increased commercialization and legal access.

The legal market has also introduced a surge in high-potency products; distillates, tinctures, and purified THC formulations; some offering doses upwards of 500–1000 mg per serving[131]. While the lethal dose of THC remains far beyond feasible human consumption, with estimated consummatory LD50 in mice around 482 mg/kg, concerns are growing that such high concentrations may bring users dangerously close to pushing that boundary[132]. A new set of side effects has emerged with this potency shift. Emergency rooms across the U.S. are increasingly reporting cases of cannabinoid hyperemesis syndrome, a condition in which heavy THC users experience uncontrollable vomiting[133,134]. More troubling is the observation that once someone develops this condition, even small doses of THC can re-trigger the symptoms, creating a long-term physiological aversion[135].

Advancement of AI and its applications in science

Humanity's innate curiosity and drive to understand the world around us has shaped every aspect of our society. Today, in 2025, we can access the entirety of global knowledge, opinions, and misinformation simply by reaching into our pockets. Over the past 30 years, breakthroughs in artificial intelligence (AI) and machine learning (ML) have given rise to large language models (LLMs) capable of scanning this vast information landscape to generate text and images in fractions of a second. While biological research has faced steep challenges—ranging from political restrictions to the inherent complexity of living systems, AI/ML have encountered relatively fewer legal or biological limitations, enabling exponential growth.

The earliest ideas behind computational learning and intelligence were deeply rooted in neuroscience. As researchers began unraveling the workings of the brain, starting at its

most fundamental unit, the neuron, computer scientists were inspired to build artificial systems capable of mimicking the brain's processing power. These systems aimed to capture not only basic memory and pattern recognition, but also higher-order reasoning and decision-making. In 1943, this vision was first formalized with a mathematical model of the neuron, reducing it to a binary unit capable of performing logical operations[136]. A few years later, psychologist Donald Hebb introduced the influential idea that "neurons that fire together wire together," laying the foundation for unsupervised learning and Hebbian learning in AI[137]. These mathematical principles opened the door for machines that could adapt and "learn" by updating their own parameters. In 1958, the first artificial neuron, the perceptron, was developed[138]. This single-layer binary classifier could intake data, apply weights and thresholds, and update those weights based on prediction error. Though primitive by today's standards, it marked the birth of neural networks and remains a cornerstone of all ML/AI systems built since.

Scientists experimented with layers and iterations of neural networks to unlock the next stages of computational brain functionality, such as pattern recognition. Human subconscious pattern recognition is well-documented, with various studies showing the remarkable ability of humans to recognize patterns effortlessly. Inspired by neuroscience, computational scientists developed Hopfield networks, the first type of recurrent neural network (RNN), based on the biological concept of associative memory[139]. This work was further enhanced by the introduction of backpropagation, a concept rooted in the neuroplasticity of synaptic connections. Backpropagation allowed scientists to train multi-layered neural networks, enabling them to learn internal representations and solve non-linear problems [140].

In the late 1990s and early 2000s, these concepts were applied widely by scientists, incorporating theoretical statistics to develop machine learning (ML) algorithms with practical success. One example of this is the support vector machine (SVM), introduced in 1995. SVMs utilized high-dimensional spaces to maximize relationships between non-linear datasets, showcasing the ability of models to identify patterns with both mathematical rigor and real-world utility[141]. In 2001, the random forest model was introduced, using layers of decision trees trained on random subsets of data. This drastically increased the diversification of the model, leading to improved performance. Random forests also introduced a method for signal-to-noise classification that could weigh feature importance without falling into the trap of overfitting, thanks to a technique called bootstrap aggregation[142]. While these models were effective for a wide variety of datasets, they struggled with visual data, such as photos and videos—one of the most complex data types to interpret. In response, convolutional neural networks (CNNs) were developed. CNNs use convolutional layers that sift through pixel data, assessing patterns in edges and textures. The first CNN, developed in 1998, was used to identify handwritten digits, marking a significant step forward in the ability of neural networks to “see” and interpret images[143].

Applications of these models grew slowly for some time until the explosion of computational power in graphics processing units (GPUs), which unlocked incredible functionality. Parallelized GPUs were utilized in deep-layered CNNs to introduce AlexNet, which incorporated overlapping max pooling, ReLU activation, and dropout regularization to train a much superior model (15.3% accuracy compared to ~26.2%) in less time[144]. This publication also set the standard for assessing visual data with their massive

ImageNet database, which contained over 1 million labeled images across a diverse range of categories. The advent of AlexNet changed how models were trained, datasets were managed, and deep learning approaches were applied in all ML/AI algorithm development. These advancements made CNNs computationally feasible and accurate enough for other fields to begin utilizing them. In 2014, CNNs were used to improve speech recognition software by modeling temporal and spectral variations across speech patterns[145]. They were also employed to analyze medical images such as X-rays, MRIs, and CT scans to enhance diagnostic accuracy and efficiency[146]. Beyond biological research, CNNs have impacted fields such as astronomy, environmental science, manufacturing, autonomous vehicles, and agriculture[147]. In neuroscience, they were used to decipher the hierarchical dynamics of visual cortical neurons in response to various stimuli, expanding our capability to understand the intricacies of the brain[148].

These applications extended to our ability to understand both animal and human behavior from video, driven by a desire to quantify behavioral changes through human pattern recognition and the unbiased observation provided by computer models. In 2015, CNNs were used to improve the accuracy and efficiency of facial recognition for psychological assessments[149]. This was later extended to enhance the accuracy of identifying complex emotions for mental health monitoring[150]. In 2020, a similar approach was applied to decipher the facial expression states in mice, attempting to correlate these expressions with "emotional" states[151]. Beyond facial expressions, body movements are equally important, which led to the use of CNNs to analyze human gait for better research into motor disorders like Parkinson's disease[152]. These models have drastically improved

researchers' ability to understand humans, animals, and the complex relationships between the brain and behavior.

Continued development of ML/AI modeling: CNNs continued to serve as the central force for deep learning approaches in the ML/AI field for some time, with researchers making small adjustments or adding additional features to improve upon AlexNet. These adjustments involved manipulations of the convolutional layers[153], running CNNs in parallel[154], and refining connection layers[155], among other developments. Eventually, this led to the creation of ResNet, which enabled the training of over 100 layers, setting a new standard for deep learning architectures that are still widely used today[156]. The next major advancement came with the introduction of Bidirectional Encoder Representations from Transformers (BERT), a new modeling approach capable of training with multi-directional movement of convolutional layers[157]. The rapid development and improvement of ML/AI models have contributed to the current AI boom, which is now pervasive in many aspects of daily life. Current language learning models, such as ChatGPT (OpenAI) and Bard (Google), can interpret language and respond with remarkable accuracy. While these models and the technologies driving them do have their drawbacks, they will undoubtedly continue to be used by scientists to advance research across a variety of fields.

Tools for researching animal behavior: Understanding the complexities of animal behavior for research has long been a difficult task, particularly given the broad diversity of species and the inability of animals to verbally communicate their thoughts, feelings, or experiences. To tackle this, three different algorithmic approaches have been developed by academic researchers. The first, introduced by Mackenzie Mathis in 2018, was DeepLabCut (DLC), a deep learning CNN-based, open-source tool designed for

academic researchers to label and train their own personal models for any given species or behavior[158]. DLC's infrastructure was developed from the Deeper Cut human pose estimation algorithm, which was based on deep CNNs like ResNet-50 or ResNet-101. A year later, an alternative was introduced called LEAP (LEAP estimates animal poses), which served the same purpose but was built from computer vision algorithms to decode animal poses[159]. It uses 15 convolutional layers without pooling to preserve spatial resolution. The team behind LEAP later developed a multi-animal version called SLEAP (Social LEAP), which addressed the challenge of tracking multiple animals simultaneously[160]. The third major open-source algorithm developed was MoSeq, a motion sequencing tool for behavioral analysis, which creatively utilized 3D cameras with a top-down view to model spatial changes in animal behavior[161]. MoSeq's unsupervised approach decomposes behaviors into "syllables" or stereotyped sequences. Together, DLC, SLEAP, and MoSeq combined forces to show an executed combinatorial approach to key point-MoSeq[162]. Other academic labs have developed personalized algorithms for deciphering animal behavior, such as locomouse and AlphaTracker, but none have gained the traction of the three mentioned above[163,164].

Summary

Since the Controlled Substances Act in the 1970s, public perception of cannabis has shifted significantly, with a growing majority of Americans supporting its legalization for medicinal purposes by 2023. This change in sentiment sparked a state-level movement toward decriminalization, medicinal legalization, and, later, recreational legalization, starting with Oregon in 1973. Over time, cannabis' legal status expanded across the U.S.,

with 24 states legalizing recreational use by 2025. As cannabis legality grew, so did the plant itself, with growers selectively breeding strains for higher THC concentrations. By 2013, THC levels in cannabis had more than tripled from 3% in the 1970s to 12%, which continued to rise, leading to the emergence of high-concentration THC products, including distillates and tinctures. Though cannabis overdose remains unlikely due to the high lethal dose required (although likely with synthetic compounds), rising THC concentrations have led to adverse effects, including a rise in emergency room visits for hyperemesis caused by overconsumption, resulting in a long-term aversion to THC.

The development of artificial intelligence (AI) and machine learning (ML) has been inspired by neuroscience, beginning with the first artificial neurons in 1958 and evolving through the introduction of deep learning models like convolutional neural networks (CNNs). These models have been used to tackle a range of complex tasks, from recognizing patterns in visual data to advancing medical imaging and behavioral research. CNNs revolutionized the field in 2012 with the advent of models like AlexNet, which applied advanced techniques for image recognition. Over time, AI applications have expanded beyond biology to sectors like astronomy, autonomous vehicles, and agriculture, with CNNs also being applied to study animal behavior. The rise of new AI models, such as BERT, has brought even greater accuracy and sophistication to language models, marking a significant shift in how AI is integrated into everyday life and scientific research.

The increasing acceptance and legalization of cannabis, paired with advancements in AI and machine learning, have both drastically shaped scientific research in unique ways. Cannabis has transformed from an illicit substance to a controlled and commercially

viable product, while AI has revolutionized the ways in which scientists' approach and understand complex systems, from human behavior to animal research.

Chapter 2.

Development of an acute gelatin formulation for the administration of cannabinoid compounds for in vivo rodent models

2.1 INTRODUCTION

The use of *Cannabis* products containing high concentrations of THC is rapidly increasing despite our limited understanding of its potential impact on physical and mental health [165-167]. These products are typically inhaled as combusted plant matter, vaporized extracts, or consumed in edible formulations. THC acts as a partial agonist at cannabinoid 1 receptors (**CB_1R**) to trigger a myriad of responses such as physiological responses (e.g., increase heart rate), altered mood and time perception, inhibition of motor control, and impaired learning and memory [168-174]. Subsequently, a relationship between *Cannabis* and psychotic/affective symptoms and an observable increase in *Cannabis*-associated vehicle crashes has become apparent without an understanding of the neural effects of higher dose THC [170,175-178]. Many of these effects translate to preclinical models where in rodents, THC reduces spontaneous locomotion and locomotor control, induces hypersensitivity to tactile and auditory stimuli, ataxia, and sedation; all of which have been shown to be mediated through action at CB_1R [179-182]. Importantly, some cannabimimetic responses are sex-dependent, as exemplified by the finding that THC (5 mg/kg, *i.p.*) triggers a more pronounced reduction in spontaneous locomotion and anxiogenic response in females than in males [183,184]. In addition to these cannabimimetic responses, preclinical investigations have pursued psychosis-related behaviors through the acoustic

startle response, finding that involuntary administration of THC impairs psychomotor/sensorimotor gaiting [185-188], emphasizing the translational value in understanding THC's bioactivity in humans.

Understanding the effects of increased THC use in humans through preclinical models of voluntary THC administration has proven difficult to establish due to the aversive behaviors to higher doses in rodent models [189,190]. In recent years, progress has been made in promoting voluntary oral consumption of THC in rodents, but results have been limited to mild, acute CB_1R-dependent cannabimimetic responses [123,191,192]. This lack of experimental tools to translate higher-dose THC intake in humans to preclinical models emphasizes the urgent need to develop and fully characterize a novel experimental approach. To bridge this translational gap, we initially developed an approach where mice are given *ad libitum* access to consume a sugar-water gelatin (**CTR-gel**) containing fixed amounts of THC [122,123]. Matching previous rodent studies, we found that mice consumed more vehicle gelatin than THC gelatin, indicating that they detected and avoided THC [116]. To overcome this limitation, in the current study we developed and characterized a palatable oral gelatin formulation that increases voluntary consumption by formulating THC in a chocolate-flavored nutritional shake, Ensure™ (**E-gel**). Previous work has shown that mice have a preference for chocolate flavor, making it an ideal THC formulant to increase palatability [193,194]. We leveraged this approach to determine whether oral consumption of high concentration THC gelatin induces commonly studied cannabimimetic responses in mice (hypolocomotion, analgesia, and hypothermia) and then we examined the effects of THC E-gel consumption on acoustic startle response, a preclinical measure of reflexive response rate and psychomotor arousal [186,195]. The model

developed here leverages acute voluntary consumption of a sweetened gelatin to investigate psychomotor and reflexive behaviors, pharmacokinetics, and triad responses following consumption of THC E-gel in mice.

2.2 RESULTS

E-gel promotes heightened voluntary oral consumption of THC and induces cannabimimetic behaviors by adult mice.

To incentivize voluntary oral consumption of high concentration THC, we utilized an E-gel formulation and optimized an exposure paradigm based on previous studies [123,196]. Here, individual mice were exposed to a control (CTR-gel) during a 2 h consumption period (Habituation, Day 1); and the following day exposed to THC formulated in either CTR-gel or E-gel (X mg/15 ml) for 2 h (**Figure 2.1a**). Gelatin mass was measured before and after access to calculate grams consumed, and gelatin concentrations are expressed as *X* mg of THC (X = mg of THC/15 ml gelatin) (**Figure 2.1b**). As expected, higher concentrations of THC-CTR-gel reduced gelatin consumption, an effect significant at 1 mg THC (**Figure 2.1c**, One-way ANOVA $F_{4,108} = 9.126$, $p < 0.001$, Sidak's). Remarkably, 7/17 (41%) of mice exposed to 4 mg CTR-gel did not consume any gelatin while all mice consistently consumed 5 mg and 10 mg THC-E-gel (**Figure 2.1d**). Thus, mice consumed 1.9 ± 0.05 g of VEH-E-gel and 1.0 ± 0.07 g of E-gel containing THC (10 mg/15 ml) (**Figure 2.1d**, One-way ANOVA $F_{5,75} = 14.10$, $p < 0.001$, Sidak's). Note that mice consumed similar amounts of VEH-E-gel and VEH-CTR-gel (1.96 ± 0.15 g and 1.92 ± 0.17 g, respectively), indicating that chocolate flavor *per se* does not increase consumption. When calculating the amount of THC consumed in mg/kg, we found that mice consumed more THC when formulated in E-gel (**Figure 2.1e**). For example, mice consumed 10.5 ± 0.7 mg/kg/2 h when exposed to 2 mg E-gel compared to only 4.6 ± 0.5 mg/kg/2 h when exposed to the same amount of THC formulated in CTR-gel. Using this experimental approach, maximal consumption reached 29.2 ± 1.8 mg of THC per kg/2 h when exposed

to E-gel containing THC (10 mg/15 ml), compared to the few mice that consumed only 8.4 ± 1.2 mg of THC per kg/2 h when exposed to CTR-gel containing THC (4 mg) (**Figure 2.1e**, Two-way ANOVA $F_{7,94} = 73.14$, $p < 0.001$, Sidak's). As previously shown, we found no statistically significant sex-dependent effects in consumption between male and female mice across all treatments (Two-way ANOVA $F_{1,60}= 3.64$, $p<0.06$) but did see an individual significance between males and females at 1 mg THC-E-gel (**Figure 2.1, Supplementary Figure S2.1**, Two-way ANOVA, $p<0.05$) [122,123]. These data show that mice consistently consume significant quantities of E-gel despite high THC concentrations. Based on these results, we next focused our study on quantifying the pharmacological effects of THC formulated in E-gel.

Considering that THC-CTR-gel triggers mild cannabimimetic responses due to limited consumption [122,123], we determined whether consumption of THC-E-gel could induce cannabimimetic responses measured immediately following the 2 h access period (**Figure 2.1f**). Thus, we selected three well-described behavioral effects of THC in mice: hypolocomotion, analgesia, and hypothermia (**Figure 2.1g-i**) [181]. THC was formulated and administered either by *i.p.* injection (grey), CTR-gel (green), or E-gel (purple) and behavioral responses to gelatin consumption were plotted from the average dose consumed, calculated in **Figure 2.1e**. **Figure 2.1g** shows that *i.p.* administration of THC reduced locomotion starting at 3 mg/kg, as previously reported [181], and that this response was significant after access to 4 mg THC-CTR-gel (avg: 8.4 mg/kg) and 2 mg THC-E-gel (avg: 10.5 mg/kg) (**Figure 2.1, Supplementary Figure S2.2b-e**, One-way ANOVA $F_{5,68} = 14.54$, $p<0.001$, Sidak's for CTR-gel and $F_{4,56} = 3.24$, $p=0.02$ for E-gel, Sidak's). **Figure 2.1h** shows the greatest THC-induced analgesia was reached at 30 mg/kg *i.p.* and after

access to 2 mg THC-E-gel (**Figure 2.1h** and **Supplementary Figure S2.2d, g**, One-way ANOVA $F_{4,104}$ = 9.4, p<0.001, Sidak's for CTR-gel and $F_{7,77}$ = 8.7, p<0.001 for E-gel, Sidak's). THC injection (*i.p.*) reduced core body temperature starting at 3 mg/kg, and that this response reached significance at 4 mg THC-CTR-gel (avg: 8.4 mg/kg) and at 5 mg THC-E-gel (avg: 17.2 mg/kg). **Figure 1i** also shows that reduced core body temperature induced by THC reached a significant effect of -5.84°C at 30 mg/kg *i.p.*, -1.5°C after 4 mg THC-CTR-gel (avg: 8.4mg/kg) and -1.8°C after 10 mg THC-E-gel (avg: 29.2 mg/kg) (**Figure 2.1, Supplementary Figure S2.2d, g**, One-way ANOVA $F_{5,61}$ = 11.16, p<0.001, Sidak's for CTR-gel and $F_{4,114}$ = 6.36, p<0.001 for E-gel, Sidak's). Analgesia and hypothermia did not plateau, matching prior studies which have also shown that 30 mg/kg THC-*i.p.* does not produce a maximal response for these cannabimimetic behaviors [197,198]. Sexual dimorphic responses were measured after THC administration through either *i.p.* injection or E-gel, although VEH-E-gel did show a significant difference in hypolocomotion between males and females (Supplementary Figure S3b-g, THC: Two-way ANOVA, Sidak's post-test, VEH-E-gel locomotion: Unpaired T-test, t=2.721, df=16, p = 0.02) Thus, **Figures 2.1g-i** show that: 1) THC reduces locomotion when administered using these three experimental paradigms, and to a greater extent at higher-dose *i.p.* THC and higher-concentration THC-E-gel; 2) THC induced analgesia only when administered *i.p.* and using THC-E-gel, though *i.p.* administration is more potent; and 3) THC reduces core body temperature only when administered *i.p.* and using THC-E-gel, though *i.p.* administration is more potent.

Next, we analyzed the cannabimimetic responses of individual mice following THC (10 mg/15 ml) E-gel access and how the CB_1R inverse agonist, SR1, administered 1 h

into the consumption window influences these responses (**Figure 2.1j**). SR1 was administered at 1 h to reach peak circulating concentrations during the behavioral testing (1-2 h post-injection) and to reduce any anorectic effects that would inhibit consumption of THC-E-gel [199,200]. Cannabimimetic responses increased as a function (linear regression) of increasing amount of THC consumed, demonstrating a significant relationship between the amount of THC consumed and the three cannabimimetic readouts: hypolocomotion (linear regression $F_{1,46}$=9.74, p=0.003), Analgesia (linear regression, $F_{1,57}$=15.73, p<0.001), and hypothermia (linear regression, $F_{1,46}$=24.72, p<0.001) (**Figure 2.1k-m**). Confirming the involvement of CB_1R, SR1 blocked the three THC-induced cannabimimetic responses: hypolocomotion ($F_{1,6}$=4.1, p=0.09), Analgesia ($F_{1,6}$=0.66, p=0.45), and hypothermia (SR1: $F_{1,6}$=0.68, p=0.44) (**Figure 2.1k-m**). As expected, SR1-treated mice did not consume maximal THC-E-gel compared to some animals exposed to 10 mg THC-E-gel, likely due in part to the SR1 injection 1 h into the consumption window and the known anorectic effects of SR1 [199,200]. We additionally compared the linear regression of all THC-E-gel consumption within the range of SR1-treated animal consumption and found that THC-E-gel alone still produced a significant correlation to all behaviors. These results indicate that consumption of THC-E-gel evokes robust CB_1R-dependent cannabimimetic behavioral responses in adult mice that are comparable to *i.p.*-THC administration when measuring hypolocomotion, and less potent when

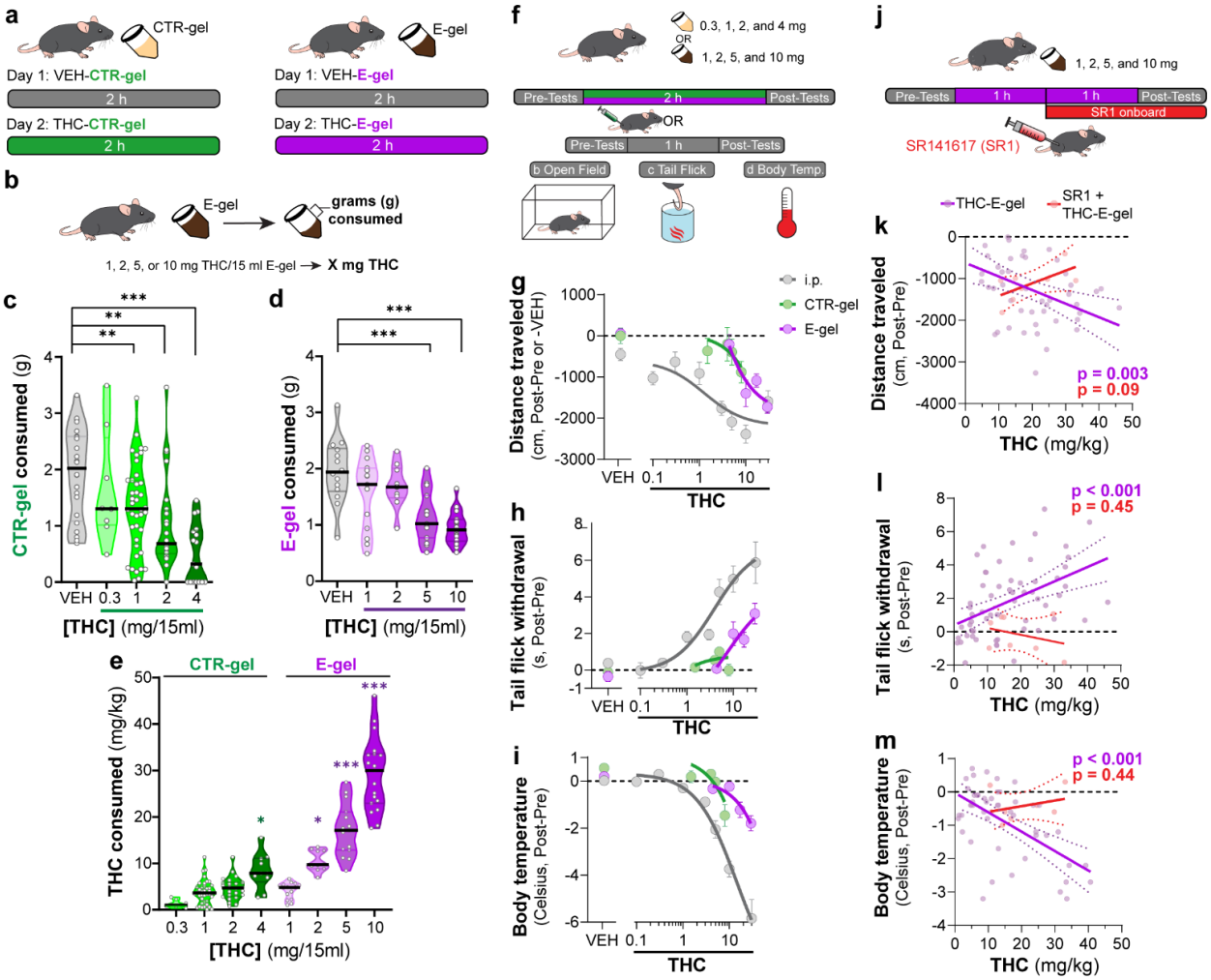

Figure 2.1: <u>E-gel promotes heightened voluntary oral consumption of THC and induces cannabimimetic behaviors by adult mice.</u>

a) Mice were given free access to vehicle (VEH), or THC formulated in either CTR-gel or E-gel for 2 h on Day 1 and Day 2. **b)** Consumption was determined by weighing gelatin at the end of each session. **c)** Consumption of CTR-gel on Day 2 is decreased after addition of THC. **d)** Consumption of E-gel on Day 2 is maintained after addition of THC. **e)** Dose of THC consumed, in mg/kg, when formulated in either CTR-gel or E-gel on Day 2. Results are mean ± S.E.M. Consumption compared ANOVA and Sidak's, *p<0.05, **p<0.01, and ***p<0.001, N=8-40. **f)** Diagram of behavioral paradigm before and after *i.p.* or gelatin administration. **g-i)** Dose-dependent behavioral responses for hypolocomotion (**g**), analgesia (**h**), and hypothermia (**i**) after THC exposure. Administration by *i.p.* (grey) is plotted on x-axis by single bolus injection while CTR-gel (green) and E-gel (purple) are plotted based on average THC consumed after 2 h exposure window shown in **e**. **j)** Diagram of THC-E-gel exposure, behavioral measurements, and SR1 injection (by *i.p.*) at 1 h into exposure window. **k-m)** Individual behavioral responses for hypolocomotion (**k**), analgesia (**l**), and hypothermia (**m**) for each animal. Individual points are plotted based on individual THC consumption with a linear regression to show correlation between consumed THC and behavioral output (p-values: **k**=0.003, **l**<0.001, **m**<0.001). SR1 treated mice are plotted (red) based on consumed THC after exposure to 10 mg/15 ml THC-E-gel with a linear regression to show no correlation across three behaviors (p-values: **k**=0.09, **l**=0.44, **m**=0.45).

compared to *i.p.*-THC administration when measuring analgesia and reduction in core body temperature.

THC-E-Gel reduces locomotion during the exposure period.

We found that mice consumed ~2 g of vehicle E-gel (VEH-E-gel) compared to ~1 g of THC-E-gel (10 mg/15 ml), indicating a 2-fold reduction in consumption (**Figure 2.2a**). To investigate the time course of this effect, we weighed gelatin every 10 min during the 2 h access period in a 3-day paradigm: access to VEH-E-gel on Day 1, access to either VEH-E-gel or THC-E-gel Day 2, and access to VEH-E-gel on Day 3 (**Figure 2.2a**). **Figure 2.2b** shows that consumption of VEH-E-gel on Day 1 started within 20 min of availability and was constant during the 2 h period. On Day 2, mice consumed comparable amounts of VEH-E-gel and THC-E-gel during the initial 40 min of access (16.3 and 13.0 mg/min, respectively) (**Figure 2.2c** and **Supplementary Figure S2.1**). However, consumption of THC-E-gel plateaued after 40 min to a rate of 4.2 mg/min (67.7% reduction), while consumption of VEH-E-gel was sustained at 9.9 mg/min (39.3% reduction), producing a significant effect by THC to modify gelatin consumption (**Figure 2.2c**, Two-way ANOVA, repeated measures $F_{1,14} = 7.604$, $p = 0.015$, Sidak's and **Figure 2.2 and Supplementary Figure S2.2**, Two-way ANOVA, $F_{1,14} = 6.05$, $p = 0.03$, Sidak's). By sharp contrast, mice that had consumed THC-E-gel the day prior consumed VEH-E-gel on Day 3 at a significantly slower rate (6.2 mg/min) during the access period, suggesting an aversive memory to THC-E-gel (**Figure 2.2d**, Two-way ANOVA, repeated measures $F_{1,14} = 4.865$, $p = 0.045$, Sidak's and **Supplementary Figure S2.2**). Consequently, mice exposed to THC-E-gel on Day 2 significantly decreased their total VEH-E-gel consumption on Days

2 and 3 (**Figure 2.2e**, Two-way ANOVA, $F_{1,83} = 37.51$, $p < 0.001$, Sidak's). These data suggest that, on Day 2, mice consumed high enough quantities of THC to induce a typically *i.p.*-high-dose (5-10 mg/kg) cannabimimetic response resulting in an avoidance to gelatin on Day 3.

Reduced spontaneous locomotion is a hallmark response to THC in mice. To address whether THC-E-gel consumption impacts spontaneous locomotion, we video-recorded the travelling distance of mice during the gelatin access period (total distance in cm over 2 h) (**Figure 2.2f**). **Figure 2.2g-i** shows that locomotion during the consumption period initially reached (1,200 cm/ 5 min) and then steadily decreased over the 2 h session on Day 1, as expected in mice that are habituating to the environment. On Day 2, spontaneous locomotor activity between mice that consumed VEH-E-gel and THC-E-gel diverged after 40 min, showing a significant decrease in total locomotion in mice that consumed THC-E-gel (**Figure 2.2h**, Two-way ANOVA, repeated measures $F_{1,14} = 11.18$, $p = 0.005$, Sidak's). Thus, this reduction in locomotion parallels a corresponding reduction in consumption in **Figure 2.2e** that is significantly different on day 2 (**Figure 2.2j**, Two-way ANOVA, $F_{1,42} = 0.3413$, $p = 0.562$, Sidak's). Importantly, spontaneous locomotion of mice exposed to VEH-E-gel and THC-E-gel was similar on Day 3. Together, these results show that consumption of THC-E-gel induced hypolocomotion on Day 2 after 40 min of access. Additionally, the decreased consumption of VEH-E-gel on Day 3 is likely due to an aversive memory of the THC exposure period and not to hypolocomotion. Thus, E-gel incentivizes voluntary THC consumption to induce robust hypolocomotion, a hallmark cannabimimetic response, within 40 min of access.

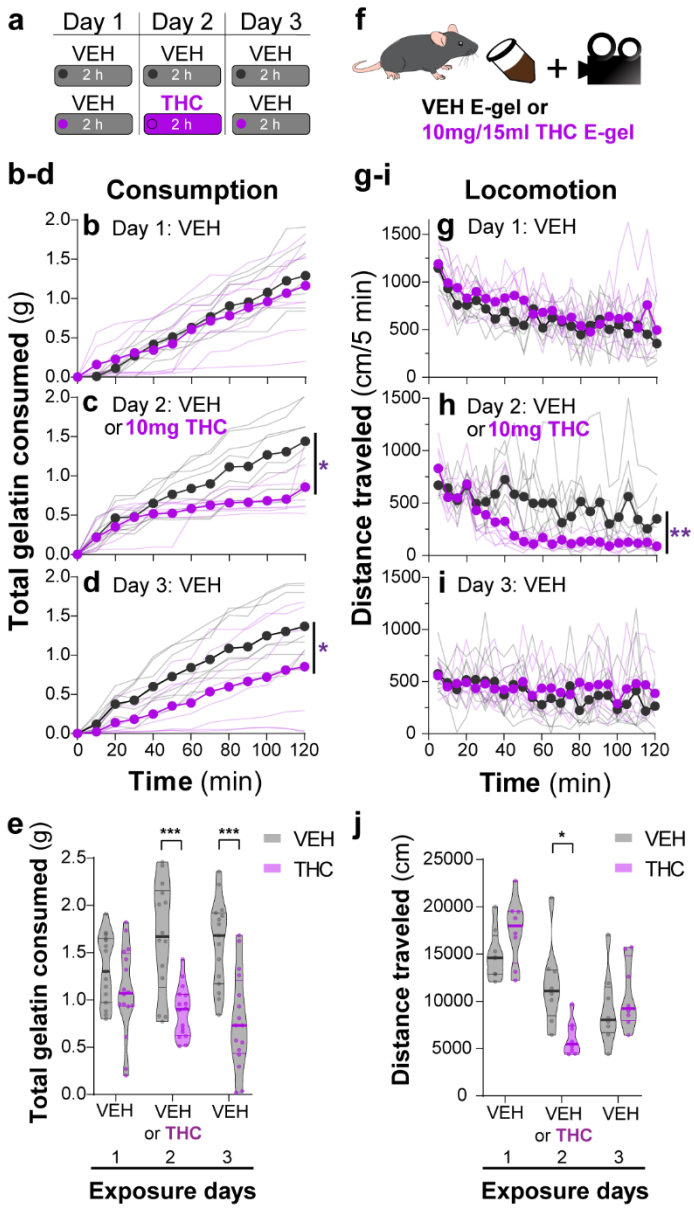

Figure 2.2: <u>THC-E-gel consumption triggers CB_1R-dependent behaviors</u>

a) Over a 3-day exposure paradigm, mice received 3 days of E-gel with either VEH or THC (10mg/15ml) E-gel on day 2. **b-d)** Cumulative gelatin consumption recorded every 10 minutes throughout the 2 h exposure window over the 3-day paradigm. VEH (black) and THC (purple) groups received access to VEH on day 1 (**b**), VEH or THC on day 2 (**c**), and VEH on day 3 (**d**). **e)** Total gelatin consumption after 2 h of access to gelatin was plotted comparing VEH and THC treatment groups. **f)** Animal consummatory and locomotor behavior was tracked during gelatin exposure window. **g-i)** Distance traveled recorded every 5 min over the 3-day paradigm, similar as to **b-d. j)** Total distance traveled (cm) after 2 h of gelatin access was plotted comparing VEH and THC groups. Main effect over 2 h exposure period (**b-d, g-i**) measured using Two-way ANOVA with repeated measures and Sidak's, main effect on total response (**e, h**) measured by One-way ANOVA and Sidak's (*p<0.05, **p<0.01, ***p<0.001) N=8-16.

Consumption of THC-E-gel results in concomitant increases in the levels of THC and its metabolites in brain tissue.

Several studies have shown that the PK profile of THC (5 mg/kg, *i.p.*) results in peak circulating concentrations of THC (1000pmol/g), its bioactive metabolite 11-OH-THC (300pmol/g), and its inactive metabolite 11-COOH-THC (100 pmol/g) in the brain after 2 h [201,202]. To determine the PK profile of THC-E-gel consumption (10 mg/15 ml) and considering the hypolocomotion behavior occurring during the consumption window, we collected plasma and brain tissue samples after 1 h of consumption, at the end of the 2 h access period, as well as 30 min (2.5 h) and 24 h (26 h) following the 2 h access period (**Figure 2.3a**). **Figure 2.3b** shows THC levels in the brain reached 500-600 pmol/g tissue between 1 h and post 2.5 h time-point and was below 50 pmol/g tissue after 24 h. Remarkably, 11-OH-THC and 11-COOH-THC levels in brain increased concomitantly to THC levels, reaching 400-500 pmol/g tissue and 200-350 pmol/g tissue, respectively, between 1 h and the post 2.5 h time-point, and both were also below 50 pmol/g tissue after 24 h. Thus, levels of both CB_1R agonists, THC, and 11-OH-THC, concomitantly peaked after 1 h of THC-E-gel consumption, a result that matches the hypolocomotion response measured starting at 40 min during the 2 h consumption period (**Figure 2.1**). Furthermore, THC and 11-OH-THC levels in brain tissue were lower, near zero, 24 h after the 2 h exposure, as previously reported [203,204]. THC levels in plasma reached approximately 400 pmol/g tissue at the 1 h time-point and decreased thereafter (**Figure 2.3c**). Statistical comparisons between the 1 h and 2 h exposure periods were limited due to different treatment paradigms, prompting the normalization of all PK values to the 1 h exposure period samples (**Figure 2.3d-e**). Brain samples were all increased at 2 h

relative to 1 h exposure but significant differences to 1 h exposure was only found at the 26 h collection time point (**Figure 2.3d**, One-way ANOVA, $F_{3,139} = 14.03$, $p < 0.001$, Sidak's). Alternatively, plasma samples were significantly decreased at 2 h for THC and COOH-THC while all three compounds were significantly decreased at the 26 h collection time point (**Figure 2.3d**, One-way ANOVA, $F_{3,141} = 35.23$, $p < 0.001$, Sidak's). Correlation of PK findings with cannabimimetic triad results did not reveal any significant relationships (**Supplementary Figure S2.3**). Note that 11-OH-THC and 11-COOH-THC levels peaked after 2 h of consumption which contrasts with the early onset

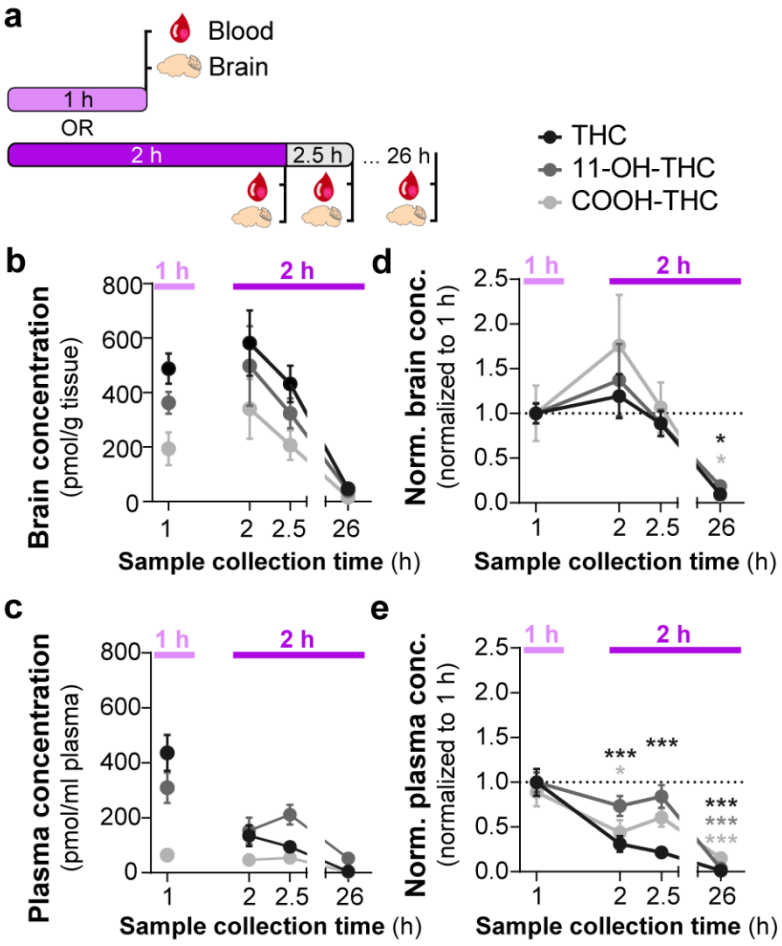

Figure 2.3: <u>Consumption of THC-E-gel results in concomitant increases in the levels of THC and its metabolites in brain tissue</u>
a) Diagram outlining gelatin exposure paradigm where blood and brain samples were collected immediately following 1 h and at 2, 2.5, and 26 hours from the beginning of 2 h access to 10mg/15ml THC-E-gel. **b)** Brain concentration of THC, 11-OH-THC, and COOH-THC after E-gel exposure, 1 h access is separated due to a reduced total access time to THC-E-gel compared to the other time points. **c)** Plasma concentrations for the three compounds plotted similarly to b. **d-e)** PK concentrations in brain **(d)** and plasma **(e)** normalized to the 1 h access period. Statistical comparison to 1 h Two-way ANOVA, Sidak's, *p<0.05, **p<0.01, and ***p<0.001, N=8-15.

hypolocomotion response measured in **Figure 2.1** after 40 min of gelatin access. Thus, PK analysis of high concentration THC-E-gel consumption demonstrates parallel accumulation of THC and 11-OH-THC in the brain, a unique profile that differs compared to previously established PK profile resulting from THC-*i.p.* injection [201,202].

Correlating *i.p.* THC and THC-E-gel triad cannabimimetic responses predicts THC-E-gel-dependent behaviors.

To further establish the pharmacological relationship between *i.p.* THC injections and THC-E-gel consumption after 1 h and 2 h consumption along with the low variability in the cannabimimetic responses triggered by both routes of administrations, we calculated "predicted THC doses" by correlating their cannabimimetic responses across experiments (**Figure 2.4a**). Thus, we extrapolated the relative *i.p.* dose for each cannabimimetic response triggered by consumption by plotting the cannabimimetic response following consumption onto the dose-response curve of THC-*i.p.* as reference (**Figure 2.4b-d**). **Figure 2.4b-d** also shows that 1 h access to high concentration THC-E-gel triggered greater cannabimimetic responses compared to 2 h access. Consequently, this resulted in a higher "predicted *i.p.* dose" shown by dotted lines tracked to the *i.p.* dose-response curves. Of note, 1 h access to high dose THC-E-gel triggered stronger hypolocomotion and reduction in core body temperature corresponding to 10.3 and 11.6 mg/kg THC *i.p.*, respectively, and analgesia corresponding to 4.5 mg/kg THC *i.p.* (**Figure 2.4b-d**). By contrast, 2 h access to high concentration THC-E-gel triggered a comparable response in the three cannabimimetic behaviors corresponding to 3-4 mg/kg THC *i.p.* (**Figure 2.4b-d**). **Figure 2.4e** illustrates the predictive value of these calculations, and the

larger variability for the 1 h access predicted dose of 8.8 ± 2.2 mg/kg *i.p.* and 3.7 ± 0.3 mg/kg *i.p.* for 2 h access, a 2.4-fold higher predicted dose after 1 h access. The variability between the cannabimimetic response for the 1 h access results suggest that a difference in the PK profile of THC at 1 h compared to 2 h access (see **Figure 2.3**). Together, these results indicate that consumption of high dose THC-E-gel triggers strong cannabimimetic responses, comparable to *i.p.* injections of THC between 4-12 mg/kg, although this is not necessarily adaptable to all behavioral readouts.

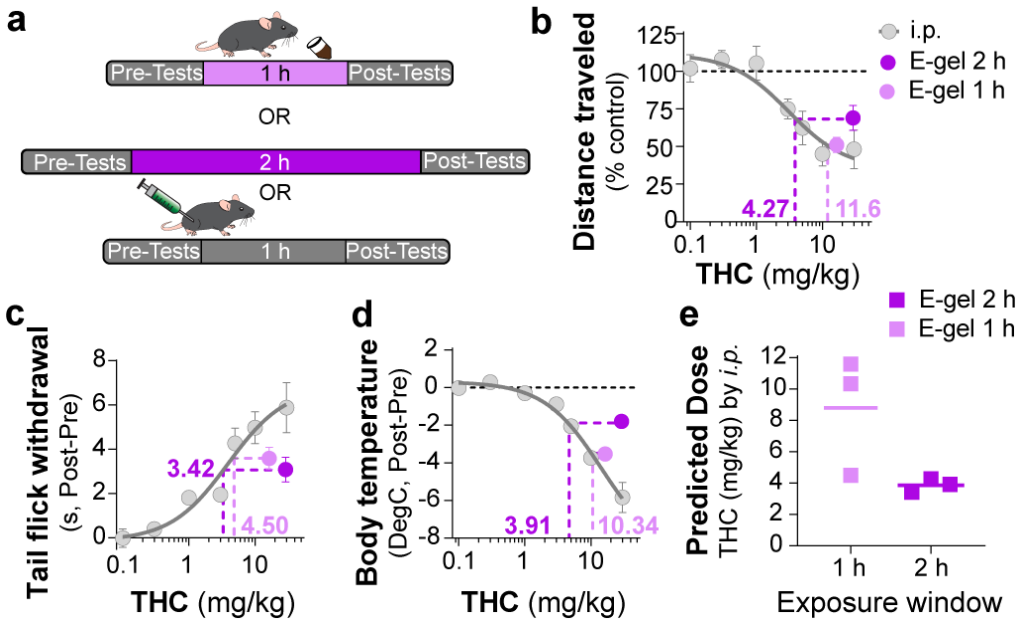

Figure 2.4: <u>Correlating *i.p.* THC and THC-E-gel triad cannabimimetic responses predicts THC-E-gel-dependent behaviors.</u>
a) Diagram of 1 h and 2 h THC-E-gel exposure and *i.p.* administration with behavioral tests. **b-d**) Cannabimimetic responses after THC administration by *i.p.* and subsequent dose-response curve in grey. Responses after 1 h or 2 h exposure to 10 mg THC-E-gel are plotted with dotted lines tracking to relative THC-*i.p.* dose response. **e**) Predicted *i.p.* dose after 1 h and 2 h THC-E-gel exposure window from all three triad behaviors.

THC-E-gel consumption and THC *i.p.* injections induce sex-dependent changes in acoustic startle responses.

Acoustic startle responses in mice represents a well-established preclinical approach to evaluate an unconditional reflex characterized by the rapid contraction of muscles to a sudden and intense startling stimulus. It is an especially useful measure in preclinical research as it is consistent across species and involves simple neural circuitry in sensorimotor gating [205]. It is known that *i.p.* injection of THC (6 and 10 mg/kg) reduces acoustic startle in male mice [186,195,206]. Thus, whether acute startle response is affected in a sex-dependent manner and by lower dose THC delivered *i.p.* or via oral consumption remains unknown. Here we compared the effect of THC-E-gel consumption and THC *i.p.* injections on acute acoustic startle in male and female mice. Acute startle responses were measured as the peak velocity of startles (Vmax) using an accelerometer and following audible tones of 80, 90, 100, 105, 110, and 120 dB delivered either 1 h after *i.p.* administration of THC (from 0.1 to 10 mg/kg) or immediately after access to THC-E-gel (10 mg/15 ml) (**Figure 2.5a**). THC administration via *i.p.* injection induced a significantly increased startle response in males at 1 and 5 mg/kg with a trend decrease at 10 mg/kg, and only a significantly decreased startle response in females at 10 mg/kg (**Figure 2.5b-c**, males: v. VEH Two-way ANOVA $F_{4,122} = 13.89$, $p < 0.001$, Sidak's; females: v. VEH Two-way ANOVA $F_{4,116} = 6.76$, $p < 0.001$, Sidak's). **Figure 2.5d** shows the male and female startle responses that occurred at the 120 dB tone exposures and follows an inverted U shape characterized by: 1] increased acute startle response at 1 and 5 mg THC (i.p.) in males, 2] absence of such response in females and 3] a comparable reduction in acute startle response in both male and female at 10 mg THC (i.p.) in males and females (Two-way ANOVA $F_{3,23} = 26.66$, $p <0.001$, Sidak's).

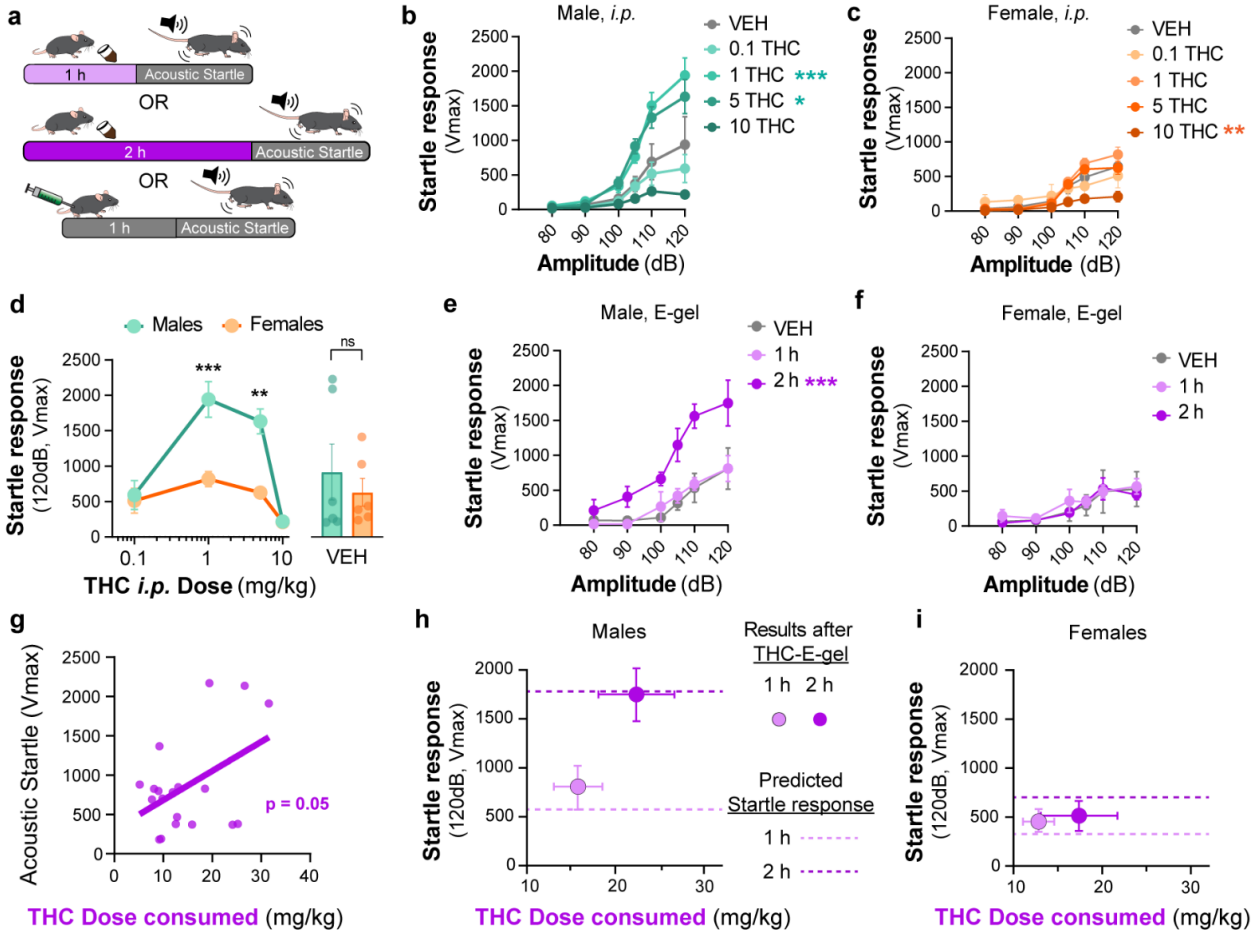

Figure 2.5: <u>Sex-dependent acoustic startle responses after *i.p.* injection of THC and high concentration THC-E-gel consumption</u>

a) Diagram of THC-E-gel exposure or *i.p.* administration followed by acoustic startle response behavioral testing. **b-c)** Male and female acoustic startle responses after *i.p.* administration of THC in response to escalating tones (80, 90, 100, 105, 110, and 120dB) following *i.p.* administration of THC in males (**b**) and females (**c**). **d)** Male and female acoustic startle dose-responses to a 120dB tone after *i.p.* THC administration. Results are mean ± S.E.M. One-way ANOVA, Sidak's comparing VEH and *i.p.* THC dose between males and females **p<0.01, and ***p<0.001, N=6-11. **e-f)** Male and female acoustic startle responses after 1 h or 2 h THC E-gel exposure in response to escalating tones (80, 90, 100, 105, 110, and 120dB. **g)** THC dose consumption based on grams consumed and individual body weight correlated with individual acoustic startle response after 2 h exposure. **h-i)** Startle response to a 120dB tone for males (**h**) and females (**i**) after 1 h or 2 h access to THC E-gel. Predicted doses calculated from a second order polynomial of *i.p.* dose responses are plotted to show the consistency in predicted dose response after E-gel exposure.

THC-E-gel consumption by males and females also triggered a sex-dependent startle response. **Figure 2.5e-f** show that only males that were allowed access for 2 h to THC-

E-gel exhibited an increase in acute startle response (2.2-fold increase) (males: Two-way ANOVA $F_{2,70} = 26.85$, $p < 0.001$, Sidak's). Further analysis of the relationship between THC-E-gel consumption and modification of the acute startle response delivered at 120 dB resulted in a significant correlation (**Figure 2.5g**, $p = 0.05$).

Finally, we sought to determine whether the predicted dose calculations from **Figure 2.4e** could be applied to the *i.p.* THC acoustic startle response dataset to test the accuracy and generalizability of the dose-prediction model. Specifically, we plotted the predicted doses of 3.7 and 8.8 mg/kg *i.p.* (from **Figure 2.4e**) on to **Figure 2.5d** depicting the acoustic startle response measured at 120dB resulting from *i.p.* injections (**Supplementary Figure S2.5-S2.6**). This produced predicted startle responses of: 310 cm/min for 1 h consumption and 688 cm/min for 2 h consumption for females, as well as 558 cm/min for 1 h consumption and 1733 cm/min for 2 h consumption for males. We then plotted the measured acute acoustic response (Vmax, 120 dB tone) following THC consumption in **Figure 2.5h-i**, as well as the predicted acute startle responses (dashed lines) from **Figure 2.5d** (**Supplementary Figure S2.7** shows methodology). The predicted acute startle responses in males exposed to 10 mg/15 ml THC-E-gel for 1 and 2 h access was close to, or within, the standard error of the measured startle response following THC-E-gel for 1 and 2 h access (**Figure 2.5h-i**). This dose-prediction model demonstrates the reliability of voluntary THC-E-gel consumption as a behavioral paradigm to produce consistent cannabimimetic responses across different experimental modalities.

2.3 DISCUSSION

Here we report a novel experimental approach that enables the behavioral impact of voluntary oral consumption of high dose THC by adult mice. Access to E-gel for 2 h over a two-day period incentivizes robust consumption, and at the highest dose tested here (10 mg/15 ml), mice of both sexes consumed ~30 mg/kg THC in 2 h on the second day. Acute consumption of THC triggers commonly established cannabimimetic responses, the potencies of which were right shifted compared to the responses measured with *i.p.* injections. Furthermore, we discovered that acute consumption of 10 mg/15 ml THC-E-gel increases the acoustic startle response in males and not in females; whereas *i.p.* injection of THC triggers a dose-dependent, inverse U-shaped, impairment of acoustic startle response that was also more pronounced in males than females. Our study provides important translational results at two levels: voluntary consumption of THC by rodents and its sex-dependent impact on acoustic startle response as a measure for psychomotor reflexive behavior.

Mice of both sexes consumed similar amounts of VEH-CTR-gel and VEH-E-gel, and none consumed more than 20% of their daily caloric intake indicating comparable consumption behaviors. However, consumption of high concentration THC-CTR-gel (4 mg) was inconsistent, and 41% of the mice completely avoided consumption (as assessed by an unbroken gelatin surface at the end of the 2 h access period) (**Figure 2.1c**). By contrast, consumption of THC-E-gel (10 mg, i.e., 2.5X more concentrated) was more consistent with a total consumption rate of 0.95 g/2 h (**Figure 2.1d**). This difference in consumption between THC-CTR-gel (4 mg/15 ml) and THC-E-gel (10 mg/15 ml) is likely due to the chocolate flavoring in Ensure™ that masks the strong odor and bitter

taste of high-concentration THC and its aversive properties. At higher doses of THC-E-gel exposure, we found more variability in dose consumed (**Figure 2.1e**), a consumption behavior similar between sexes (**Figure 2.1-figure supplemental 1b**). Future studies of such increased variability at even higher doses of THC may reveal differences in absorption or metabolism for example. Significantly, mice that consumed the higher dose THC-E-gel on Day 2 consumed remarkably less VEH-E-gel on Day 3 (**Figure 2.1-figure supplemental 2c**). This decrease in consumption is likely due to the development of aversive conditioned associations to higher dose THC. Thus, the THC-E-gel experimental approach reported here also enables the study of aversive memory to voluntary oral consumption of high dose THC.

I.p. injection of THC induces hypolocomotion, analgesia, and hypothermia in mice with different median effective doses (ED_{50}, 1.3, 3.9 and 14.4 mg/kg, respectively) (**Figure 2.2b-d**). By comparison, 1 h access to 10 mg THC-E-gel produced cannabimimetic responses that paralleled the ED_{50} of *i.p.* injections and are equivalent to an *i.p.* dose of ~9 mg/kg. Also, 1 h access to 10 mg THC-E-gel evoked a more pronounced cannabimimetic response compared to 2 h access, agreeing with prior studies which have shown that oral gavage increases brain peak concentration of THC 1-2 h after administration [207]. Oral consumption also increases 11-OH-THC levels in the brain with comparable kinetics and concentration as THC, and the levels of both cannabinoids decrease in parallel (**Figure 2.3b-c**). Considering that ~600 pmol/g of THC and 11-OH-THC is roughly equivalent to 3 nM of both compounds in the brain that persists over several hours, and both activate CB_1R with comparable potencies, our results suggest that the accumulation of both THC and 11-OH-THC in the brain might contribute to

cannabimimetic responses [208]. Because of the experimental design implemented for this study, we did not determine if variation in the time course of distinct cannabimimetic response we different following consumption. Thus, future studies that prioritize behavioral responses at multiple time points following consumption of THC using E-gel results might reveal differences in the dynamics of onset and decay in cannabimimetic responses.

We found that oral consumption of THC-E-gel produced a higher brain concentration of the primary metabolite 11-OH-THC in the brain compared to previously published concentrations after *i.p.* administration [201]. This suggests oral administration may modify the accumulation of 11-OH-THC or its metabolism in the brain. Both males and females were studied for all pharmacokinetic timepoints, and we found no significant sexual differences (**Supplementary Figure S2.3**). Finally, considering that voluntary oral consumption of 10 mg/15 ml THC results in nanomolar concentrations of THC and 11-OH-THC for several hours, the time-dependent reduction in cannabimimetic response that follows their maximal response may also be due either to CB_1R desensitization/tolerance or to redistribution of the drug within brain parenchyma.

An *i.p.* injection of THC 6 and 10 mg/kg in male mice reduces acoustic startle behaviors [195,206]. We show here that THC-*i.p.* induces a dose-dependent biphasic behavioral response that is more pronounced in males than females, demonstrating sex-dependent sensorimotor behaviors, and confirming that THC impacts neurocognitive function in a sex-dependent manner (**Supplementary Figure S2.4**) [209-211]. THC-E-gel (10 mg/15 ml) consumption also increased the response to acoustic startle preferentially in males compared to females. Whether the dose of THC formulated in E-gel can be

increased to levels that remain palatable to mice and might trigger the pronounced reduced acoustic startle measured with 10 mg THC injection *i.p.* remains an open question.

Analysis of the behavioral responses following *i.p.* injection and consumption of THC-E-gel enabled us to propose a model that correlates the doses of THC capable of producing comparable behavioral responses, emphasizing the robustness of this experimental approach. Thus, the flexibility of the THC-E-gel experimental approach may extend its utility as a substitute for traditional *i.p.* injections, better bridging the translational gap between preclinical investigations and human use. For example, the THC-E-gel experimental model can be easily modified and implemented to measure, in a less invasive manner, the impact of oral THC consumption on additional mouse behaviors, including self-administration and preference/aversion, paradigms that require multiple treatment regimens.

In conclusion, we report a new experimental approach that achieves robust voluntary oral consumption of THC in adult mice by formulating THC in a chocolate-flavored sweetened E-gel. Given the recent rise in use of *Cannabis* products that contain high doses of THC such as edibles [212], this voluntary consumption model allows the study of its effect on translational relevant behaviors, including sex-dependent psychomotor reflexes in mice.

Chapter 3.

Adolescent exposure to THC and its modifications to opioid addictive potential behaviors

3.1 INTRODUCTION

The legal use of the *Cannabis* plant and *Cannabis*-based products for medical and recreational purposes is rapidly evolving and thus there is an urgent need to understand how this might impact human health and society. The recent recreational legalization of *Cannabis*-based product use in several states of the US, with Washington and Colorado having led the way, has implemented a *Cannabis* market. Thus, the bioactivity of cannabinoids occurs along a continuum, from beneficial effects to harm reduction properties and potential harm in vulnerable population, a continuum that also occurs along the market-oriented legalization of the use of cannabis-based products (**Figure 3.1C**). The recently developed cultivation methods of the *Cannabis* plant either boost THC concentrations or boost CBD concentrations while reducing THC concentrations below 0.3%, a plant now referred to as *Hemp*. Specifically, the THC:CBD ratio has increased from 14-fold in 1995 to 80-fold in 2014, and more recent *Cannabis*-based products using *Cannabis* extracts can contain up to 90-95% THC[213]. Concomitantly, *Cannabis* use seems to be increasingly accepted as a safe recreational drug, as indicated by 16.4% of individuals ages 12–17 and 51.9% of individuals ages 18–25 years in the US reporting the use of *Cannabis* in their lifetime (2021 NIDA). Furthermore, the age of onset of daily use of *Cannabis*-based products is rapidly shifting towards younger ages (2021 NIDA). Together, these alarming statistics indicate that there is a shift toward increased use of high potency *Cannabis*-based products by adolescents, a scenario that may have

important consequences on adolescent brain development and subsequent adulthood behavior.

The relatively young field of Cannabis research has provided a strong understanding of the mechanism of action and bioactivity of phyto-CBs at the molecular, cellular, and systems levels. THC and CBD modulate neuronal activity by interacting with distinct receptors: THC acting principally on cannabinoid 1 and 2 receptors (CB_1R and CB_2R) and the glycine receptor (GLRA3), and CBD acting on G protein-coupled receptor 55 (GPR55) and transient receptor potential cation channel subfamily V member 1 (TRPV1), at least as evidenced by preclinical *in vivo* studies that validated the involvement of these receptors using genetic knockout mice. Thus, both THC and CBD modulate the activity of GPCRs and ligand-gated ion channels that are normally modulated by endogenous ligands. This includes lysophosphatidic acid (LPA) at GPR55, eicosanoids and protons at TRPV1, and the amino acids glycine at GLRA3 and GABA at $GABA_AR$.

More than two decades of peer-reviewed studies have demonstrated that the adolescent brain exhibits significant vulnerability to continued exposure of THC [214]. Functional neuronal connectivity between the ventral tegmental area (VTA), prefrontal cortex (PFC), and nucleus accumbens (NAc) (i.e., mesocorticolimbic circuitry) underlie executive function, reward processing, and appropriate decision-making, and are precisely defined during critical stages of brain development: childhood, adolescence, and young adulthood [215,216]. This places *Cannabis*-based products in the bull's-eye of public health concerns and suggests that thousands, if not millions, of adolescents will be exposed to these chemically complex products over the coming decades. Specifically, THC can have acute and durable impacts on the mental health of adolescents and can

influence mental health much later in adulthood. For example, daily use of *Cannabis*-based products with high THC by adolescents increases the risk of developing a psychotic disorder, including schizophrenia, and is related to an earlier onset of symptoms compared to people who do not use cannabis [217-220]. Relevant to this chapter, the dopaminergic system encompasses neurons that release dopamine, originating in the midbrain and sending their axons to select areas of the forebrain, a system well known to regulate motivated behaviors. Dysregulation of the dopaminergic system is associated with several neurological and cognitive diseases, including drug addiction and schizophrenia.

The marriage of pharmacological PK/PD approaches with molecular, genetic, and behavioral approaches has greatly increased our understanding of the bioactivity of THC on brain development; particularly on the development of mesocorticolimbic brain areas. This chapter was written to bridge our current understanding of the available evidence on the relationship between THC content and health outcomes, and adverse events associated with consuming highly concentrated, manufactured *Cannabis*-based products. We focused our discussion on peer-reviewed surveys and controlled studies (controlled intake and readouts). The body of work reviewed in this chapter has provided an interdisciplinary framework to generate data-driven messages about the impact of THC use on adolescent brain and highlight directions for future research objectives.

***Cannabis*-based products and devices**

Cannabis is a dioecious plant that grows around the world and is one of the world's oldest crops whose use dates back about 12,000 years [2]. THC produces psychotropic effects,

typically described as enhanced sensory perception, distorted perception of space and time, and altered interpersonal relationships and thought processes [171,221]. CBD, often referred to as a non-psychotropic phyto-CB because it does not induce the euphoria and intoxication triggered by THC [222]. CBD does greatly influence specific brain functions and behaviors such as neuronal activity and seizure incidence through a different mechanism than THC [104,223]. Additional phyto-CBs that exhibit a certain level of bioactivity include cannabinol, cannabigerol, and cannabichromine [224,225]. Thus, while hundreds of structurally related phyto-CBs are synthesized by *Cannabis* plant expressing enzymes, only a handful of them appear to exhibit significant bioactivity when taken alone or in combinations.

A key question is the potential difference in the bioactivity of whole extract *Cannabis* that include terpenes versus the bioactivity of phyto-CB isolates [226,227]. Terpenoids (terpenes) are another major bioactive constituent of the *Cannabis* plant, although present in lower quantities than phyto-CBs [228]. These 5-carbon compound isoprenes generally add fragrance to a strain of *Cannabis*, as limonene, pinene, myrcene, and caryophyllene all have distinctive odors. They bind to odorant receptors [229] and there is growing evidence that terpenoids can also engage CB_1R and CB_2R [230], here providing plausible support to the idea that terpenoids might modulate phyto-CB bioactivity. Thus, *Cannabis*-based products generated by extracting the plant material and adding the principal bioactive compounds, THC, CBD and terpenes at set ratios might produce comparable biological effects.

The legalization of *Cannabis* use bolstered the development of novel *Cannabis*-based products and devices. The most common are flower cigarettes (joints) and edibles

(cookies and candies). The newly developed devices greatly increase THC intake and provide both faster and higher quantities of phyto-CBs delivered per use (**Figure 3B**). Examples include electronic vaping devices that deliver 60-80% THC and dabbing devices that delivers high dose of concentrated cannabis resin containing 90-95% THC in one hit exposure [231]. Unlike *Cannabis* flower cigarettes and edibles, vaping and dabbing devices, as well as colorful candies and soft drinks, tend to be more common among adolescents who use more *Cannabis* overall. The ever-increasing landscape of devices that deliver high-dose THC further promotes potentially dangerous consummatory behaviors. For example, these riskier methods of consuming THC does not allow effective titration of their dose [232]. In Washington state, epidemiological data available since legalizing Cannabis use in 2012 show that *Cannabis* users are now more likely to use concentrated forms through dabbing, eating, or vaping than prior to legalization [233]. Further, it is important to better understand the diversity in THC's impact on human health, whether it varies depending on health, sex, ethnicity and age. To summarize, the legalization of *Cannabis*-based products resulted in the production of new devices that rapidly deliver THC concentrates of high potency and thus increase their psychotropic response, which raise serious concerns of the impact of such products on vulnerable population, in particular adolescents.

Cannabinoids, endocannabinoid signaling, and brain development

THC and its primary metabolite, 11-hydroxy-Δ^9-THC, activate CB_1R, GPCRs expressed by select types of neurons and glial cell [234,235]. CB_1R activation modulates neuronal functions by reducing the release of many neurotransmitters, including glutamate and GABA, and adjusting synaptic circuits and energy metabolism [236,237]. Recent evidence

also emphasizes a prominent role for CB_1R expressed by astrocytes in the modulation of neuronal functions [237]. At the molecular level, THC modulated that activity of CB_1R, CB_2R and GLRA3, receptors normally modulated by eCBs and glycine, respectively. Thus, the psychoactive responses produced by THC exposure are mediated through various receptors expressed by a complex network of neuronal and glial cells in the central nervous system. The pharmacological activity of CBD appears to involve multiple receptors. For example, evidence suggests that CBD might modulate CB_1R as a negative allosteric modulator [238], a positive allosteric modulator at $GABA_A$ receptors [239], antagonizes GPR55, activate TRPV1 and inhibit ENT-1 that mediated adenosine uptake [240-243]. As mentioned above, much less is known about the bioactivity and mechanism of action (MOA) of other phyto-CBs, including cannabinol, cannabigerol, and cannabichromine.

Significant medicinal chemistry efforts were dedicated to the synthesis of artificial cannabinoids (often referred to as “synthetic cannabinoids”) that are not produced by the *Cannabis* plant (or in fact any biological organism) and activate CB_1R. Some of the most notorious artificial cannabinoids include JWH-018, the bioactive ingredient in *Spice* and *K2* [244,245]. *Spice* has been made illegal in many countries in the world; however, the development of potent analogues, such as JWH-019, JWH-073, JWH-081, and other synthetic cannabinoids have circumvented conventional drug laws before their novel structures are made illegal. Additional artificial cannabinoids such as WIN55,212-2 (WIN) and CP55,940 (CP) are used primarily for preclinical study, as referenced below. Artificial cannabinoids exhibit a pronounced toxicity profile, and adolescents are particularly vulnerable to this class of compounds [104,246].

Cannabinoid receptors are endogenously activated by eCBs, including AEA and 2-AG, signaling lipids produced and inactivated by distinct enzymes expressed by neurons and glial cells, resulting in functionally parallel eCB signaling systems [237,247,248]. Specifically, eCBs are produced on-demand by neurons and glial cells in response to select stimuli and increased cellular activity (typically associated with increases in intracellular calcium) via lipase activation. NAPE-PLD and DAGL release eCBs from their plasma membrane precursors to generate AEA and 2-AG, respectively [63,249-253]. Released eCB's act in a retrograde manner from the post-synaptic production site to the pre-synaptically expressed CB_1R, a concept that stems from the post-synaptic expression of eCB synthesizing enzymes and presynaptic expression of CB_1R [254]. Furthermore, glial cells produce eCB and activate cannabinoid receptors expressed on other neural cells, here emphasizing the paracellular signaling mechanism of eCBs. 2-AG (functioning as a full agonist) and AEA (functioning as a partial agonist) stabilize CB_1R in conformations that activate $G_{i/o}$-proteins, induce β-arrestin signaling, and inhibit neurotransmitter release [255]. 2-AG and AEA also activate the CB_2R, primarily expressed on non-neuronal cell types, to modulate immunological activity [248]. Inactivation of eCBs occurs in two steps: a rapid uptake across cell plasma membranes via active transport followed by intracellular hydrolysis: FAAH for AEA [256-258] and MAGL and α/β-hydrolase domain 6 (ABHD6) for 2-AG [247]. 2-AG and AEA can additionally activate CB_2R, a CB_1R homolog that is primarily expressed in immune cells to modulate anti-inflammatory activity [259]. Thus, eCB signaling in the CNS encompasses CB_1R, AEA and 2-AG, and the enzymes that produce and inactivate these two main eCBs, which both mediate paracellular signaling between cells and intracellular signaling in mitochondria.

GPR55 is a newly de-orphanized Class A GPCR that has been implicated in neuronal development and regulation of neurotransmission in the adult brain [260,261]. Several endogenous ligands for GPR55 have been identified, including the signaling lipid LPI, PACAP-27 and several newly discovered small peptides [262,263]. CBD acts as an antagonist at GPR55 and modulates neurotransmission under both physiological and pathological conditions and exhibits clearly promising anti-epileptic properties for the treatment of juvenile epilepsy [264-267].

Relevant to this chapter, eCB signaling plays an overarching regulatory role in development, starting during the initial stages of embryonic development, ensuing prenatal development and differentiation [268,269]. This signaling system then undergoes a switch in function from the determination of cell fate during adolescence to the homeostatic regulation of metabolic pathways and transmission in the mature CNS [270,271]. Thus, the developing adolescent brain undergoes substantial structural remodeling that makes it particularly vulnerable to the harmful effects of exogenous bioactive agents, such as THC [272]. For example, excessive activation of CB_1R during brain development influences multiple fundamental cellular functions, including cell proliferation, migration, and differentiation through control of select signaling pathways and changes in the expression of morphogenetic factors [95-97]. Thus, the molecular diversification into neuronal and glial progenies during brain development is regulated by morphogenetic signaling molecules, including eCB signaling that contribute to the building of complex tissues. An interesting example is provided by eCB-mediated activation of CB_1R expressed by neural stem cells, which enhances differentiation into neurons without affecting astrocytes and oligodendrocytes, as evidenced by increased neurite outgrowth

and expression in neuronal markers [96]. By contrast, activation of CB_1R expressed by post-natal radial and neuronal stem cells controls differentiation in the adult brain by promoting astroglial differentiation of newly born cells [273,274]. Such remodeling occurs in many brain areas involved in vital neuronal function, including sensory inputs and higher-order cognitive processes such as learning, memory, and decision making [275]. Given that CB_1R expressed by neural progenitor cells in the adolescent developing forebrain regulates the ratio of neurons to astrocytes in areas such as the hippocampus and cerebral cortex, THC triggered activation of CB_1R during this critical period is likely to influence the connectivity of these brain regions [276,277]. In addition, evidence suggests that focal eCB gradients are generated to guide the direction of cell migration [278]. Accordingly, the downregulation of

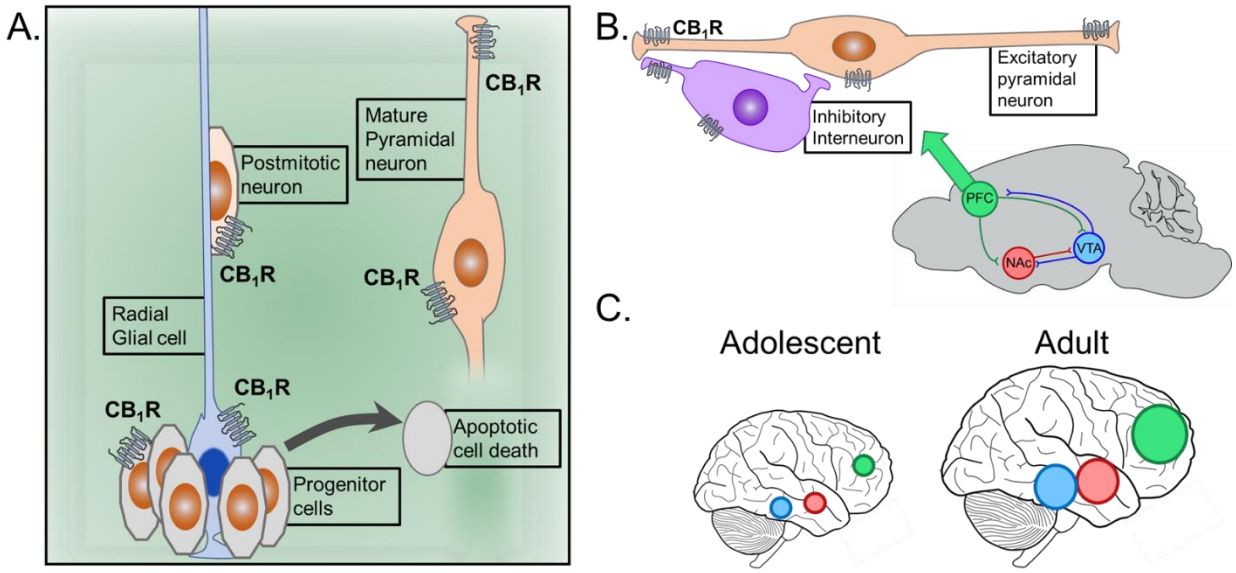

Figure 3.1. Endocannabinoid signaling and brain development: A) CB_1R are involved in brain development by their ability to control cell viability, proliferation, migration and fate, as well as neurotransmission, metabolism and connectivity. **B)** CB_1R are abundantly expressed by excitatory pyramidal neurons and inhibitory interneurons in mesocorticolimbic structures of the developing adolescent brain, a circuitry that connects the prefrontal context (PFC, green), nucleus accumbens (NAc, red) and ventral tegmentum area (VTA, blue) in rodent brain. **C)** Mesocorticolimbic brain areas are actively developing during human adolescence.

DAGLα and DAGLβ expression (enzymes involved in 2-AG release as well as production

from membranes) following neuronal specification represents an essential step to increase the reliance of post-mitotic neurons on extracellular 2-AG [278]. Relevant to this chapter, cortical plate pyramidal neurons produce and release enough quantities of 2-AG to provide positional cues [278]. Additional molecular mechanisms involving eCB signaling that regulate directed migration include the transactivation of specific receptor tyrosine kinases following activation of CB_1R [97,275,279,280]. Together, these studies provide a detailed molecular picture depicting the role eCB signaling in brain development and the vulnerabilities to exogenous cannabinoid compounds such as THC.

The prefrontal cortex (PFC) is considered one of the most evolved brain regions enabling evolutionary cognition and the emotional and cognitive capabilities of the developed, matured brain, making it particularly vulnerable during its developmental stages [281,282]. To develop the PFC and establish its complex network with other brain structures, this tissue undergoes vast number of molecular and cellular changes during adolescence that are crucial to properly form and connect brain structures, a process that is highly sensitive to bioactive agents known to impair development [99]. Specifically, the PFC undergoes significant synaptic pruning, enhanced myelination, and interneuron migration that contributes to proper adolescent maturation [283]. The complex maturation that the PFC must undergo during adolescence leaves it as one of the final brain regions to fully develop. Structural maturation of brain regions commonly occurs concurrently to functional maturation and therefore the proper maturation of the PFC is critical for developed executive functioning [284]. Given the importance of proper PFC development, several studies have linked impaired development with future psychiatric disorders [100,101,285]. More recently, dysfunction of microRNA-mediated maturation of the PFC

leading to psychiatric disorders has been reported [100]. In line with these findings, studies have linked *Cannabis* use during adolescence to neuro-psychiatric disorders in adulthood [285].

To conclude this section, eCB signaling plays a pivotal role for appropriate neuronal maturation during adolescence and neuronal maintenance during adulthood. Exogenous tampering from phyto-CB's impacts the CB_1R-driven proliferation, differentiation and maturation and pruning processes during adolescence. Further, the PFC appears to be a highly vulnerable brain region to the deleterious effects of *Cannabis* used during adolescent given that its development occurs through adolescence and that this intricate process depends on eCB signaling. The following two sections detail human clinical evidence and preclinical evidence showing that adolescent cannabinoid intake disrupts brain physiology and behavior, with particular attention paid to the PFC and mesocorticolimbic network, and its impact on adulthood anatomy and behavior.

Evidence from human studies

Several studies have addressed the health impact of *Cannabis* use during human adolescence, however only few studies offer interpretable results by providing key parameters on the population that was studied, the product used, and the amount and regimen of THC use. The gold standard of research is Randomized Control Trials (RCTs) in which study participants are randomized to two or more conditions. However, RCTs are not always possible or ethical to conduct in humans. Research on the impact of *Cannabis* use during human adolescence must therefore rely on alternative study designs and use sophisticated statistical methods to mimic RCTs to draw conclusions. Here we selected peer-reviewed human studies that were rigorously designed as emphasized by

1) the recruitment protocol of subjects with a specific health outcome and 2) a documented dose and frequency of *Cannabis* use. We also relied on surveys and secondary data analysis, where people report their cannabis use patterns, health behaviors, and health outcomes.

Because measuring THC content in *Cannabis*-based products is not feasible for large population-based studies, a more common approach is to collect detailed information on the modes of *Cannabis* administration that typically use concentrated *Cannabis*-based products. For example, using this approach, a recent study show that adults who regularly consume *Cannabis* can self-titrate their use and adjust their intake to compensate for potency [286]. While for adults this might mitigate a potential increase in the detrimental effects of high potency products, this might not be the same for adolescents. Specifically, adverse effects linked to the use of manufactured products are especially high among adolescents, and exposure to vaping *Cannabis* products is more likely to need medical intervention [287]. Many current *Cannabis*-based products use formulations with higher levels of THC content compared to *Cannabis* flower, and these modes of use have been associated with adverse health events like acute toxicity, emergency department visits, and poison center calls [213,288,289]. Thus, the increase in high potency *Cannabis*-based product is now associated with various acute toxicities, a scenario that contrasts with the previously common belief that *Cannabis* use is safe and not be associated with acute toxicity.

An additional alarming change is the recent identification of a “new” psychiatric disorder introduced in the DSM IV, the development of *Cannabis* use disorder (CUD) or addiction to *Cannabis*, particularly among adolescents [290]. It should be emphasized that

use of high potency *Cannabis*-based products increases the risk of developing CUD, a condition that impairs social functioning, memory, decision-making, school/work performance, and is more likely to be expressed by adolescent long-term users of high-dose THC compared to adults using similar amounts [291-294]. Furthermore, in a population of adolescents experimenting with *Cannabis*-based products, the use of highly concentrated THC is associated with the progression and persistence of further use compared to adolescents that use less potent products. This suggests that THC potency may represent a contributing factor to experimental use as adolescents transition to frequent use [292]. For example, a study performed in the U.S. monitored THC potency and CUD symptom onset and found that high potency cannabis products used at *Cannabis* initiation is associated with over 4 times the risk of CUD symptom onset within the first year of initiation [293]. Further, adolescents that frequently used high potency products report a higher risk of *Cannabis* dependence [294]. Other distressing studies indicate that daily use of high-potency *Cannabis* during adolescence is associated with an earlier onset of psychotic symptoms (6 years earlier) than non-cannabis users [218]. Together, this evidence suggests an increased risk of experiencing CUD and other mental disorders when adolescents frequently use high THC *Cannabis* products.

Cognitive aptitude and behavior of adults who used cannabis during adolescence

Several studies explored how cognitive aptitude and behavior during adolescence might influence *Cannabis* use behavior in adulthood. For example: “Does cognitive aptitude during adolescence influence the pattern of *Cannabis* use during adolescence and later in adulthood?” An analysis of a nationally representative longitudinal cohort identified 5 latent trajectories of *Cannabis* use frequency between ages 16 and 26: abstainers,

dabblers, early heavy quitters, consistent users, and persistent heavy users [295]. When examining how cognitive aptitude in early adolescence is associated with heterogeneous pathways of *Cannabis* use, there was a statistical relationship between adolescents with a higher rating of cognitive aptitude who start using *Cannabis* products in early adolescence and the likelihood to enter consistent patterns of use (i.e., without extreme trajectories of *Cannabis* use as they age into young adulthood) [295].

A systematic review and meta-analysis of 11 studies encompassing 23,317 individuals younger than 18 years of age indicated that adolescent *Cannabis* consumption is likely associated with increased risk of developing mental health disorders, specifically depression and suicidal behavior later in life, even in the absence of a premorbid condition [296]. Notably, this study did not find any association with anxiety incidence. This study measured *Cannabis* use in the last year or the last 6 months using self-reported questionnaires, and distinguished weekly users, daily users, and occasional users. Considering the high prevalence of adolescents consuming *Cannabis*-based products, this study suggests that the large number of young adults who develop depression and suicidality might be partially attributable to *Cannabis* use. Another recent study explored associations between *Cannabis* potency, substance use and mental health outcomes, while accounting for preceding mental health and frequency of *Cannabis* use; finding that use of high-potency *Cannabis* was associated with both increased frequency of *Cannabis* use and increased likelihood of anxiety disorder onset [297]. This result was based on analyzing outcomes and exposures collected from 1087 participants with an average age of 24 who self-reported *Cannabis* use during adolescence (average onset of use: 16.7

years of age). Of note, this study found no evidence of association between the use of high-potency *Cannabis* on either alcohol use disorder or depression [297].

Thus, the few reports on *Cannabis* use by human adolescents suggest that cognitive aptitude and behaviors during adolescence influences the pattern of *Cannabis* use, and that increased use of high THC products is associated with increased risk of developing mental health disorders, including CUD and possibly depression. Together, these studies provide a clear message of caution: preadolescents and adolescents should avoid using *Cannabis*-based products as it might be associated with a significant increased risk of developing mental health disorders in adulthood.

Disruption of brain anatomy, connectivity and dopamine function in human adults that used cannabis during adolescence

Several laboratories studied whether *Cannabis* use during adolescence affects brain anatomy and connectivity in adulthood by combining self-reports of *Cannabis* use and brain imaging technologies. A 2014 study used high-resolution MRI scans of adolescent *Cannabis* users and compared them to non-using controls [298]. They measured several morphometry readouts, including gray matter density, brain and regional volumes and shapes, and found greater gray matter density and brain structure shape differences in *Cannabis* users compared to non-using participants, particularly in the left nucleus accumbens (**NAc**) that extended to subcallosal cortex, hypothalamus, sublenticular extended amygdala [298]. Participants in this study were 20 young adults (age 18–25 years) that currently used *Cannabis* and 20 non-using controls. *Cannabis* participants used it at least once a week but were not dependent according to a Structured Clinical Interview for the DSM-IV. Thus, this study suggested that *Cannabis* exposure during young adulthood

might be associated with exposure-dependent alterations of the neural matrix of core brain reward structures.

The first longitudinal study that compared resting functional connectivity of frontally mediated networks (cingulate cortex and frontal gyrus) that mediate cognition and executive function using fMRI scan compared 43 healthy controls and 22 treatment-seeking adolescents with CUD [299]. This study found the expected increase in resting functional connectivity measured in healthy controls did not occur in adolescents with CUD, and that high amounts of *Cannabis* use during the 18-month interval predicted lower intelligence quotient and slower cognitive function as measured by full-scale IQ and reaction time. Here, the average age of cannabis use onset in the CUD cohort was 17.6 years of age and all were lifetime *Cannabis* users, representing 1000-1200 days of *Cannabis* use/individual. This study suggests that repeated exposure to *Cannabis*-based products during adolescence may have detrimental effects on brain resting functional connectivity, intelligence, and cognitive function, notably in the PFC [299]. In line with this report, a study following 799 adolescent participants found increased thinning of the PFC associated with dose-dependent experimental *Cannabis* use [300]. Participants were *Cannabis*-naïve (mean age: 14.4 years) at initial magnetic resonance (MR) image collection and 5-year follow-up MR images evaluated based on *Cannabis* use throughout the adolescent window. They also determined, by a self-report questionnaire, that *Cannabis* use and cortical thinning throughout adolescence was associated with increased impulsive behaviors [300].

A 2019 study measured the gray matter volume (**GMV**) by voxel-based morphometry of 46 individuals that reported just one or two instances of cannabis use at 14-year-old

human adolescents (males and females). The results indicated greater GMV in *Cannabis* users of the bilateral medial temporal lobes and posterior cingulate, and of the lingual gyri and cerebellum, compared to carefully matched THC-naive controls [301]. The authors noted that the GMV differences were unlikely to precede *Cannabis* use and were more likely linked to generalized anxiety symptoms in the *Cannabis* users [301]. This study outlines the provocative idea that structural brain and cognitive effects might occur after just one or two instances of *Cannabis* use in adolescence.

A 2018 study leveraged two positron emission tomography scans to measure striatal dopamine release and found a lower dopamine release 30-50% in the associative striatum of adults that use cannabis during adolescents qualify as severely cannabis-dependent participants (onset *Cannabis* use at 16.3± 3.2 years of age, used *Cannabis* for an average of 11.3± 3.6 years). The authors also reported a correlation between inattention and negative symptoms in severely *Cannabis*-dependent participants such as poorer working memory and probabilistic category learning performance [302].

Together, these studies provide independent evidence that *Cannabis* use during human adolescence may result in disrupted brain anatomy and connectivity in adulthood. To address these detrimental effects of adolescent *Cannabis* use, we urgently need additional studies to confirm and extend the current pool of knowledge. More specifically, the necessity for studies that report PK data in humans using different products, routes of administrations, and quantitative measures of any impact on brain anatomy, connectivity, and neurotransmitter functions (e.g., the dopaminergic system) are increasingly prevalent. An additional approach is to study the impact of THC use on adolescent non-human primates. A recent study in squirrel monkeys treated daily for 4

months with escalating dose of THC (0.1-1 mg/kg) showed that initial low doses of THC impair the performance of adolescent monkeys in a cognitive test designed to study repeated acquisition and discrimination reversal using a touchscreen-based cognitive test [303]. THC treatment also reduced motor activity and increased sedentary behavior during the initial week of treatment, and progressive tolerance to treatment developed, starting the second week [303]. This study provides an example of a highly translational model system to study the impact of THC use during adolescence.

Evidence from rodent studies

There has been a recent increase in the number of studies reporting the impact of THC in preclinical adolescent rodent models. Considering the well-known neuro-developmental stages that occur during rodent adolescence, conclusions can be accurately drawn when comparing THC-treated rodents to controls. An additional advantage of such studies is the ability to precisely deliver set regimens of THC, and measure changes in molecular, cellular, and behavioral parameters as a proxy of the acute impact in adolescence and subsequent consequences in adulthood. On the other hand, rodents do not model all aspects of human physiology and behavior, and many studies deliver THC using i.p. injections, which do not accurately recapitulate human use. Additionally, exposure to THC, CBD, other phyto-CBs, and terpenes as single agents does not encapsulate the full bioactive profile of the *Cannabis* plant. These important limitations must be considered when interpretating the results of preclinical studies and their translational values.

Considering an average THC content of herbal *Cannabis* is approximately 10% in Europe, and using the transformation of human-equivalent doses proposed by the Food

and Drug Administration (FDA), one can extrapolate that i.p. injections of 2.5, 5, and 10 mg/kg THC corresponds to half, one, and two joints, respectively [304,305]. Several studies reported the PK profile of THC injected i.p. and delivered orally to mice and rats [306], and it is known that THC is mainly metabolized by select P450 enzymes expressed in the liver [307]. Meanwhile, the ABC transporters P-glycoprotein (P-gp, Abcb1) and breast cancer resistance protein (Bcrp, Abcg2) regulate the brain disposition of THC [308,309]. Relevant to this chapter, there are multiple differences in the distribution and metabolism of THC between adolescent and adult mice, which might influence the pharmacological response to the drug [201]. For example, i.p. injections of THC (5 mg/kg) reaches 50% higher circulating concentration in adolescent male mice (PND 37) compared to adult mice (PND 70). Conversely, THC brain-to-plasma ratios measured in adolescent mice brain relative to adult mice brain indicate 40-60% lower brain concentrations in adolescents, most likely due to higher expression of P-gp by endothelial cells of the adolescent blood brain barrier [201]. Accordingly, i.p. injections of THC (5 mg/kg) reduces spontaneous locomotor activity in adult, but not adolescent, mice [201]. Further, adolescent female rats (PND 27-45) show a stronger metabolism compared to males. Here, the 0.5 mg/kg dose of THC i.p. was selected based upon those that typically produce rewarding and anxiolytic effects (<1 mg/kg), and the 5 mg/kg dose i.p. was selected because it typically produces anxiogenic and aversive effects (>5 mg/kg) in rodents [310]. Thus, this study reports dose-dependent and sex-dependent effects on behavior, neural activity, and functional connectivity across multiple nodes of brain stress and reward networks as measured by the elevated plus maze, novel environment activity, conditioned place preference (CPP), as well as

changes in cFOS expression using network analysis [310]. In summary, THC metabolism in rodents varies depending on the sex and species of rodents.

Treating rodents with cannabinoid agonists triggers characteristic cannabimimetic behaviors, including four hallmark responses referred to as the "tetrad response": hypothermia, hypolocomotion, analgesia, and catalepsy [181,311]. However, acute treatment with cannabinoids and pharmacological agents that target eCB signaling influence additional mouse behaviors, including ambulation, motor coordination, stress, short term memory, spatial memory, and acoustic startle [206,312-314]. Thus, it is important to study the impact of THC in adolescent mice using multiple behavioral readouts.

Molecular and cellular responses to THC treatment during adolescence in rodents

How does THC treatment impact CB_1R function, gene expression, and neuronal functions in adolescent rodents? One answer is provided by studies showing that CB_1Rs activation on the axonal surface induces repulsive growth cone turning and eventual collapse [277,315,316]. The molecular mechanism of CB_1R-mediated cytoskeletal instability in growth cones involves RHO-family GTPases, RAS, and PI3K–AKT–β-catenin signaling [277,317,318]. Accordingly, THC exposure leads to ectopic formation of filipodia and alterations in axon morphology, together limiting the computational power of neuronal circuits involved in higher cognitive function, such as the mPFC, in affected individuals [249,278]. Another molecular and cellular response linked to repeated activation of CB_1R by THC during the sensitive period of adolescent brain development are the pronounced changes in the expression and functionality of signaling proteins, including dopamine receptors critically involved in higher cognitive functions [103,105].

While it is known that the hippocampus is particularly sensitive to THC treatment [319], increasing evidence indicates additional brain structures are also sensitive, including the PFC. Specifically, as a vital cortical region with a high glutamatergic to GABAergic anatomical distribution, the balance of excitatory and inhibitory function within the PFC is critical to proper development and adult cognitive function [320]. Increased eCB production and treatments with THC or synthetic cannabinoids activate CB_1Rs expressed by different neuronal subpopulations and fine-tuned excitatory and inhibitory neurotransmission and neuronal function [237,321]. Distinct neuronal subpopulations in the PFC express CB_1R at different levels: higher levels by GABAergic neurons and parvalbumin (PV)-expressing interneurons and lower levels by cortical neurons that project to the striatum [322]. In fact the levels of *Cnr1* mRNA (which encodes CB_1R) in PFC are reduced during adolescence [323]. Given the sensitive balance of glutamatergic and GABAergic transmission with the PFC, decreased *Cnr1* mRNA suggests a shift in eCB-mediated control of synaptic development that may be uniquely vulnerable to exogenous treatment [324]. In line with this notion, activation of CB_1R shifted the balance between excitation and inhibition towards excitation [325], and results in a remarkable up-regulation in CB_1R expression and down-regulation of BNDF in the PFC, as expected by down regulation of CB_1R that controls BDNF expression [97,326].

Additional studies show that THC treatment of adolescent rodents modifies the excitatory/inhibitory balance in the mPFC. Adolescent female rats (PND 35- 45) treated with increasing doses of THC twice a day (i.p., 2.5 mg/kg 35–37 PND; 5 mg/kg 38–41 PND; 10 mg/kg 42–45 PND) show decreased expression in components of eCB signaling: CB_1R, MAGL and FAAH [102]. Accordingly, the authors found reduced eCB-

mediated LTD in the adult PFC as indicated by electrophysiological slices recordings in the cortical layer V (L-V) upon stimulation of layer II (L-II). Females presented with increased GluN2B in adulthood and AMPA GluA1 with no changes in GluA2 subunits. Adolescent exposure to the CB_1R agonist WIN impairs neuronal development and downregulates local inhibitory GABA transmission in the mPFC [105,327]. By contrast, chronic THC exposure in adolescent mice decreases NMDA current and plasma membrane expression of GluN1 in adulthood [328]. Together, this evidence suggests that THC exposure may delay adolescent maturation of the glutamatergic system, thus resulting in a less functional adult mPFC. Of note, fluctuations and dynamic state of eCB levels (2-AG and AEA) in the PFC do not appear impacted by chronic THC exposure during adolescence, thought these levels were measured by LC-MS which has clear limitations [329]. Specifically, our understanding of eCB dynamics in vivo has been limited by the low spatiotemporal resolution of common analytical chemistry approaches (rapid freezing of tissue follow by LC-MS quantification). While well suited for measuring changes in eCB tone, quantification of bulk brain eCBs does not resolve their fluctuations occurring in sec to min triggered by transient changes in brain activity. To overcome this limitation, novel genetically encoded eCB sensors, e.g., $GRAB_{eCB2.0}$, are paving the way to study localized changes in low micromolar eCB concentrations within seconds [109,330]. Together, this significant body of works convincingly shows that THC treatment of adolescent rodents results in profound changes in the molecular and cellular components involved in healthy neuronal maturation and development.

Impact on adult mesocorticolimbic systems and reward/addiction-like behaviors associated with THC use during adolescence in rodents

The THC-triggered changes in the expression of select proteins and neuronal functions in adolescent rodent brain has a pronounced impact at the system's level of adult brain function. Subsequent rodent behaviors are commonly studied as a proxy of behaviors, cognitive tasks, and pathological behavioral impairments in humans. Early studies from the laboratory of Dr. Yasmin Hurd addressed this important question in the context of the mesocorticolimbic systems and reward/addiction-like behaviors, setting a solid foundation for future studies.

One persistent claim is that *Cannabis* acts as a gateway drug; that its use may predispose individuals to want to take 'harder' drugs like opiates or psychostimulants. Because adolescence represents a time of marked plasticity, it is possible that *Cannabis* use during this period may change the underlying neurophysiology to make already reinforcing drugs more rewarding. A handful of preclinical studies have attempted to behaviorally model this 'gateway' hypothesis. Those that have typically treated adolescent rats with THC between the ages of PND 21-45 and use operant self-administration (**SA**) of the secondary drug in adulthood. Note that most studies are almost exclusively performed in rats, and it is noted when mice were used.

Opiates. In one of the earliest attempts to model the gateway hypothesis, the Hurd lab reported that adolescent THC exposure increases heroin SA in adult rats [331]. Rats with THC exposure (1.5 mg/kg, i.p., 8 injections over 21 days) pressed the heroin-associated lever more and received more total heroin after 15 days of heroin exposure. Analysis of changes in mRNA levels showed increases in pro-enkephalin mRNA in the NAc as a function of ado-THC exposure that correlated with increases in heroin SA [331]. A follow-up study showed that this pro-enkephalin was critical for expression of heroin SA after ado-

THC [332]. Studies from other groups using opiates generally support this initial behavioral finding, including identifying reinstatement of heroin seeking as influenced by ado-THC [333]. Note that the genetic makeup contributed to specific aspects of opiate-seeking behavior [334]. Using two rat strains, Lecca et al. showed that the Lewis rat strain (a more addiction prone strain) exhibit increased heroin SA after ado-THC, while the effect was largely absent in the Fischer 344 strain [334]. This study suggests that individuals who may already be addiction-prone may further increase risk of subsequent secondary drug use when using THC in adolescence. Thus, results from preclinical rodent models point to a direct relationship between adolescent *Cannabis* use and heightened opiate consummatory behavior in adulthood.

Cocaine. In contrast to the consistent results reported on opiates, three studies investigating adolescent cannabinoid exposure on cocaine-triggered behaviors in adulthood and provided opposing results. In CP treated adolescent rats (0.4 mg/kg, i.p., 11 days), adult female but not male rats increased acquisition of cocaine SA [335]. In a study published decade later, this effect was repeated with THC in adolescents (1 mg/kg, i.p., 18 days) and importantly, only using lower cocaine doses as adults [336]. Finally, using mice, Gobira *et al.,* 2021 found that adolescent exposure to WIN (3mg/kg, 8 injections over 21 days) blunted conditioned place preference (CPP) to cocaine (15 mg/kg, i.p.), a dose that is typically rewarding[337]. The authors also report an increase in PFC expression of a methyltransferase protein important in epigenetic regulation. Interestingly, this parallels another report which shows WIN-induced reduction in HDAC6 [338], suggesting both methylation and acetylation changes as a result adolescent WIN exposure. Thus,

while there appear to be effects of cannabinoids in adolescence on later cocaine sensitivity/intake, it may be both sex and dose dependent.

Other drugs of abuse. Similar to cocaine, the effect of cannabinoid use during adolescence on other non-opiate drug reward behaviors in adulthood are less conclusive. When adolescent THC (escalating dose up to 12 mg/kg) was paired with adult nicotine self-administration, no effects were found on adult acquisition of nicotine SA, extinction, or reinstatement [339]. When adolescent mice were instead injected with WIN (0.2 mg/kg, 12 injections), this did enhance subsequent adult nicotine SA at lower doses of nicotine [340], but this effect was seen only in males. The impact of THC use during adolescence on its use in adulthood also appears to be variable. One study indicated that adolescent THC exposure produced an increase in adult WIN SA [338], and showed that this THC exposure lowered DA cell activity in the VTA as well as DA release in the NAc. However, another study published the same year found that THC exposure during adolescence did not alter subsequent place preference to THC itself [341].

Taken together, two main conclusions may be drawn from this limited set of studies. The first is that adolescent exposure appears to enhance adult opioid intake, while its influence on other drug effects are unclear. However, the type of behavioral test may also be important, as CPP studies tended to produce more negative results compared to SA within each drug category. A second conclusion is that synthetic cannabinoid agonists (CP and WIN) have distinct pharmacological activity from THC, including their ability to both produce long-term changes in abuse liability and be abused themselves. This has extremely important ramifications considering the increase in artificial cannabinoid agonists that are illegally sold, such as *Spice*. If these potent CB_1R agonists are uniquely

detrimental during adolescence because of their ability to alter future drug taking, further consideration of legal status is warranted.

Additional systems-level and behavioral responses to THC treatment during adolescence in rodents

Adolescent use of THC in rodents also produces significant changes in non-addiction models of anxiety and locomotor behavior suggesting potentially dose-dependent modifications to the systems level neural connectivity of the adult brain. Adolescent chronic exposure of male mice to THC (daily 3 mg/kg i.p. for 3 weeks) increases repetitive and compulsive-like behaviors, as measured by the Nestlet shredding task [120]. Chronic administration of THC, either during adolescence or during adulthood, leads to a delayed increase in anxiety as measured by the elevated plus maze (**EPM**). Adolescent male rats (PND 35–37) treated with escalating low-doses of THC for 10 days (twice daily, 0.3-3 mg/kg) show increased spontaneous open-field activity without affecting pre-pulse inhibition (**PPI**) and attentional set-shifting performance in adulthood (PND 75, i.e., 30-day interval) [326]. Specifically, a study investigating acute THC use in adolescence report that adolescent mice responding to THC do not show significant locomotor impairments or anxiogenic behaviors in adulthood [184]. One study showed that a combination of formalin-induced chronic pain and adolescent THC exposure impaired sociability in mice, a behavior not observed from either stimulant alone [342]. Locomotion and sociability activity of adolescent male and female rats was also not affected 24 h after a single dose of WIN given that sex-dependent differences were noticeable in female adult rats [343]. Here it is important to emphasize that their THC exposure paradigm was shorter (single dose of WIN) than studies showing negative consequences such as impaired recognition

memory in adult mice after three weeks of 8 mg/kg THC exposure per day in adolescence [344]. Another set of studies with a longer THC exposure paradigm (3 weeks of daily 3 mg/kg exposure) showed cognitive and behavioral dysfunction in adulthood as measured by deficits in working memory and novel object recognition behavioral tasks [120,345].

At the mechanistic level, a recent study shows that the behavioral changes measured in adulthood resulting from THC treatment of adolescent mice depend on the expression of reelin, a signaling protein cardinally implicated in brain development implicated in psychiatric disorders when its function is impaired. Specifically, mice (PND 28) injected daily with THC (10 mg/kg, i.p.) for 3 weeks and studied 2 weeks after the last injection exhibited sex-dependent and reelin expression dependent impaired social behaviors as determined by measuring working memory, social interaction, locomotor activity [346]. THC treated adolescent mice heterozygote for reelin also exhibited elevated disinhibitory phenotypes as measured by anxiety-like responses and stress reactivity, and increased reactivity to aversive situations as measuring using pre-pulse inhibition of acoustic startle [346].

Long-term ‘two hit’ behavioral effects of chronic young-adult treatment with CP (0.2 mg/kg, 8–10 weeks of age) in combination with maternal separation (3 h every day from postnatal days 2–14) was studied in male and female rats [347]. In male rats, the combination of maternal separation and CP exposure decreased sucrose preference and time spent on the open arms of the elevated plus maze. By contrast, no effect was detected on PPI, memory performance in the Y-maze and novel object recognition. This difference in behavioral consequences due to varied THC exposure paradigms may point

to a unique vulnerability of the mPFC during this adolescent period due to its complexity and developmental complexity and timeline.

Together, these studies paint a picture of diverse behavioral modifications in anxiety, sociability, locomotion, and sucrose preference that are initiated by adolescent exposure of THC. The diversity of behaviors impacted in adulthood suggests that THC's bioactivity during neurodevelopment is modifying a larger systems-level connectivity throughout the nervous system. Further investigations to understand the molecular, cellular, and systems-level effects of adolescent THC exposure will contribute to deciphering the alterations in region-to-region connectivity.

CBD interactions with THC during adolescence

Several studies have shown that the bioactivity of CBD is often biphasic, producing one set of behavioral changes at low doses and exhibiting a distinct bioactivity at high doses, including reducing seizures [129]. Specifically, high dose of CBD (approximately 300 mg/kg in both humans and rodents) proved to exhibit groundbreaking anti-seizure activity for the treatment of early-onset epilepsies that develop in adolescent patients with Dravet syndrome and Lennox-Gaustat; and this treatment regimen exhibits a promising safety profile characterized by mild side-effects (somnolence, decreased appetite, diarrhea and fatigue) [264,265,348]. These studies emphasize the promising safety profile of CBD even at relatively high doses. One also need to consider non-medicinal preparations often referred to as "cannabis light" that contain CBD (e.g., 1-30 mg/kg) and low levels of THC (e.g., 0.2 to 1%), products that are legally available in select countries [305,349]. Thus, one approach to study the mitigating effect of CBD on THC's bioactivity is to consider THC/CBD ratios currently used by human adolescents. For example, THC/CBD ratios of

3 and 0.33 are reminiscent of THC-rich/CBD-poor and CBD-rich/THC-poor cannabis-based product that were confiscated in the illegal market [305,350].

To our knowledge, the first study reporting the mitigating effect of CBD on THC use in adolescent rodents was published in 2017 by the laboratory of Dr. Kenneth Mackie. Adolescent mice were treated for 15 days (PND 28–48) with daily i.p. injections of either THC (3 mg/kg), CBD (3 mg/kg) or both [120]. THC triggered immediate and long-term impairments in working memory measured by the novel object recognition task, as well as in increased adulthood anxiety measured on the elevated plus maze (**EPM**), and increased repetitive and compulsive-like behaviors measured with the Nestlet shredding task and marble burying [120]. All THC-induced behavioral abnormalities were prevented by the coadministration of CBD + THC, and CBD alone did not influence behavioral outcomes [120]. Additionally, a study investigated the potential effects of CBD to mitigate the negative anxiogenic effects experienced from THC, finding that a single co-administration of CBD (3mg/kg) alleviates the anxiogenic behavior produced from THC (1mg/kg) [351].

A recent study in adolescent female rats (PND 35-45) explored the impact of 15 days treatment with twice daily i.p. injections of increasing doses of THC (2.5, 5 and 10 mg/kg), CBD (0.8, 1.7 and 3.3 mg/kg), or of THC:CBD (1:1) [305]. This paradigm results in adulthood impaired emotional behaviors measured by the swim test, sucrose intake, palatable food intake, and elevated plus maze; as well as deviations in social interaction behaviors measured with short-term recognition memory, and impaired memory measured with novel object recognition [305]. These behavioral changes correlate with molecular and cellular changes in the PFC, including reduction in CB_1R and Glutamic Acid

Decarboxylase-67 (GAD67) expression measured by Western blot, increased CD11b expression measured by Western blot, and microglial cell activation measured by changes in cell morphology analyzed by IHC [305]. These results suggest that PFC activity in adulthood is impacted by changing the balance between excitatory and inhibitory neurotransmission and concomitant neuroinflammation. Here too, CBD mitigates some of the long-term behavioral alterations induced by adolescent THC exposure as well as the changes in long-term changes in PFC molecular components [305].

Due to the recent shift towards the legalization of the consumption of *Cannabis*-based products, understanding its impact on public health is increasingly urgent, particularly its consequences for the developing adolescent brain (see our recent reviews [352,353]). In 2014, over 60% of new cannabis users in the US were under 18 at the initiation of use [131,354,355]. This statistic is alarming given the emerging research identifying that the best predictor of substance use disorders is the age of onset of substance use [356-358]. Accordingly, both human and preclinical studies suggest that THC exposure during adolescence may lead to psychiatric and neurological impairments in adulthood that include compromised motivation, spatial memory and reward sensitivity [298-302,359-365]. THC is the primary psychoactive compound produced by the *Cannabis* plant. Its psychotropic is mediated by cannabinoid 1 receptor (**CB_1R**) , a GPCR abundantly expressed in the brain, particularly in areas involved in motivated behavior [366]. Activation of CB_1R expressed by developing neurons influences their phenotype, connectivity, and release of neurotransmitters [367-369]. Accordingly, adolescence represents a critical period of brain development that is highly vulnerable to the effects of exogenous drug exposure. Specifically, the brain is sensitive to the THC activation of CB_1R, and evidence shows that

i.p. delivery of THC during adolescence modifies the endocannabinoid (**eCB**)-CB_1R dependent signaling pathway, neural activity, and behavior in adult mice. THC exposure during adolescence in rodents changes the functionality of key receptors in adulthood, including reductions in CB_1R expression [103,105,191] and repeated i.p. injections of THC in adolescent rodents results in selective behavioral impairments in adulthood, including increased repetitive and compulsive-like behaviors measured by the Nestlet shredding task [120], as well as anxiety-like behavior as measured by the elevated plus maze (EPM) and increased spontaneous locomotion in open-field; yet it does not affect pre-pulse inhibition (PPI), an attentional set-shifting performance [326]. This diversity of motivated behaviors impacted in adulthood suggests that THC's activation of CB_1R during brain development impacts multiple systems-level connectivity throughout the brain and ensuing the behaviors. However, we still do not understand how continuous adolescent voluntary consumption of edibles containing THC (a model very similar to human adolescent consumption and lacking the confounds of i.p. injection kinetics and investigator induced stress) behavioral readouts in adult mice.

The understanding the impact of THC use using preclinical models of voluntary THC administration has proven difficult to establish due to the aversive behaviors to higher doses in rodent models, and has been limited to mild, acute CB_1R-dependent cannabimimetic responses [123,189-192]. This lack of experimental tools to translate higher-dose THC intake in humans to preclinical models emphasizes the urgent need to develop and fully characterize a novel experimental approach. To bridge this translational gap, we developed an approach where rodents are given *ad libitum* access to consume a sugar-water gelatin (CTR-gel) containing fixed amounts of THC [122,123]. Here we allowed

adolescent mice to voluntarily consume CTR-gel and THC-gel during adolescence and studied whether this impacted their locomotor behavior in adulthood, an index of impairment.

3.2 RESULTS

Voluntary consumption of THC-Gel by adolescent mice. The bioactivity of THC in rodents has been studied using i.p., i.v., and s.c. injections, inhalation, solution drinking, and oral gavage [116,120,121]. Limitations of these approaches include the absence of voluntary consumption, the stress response in rodents during injection or exposure to experimenter-administered smoke, as well as the necessity of food/water-deprivation to

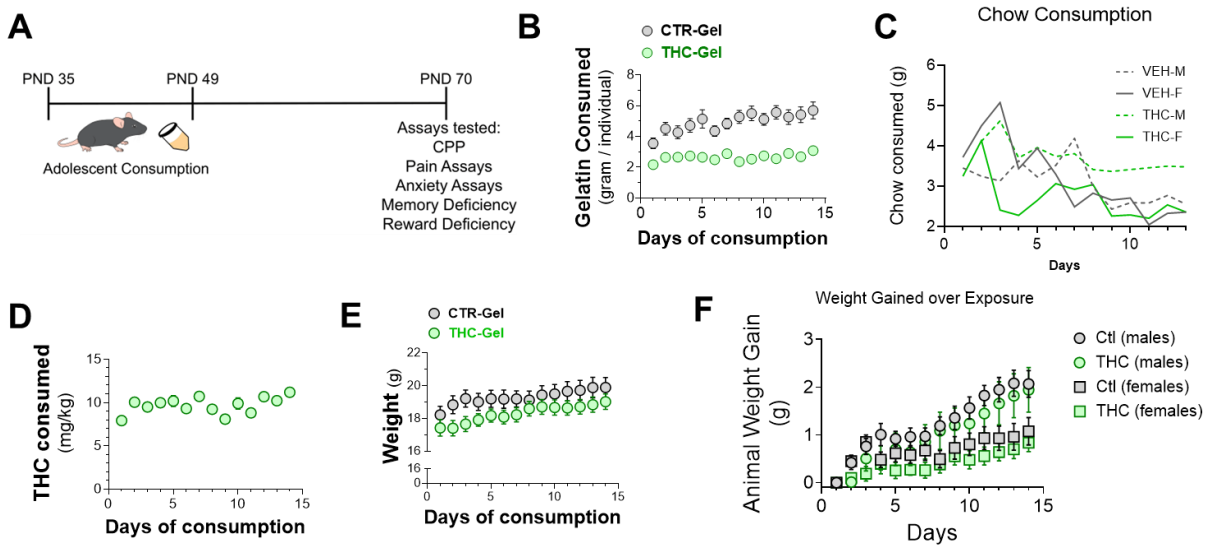

Figure 3.2: Voluntary consumption of THC-Gel by adolescent mice: A**)** Timeline of adolescent gelatin exposure to CTR-gel or THC-gel from PND 35-49, with experimentation occurring on PND 70. **B**) Gelatin consumed of vehicle and THC gelatin over 14 day exposure. **C)** Total chow consumed per animal by cage during the gelatin exposure window. **D)** THC consumed per animal of the 14 day gelatin exposure when exposed to THC gelatin. **E**) Average animal weight for mice exposed to CTR-gel or THC-gel. **F**) Animal weight gained over the gelatin exposure window, separated by male and female.

facilitate robust consumption. Here we used the voluntary consumption of THC-gelatin that we previously developed and validated[123]. Specifically, adolescent mice of both sexes (PND 35-49) were allowed free access to either CTR-Gel or THC-Gel (15 mg/15 ml) for 24h every day for 14 days (**Figure 3.2A, Supplementary Figure S3.1**). As expected, both adolescent males and females voluntarily consume comparable amounts

of CTR-Gel, and lower amount of THC-Gel daily, and for multiple days (**Figure 3.2B** and Figure S1A-B). Importantly, adolescent mice of both sexes consumed a similar amount of chow during that period, excluding any involvement of satiety (**Figure 3.2C, Supplementary Figure S3.2**). **Figure 3.2D** shows that adolescent mice consumed a constant about of THC resulting in ≈ 8-11 mg/kg/day over 2 weeks. Adolescent mice exposed to CTR-Gel and THC-Gel increased in total body weight at similar rate, as well as similarly gained weight as a percent of exposure (**Figure 3.2E**). Of note, adolescent mice consumed a total of VEH-CTR-gel (1.96 ± 0.15 g and 1.92 ± 0.17 g, respectively), which are equivalent to 1.70 kcal (~13% of daily kcal intake and thus unlikely to affect overall nutrition). As previously shown, we found no statistical difference in consumption between male and female mice [123,191,353,370]. Together, these results show that adolescent mie of both sexes similarly consumed CTR-Gel and THC-Gel daily and for multiple days without any significant effect on their body weight and chow consumption.

Sex dependent impact of THC-Gel consumption during adolescence on adulthood memory and motivated behaviors, without affecting locomotion in an open field and canonical pain responses. We first tested memory behavior in adult mice (PND70) exposed to CTR-Gel and THC-Gel during adolescence by measuring the Barnes Maze escape time on the last final trial of a over 4 days testing. **Figure 3.3A-B** show that while male adults showed no difference between CTR-Gel and THC-Gel treatments, adult females exposed to THC-Gel did not reduce their escape time compared to adult females exposed to CTR-Gel, suggesting that THC exposure during adolescent only impact spatial memory in females. We then tested motivated behavior using the condition place preference (CPP) test of adult mice exposed to morphine (5 mg/Kg). **Figure 3.3C** shows

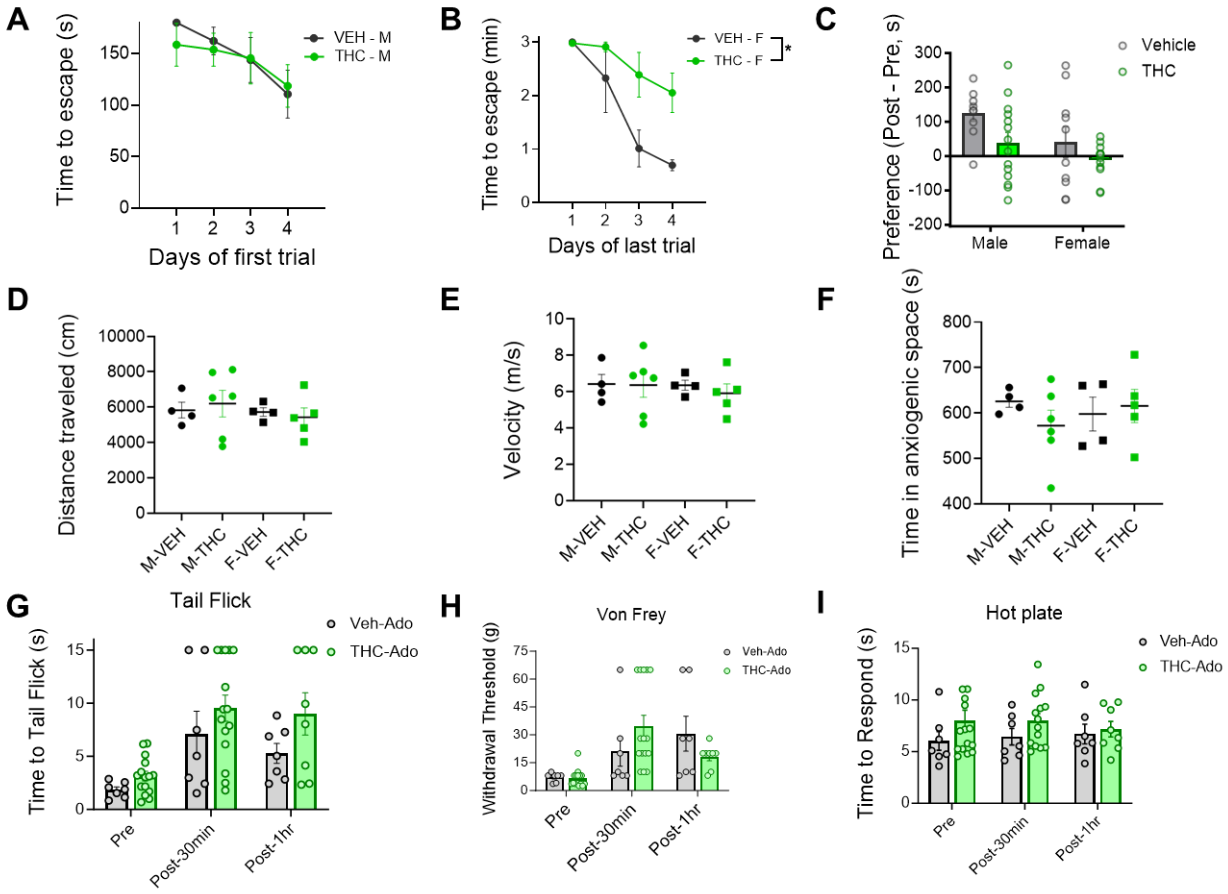

Figure 3.3: Sex dependent impact of THC-Gel consumption during adolescence on adulthood memory and motivated behaviors, without affecting locomotion in an open field and canonical pain responses. A-B) Barnes Maze escape times of trial one over 4 days of testing in male (A) and female (B) mice on PND 70 after exposure to either CTR-gel or THC-gel in adolescence. **C)** CPP for morphine in male and female mice after ado exposure. **D-F)** Distance traveled (D), velocity(E), and anxiety score (F) as measured by time in anxiogenic space during CPP test day. **G-I)** Pain scores before, 30 min after, and 1 hour after morphine administration. Tests performed were Tail flick assay (G), Von Frey (H), and Hot plate assay (I). One-Way ANOVA (*p<0.05).

that adult male mice exposed to CTR-Gel during adolescence spend more time in the morphine chamber compared to adult male mice exposed to THC-Gel during adolescence as exemplified by the lack of place preference. Remarkably, adult female mice exposed to both CTR-Gel and THC-Gel during adolescence showed no place preference (**Figure 3.3C, Supplementary Figure S3.3**). Reduced spontaneous locomotion in an open field is a hallmark cannabimimetic response to THC administration

in mice[181]. **Figures 3.3D-F** show that adult mice of both sexes exposed to CTR-Gel and THC-Gel during adolescence exhibited similar spontaneous locomotor behaviors in the open field when measuring distance traveled, velocity and time spent close to the borders. Basal pain behaviors were also not different in adult mice of both sexes exposed to CTR-Gel and THC-Gel during adolescence as measured by the tail flick, Von Frey and hot plate assays (**Figure 3.3G-I, Supplementary Figure S3.3**). Together, these results show that exposure to THC during adolescence results sex-dependent behavioral impairments in adulthood, specifically spatial memory impairment in females and impairment of CPP to morphine in male adults, without affecting spontaneous locomotion measured in an open field and canonical pain behaviors.

Adolescent THC exposure alone does not produce robust behavioral changes but does reduce grooming. We recently developed an unbiased analysis of spontaneous locomotion in adult mice using a rigorous, machine learning analysis designed to isolate critical behavioral features in a linear track. Such analysis is particularly relevant as we discovered that acute treatment of adult mice with THC reduces spontaneous locomotion events and affects motor coordination, a behavioral response seen in humans [371-373], which was not captured in sufficient detail by previous analyses of rodent cannabimimetic responses. Specifically, we used the machine learning pose estimation algorithm, SLEAP, to automatically classify a variety of defined behavioral states in a clear-bottomed behavioral corridor, adapted from, allowing for high frame rate behavioral tracking of discrete animal movement, simultaneously from the ventral (bottom) of the mouse and from the lateral position (side) [158,164] (**Figure 3.4, Supplementary Figure S3.5-S3.6**). We found striking changes in anxiety-like measures and time grooming, establishing this

model as high resolution and having utility in decoding the impact of adolescent THC on

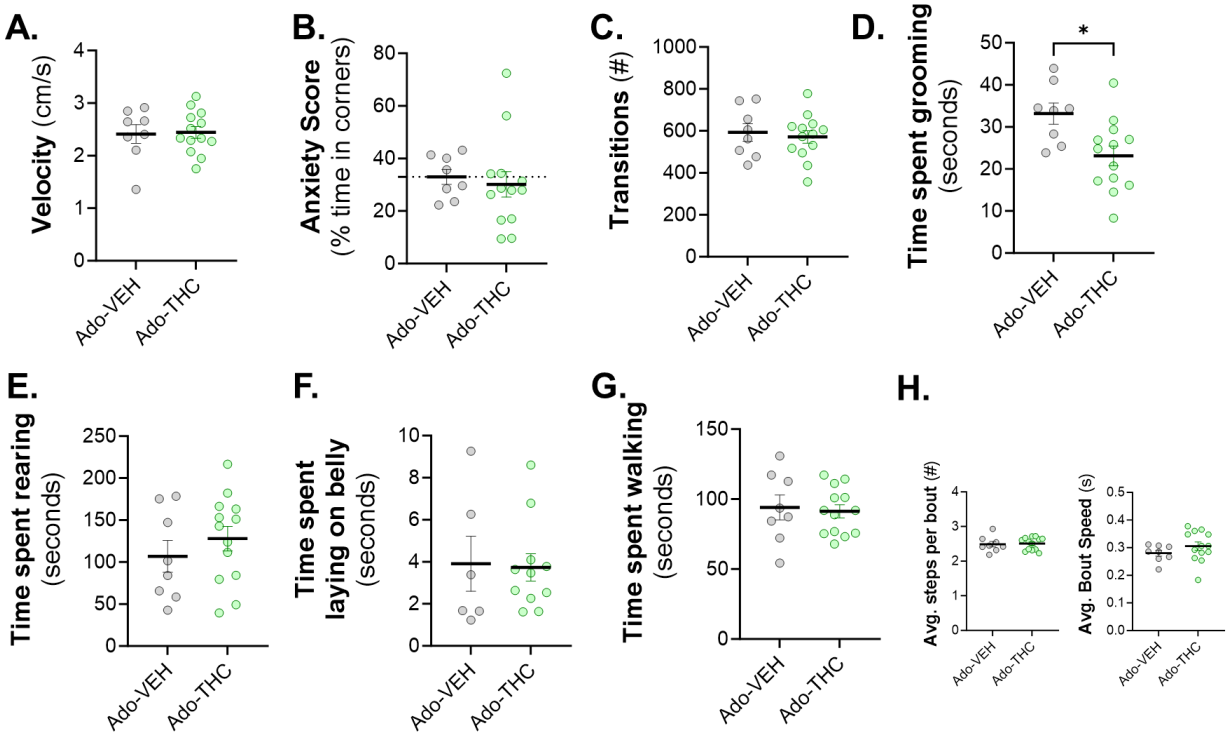

Figure 3.4: Adolescent THC exposure alone does not produce robust behavioral changes but does reduce grooming. All linear track behavioral data analyzed after first exposure into the linear track to determine natural behavioral changes after adolescent exposure. Data quantified were **A**) Average velocity during session, **B**) Anxiety score as measured by time spent in corners of the linear track, **C**) Transition frequency between core behaviors, **D**) Time spent grooming, **E**) Time spent rearing, **F**) Time spent laying on belly, **G**) Time spent walking, **H)** average steps and bout speed per each walk event. Student's T-test (*p<0.05).

adult behavioral responses.

Multiple behavior algorithms were combined to construct the full behavioral paradigm over the experimental session to track 4 common behavioral states of mice (**Figure 3.4D-G**, grooming, rearing, walking, and laying on belly) [205,374,375]. Further investigation into fine locomotor kinematics through key point analysis revealed no apparent kinematic deficits by adolescent exposure to THC (**Figure 3.4H, Supplementary Figure S3.7**).

Adolescent THC exposure does not overtly modify THC impaired behavior in adulthood.

Adolescent THC exposure revealed only a minor change on the persistence of grooming behaviors in adulthood. However, re-introduction of THC as a stimuli in adulthood could reveal a greater underlying modification in CB_1R expression or signaling. To perform this, mice were treated with THC at 5mg/kg *i.p.* and placed into the same linear track as in **Figure 3.3** one hour later. Animals that received either vehicle or THC gelatin in adolescence were placed into a linear track chamber as described in English et al for 15 minutes. Videos were recorded at 100 frames per second. Videos were then labeled for 30 key points of interest across a side and bottom up view of the animal at every frame using a SLEAP-designed algorithm. General metrics such as locomotion and speed were measured and revealed no THC-dependent effect from adolescent exposure. The x and y coordinates of these points were then analyzed to extract key features of each positional frame. These were then fed into a classification algorithm to identify core behavioral frequencies for walking, rearing, grooming, and laying on belly (**Figure 3.5**). No overt behavioral differences occurred in the frequency of the 4 behavioral metrics by THC exposure during adolescence (**Figure 3.5**). Walk events were isolated and locomotor kinematic features were calculated to determine if adolescent THC exposure modified basal locomotor balance. Across all metrics measured, no consistently observable kinematic feature was statistically modified by THC adolescent exposure (**Figure 3.5**). This result suggests no overt behavioral effects by adolescent THC exposure on THC's activity in an adult animal. This could further suggest that any modifications in CB_1R expression or signaling, if they occur, are minor enough to have intangible effects on relevant behaviors.

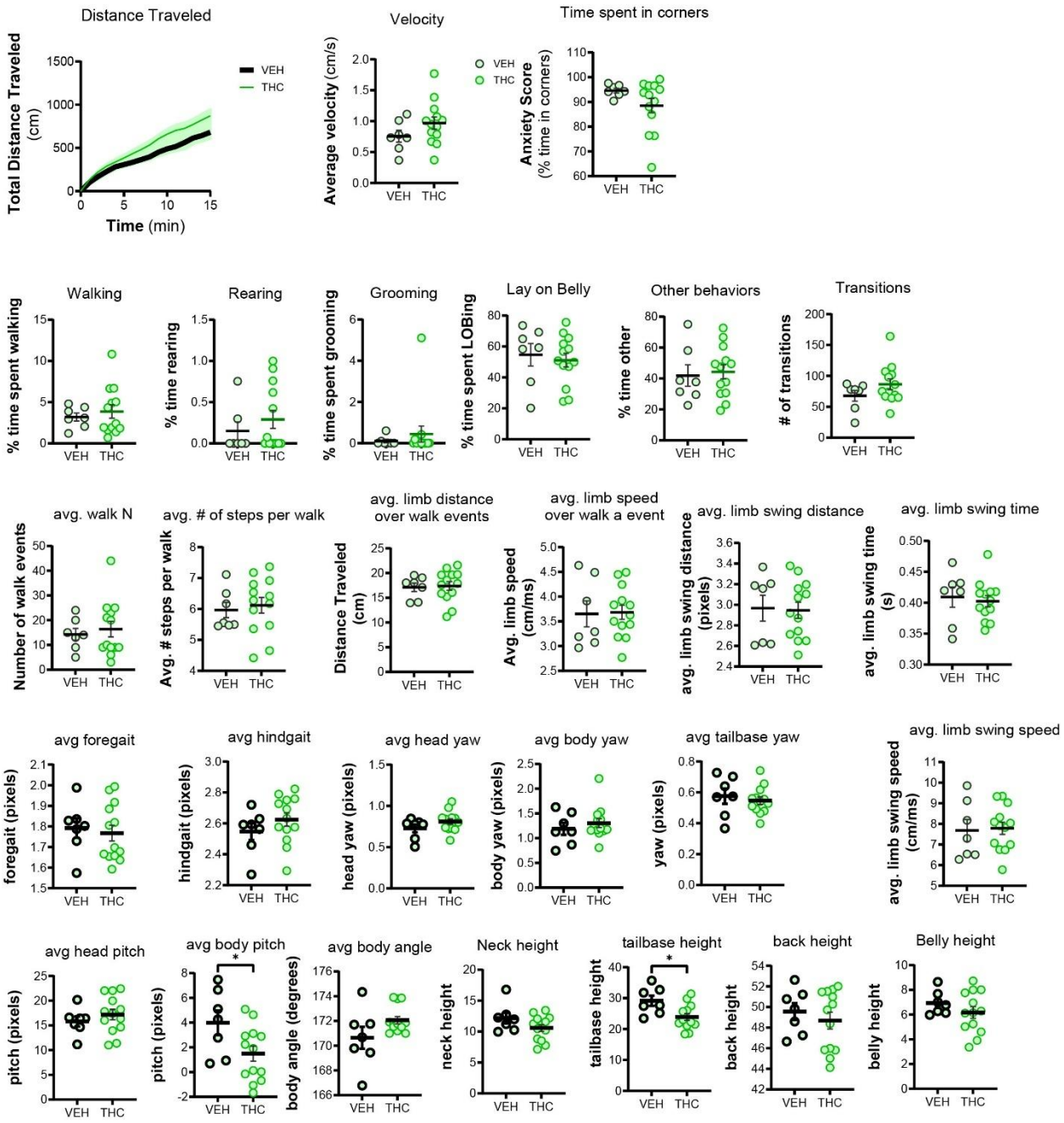

Figure 3.5: Adolescent THC exposure does not overtly modify THC impaired behavior in adulthood.

Series of metrics calculated after a 15 minute recording in the linear track after treatment with 5 mg/kg THC 1 hour prior. General metrics such as distance traveled, velocity and location tracking (anxiety score) were measured. Quantification of core behavioral frequencies fro walking, rearing, grooming, and laying on belly along with transition frequencies were quantified. Further locomotor kinematic metrics ranging from key point analyses such as forepaw gait width to stride metrics and positional metrics such as neck and belly height during walking.

Unsupervised Analysis of nuanced mouse behavior after adolescent THC exposure

revealed a novel behavioral signature inhibited by THC. Unsupervised deep learning algorithms have allowed researchers to drastically improve their capabilities to interpret biological phenomena, from microscopy to behavior. Here, we utilized an unsupervised analysis approach on videos of animal behavior analyzed in Figure 3 to identify nuanced behavioral effects that would otherwise go unnoticed by the train observer. Additional features were selected from the x and y coordinates of positions throughout the videos recorded. Features were then fed in a dimensionality reduction algorithm and plotted using a 2 dimensional tSNE (**Figure 3.6**). These tSNE plots were then analyzed with a watershed analysis to identify key potential clusters of behavior (**Supplementary Figure S3.6**). Vehicle exposure within the chamber and THC 5mg/kg treatment within the chamber identified a series of clusters primarily shared between both experimental groups. Interestingly, in the control group, where adults had first been exposed to the linear track, a cluster of behavior was segmented which occurred primarily in mice exposed to THC during adolescence (**Figure 3.6**). This behavior was identified by human eye to be similar to a scanning or upward sniffing behavior. This adolescent THC-dependent behavior suggests further that THC exposure during adolescence may induce nuanced and subtle effects that could have potential impacts in adulthood. Interestingly, this behavior was not observed when the animals were re introduced to the linear track chamber without a treatment, suggesting it may also be a novelty-related nuanced behavior difference (**supplementary Figure S3.6**). Further investigation into this behavior and its potential implications is further warranted.

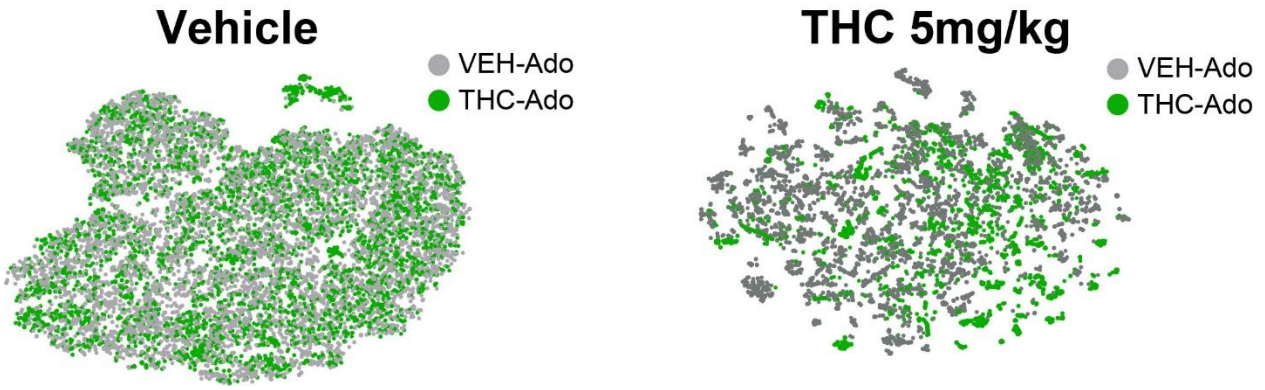

Figure 3.6: Unsupervised analysis of natural behavior identifies a novel behavior increased after adolescent exposure to THC.
Positional frames (90,000 frames per animal) were fed into an unsupervised algorithm to identify nuanced behavioral changes between experimental groups. Vehicle treated group represents the first exposure within the linear track as adult mice, with an identified novel behavior clustered away from the norm. THC treated mice developed islands of throughout dimensionality reduction.

3.3 DISCUSSION

The CB1 receptor plays a central role in neuronal development, yet the consequences of Cannabis exposure during adolescence, a critical period of brain maturation, remain poorly understood. A particularly compelling area of inquiry is the interaction between adolescent THC exposure and vulnerability to other drugs of abuse, especially opioids. The long-standing “gateway drug” theory, popularized through media and anti-drug campaigns, posits that early Cannabis use increases the likelihood of progression to more dangerous substances such as cocaine or heroin[376,377]. However, extensive human epidemiological data have challenged this idea, instead suggesting that shared underlying risk factors (e.g., predisposition to addiction) are more predictive of later drug use than Cannabis exposure itself[378,379]. Despite the lack of conclusive support for the gateway hypothesis, there is a biologically plausible and understudied intersection between the endocannabinoid (eCB) and opioid systems that could have therapeutic implications[380].

To clarify these relationships at the biological level, we administered THC-infused gelatin or vehicle during adolescence and assessed opioid-related behaviors in adulthood. Opioids remain among the most potent analgesics available, but their use is limited by their reinforcing euphoric effects and high addiction potential, particularly in the context of chronic pain. While we did not directly assess withdrawal responses, a key feature of

opioid dependence, we evaluated whether adolescent THC exposure modulates morphine's analgesic or rewarding properties.

Across multiple pain modalities, including acute thermal (tail flick and hot plate) and mechanical hypersensitivity (Von Frey), we found no effect of adolescent THC exposure on morphine's analgesic efficacy. We also conducted a conditioned place preference (CPP) test to examine whether adolescent THC exposure influenced morphine-associated reward learning. No significant differences were observed in male or female mice, although the relatively low baseline CPP responses suggest that environmental or methodological factors may have limited our ability to detect potential THC-related modulation[381,382].

Addiction vulnerability is also shaped by cognitive processes, particularly learning and memory, which are tightly linked to dopaminergic signaling and prediction error frameworks[383]. We therefore evaluated spatial learning and memory in the Barnes maze task over four days. Notably, female mice exposed to THC during adolescence exhibited impairments in memory recall, as reflected in longer latencies during the first trial of each day. While sex differences in Cannabis effects are rarely observed due to the broad distribution of cannabinoid receptors throughout the brain[384], prior studies have reported some sex-specific responses to THC exposure[385]. Our findings suggest that adolescent THC exposure may selectively impair memory retrieval in females, warranting further investigation using complementary paradigms such as operant or Pavlovian conditioning tasks.

Finally, we employed our custom linear track pose estimation system to assess naturalistic behavior after adolescent THC exposure. Two key time points were analyzed: initial exposure to the linear track (baseline behavior) and following acute THC administration in adulthood. No overt motor deficits were observed post-THC treatment, but more sophisticated analyses, such as unsupervised behavioral clustering—may uncover subtle or nuanced effects. One particularly intriguing behavioral phenotype emerged during baseline assessment: adolescent-THC-exposed mice showed a consistent, upward-facing investigative posture not present in controls. The specificity and recurrence of this behavior suggest it may reflect a previously unrecognized THC-induced modulation of exploratory or attentional processes. Integrating this finding with neural recordings could reveal the motivational or affective underpinnings of the altered posture and further illuminate how adolescent THC alters adult brain function and behavior. Future studies might vary the experimental context or add social, reward-based, or aversive stimuli within the linear track to expand on these results.

Chapter 4.

Deep learning dose prediction modelling of natural behavior reveals THC-impaired mPFC transients

4.1 INTRODUCTION

Emerging technologies provide a pathway to overcome these limitations and enable more sophisticated analyses. In recent years, computer vision tools like DeepLabCut and SLEAP have transformed behavioral research by allowing detailed tracking of individual points on animals during experiments, while other tools like MoSeq employ 3D imaging to capture broader behavioral patterns[158,159,162]. These methods have substantially improved our ability to analyze animal behavior, yet they remain underutilized and lack standardization across laboratories. In this manuscript, we utilize the SLEAP pose estimation algorithm developed in the Pereira laboratory within a linear track system that enables consistent visualization of mice side and bottom-up profiles. We take this technology and adapt machine learning classification algorithms and more intricate unsupervised AI approaches to decipher THC-impairment within this linear track system. Further, we apply a novel approach wherein THC-specific dose prediction algorithms are utilized to identify the “presented behavioral dose” of control and genetically manipulated mice during naturalistic behavioral recordings.

The increasing prevalence of using products that contain high-doses of THC resulting from their greater accessibility has raised significant concerns about the acute THC’s induced motor and behavioral impairment[386,387]. While THC’s ability to impair motor

behavior and cognition is well-recognized, our fundamental understanding of these effects is limited by the current experimental approaches to for their assessment[371,388]. Genetic and molecular approaches have established that THC modifies neuronal activity by activating cannabinoid 1 receptor (CB_1R). Rodent studies have demonstrated that high-dose THC significantly reduces locomotion by interacting with CB_1R expressed by glutamatergic excitatory neurons within the cortex and forebrain[106,321]. However, the cellular and molecular mechanisms underlying its impairing effect on finer locomotor behaviors, including how THC influences movement initiation and walking strides, remains unknown.

The medial prefrontal cortex (mPFC) plays a pivotal role in motor planning and preparation, earning it a reputation as a secondary motor cortex[389]. Notably, the mPFC expresses a higher density of CB_1R compared to the motor cortex, suggesting it may be a key target of THC's motor-impairing effects[390]. Despite this, the relationship between THC-induced mPFC activity and behavior is understudied. Specifically, prior studies investigating THC's effects on rodent behavior has largely relied on conventional methods that lack the precision and time resolution needed to uncover nuanced impairments. In parallel, advancements in endocannabinoid (eCB) biosensors $GRAB_{eCB2.0}$ now allows to measure the real time dynamics of the activity-dependent production of these highly lipophilic signaling molecules[109,110,112]. Thus, combining these innovative tools and experimental approaches offers the potential to precisely analyze THC's effects on both naturalistic behavior and neural dynamics at unprecedented resolution at the circuit level[110]. Here, we leveraged this integrative approach represents a significant step

forward in understanding the nuanced behavioral and neural consequences of THC exposure.

4.2 RESULTS

Figure 1: Machine learning behavioral tracking reveals the importance of mPFC activity during THC-impaired locomotor behavior

THC locomotor impairment is traditionally quantified in rodents by calculating total distance traveled or average velocity over a limited experimental session[181]. In rodents, this is a facet of the "tetrad" response that was developed as the industry standard for measuring the cannabimimetic effects of THC and other eCB-targeting drugs[181]. This behavioral analysis identifies a gross decrease in behavior but fails to identify the nuances of motor behavior when animals do move, let alone decipher naturalistic behavior. To investigate the nuances of this THC-impaired movement we implemented the pose estimation algorithm SLEAP (**Figure 4.1a**) in a linear track corridor with a mirror positioned below at a 45 deg angle to allow dual-view (side and bottom-up) of the animal from a single camera[164,391]. An AI pose estimation algorithm was developed with points on both views of the animal and trained from hand-labeled videos (N = 72; 51% male, 49% female) of WT behavior in the chamber after a two-day habituation paradigm (Supplemental Data). A secondary supervised classification (random forest) algorithm was developed to automatically classify 4 core behaviors (walking, rearing, grooming, and laying on belly (LOB)) with >95% accuracy (**Figure 4.1a, Supplementary Figure S4.1-S4.3, and S4.13**). WT male and female mice (N=179) were treated with a dose range of THC (0.1, 0.3, 1, 3, 5, 10, and 30 mg/kg) and recorded for 15 min, 1 h post-injection, within the linear track chamber. A behavioral ethogram snapshot (**Figure 4.1b**) exemplifies the high accuracy of behavioral identification over the course of the first 5 minutes of treated animals in the linear track. Quantification of time spent across the four

core supervised behaviors revealed a dose-dependent decrease in grooming (IC50 = 0.10 mg/kg), rearing (IC50 = 0.62 mg/kg), and walking (IC50 = 0.83 mg/kg) while a dose-dependent increase in laying on belly (EC50 = 1.23 mg/kg) (**Figure 4.1c**). To assess the nuances of THC impairment, classified walk events were isolated and points of interest from the side and bottom-up profile were measured to calculate motor kinematic effects (**Figure 4.1d, Supplementary Figure S4.14**). Motor kinematics such as the gait width is a known indicator of motor instability, being used as a metric in Parkinsonian and other motor-impaired behavioral models[392]. Of the kinematic effects calculated, the forepaw gait width and hind paw gait width (the average widths of the paws over the walk event) induced a THC dose-dependent increase, suggesting THC induces impaired motor kinematics in a dose-dependent manner (**Supplementary Figure S4.20, S4.22**). These kinematic metrics across all THC doses tested were standardized to their respective vehicle control and visualized to show the intensity of kinematic discoordination, as measured by our kinematic points of interest metrics (Figure 1e). Animals treated with 30 mg/kg were excluded due to the near zero frequency of walk events to quantify. No kinematic metrics were found to be sex-dependent (**Supplementary Figure S4.21**).

This linear track supervised classification identified robust dose-dependent effects in core behavioral presentation. Given this high accuracy, we hypothesized that constructing a non-linear regression model, trained from the large THC-treated dataset we've constructed, could identify the exact "presented dose" of an animal's behavior. In doing so, the regression model predicted fractional differences in "treated dose" based solely on behavior output, allowing us to identify potential changes in naturalistic behavior otherwise too nuanced for standard readouts. We trained two random forest regression

algorithms to identify general behavior and specifically kinematic behavior on a behavioral test dataset of mice treated with a range of THC doses (0.1-7 mg/kg) (**Figure 4.1f**). High doses over 7 mg/kg were excluded as they reduced the accuracy of the model, likely due to significant inactivity. The general behavior and kinematic models produced mean square errors (MSE) of 0.48 and 0.92, respectively, suggesting that general behavioral metrics are a more effective predictor of treated dose than kinematic metrics. To test the general model's predictions were valid, we used the model to identify a training dataset of animals treated with a range of THC and scrambled the features across doses, which eliminated the dose prediction accuracy for the general and kinematic models (**Figure 4.1g**). Both models displayed their nearest to ideal accuracy in the effective dose range between 2 and 5 mg/kg, matching the dynamic dose range seen in classical readouts of cannabimimetic behavior. These behavioral dose prediction models mark a first-in-class approach to deciphering animal behavior with modern AI approaches for behavioral research. The differential effectiveness of the General and Kinematic models supports the capabilities of this modelling approach to decipher naturalistic behaviors.

Figure 2: Unsupervised analysis of nuanced animal behavior predicts THC treatment dose.

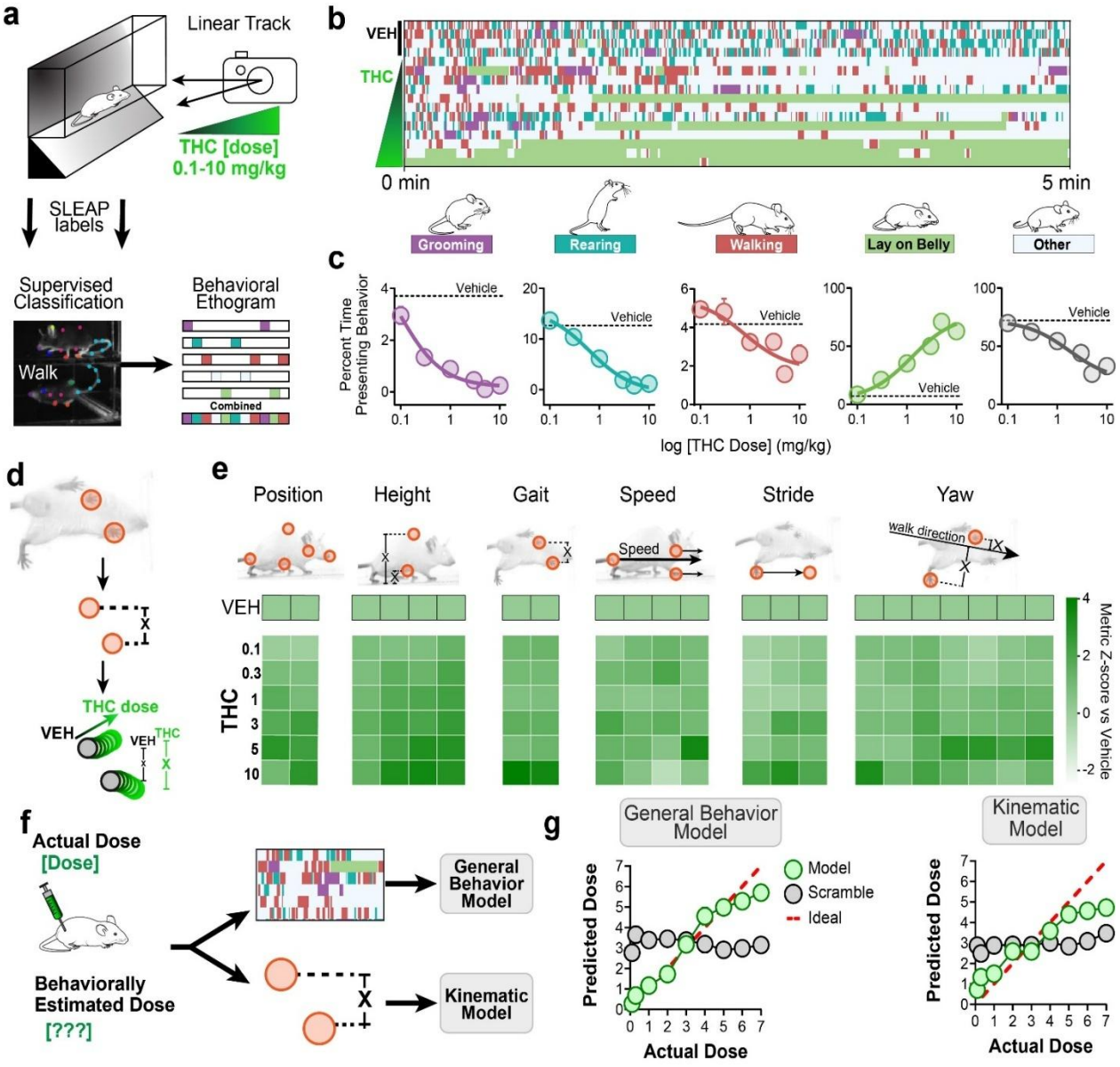

Figure 4.1: Machine learning behavioral tracking reveals importance of mPFC activity during THC-impaired locomotor behavior: a) Schematic of analysis pipeline for linear track recordings first analyzed with a supervised classification algorithm. **b)** Behavioral ethogram over 5 minutes in the linear track identifying core behaviors (grooming, rearing, walking, and laying on belly. Each row represented one mouse treated with vehicle or increasing doses of THC. **c)** THC dose-dependent response curves for percent time in four core behaviors as assessed by supervised classification algorithm. **d)** Schematic of kinematic analysis as calculated by POIs during walk events. **e)** Kinematic metrics during walk events after increasing doses of THC with Z-scores standardized to vehicle treatment. **f)** Schematic for training random forest regression models to predict THC dose from general behaviors and from kinematic features. **g)** Dose prediction accuracy of general and kinematic behavioral models against a test set (green) and a dataset scrambled across doses (grey) compared to an ideal prediction (red). Full experimental dataset: vehicle (N=179) and THC (0.1-10 mg/kg: N = 10-35 each). Random forest regressor training set: THC (0.1-5 mg/kg: N = 16-35 each).

Identifying animal behavior is a challenging task due to effort taken to label videos, the variety of animal behavior, and the inherent bias afforded to interpretation of behavior by scientists. To tackle this, researchers have successfully utilized multi-dimensional clustering approaches to identify behaviors without excessive human oversight[393]. Therefore, to further assess THC impairment behavior, we sought to employ cutting edge AI analysis frameworks with high dimensional clustering of naturalistic behavior. We sought to develop a model that could identify the nuanced changes in animal behavior that would otherwise go unnoticed or be too vague to characterize. To do this, we first

analyzed videos (N=176) with our supervised algorithm, where only behavioral frames

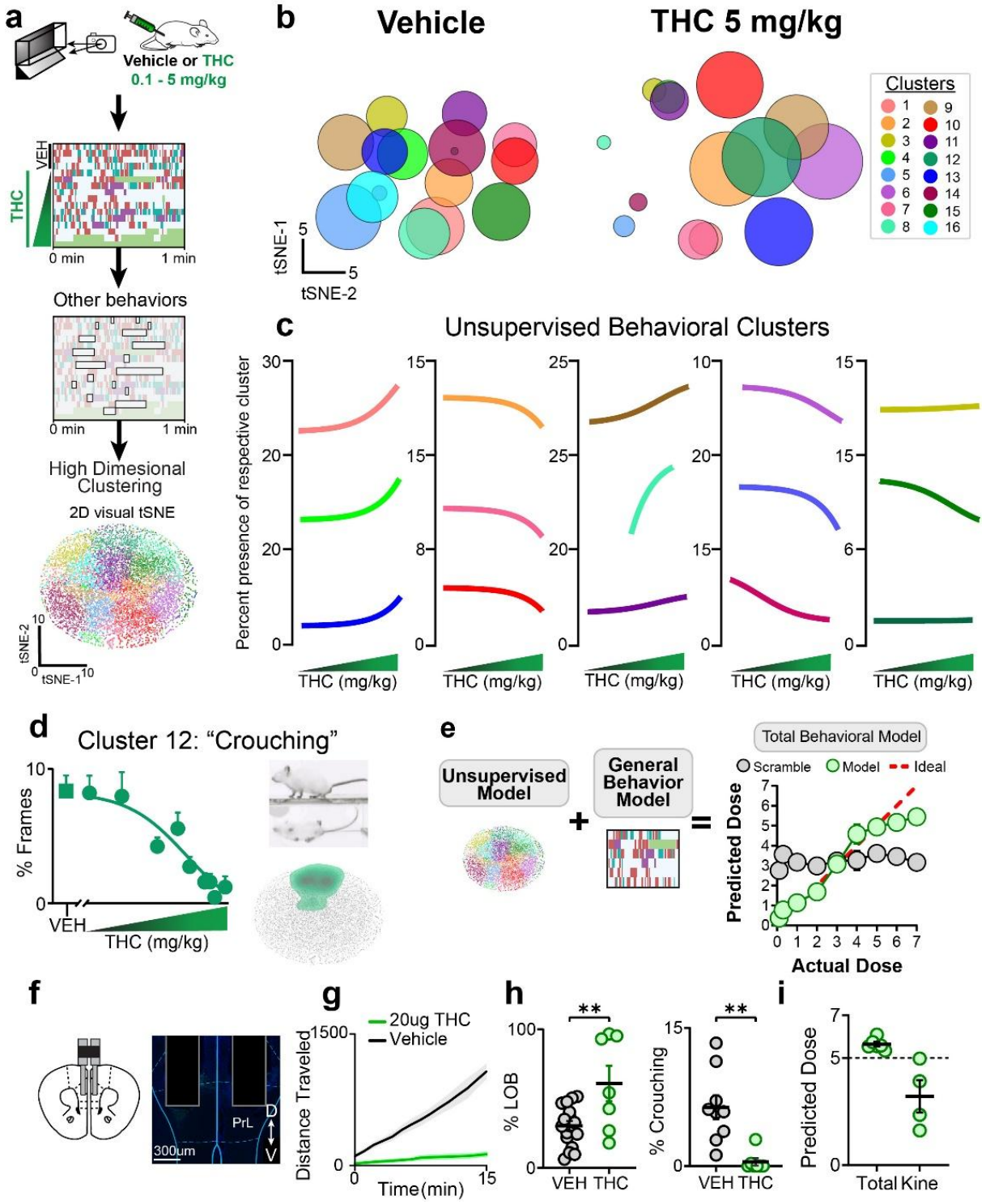

Figure 4.2: Unsupervised analysis of nuanced animal behavior predicts THC treatment dose: a) Schematic of analysis pipeline for extracting nuanced "other" frames to generate features for high dimensional Kmeans clustering (N=179, 53% male, 47% female, treatment range vehicle, 0.3, 0.1, 1, 2, 3, 4, 5, 6, 7, or 10 mg/k THC). 2 dimensional (2D) tSNE shows representative segmentation of clusters. **b)** Vehicle and 5 mg/kg THC treated behavioral frames with unsupervised cluster centroids sized to relative contribution for given treatment. **c)** THC dose-dependent effects of 16 identified clusters. **d)** Crouching "squatting" dose response curve along with a visual snapshot of behavior and 2D tSNE with cluster highlighted. **e)** Schematic for training of a random forest regressor for dose prediction by combining an unsupervised model using only nuanced behavioral clusters and the combination with the general model to train a total behavioral dose prediction model. **f)** bi-lateral intracranial infusion of high concentration THC (10 ug each side). **g)** Standard behavioral effect of total distance traveled in linear track. **h)** Percent laying on belly and expression of Crouching exemplifies THC effect. **i)** Application of total and kinematic dose prediction models reveals high dose THC behavioral presentation. N=7-15 Student's unpaired T-test (**p<0.01).

not classified as walking, rearing, grooming, or LOB were selected. These "other" behavioral frames represent the more nuanced naturalistic behaviors. From these frames, we calculated an optimized set of 29 positional features for each "other" frame which accounted for individual positions and relationships to temporally relevant frames (**Supplementary Figure S4.13**). Then, these features were used within a 29-dimensional Kmeans clustering framework to generate 16 nuanced behavioral clusters (**Figure 4.2a**). For visualization purposes, the same features and dataset were used as training data for a dimensionality reduction t-SNE plot with the 12 original clusters from the higher order clustering colored. This visualization revealed good separation in a 2-D space, given the core relationships were distinguished in 27 more dimensions. Clusters were assessed for their prevalence across dose, sex, and time throughout the experimental datasets with a human-in-the-loop surveyance of examples frames for relevance (**Supplementary Figure S14.5**). THC dose-response curves for each cluster's relative expression per "other" contributions were plotted (**Figure 4.2b**), revealing a dynamic range of behaviors that decreased, increased, or were unaffected by THC. Crouching (post-hoc named

“squatting”) was isolated due to its robust THC-dependent decreased (**Figure 4.2c**). The dose response curve was plotted as percentage of time animals spent performing that cluster relative to the total percentage of “other” frames. An example image for Crouching, and its location within the 2-D tSNE plot is shown for visualization purposes (**Figure 4.2c**). The ability of our clustering methodology to identify robustly THC-dependent, naturalistic behaviors that would otherwise go unnoticed, emphasizes the impressive capabilities of black box classification for behavioral datasets.

To identify whether these nuanced behavioral metrics could effectively predict THC “presented dose”, we constructed another random forest regressor algorithm from features constructed solely in regard to the cluster distributions within the THC training dataset. These features were then combined with the general features to train one “total behavior” dose prediction model (MSE: 0.4711) which can be used to effectively a holistic THC-treated dose (**Figure 4.1e**). The model accuracy plot emphasized the high accuracy of this finalized Total behavioral model, showcasing the value of these nuances behaviors to improve the deciphering of behavior. To test the effectiveness of this model in animals treated with THC in a non-systemic manner, we infused THC directly into the mPFC and recorded behavior in the linear track. We implanted a bi-lateral cannula into the prelimbic cortex region (AP = 1.8, DV = -2.0, ML = 0.4) of the mPFC and infused either vehicle (1:1:1:17, ethanol:DMSO:Cremophor:50 mg/kg BSA in saline) or 20 ug THC (10 ug in 1 nl, each side) bi-laterally (**Figure 4.2g**)[394]. Local THC infusion caused robust hypolocomotion as distance traveled, a standard metric of cannabimimetic behavior. Additionally, our supervised classification algorithm identified a significant increase in time spent LOB and a significant decrease in the relative behavioral presentation of Crouching

behavior after THC infusion. Dose prediction with our Total and Kinematic models was applied to assess the general THC behavior and the specific locomotor THC-impairment effects. Interestingly, the kinematic only model revealed an even lower predicted dose compared to WT animals treated with a similar THC dose, suggesting a role for mPFC activity in THC's locomotor impairing effects.

Figure 3: Activity monitoring of the mPFC during walk behavior reveals THC modifies E/I balance correlated with locomotor impairment.

The mPFC is often referred to as the "the secondary motor cortex" and is involved in the coordination of nuanced locomotor behavior[395]. To investigate the potential neural relationship between the mPFC and THC's locomotor impairing effects, we expressed GCaMP6f in WT male and female mice with a CAMKII promoter to select for pyramidal neurons, within the mPFC (**Figure 4.3a**). WT-GCaMP6f-expressing (AAV-DJ-CaMKIIa-GCaMP6f) mice were exposed for 15 min in the linear track with fiber photometric recordings taken 1 hour after treatment of either vehicle or 5 mg/kg THC. Neural activity during the session was timelocked to the supervised behavioral classes, revealing a robust THC-dependent response at the initiation of a walk event (**Figure 4.3b**). Averaging neural signal across all walk events reveals an increase in signal seconds before the walk

before

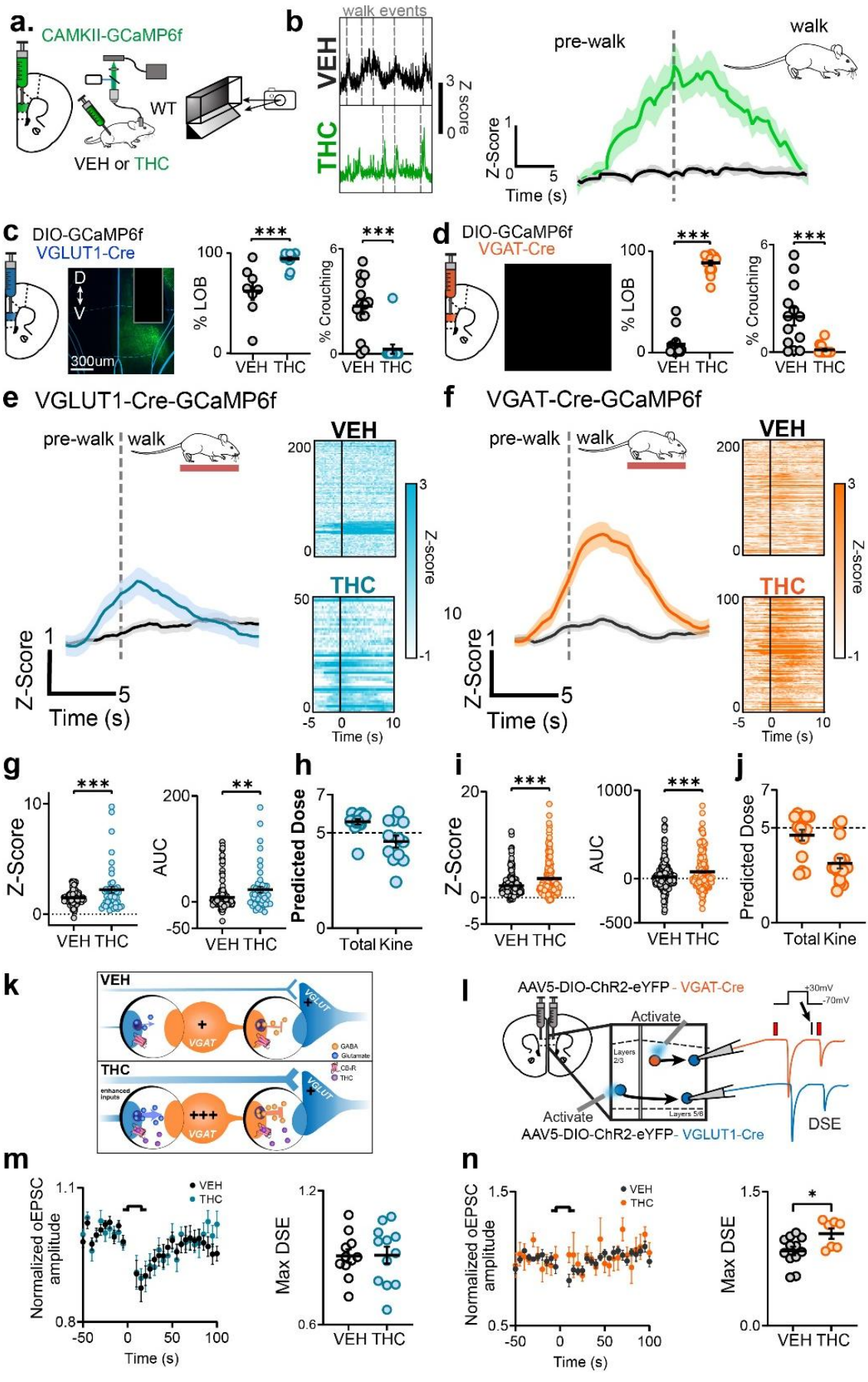
a.
CAMKII-GCaMP6f
WT
VEH or THC
b
walk events
VEH
THC
Z score
pre-walk
walk
Z-Score
Time (s)
c
DIO-GCaMP6f
VGLUT1-Cre
D
V
300um
% LOB
% Crouching
VEH THC
d
DIO-GCaMP6f
VGAT-Cre
e
VGLUT1-Cre-GCaMP6f
pre-walk
walk
VEH
THC
Z-score
Z-Score
Time (s)
f
VGAT-Cre-GCaMP6f
g
Z-Score
AUC
VEH THC
h
Predicted Dose
Total Kine
i
j
k
VEH
THC
VGAT
VGLUT
GABA
Glutamate
CB-R
THC
enhanced inputs
l
AAV5-DIO-ChR2-eYFP - VGAT-Cre
Activate
+30mV
-70mV
Layers 2/3
Layers 5/6
DSE
AAV5-DIO-ChR2-eYFP- VGLUT1-Cre
m
Normalized oEPSC amplitude
Time (s)
Max DSE
n

Figure 4.3: Activity monitoring of the mPFC during walk behavior reveals THC modifies E/I balance correlated with locomotor impairment: a) mPFC injection of AAV-DJ-CAMKIIa-GCaMP6f for fiber photometry linear track experimentation. **b)** Time locked CAMKII neural signal at walk initiation during WT-CAMKII behavior. Averaged walk event traces after vehicle or 5 mg/kg THC treatment. **c-d)** Schematic and histology for Cre-dependent expression of GCaMP6f in VGLUT1-GCaMP6f (**a**) and VGAT-GCaMP6f (**b**) mice. Percent LOB and Crouching behavioral presentation in vehicle and 5 mg/kg THC-treated VGLUT-GCaMP6f (**c**) and VGAT-GCaMP6f (**d**) mice. **e-f)** Fiber photometry signal of glutamatergic (**e**) and GABAergic (**f**) neuron activity at walk initiation and subsequent heatmaps for each walk event. **g)** Peak Z-score and AUC over neural recordings of walk events in VGLUT-GCaMP6f mice. **h)** Application of Total and Kinematic dose prediction models to VGLUT-GCaMP6f behavior during fiber photometry recording. **i)** Peak Z-score and AUC over neural recordings of walk events in VGAT-GCaMP6f mice. **j)** Application of Total and Kinematic dose prediction models to VGAT-GCaMP6f behavior during fiber photometry recording. **k)** Cartoon schematic of mPFC neurons after THC administration during walk behavior. **l)** Schematic of electrophysiological reocrdings in VGLUT1-Cre and VGAT-Cre mice. **m-n)** Normalized oEPSC amplitude after optogenetic stimulation with and without THC bath reveals enhanced maximum DSE in VGAT neurons. N=8-14 Student's unpaired T-test (**p<0.01, ***p<0.001).

returning to baseline. This response seems to only occur in animals treated with higher doses of THC (peak Z-score = 2.733 +/- 0.03) and not in vehicle-treated animals (peak Z-score = 0.237 +/- 0.01). These neural findings alongside the motor kinematic effects induced by THC support the mPFC's involvement as a key factor in modifying THC-impairment.

Pyramidal glutamatergic excitatory and GABAergic inhibitory neurons within the mPFC represent a processing neuronal hub that orchestrates signals throughout the brain to mediate nuanced drug effects[396-398]. This balance of excitation and inhibition (E/I) is a critical feature of the cortex where this balance is relevant to a myriad of disease states[325,399,400]. To selectively disentangle the E/I balance, we first performed an *in situ* hybridization technique, RNAscope and identified that CAMKIIa mRNA is expressed in both GABAergic and glutamatergic neurons within the mPFC (**Supplementary Figure S4.4**). Thus, we sought to assess the activity of both populations by utilizing genetically

modified VGLUT1-Cre and VGAT-Cre injected with an AAV5-DJ-EF1a-DIO-GCaMP6f and implanted with an optic fiber above the mPFC (550nl: AP = 1.8, DV = -2.0, ML = 0.4) (Figure 3c-d). Animals were treated with either vehicle or THC (5 mg/kg) and left to explore within the linear track for 15 min. Percent LOB and presentation of behavioral Crouching show robust cannabimimetic responses by 5 mg/kg THC in fiber photometry animals (**Figure 4.3c-d**). Isolated walk events were classified with our supervised algorithm and these time stamps were used to time lock the initiation of walking to neural signal. This revealed a THC-dependent increase of glutamatergic activity only in THC-treated animals which began increasing 3-4 sec before movement onset and reached a peak Z-score of 1.53 +/- 0.02 (**Figure 4.3e**). Vehicle activity showed a small increase in activity due to a lone mouse with significant activity. GABAergic activity was similarly time locked to walk initiation, revealing a significant increase in inhibitory activity (**Figure 4.3f**). This transient, like excitatory glutamatergic neurons, began increasing in THC-treated mice 3-4 sec prior to walk initiation but reached a much higher peak activity (Z-score = 2.51 +/- 0.03). Vehicle treated animals were found to express minor transient activity associated with movement onset with a peak Z-score of 0.815 +/- 0.01. THC-treated VGLUT1 and VGAT animals showed significantly higher peak Z-scores and AUC during walk events compared to vehicle (**Figure 4.3g and 4.3i**). Total dose prediction of fiber photometry animals predicts for VGLUT1-Cre and VGAT-Cre mice at 5.58 +/- 0.14 and 4.62 +/- 0.29 mg/kg, respectively showing that fiber implantation and patch cable during experiment does not obscure THC's gross cannabimimetic effects (**Figure 4.3h and 4.3j**). Alternatively, the kinematic dose prediction model predicted 4.54 +/- 0.31 and 3.13 +/- 0.27 mg/kg for VGLUT-Cre and VGAT-Cre fiber photometry animals, respectively, well

below the 5 mg/kg treatment. This drop in predicted kinematic dose supports that the act of having the patch cable attached to the fiber implant during the experiment modifies the animal's natural walking behavior. These findings suggest that the GABAergic transient is indicative of walk stability, wherein the greater activity of GABAergic activity, the more stable to walk event is, suggesting this shift in E/I balance could be modified directly by THC to impair motor behavior, or could be a compensatory response to correct for impaired movement (**Figure 4.3k**). To further investigate this cannabinoid-mediated shift mPFC E/I balance, depolarized suppression of excitation (DSE) was measured from glutamatergic and GABAergic neurons. VGLUT1-Cre and VGAT-Cre mice were injected with the light-activated opsin ChannelRhodopsin (AAV5-DIO-ChR2-eYFP) into the contralateral or ipsilateral mPFC, respectively to where *ex vivo* electrophysiological recordings were performed (**Figure 4.3l**). Tissue were bath treated for 1 hour in either vehicle solution or 20 uM THC. Maximum DSE measurements revealed a THC-dependent increase in maximum DSE from local glutamatergic neurons onto GABAergic neurons (**Figure 4.3m-n, Supplementary Figure S4.18**). These findings further support the THC-dependent shift from excitation to inhibition within the mPFC.

Figure 4: Manipulation of mPFC activity reveals GABAergic neuronal activity important in mediating fine locomotor behavior during THC-impaired locomotion.

We sought to determine if differential mPFC neuronal population activities mediate THC-impaired locomotion by modifying motor stability. To test this, we deleted CB_1R expression from select neuronal population within the mPFC using an AAV-CRISPR-Cas9 virus approach[401]. A CB_1R CRISPR (AAV1-FLEX-saCas9-sgCnr1) or ROSA control (AA1V-FLEX-saCas9sgROSA26) virus was injected bi-laterally into the mPFC (400nl: AP

= 1.8, DV = -2.0, ML = +/- 0.4) (**Figure 4.4a**). Validation of the CRISPR was performed with FACS, revealing a ~30% deletion via insertion/deletion modifications of the Cnr1 gene (**Supplementary Figure S4.17**). Further validation of gene deletion was tested for each animal post-hoc with *in situ* hybridization to identify mRNA knockdown (**Supplementary Figure S4.16**). Four weeks later, a uni-lateral injection of GCaMP6f into the right hemisphere at the same coordinates to visualize changes in neural activity of VGLUT1-Cre and VGAT-Cre animals during behavior. Percent LOB and behavioral Crouching presentation were modified consistently with vehicle and 5 mg/kg THC treatment except for vehicle-treated VGLUT1-Cre-ROSA mice who displayed behavioral Crouching to a small degree (**Figure 4.4b-c**). Neural recordings of both neuronal

populations were recorded and time locked to walk behavior in ROSA and CRISPR mice

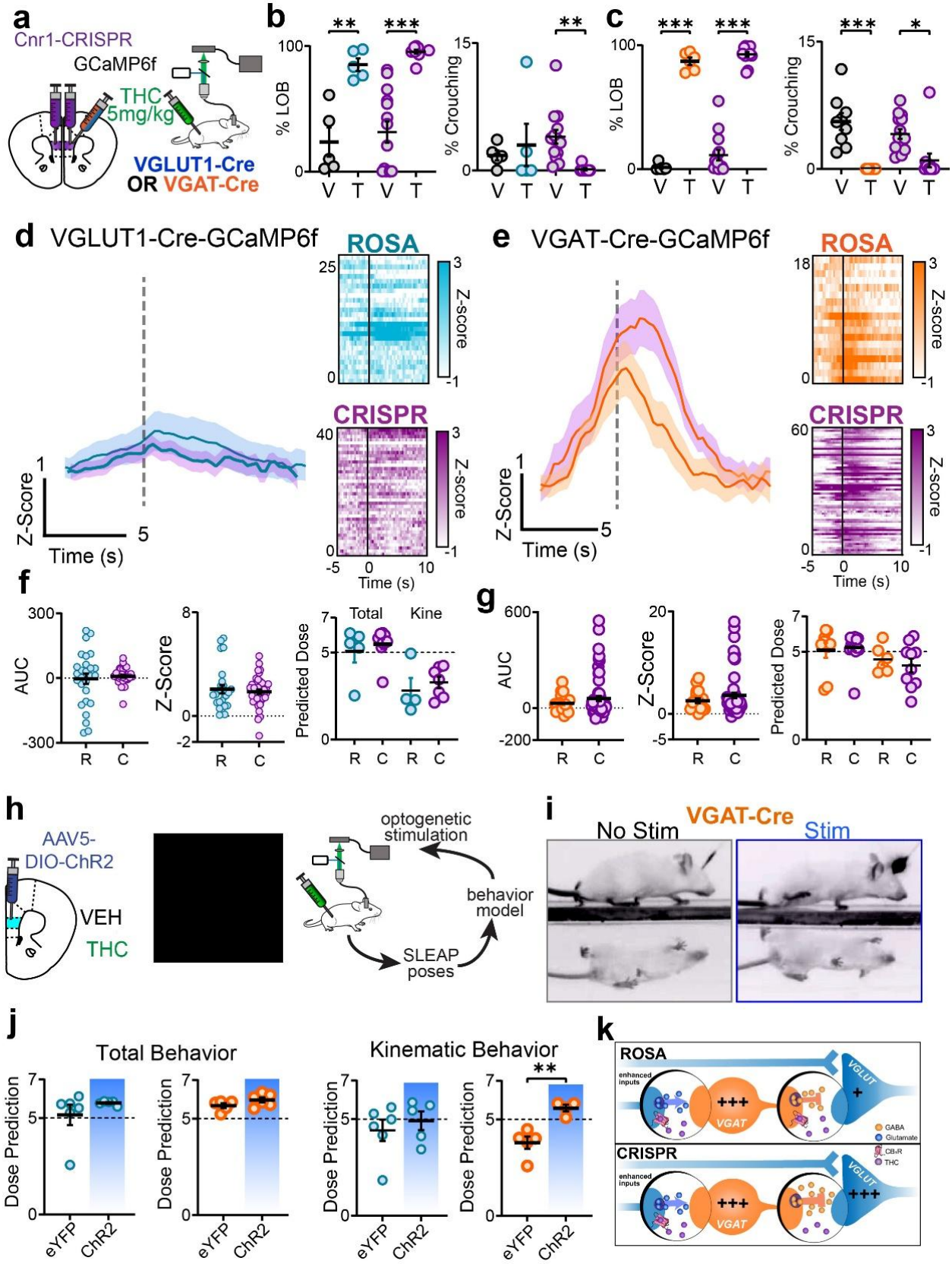

Figure 4.4: Manipulation of mPFC activity reveals GABAergic neuronal activity important in mediating fine locomotor behavior during THC-impaired locomotion: a) Schematic of bi-lateral AAV-SaCas9-Cnr1 (or ROSA control) injection and unilateral DIO-GCaMP6f injection with fiber implantation for fiber photometry. **b-c)** Percent laying on belly and Crouching behavioral presentation across ROSA and CRISPR animals treated with vehicle or THC in VGLUT1-Cre (**b**) or VGAT-Cre (**c**) animals. **d-e)** Fiber photometry signal at walk initiation of VGLU1-Cre (**d**) and VGAT-Cre (**e**) ROSA (blue and orange) and CRISPR-expressing (purple) mice, shown as calculated Z-score. **f)** Quantification of AUC and peak Z-score for each walk event in VGLUT1-Cre ROSA (blue, R) and CRISPR (purple, C) recordings. Dose prediction of Rosa and CRISPR VGLUT1-Cre animals with total and kinematic models. **g)** Same as **f**, except with VGAT-Cre ROSA (orange, R) and CRISPR (purple, C) animals. **h)** Schematic for closed-loop optogenetic experimentation within the linear track chamber. **i)** Image of VGAT-ChR2 mouse walk behavior with and without stimulation within video, mid-stride. **j)** Total and Kinematic dose prediction of eYFP and ChR2 animals. Kinematic dose prediction only applied to walk events where stimulation occurred. **k)** Cartoon Schematic of mPFC after THC administration. N=5-10 Student's unpaired T-tests, (*p<0.05, **p<0.01, ***p<0.001).

after treatment with 5 mg/kg THC (**Figure 4.4d-e**). Here, glutamatergic activity was unaffected by CRISPR-deletion of CB_1R while GABAergic neurons increased slightly. Quantification of AUC and peak Z-score did not reveal a statistically significant modification by CB_1R CRISPR-deletion in either glutamatergic or GABAergic neurons but did show a trend in the GABAergic neurons. Further, application of the total and kinematic behavioral dose prediction models did not reveal a CRISPR-deletion modification in total or walk-specific behavioral presentation. The CRISPR knock out of the CB_1R in GABAergic neurons showed trending effects on neural activity and behavior that support eCB involvement in the critical E/I balance of the mPFC. Given the relatively low knock out of the Cnr1 gene (~30%) and the trending effects, more aggressive intervention would likely be necessary to see robust changes if CB_1R was directly modifying THC's effects. To test this hypothesis, we sought to modify neuronal activity during locomotor events within the linear track system. Therefore, VGLUT1-Cre and VGAT-Cre mice were injected

to express the light-sensitive opsin Channel Rhodopsin (AAV5-EF1a-DIO-ChR2-eYFP) or an eYFP control (AAV5-EF1a-DIO-eYFP) uni-laterally and implanted with an optic fiber 4 weeks prior to testing. A major challenge in investigating naturalistic behavior is the unpredictability of such behavioral events, and the timing of triggering optogenetic stimulations. To this end, we constructed a closed loop optogenetic system within our linear track chamber which records behavior in real time (**Figure 4.4h**). We constructed a new supervised classification algorithm trained solely to identify walk and "pre-walk" events described as the 30 ms immediately prior to walk initiation (**Supplementary Figure S4.13**). Here, we set parameters to trigger optogenetic ramping stimulation when the pre-walk model identified that a walk behavior was about to occur. Optogenetic stimulation was triggered at 5 Hz (5 ms pulse width and 10 s inter-trial-interval [**ITI**]) to avoid potential confounding overstimulation effects that might be seen with high frequencies[402]. A ramping of stimulation frequency was also utilized to mimic the natural increase in activity shown from fiber photometric recordings in **Figures 4.3 and 4.4**. These identified walk events were also identified by eye to orchestrate a further "human-in-the-loop" validation to ensure the model was not mis-identifying preparatory/lunging behavior that did not develop into a full walk. VGLUT1-Cre and VGAT-Cre mice were treated with vehicle or 5 mg/kg THC and tested using the closed-loop system. General behavioral metrics of percent time LOB were quantified and followed expected trends (**Figure 4.4i**). Crouching behavioral presentation was also quantified and followed expected trends except for vehicle-treated VGAT-ChR2 animals who did not display the behavior (**Figure 4.4j-k**). Total behavioral dose prediction of THC 5 mg/kg treatment conditions for eYFP and ChR2 was compared to reveal that local stimulation of

glutamatergic or GABAergic neurons did not overtly modify general THC-induced behavioral effects. Before applying the kinematic dose prediction model, all stimulated walk events were separated from those where stimulation did not occur due to either events occuring during the ITI or them being missed by the closed-loop system. Kinematic dose prediction of stimulated walk events revealed a significant increase in the predicted dose after enhancing the activity of GABAergic neurons. This less stable motor behavior caused by increasing GABAergic neuron activity implicates the GABA neurons of the mPFC as mediators of nuanced locomotor impairing effects by THC. Further, it supports that a greater knockout of CB_1R expression in mPFC GABA neurons could have caused an even greater increase in neural activity and therefore more robustly modify kinematic behavior. The potential of the CB_1R on GABAergic neurons to modify THC impairment suggests an action of endocannabinoids from some neuronal population is enhanced after the treatment of THC.

Figure 5: THC treatment induces 2-AG release from mPFC glutamatergic neurons during walking.

The most abundant eCB, 2-arachidonyl glycerol (**2-AG**), is produced post-synaptically and acts in a retrograde manner to activate pre-synaptic CB_1R as a full agonist[63]. In Figure 4, we showed a potential link between the CB_1R on GABAergic neurons and THC's locomotor impairing effects, but the source of this cannabinoid activity is unclear. GABAergic neurons in the mPFC project onto glutamatergic pyramidal neurons in layers 4/5 but also onto other GABAergic neuronal subpopulations. To decipher this cannabinoid activity, we operationalized the $GRAB_{eCB2.0}$ (**Figure 4.5a**). $GRAB_{eCB2.0}$ driven by the synapsin promoter (AAV1-hSyn-GRAB-eCB2.0) was injected into the mPFC of WT mice

(550nl: AP = 1.8, DV = -2.0, ML = 0.4), and implanted with an optic fiber to see general expression of the sensor is all neuron types. WT-GRAB$_{eCB2.0}$ mice were treated with vehicle, 1, 5, and 10 mg/kg 1 h before recording eCB signal in the linear track. Percent LOB and behavioral Crouching presentation showed a dose-dependent decrease and increase, respectively. Analysis of walk behavior revealed a similar dose-dependent transient at movement initiation with the most prominent activity being apparent at 5 and 10 mg/kg (**Figure 4.5c**). The trace also presented transients of spiking activity that corresponded with identified initiation of walk events as seen with glutamatergic and GABAergic neurons. Total AUC and peak Z-score quantification of the tested doses reveal a dose-dependent effect with significance at 5 and 10 mg/kg compared to vehicle confirms the significant THC-dependent cannabinoid response during walk behavior (**Figure 4.5d**). Additionally, predicted doses by the total and kinematic prediction models follow the same behavior trajectory as LOB (Figure 5e). The GRAB$_{eCB2.0}$ sensor is responsive to all cannabinoids and therefore difficult to decipher which ligands may be causing this transient[109-111].

To further understand the capabilities of the sensor, we performed *in vitro* validation studies in culture following Singh et al by testing the endogenous ligand 2-AG and the exogenous ligand THC (**Supplementary Figure S4.19**). Our results support the sensor's sensitivity to measure 2-AG and THC activation as a full and partial agonist, respectively. THC showed about 25% maximal response compared to 2-AG, a previously published relationship at the native CB_1R[403]. Therefore, to decipher *in vivo* which ligand is the cannabinoid triggering activity during walking, we performed a long, 100 min session to visualize the eCB dynamics before and after THC administration. The GRAB$_{eCB2.0}$ signal

was measured in a representative mouse which displayed an increase in total activity starting immediately after THC injection and continuing until the end of the session (**Figure 4.5f**). To disentangle 2-AG's potential role, we pre-treated mice 1 h prior with the diacylglycerol lipase (DAGL, 2-AG synthesizing enzyme) inhibitor DO34 (30 mg/kg) prior to the experimental Vehicle (black) or THC (maroon) exposure (**Figure 4.5f**). We detected a pronounced increase in $GRAB_{eCB2.0}$ signal resulting from THC's accumulation in the brain over the entire session. This time course aligns with previously published literature on the circulating THC levels in the brain[201,404]. DO34 pretreatment eliminated the $GRAB_{eCB2.0}$ transient increases in signal throughout the session without modifying the overall THC induced increase in $GRAB_{eCB2.0}$ signal or walk behavior (**Supplementary Figure S4.5-4.9**). To further confirm the involvement of 2-AG, we employed the monoacylglycerol lipase (MAGL, 2-AG metabolizing enzyme) inhibitor JZL-184 (10 mg/kg). As expected, JZL-184 blocked 2-AG hydrolysis causing the accumulation of 2-AG and increase in $GRAB_{eCB2.0}$ signal at every walk event (**Figure 4.5g**). The average of these treatments to walk events showed that transient activity increased similarly to THC-treated mice but continued to increase rather than return to baseline. JZL-184 alone also caused an increase in time spent LOB, matching previous publications where it has been found to decrease total movement wherein DO34's increase in LOB does not match previous results where it has been expected to not alter movement[405,406] (**Figure 4.5h**). Behavioral Crouching presentation was unexpectedly unaltered by any pharmacological treatment, with each treatment arm showing high variability. Total behavioral dose prediction did not reveal any significant changes whereas kinematic dose prediction did reveal a DO34-mediated effect on motor stability (**Figure 4.5i**). DO34 alone significantly

increased the kinematic predicted dose compared to vehicle and DO34 with THC barely modified that predicted dose (trending lower than THC alone). DO34 has not been published on before showing any robust modification in kinematic or fine locomotor behavior but enhancement of 2-AG has been shown to modify fine motor behavior, supporting these results[407,408]. Altogether, the pharmacological treatments emphasize these cannabinoid transients are 2-AG release events are THC-dependent during walk behaviors.

$GRAB_{eCB2.0}$ is expressed in all neurons; it does not help us distinguish which neuronal population is producing the 2-AG. Given the importance of GABAergic activity in this THC-dependent motor phenomena, we anticipated glutamatergic neurons to be the primary 2-AG production neurons. To test this, we sought to stimulate the neuronal populations directly and record eCB activity in vivo. We prepared VGLUT1-Cre and VGAT-Cre animals with a Cre-dependent uni-lateral injection of the red-shifted opsin Chrimson (AAV5-FLEX-ChrimsonR-td-Tomato) and the same $GRAB_{eCB2.0}$ virus to express in all neurons along with an optic fiber (**Figure 4.5j**). Animals were pre-treated with vehicle or 5 mg/kg THC 1 h prior to stimulating and then recording eCB activity at 20 Hz (5 ms pulse width, 90 s ITI) not in the linear track. The glutamatergic neurons responded dramatically while the GABAergic neurons showed no response in either treatment case (**Figure 4.5k-l**). THC treatment decreased maximal $GRAB_{eCB2.0}$ signal, suggesting a competitive partial antagonism of the endogenous 2-AG being released. This decrease in activity matches what would be the reduced activity of the native CB_1R on GABAergic neurons leading to a shift in the E/I balance with enhanced GABA activation seen in **Figure 4.3f** which, when

heightened further, worsens the kinematic locomotor impairment induced by THC as shown in **Figure 4.4k**.

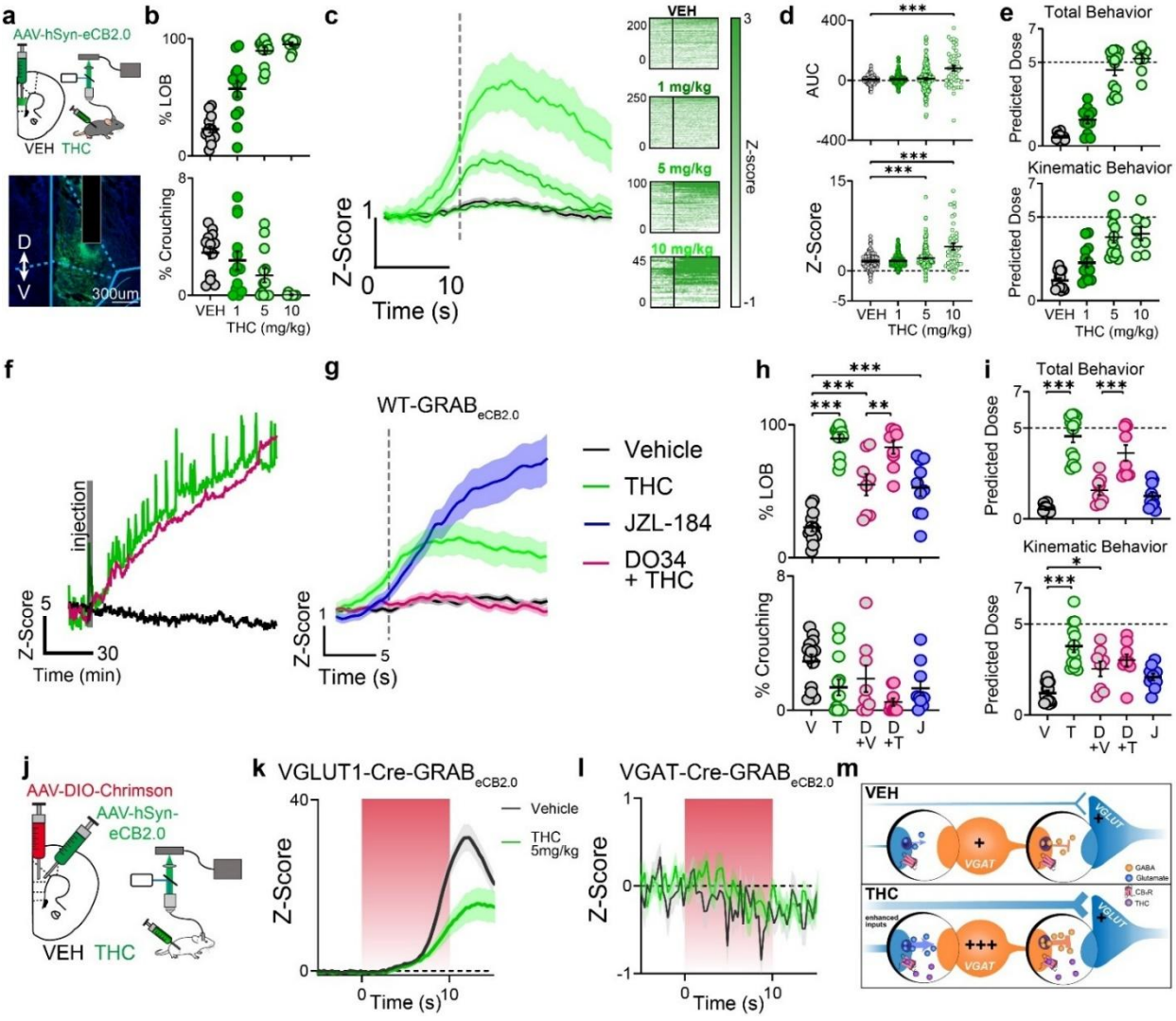

<u>Figure 4.5:</u> THC treatment induces 2-AG release from mPFC glutamatergic neurons during walking: a) Schematic for $GRAB_{eCB2.0}$ expression and histology with optic fiber placement. **b)** Percent laying on belly and Crouching behavioral presentation across WT- $GRAB_{eCB2.0}$ animals treated with vehicle, 1, 5, or 10 mg/kg. **c)** Fiber photometry signal of $GRAB_{eCB2.0}$ signal in WT mice treated with vehicle or a range of THC doses (1, 5, or 10 mg/kg) at walk initiation with their subsequent heatmaps for each walk event. **d)** AUC and peak Z-score from walk events. **e)** Dose prediction with total and kinematic behavioral models for vehicle and THC-treated animals. **f)** Example fiber photometry trace of a 100 min experimental session with 10 mg/kg THC (green) injected systemically at 10 min. Animal was pre-treated 1 h before with 30 mg/kg DO34 before systemic injection of vehicle (black) or 5 mg/kg THC (purple). **g)** Fiber photometry signal at walk initiation after treatment with vehicle (black), 5 mg/kg THC (green), 30 mg/kg DO34 then 5 mg/kg THC (purple), or 20 mg/kg JZL-184 (maroon). **h)** Percent LOB and Crouching behavioral presentation across all eCB pharmacological treatments of vehicle (V), 10 mg/kg THC (T), 30 mg/kg DO34 + vehicle (D+V), 30 mg/kg DO34 + 10 mg/kg THC (D+T), and 20 mg/kg JZL-184 (J). **i)** Dose prediction of all eCB pharmacological treatments with total and kinematic behavioral models. **j)** Schematic for Cre-dependent expression of red-shifted opsin, Chrimson, and $GRAB_{eCB2.0}$ with hSyn promoter in WT mice. **k-l)** $GRAB_{eCB2.0}$ signal in vehicle and THC-treated (5 mg/kg) mice during 10 s, 20Hz stimulation (5 ms pulse width) stimulation. **m)** Cartoon schematic of local mPFC circuitry during walk behavior of THC treated mice. N=8-16 Student's unpaired T-tests, (**p<0.01, ***p<0.001).

4.3 DISCUSSION

In this paper, we utilized computer vision AI models to identify naturalistic kinematic motor and fine nuanced behaviors otherwise missed by standard experimental approaches. From these, we calculated key features to predict the dose of THC an animal was treated with to standardize a generalizable “total” and a locomotor “kinematic” behavioral effect. Neural recordings revealed that THC modifies GABAergic inhibitory and glutamatergic excitatory neuronal balance to by differentially enhancing neuronal signaling during natural walking behavior. Manipulation of the GABAergic mPFC neurons during walk behavior modified the predicted locomotor dose, showing the direct control of the mPFC in modifying fine locomotor control in a THC-impaired state. We then, used the novel $GRAB_{eCB2.0}$ sensor to identify that THC treatment induces endogenous 2-AG release during walk behavior, a novel link between exogenous THC and endocannabinoids.

The dose prediction analyses displayed here display the potential of insights that behavioral analysis can contribute with supported AI analysis. Predicting a therapeutic dose based on behavior alone was effectively showcased in this publication as a method to standardize treatment and to identify the nuanced impacts of neural manipulations on behavior. This use of random forest nonlinear regression algorithms marks the first combination of cutting-edge AI/ML algorithms to decipher animal behavior. Further development of this algorithm would potentially improve with the introduction of a transitory element capable of more thoroughly accounting for the temporal relationship between frames of poses. Applications such as MoSeq have implemented similar functions and incorporations of a Recurrent Neural Network of Hidden Markov Model could account for these behavioral transitions[162]. Additional efforts to predict behavioral

progression throughout an experiment could further be enhanced with the implementation of techniques utilized by the gene sequencing fields as showcased in Patton et al, 2023[409]. Further development with a larger dataset of videos across doses trained with a personalized deep learning model such as a variational auto-encoder could identify significantly more valuable insights of behavioral features. The applications of such behavioral analysis could extend to the research efforts of neurological, behavioral-presenting diseases and to the development of neurologic therapeutics.

In vivo animal models introduce an inherent variability in experimentation that provides significant difficulty to many behavioral experiments. The dose prediction algorithms employed here provide the most holistic approach thus far to decipher behavior induced by an exogenous substance. Even within the variability of our developed models, we were able to identify nuanced changes in general and nuanced behavior over a range of doses. These applications set the groundwork for further applications in the drug development pipeline for screening novel therapeutics and potentially the human clinical space where behavioral identification is even more complex. Specifically for Cannabis, identification of “impairment” has been an increasing issue and concern for physicians, law makers, and law enforcement. Cannabis availability and concentration has been increasing over the last decade with now 24 states in the U.S approved for recreational use while the average concentration of market products has reached a percentage over 4-fold greater than what was available in the 1980s[386]. These increased parameters have led to increased hospitalizations, complications with other therapeutics, and increases in motor vehicle crashes without a clear understanding of how to identify an Cannabis-impaired state. THC deposits in fat tissue throughout the body and is detectable up to 24 h after use for a first

time user and over a week after use for a chronic user, making detection of a THC-impaired state highly variable and subjective. Applications to effectively identify impaired human behavior with a standardized method is one step closer to reality with a validation in animals.

Exogenous neurological drugs, such as THC, modify synapses throughout the brain, causing a shift to a differential state space compared to a non-drugged state. This differential state allows new perspectives on biological relationships otherwise invisible to standard experimentation. In this paper, we showed that in a THC-impaired state, the mPFC GABAergic interneurons mediate fine locomotor behavior, a relationship that has not been clearly defined. However, given the integrative capacity of the mPFC as a central processing hub, there is more to understand regarding the input and subsequent outputs from the mPFC that results in the modified locomotor behavior. Deciphering these neuronal populations introduces a further novel avenue to decipher how a THC-impaired state modifies the communication networks within the brain. Further investigation into these neuronal populations may be critically important to disentangle THC's impairing effects from its therapeutically valuable effects, which has been a focus of some dedicated research.

THC acts directly on the native CB_1R as a partial agonist where, at high concentrations and activity, it can compete with the endogenous cannabinoids 2-AG and AEA. This relationship between an exogenous drug and its endogenous competitive ligand(s) is a complex one that is uniquely difficult to understand. In this paper, we revealed a relationship between THC and the endogenous cannabinoid ligand 2-AG that was behaviorally dependent wherein 2-AG release was enhanced after THC-impaired

behavior. Before access to the $GRAB_{eCB2.0}$ sensor, identifying cannabinoid activity in a tight temporal window was limited to mass spectrometry or other temporally deficient techniques. This new high-resolution technology developed by the Li lab allowed us to investigate this dynamic relationship, marking another significant advancement in the field of cannabinoid pharmacology research.

Chapter 5.

Conclusions and Discussion

The Cannabis plant has been an important ecological entity throughout human history. Its commonality through different cultures and communities allowed it to leave a significant mark impacting literary minds and supporting burgeoning infrastructure, among others. However, the innate curiosity of scientific minds to understand Cannabis has been met with significant barriers throughout history. Specifically for Cannabis, this has been made difficult due to political/administrative intervention, the natural lipophilicity of cannabinoid compounds, and the subjectivity of nuanced effects[57]. Despite this, humanity's innate scientific intrigue and curiosity luckily has continued to drive innovation further, unlocking the capabilities to research Cannabis and its effects on the human body. Over the past several decades, technological innovations such as LC-MS/MS and the recent $GRAB_{eCB2.0}$ have allowed researchers to circumnavigate the high lipophilicity of cannabinoid compounds. For my doctoral thesis I have developed innovative tools and applied them to provide objectivity to previously complex and convoluted effects of THC. This was done in three major ways outlined here: 1) the development of a gelatin formulation to promote the consistent self-administration of THC to more accurately imitate the biologically relevant consumption pattern of humans; 2) investigating and discovering nuanced behavioral effects of adolescent THC exposure otherwise missed by standard experimental procedures; and 3) Developing standardized dose prediction AI algorithms to identify THC dosage from either the collective nuanced behavioral changes or the specific locomotor kinematic modifications, uncovering a THC-dependent shift in cortical excitation/inhibition activity during walking behavior.

Gelatin formulation for THC self-administration

I found that dissolving THC in the fat-rich, sweetened dark chocolate drink (Ensure) was easily capable of suspending the THC evenly after gelatinization. This gelatin was palatable enough that rodents consumed it quickly enough to induce robust cannabimimetic responses as measured by body temperature, general locomotion, and analgesia. This is the first example, published in eLife, of high dose Cannabinoid oral self-administration of THC in rodents, who are typically avoidant due to the flavor and smell of the THC oil[410,411]. This formulation is valuable for acute treatments of THC that wish to model oral ingestion without the aversive side effects induced by standard oral gavage procedures[412].

Other laboratories have developed oral formulations for THC or other cannabinoids but such as a peanut butter mixture, but none were developed specifically for acute administration[413]. Development of a standardized formulation opens opportunities for further experimentation by scientists. Specifically, there has been significant increases in the rates of accidental THC/edible exposure in emergency rooms (especially for children) in the U.S. since the wave of recreational legalizations[414]. This means that models of this “accidental” exposure can be effectively modelled in rodents to understand the potential outlying risks/impacts. Further valuable applications of the gelatin formulation could be applied to discrimination tasks with the introduction of other flavors of the Ensure drink. It would not be advisable to modify the concentration of the Ensure by dilution. When I tested this, it did modify the texture of the gelatin.

Interestingly, I found that rodents consumed less of a vehicle or THC gelatin the day following high dose consumption. This effect is likely to an associative aversion to the

gelatin after a negative affective experience during the “accidental” exposure. It’s been shown previously that rodents present a small but consistent aversion to THC in the conditioned place preference test[410].

Another interesting finding is that animals consumed less total gelatin the higher the dose got. This was due in part to the effects hitting sooner, causing the animals to lay down and reduce their consumption. Another potential reason is that the animals could sense the effects of the THC as they happened. If this were true, the THC gelatin concentration could be tuned along with the animals trained to test if mice are capable of self-titrating THC. This could be relevant for therapeutic purposes as THC is commonly taken for a multitude of ailments, many of which are commonly self-dosed by lay consumers[415]. Mimicking this behavior in an experimental environment could be valuable to investigating THC’s therapeutic impacts and the addictive nature of its consumption which can develop into Cannabis Use Disorder (CUD)[165]. This is increasingly relevant as CUD prevalence has spiked with enhanced access to high concentration products recreationally available[293].

Adolescent THC exposure modifies nuanced behaviors

The native CB1 receptor is important in neuronal development, but the effects of Cannabis exposure during key periods of adolescence is poorly understood. A uniquely interesting topic surrounding Cannabis’ potential impact on the addiction potential other drugs of abuse, specifically opioids. For decades now, an old scientific theory surrounding the “gateway effect” as percolated in popular culture, and weaponized in the war on drugs[377]. The basis for the theory surrounds usage of THC/Cannabis as a predominantly non-dangerous illicit substance will promote the usage of stronger substances such as

cocaine and opioids like heroin. Most evidence shows that human users that eventually continued to use harder" drugs did so due to an underlying factor such addiction potential risk rather than an instigated THC primer[416]. However, there is a unique and poorly understood relationship between the endocannabinoid system and the opioid system which could prove promising for therapeutic value[380]. Therefore, with ambiguity surrounding the biological level effects of the eCB system and opioid system, I exposed mice to vehicle or THC gelatin during adolescence and measured key metrics of opioid addiction potential in adulthood.

Opioids are the strongest and most effective analgesics developed. The greatest danger of course being the euphoric effects of opioids which promote the highly addictive intake. This is heightened for patients in chronic pain where opioids are highly effective at reducing pain, helping aid to a euphoric and positive affective state. Withdrawal symptoms are also an incredibly important factor in addiction potential for a compound, which are high for opioids, but we did not test this factor. We found that adolescent THC exposure did not modify morphine's analgesic properties across multiple pain modalities: analgesia (tail flick test and hot plate assay) and hyperalgesia (Von Frey assay). We also performed a conditioned place preference (CPP) test where morphine was paired to one side to determine if adolescent THC exposure modified morphine seeking. There was no observable effect in male or female mice. Although, the baseline morphine CPP results were low compared to previously published results, suggesting an adolescent THC effect could potentially have been observed given different and more optimized environments[190]. Another key underlying aspect of addiction potential is learning behavior, since dopamine prediction error patterns in learned behavior are believed to be

the core feature of associative drug seeking[417]. To this end, I tested animals in the Barnes Maze task over four days. This assay investigated consolidation, recall, and long-term memory over the course of four days. Interestingly, female mice did show an adolescent THC-dependent response where their recall was modified as shown by their trial one for each day being worse compared to mice that didn't receive THC in adolescence. Cannabis has rarely shown to have sex-dependent effects, due in part to the robust expression throughout the brain. However, there have been instances where THC sex dependence was shown to have increased CB_1R desensitization, a potential underlying cause of trends in female capacity for Cannabis abuse[418]. Here, it suggests that adolescent THC sex-dependently modifies some underlying aspect of memory recall. A further investigation into the extent of this finding through other learning paradigms, such as operant conditioning tasks and Pavlovian conditioning could potentially prove interesting.

Going further to understanding the potential underlying neural mechanisms modified by adolescent THC, we had proposed, but ran out of time to perform, a series of tests to investigate neural mechanisms directly. This would be done by exposing adolescent mice to vehicle or THC gelatin during adolescence (as done previously) and the injecting an AAV-GCaMP virus to a specific brain region at PND42 (7 weeks of age) along with an optic fiber. Then, when the animals were of age on PND70, they would have had 3 weeks to effectively express GCaMP in given neurons (be that GABAergic, dopaminergic, etc). Then, you could perform learning and memory behaviors while recording the neurons to determine if any robust effects were observed in changes in neural signal. This would likely be performed in the Hippocampus first as a central and

core memory/learning brain region. The mPFC as a central and complex brain region would also be of interest. Really, any brain region within the mesocorticolimbic system would provide a good basis for these studies. Further usage with a pose estimation system as outlined in Chapter 4 could then be utilized during the conditioning memory/learning tasks to further identify granular and nuanced behavioral changes that may correspond with modified signal.

Lastly, we utilized the linear track pose estimation system to track natural behavior after vehicle or THC adolescent exposure. The two primary recordings occurred when the animals were first placed in the linear track to determine if any native natural behavior was modified alone in untreated mice while the second was post THC treatment to determine if the motor deficits by THC were impacted by adolescent exposure. No overt behavioral change was observed after THC administration, but further investigation with unsupervised high dimensional clustering could potentially reveal nuanced differences after adolescent THC treatment. There was an anomalous behavior noticed in the first trial within the linear track. This behavior appeared to be a staunch upward investigation-like behavior that appeared clearly in THC-adolescent animals but not in vehicle-adolescent animals. The extent by which this behavior could insist or support further expansion of THC adolescent exposure impacts on adult behavior and brain activity. Further analysis of this specific behavior alongside neural recordings could be valuable to understand what motivation may underlie the behavioral position that is being modified. Additionally, placing animals within the LT with a different experimental procedure could potentially reveal a more specific relationship between this position and the potential biological impact on a greater scale that is relevant for THC exposure.

mPFC cortical activity modified during THC impaired locomotion

It's well established that THC induces hypolocomotion in a dose-dependent way as a one of the four key metrics as part of the tetrad response[181]. Additionally, in humans, it's been shown that THC/Cannabis reduces reaction time and fine motor skills. Beyond this, there is a poor understanding into the nuances of THC's fine motor impairment effects, let alone the underlying neural mechanisms modified to modify those behaviors. I utilized and constructed AI/ML algorithms to classify/identify walking behaviors and then further key point analysis to quantify different locomotor kinematic metrics. Then, I built an unsupervised analysis algorithm to cluster poses of the animals treated with varying doses of THC which were then clustered in high dimensions to segment behavioral trends. Features were then calculated to train THC dose prediction algorithms built off the backbone of random forest regressors capable of identifying THC treatment dose based on general behaviors and specifically motor behavior. These models mark a novel application of modern AI deep learning to decipher animal behavior. Their creation allows for a standardized and centralized quantification of behavioral metrics that automatically accounts for statistical multiplicity.

The applicability of this novel model type has potential to extend to other related fields. Applications of dose prediction models could be built for other drugs of abuse such as cocaine, opioids, and amphetamines. This would allow a standardization across experimentation to further investigate modified neural mechanisms similar to what I performed. It would not be that difficult given the robust effects of these compounds. I ran a test with data shown in **Supplementary Figure S4.23** of animals treated with increasing doses of cocaine which did cause robust and potentially nuanced behavioral deficits.

Opioids would be quite easy to identify given the robust Straub tail effect seen in mice. Additionally, it could be applied in time-dependent experiments such as operant conditioning to investigate how drug-seeking is modified. The logic would be to build models that are drug dependent but more specifically designed for drug-dependent behavior when introduced to different stimuli.

The greatest extended application of the dose prediction algorithms would be to identify anomalous behaviors that indicate toxicological side effects seen during the drug development process. With a large enough dataset of control-treated mice, mice treated with drugs that did not produce negative side effects, and drugs that produced known side effects, you could effectively build a model to identify anomalous toxic behaviors for drug screening. This approach would need a large dataset to succeed and would need an expansion on the deep learning models employed here. The most effective and logical next step, given the current AI architecture available would be to employ variational auto-encoders which can more effectively look at series of data, such as the temporal relationship across frames. This touches on an aspect our current model identified but was not capable of fully describing. In **Supplementary Figure S4.24**, we found that transitions of clustered behaviors over animals treated with THC or Vehicle tended to follow one another, going back and forth. This trends of behaviors suggests a flipping frequency of clustered positions that collectively define a more holistic “behavior”. Application of an integrated variational auto encoder could help account for some of this temporal variability. Alternatively, you could employ a similar approach to language learning models (LLM) which look for trends and sequences of data. Finally, the models could be developed for specific stereotypical behaviors to help quantify metrics of

nuanced grooming behaviors, for example, which are valuable for some studies such as pruritic.

The other aspect of this project was investigating the neural modifications of the mPFC during motor behavior. The mPFC has been considered the “pre-motor” cortex as it is shown to be involved in motor planning (shown by ablation studies)[395]. And for the purposes of investigating THC, it has a dense expression of the CB1 receptor, even more so than the primary motor cortex[325,390]. The primary findings of this study were focused around the excitation/inhibition dynamic shift during motor behavior after THC administration. A shift in E/I within the cortex has been a common descriptor used to understand the misbalance of the cortical structures which have highly conserved distributions of excitatory glutamatergic pyramidal neurons and local GABAergic inhibitory neurons known to cause direct and indirect (disinhibition) inhibitory drive[325]. The functions of the cortex to be processing hubs is a complex and intricate network of neuron communication platforms that will take time and technological advancements, such as those utilized in 2-photon imaging with prism lenses[419]. Here, we do show a heightened increase in GABAergic inhibitory activity compared to glutamatergic activity. For this to occur, the GABAergic neurons would need to be stimulated by some upstream excitatory neurons. This effect could, in part, arise from contralateral glutamatergic activity, but it is also likely to come from other sensorimotor brain regions involved in incorporating sense notations. Given that the animals walk infrequently, and activity is only heightened when THC-impaired walk events occur, it stands to reason that something different in terms of neural activity as a whole may be occuring upstream, and downstream, of the observed mPFC activity. This is further supported by the nature of THC, an exogenous and activity-

independent compound which enhances the threshold that would need to be met for a neural signal to be transmitted. Therefore, a sensory signal, or some other enhanced signal would need to overcome this to trigger the walk event. The alternative argument can be made, however, given that we did not test if auditory queues or motivated behavioral stimuli would induce a similar THC-dependent increase in activity. Separating motivation versus natural behavior in this regard would be too nuanced to describe in mice.

Altogether, the described processing of the mPFC to plan motor initiations supported by the increases in GABAergic and glutamatergic activity increasing well before the initiation of walking. This does call into question what downstream partners may be impacted by the enhanced glutamatergic pyramidal neurons that actually leave the mPFC. Most likely, these neurons communicate with those in the direct and indirect pathways to balance a motor initiation event. Given the animals do not present transient activity outside of the walk events, it suggests the mPFC is not the decision point in the go/no-go for THC-impaired locomotion, unsurprisingly. Given the cortex's relationship to the direct and indirect pathways, it would be likely that the dorsal striatum would be the most immediate target. I did one test in animals where optic fibers were placed in the Nucleus Accumbens (NAc) along with a synapsin promoted $GRAB_{eCB2.0}$. This one test revealed in **Figure 4.9** a similar increase in endocannabinoid activity that was shown in the mPFC. Differently, however, this activity continued to increase after the walk event, persisting over 10 seconds post-walk initiation. This does suggest an alternate activity pattern of downstream neurons.

To continue this investigation, it would be prudent to effectively probe both D1 and D2 neuronal populations (to select for direct/indirect neurons) in the striatum in vehicle and THC treated animals to record neural activity. Distinguishing anatomically between the dorsal lateral striatum (DLS) and the dorsal medial striatum (DMS) would prove interesting to hopefully decipher underlying habitual versus “motivational” as these brain regions have been associated with these types of behavior, respectively[420,421]. Another interesting brain region to investigate downstream would be the Globus Pallidus (GP). The GP is involved in the direct pathway motor initiation but also has one of the densest expressions of the native CB1 receptor of any brain region, making it a prime target for THC’s activity[390]. This touches on another interesting effect observed in this study, observing the enhanced eCB signaling (specifically 2-AG) during THC-induced motor behavior. The direct cause for this increase in 2-AG is due highly in part to the enhanced activity of neuronal depolarization which triggers eCB production. That being said, Chrimson stimulation in **Figure 4.5** showed that only the glutamatergic neurons robustly released eCB production whereas activation of GABAergic neurons did not. In this case, the proportionate small increase in glutamatergic neurons compared to the robust increase in 2-AG does not align, suggesting a greater potential underlying force by THC to directly, or indirectly, adjust endogenous cannabinoids production. This result of course would be exciting, but difficult to put in the greater context where THC has not been shown to robust modify eCB metabolic pathways, except in the case of competition at the CB_1R during high stimulation events[108]. The specific dissection of 2-AG versus AEA activity was not directly tested with the $GRAB_{eCB2.0}$. I did evaluate and test 2-AG and AEA specific biosensors developed from the lab of Yulong Li shown in **Figure 4.12**. The results were

not promising, suggesting significant restructuring in the design of the biosensor for selectivity. Although further development of highly selective biosensors for any compound, including THC, could greatly improve our technical capabilities to decipher acute biological activity.

Together, this series of studies sets the groundwork for follow-up studies both in the specific field and with applications to other related fields. This work also prompts the potential functionality and application to industrial uses for the sake of drug development. The research collected during this PhD concludes a significant body of work which both extends the academic fields' understanding of THC's effects on behavior and the brain and builds upon innovations with potential applications to advance other fields.

Chapter 6.

Materials and Methods

Animal Studies

Animal studies followed the guidelines established by AAALAC and were approved by IACUC of the University of Washington. Male and female C57BL/6J mice ranging from 8-14 weeks of age were used. Animals were housed with sibling littermates and were provided with standard chow and water, *ad libitum,* and without any additional environmental enrichment. Investigators were not blinded to experimental exposure conditions throughout assays due to the noticeable behavioral effects measured in response to THC. Animal procedures were approved by the Institutional Animal Care and Use Committee of the University of Washington and conform to the guidelines on the care and use of animals by the National Institutes of Health.

Pharmacological Agents

Animals received THC (0.1, 0.3, 1, 3, 5, 10, and 30 mg/kg) and SR141716 (**SR1**, 1 mg/kg) *i.p.* or were exposed to THC suspended in gelatin. THC and SR141716 (SR1) were provided by the National Institute of Drugs abuse Drug Supply Program (Bethesda, MD). THC in ethanol (50 mg/ml) was either added to gelatin mixtures (CTR or Ensure®) or prepared for *i.p.* injection. For *i.p.* injection, both THC (0.1, 0.3, 1, 3, 5, 10, and 30 mg/kg) and SR1 (1mg/kg) were dissolved in 95% ethanol and then vortexed thoroughly with equal volume Cremophor and finally dissolved in sterile saline to reach a final 1:1:18 solution consisting of ethanol:cremophor:saline.

Gelatin formulation

Control gelatin (CTR-gel): Deionized water (100 mL) was warmed to 40°C and stirred at a constant rate. 2.5 g of Polycal™ sugar and 3.85 g of Knox™ Gelatin were added and the mixture was maintained at a temperature below 43°C. The mixture was removed from heat, and THC (50 mg/ml in ethanol) was added to reach a concentration of 0.3, 1, 2, or 4 mg/15 ml. An equal volume of ethanol was added to vehicle gelatin (<1% total volume). Gelatin was poured into plastic cups ranging from 2-10 ml and set into a 4°C fridge to solidify overnight.

Ensure gelatin (E-gel): Chocolate-flavored Ensure™ (100 ml) was warmed to 40°C and stirred at a constant rate. 3.85 g of Knox™ Gelatin were added and the mixture was maintained at a temperature below 43°C. The mixture was removed from heat and THC (50 mg/15 ml ethanol) was added to reach a concentration of 1, 2, 5, or 10 mg/15 ml. At the 10 mg/15 ml concentration, ethanol was evaporated off to 50% volume before being added to the mixture to reduce total alcohol concentration below 1%. An equal volume of ethanol was added to vehicle gelatin (<1% total volume). Gelatin was poured into plastic cups ranging from 2-10 ml and set into a 4°C fridge to solidify overnight. Mice were always exposed to more gelatin than they could consume, smaller volumes were used to conserve THC.

Acute gelatin access: Animals were first habituated to gelatin by receiving an excess of gelatin in their home cage the day before the first timed access. On the first day of access, mice were placed into a home cage-like environment equipped with a vehicle gelatin cup that was stabilized to the cage. Behavior was recorded during the consumption window via an overhead camera. On the second day of access, animals were placed into the same gelatin access cage with either a vehicle or THC gelatin cup. Animals experienced

either a triad of behaviors (open field, tail flick, and body temperature) measured immediately preceding and following the consumption window or an acoustic startle trial immediately following consumption. On the third and final day of access animals were placed into the same cage with a vehicle gelatin cup. For all gelatin access days, gelatin cups and animals were weighed before and after the consumption window. Access to gelatin during the consumption window was limited to either 1 or 2 h after which the animals were removed and returned to their home cage.

Triad of Cannabimimetic behaviors

Hypolocomotion, hypothermia, and analgesia were measured 1 h post-*i.p.* injection or immediately following gelatin exposure. Pre-tests were collected immediately prior to injection or gelatin exposure.

Open Field: A 50 cm x 50 cm chamber (25 LUX) was equipped with an overhead camera to record movement. Animals were placed in the chamber for 15 minutes and then returned to their home cage. Total distance traveled (cm) was measured using Noldus Ethovision behavioral tracking software. Locomotion behavior was measured immediately before and after gelatin access to calculate a gelatin dependent difference score (post-pre). Pre-test measurements for CTR-gel were not collected and pre-test values were instead normalized to vehicle post-tests to produce a difference score as Post-VEH.

Tail Flick Analgesia: A hot water bath was set to 52.5°C. Mice were securely held upright in the air with their tail hanging downward. A timer was started as 75% of their tail was submerged into the water. Time was measured once a painful response was presented, marked as a latency to flick their tail out of the hot water. Tail flick responses were

measured immediately before and after gelatin access to calculate a gelatin-dependent difference score (post-pre).

Measuring body temperature: Animals were placed on a stable surface with their tails lifted. A rectal thermometer probe (RET-3 Kent Scientific) was inserted into the anus for 10-20 s until the temperature recording stabilized. This test was always performed prior to the Tail Flick test to reduce any potential temperature contamination effects. Body temperatures were measured immediately before and after gelatin access to calculate a gelatin dependent difference score (post-pre).

Blood and brain tissue collection and quantification

Animals underwent the same gelatin access paradigm for day 1 and 2 described in acute gelatin access. After 2 h of gelatin access, blood was collected by cardiac puncture with a 23-gauge needle and placed on ice. Immediately following, brain tissue was collected and flash frozen in liquid nitrogen. Blood samples were spun in a 4°C centrifuge at 1450 x *g* for 15 min. Plasma was transferred to another tube and stored alongside brain samples in -80°C until being shipped on dry ice to the Piomelli Lab at UCI for sample analysis. Samples were collected immediately following 1 and 2 h gelatin access and 30 min and 24 h after 2 h gelatin access. THC and its first-pass metabolites 11-OH-THC and 11-COOH-THC were quantified in plasma and brain tissue using a selective isotope-dilution liquid chromatography/tandem mass spectrometry assay (26). Concentration data after E-gel consumption were compared to blood and brain tissue concentrations after *i.p.* administration from previous publications from the Piomelli Lab [202].

Acoustic startle

Acoustic Startle behaviors were measured after 1 or 2 h THC-E-gel exposure (10 mg/15 ml) and THC-*i.p.* (0.1, 1, 5, 10 mg/kg) injection. Sound-buffered startle chambers (SR-Lab, San Diego Instruments) were used to measure acoustic startle responses, equipped with a holding tube and an accelerometer. Background sound was maintained at 65 dB from a high-frequency speaker producing white noise. Startle tests were conducted 1 h post-THC-*i.p.* injection or immediately following THC-E-gel exposure. Animals were set in the holding tube for 5 min to habituate prior to a series of seven trials presenting escalating sound levels of null, 80, 90, 100, 105, 110, and 120 dB. Tones were presented for 40 ms with an inter-trial interval of 30 s. Animals were only ever exposed to the acoustic startle paradigm once, immediately after gelatin access, to avoid auditory habituation.

Data/Statistical analysis

All data were analyzed using GraphPad Prism 10-11. For all statistical analyses (unpaired *t* test, one- and two-way ANOVA, and post hoc analyses), alpha level was set to 0.05. For all ANOVA analyses, Sidak's post-test was performed for increased power and repeated measures analysis was performed for time-dependent consumption data. All behavioral locomotor tracking was analyzed using Noldus Ethovision software and statistical analyses performed through GraphPad Prism 10-11. Nonlinear regressions (**Figure 2.4B-d and Figure 1-figure supplemental 3B-G**) were performed with a 3-parameter nonlinear, least squares, regression.

Gelatin formulation for adolescent exposure

Gelatin 3.85 g of Knox Gelatin was dissolved into 100 ml of deionized H2O and raised to a temperature of 40 °C. Then either 5, 2.5, or 1 g of Polycal sugar was dissolved into the

mixture to make the 5, 2.5, and 1% sugar content gels, respectively. While maintaining the temperature of the mixture between 41 and 43 °C, THC or CBD (20 mg/ml) was added to achieve a final drug concentration of 1 mg/15 ml (g) of gelatin (or 0.5, 2, and 4 mg/15 ml for THC). Morphine was added to achieve a concentration of 1.125 mg/ 15 ml (g). Gelatin cooled in a 4 °C refrigerator before use.

Adolescent gelatin exposure

Animals were singly housed, and a small plastic cup was secured to the metal wire top using a hose clamp. Approximately, 10 g of control gelatin (no drug) at 5% Polycal content was inserted into each of the plastic cups at ~2:00 p.m. for 3 days. The weight of the gelatin from the previous day was recorded and the remaining gelatin was discarded. After this, the Polycal content was reduced to 2.5% for 2 days, and again to 1% for 5 days. Two days prior to sciatic nerve ligation, gelatins were removed, and gelatin with drug was introduced 1 day after ligation, and every day thereafter until the study was concluded.

Conditioned Place Preference

Mice were trained in an unbiased, balanced three-compartment conditioning apparatus as described (5). Briefly, mice were pretested by placing individual animals in the small central compartment and allowing them to explore the entire apparatus for 30 min. Time spent in each com-partment was recorded with a video camera (ZR90; Canon) and analyzed using Ethovision software (Noldus). Mice were assigned to saline and drug compartments and received saline in the morning (10 mL/kg, i.p.) and morphine (10 mg/kg, i.p.) in the afternoon at least 4 h after the morning training on 3 consecutive days. CPP was assessed on day 4 by allowing the mice to roam freely in all three compartments

and recording the time spent in each. Scores were calculated by subtracting the time spent in the morphine-paired compartment post test minus the pre test

Barnes Maze

The escape box is prepared, and mice can access it through a transparent plastic tube (50 cm long, 5 cm diameter), which is found under the target hole. The paradigm consists of a circular platform (92 cm in diameter) with 20 holes (hole diameter: 5 cm) along the perimeter. During testing, the mouse learns the spatial location of the target box. Extra-maze cues were all around the room as reference cues to learn the position of the target hole (escape hole). During the experimentation there were bright lights positioned above the chamber and a BSC hood was turned on to provide bussing to promote escape. At the beginning of each trial, the mouse was placed in the middle of the maze with their nose directed in a random direction of the escape port. The trial ended when the mouse enters the goal tunnel or after 3 min have elapsed. The mouse was allowed to stay in the tunnel for 1 min before being removed and return to their home cage. Nose pokes/investigations to correct, incorrect, and near-correct ports. Mice were trained four trials per day/4 days. Trials were separated by 15 min. After each trial the entire maze was cleaned with 70% ethanol her). Trials were recorded by using computerised tracking/image analyzer system (video camcorder: 1/3 in. SSAM HR EX VIEW HAD coupled to computational tracking system: TiBeSplit). The following parameters were recorded: errors, distance from tunnel, search strategy and time that the mouse took to escape into the tunnel. If mice did not escape after 3 minutes, they were taken, dragged by their tail to the escape port where they were gently suggested to enter the escape port.

Von Frey Assay

Von Frey hairs (IITC Life Science) of various, predetermined weights were used (0.1–8 g). Individual hairs of increasing weight (force) were pressed against each hind paw until a response (voluntary hind paw lift) was observed. The lowest weight that elicited a response for 2 out of 3 presses was recorded. We observed no differences in the ipsilateral and contralateral paw withdrawal scores [22, 23], so the two paws were averaged for each mouse.

Hot Plate assay

A hot plate apparatus (IITC Life Science) was set to a temperature of 57.5 °C. Mice were gently placed onto the hot plate, and the latency of a pain response was recorded. A pain response was defined as either a paw lick, jump or a hind paw shuffle.

Animals

Adult (16-35g, 12-52 weeks) male and female WT, VGAT-Cre, VGLUT1-Cre, SST-Cre, and VIP-Cre mice were group house, given ad libitum access to food and water, and maintained on a 12 hour light dark cycle (lights off at 9:00 AM, lights on at 9:00 PM). Mice were bred in a barrier facility and transferred to the holding facility at least 1 week before the start of surgical interventions or experiments. All animals were drug and test naïve, unless otherwise noted. Unless otherwise noted, statistical comparisons did not detect any sex differences, and therefore male and female mice were combined for the data presented in this manuscript. All animals were monitored daily by either facility staff or experimenter throughout the duration of the study. All procedures were approved by the Animal Care and Use Committee at the University of Washington and conformed to US National Institutes of Health guidelines. Animal studies followed the guidelines established by the Association for Assessment and Accreditation of Laboratory Animal

Care (AAALAC) and were approved by the Institutional Animal Care and Use Committee (IACUC) of the University of Washington. Investigators were not blinded to experimental exposure conditions throughout assays due to the noticeable behavioral effects measured in response to THC. Animal procedures were approved by the IACUC of the University of Washington and conform to the guidelines on the care and use of animals by the National Institutes of Health.

Pharmacological agent handling and treatments

All pharmacological treatments were performed via intraperitoneal (*i.p.*) route of administration. Animals received vehicle, THC (0.1, 0.3, 1, 3, 5, 10, or 30 mg/kg), SR141716 (SR1, 1 mg/kg), DO34 (30 m/kg), or JZL-184 (10 mg/kg). THC and SR141716 (SR1) were provided by the National Institute of Drugs Abuse Drug Supply Program (Bethesda, MD). DO34 and JZL-184 were purchased via Sigma-Aldrich. For injections, THC, SR1, and DO34 were dissolved in 95% ethanol and then vortexed thoroughly with equal volume cremophor and finally dissolved in sterile saline to reach a final 1:1:18 solution consisting of ethanol:cremophor:saline. JZL-184, due to its low solubility was dissolved in a 1:1:8 solution (DMSO:Cremophor:saline) with JZL-184 being dissolved in DMSO first. Appropriate controls were used for JZL-184.

Hand-labeled behavioral tracking

Behavioral datasets and time point markings for walk behaviors in chambers other than the linear track were performed by hand. All walk events were filtered for 20 second intervals from the previous walk event to be counted as a new event. The conditions for

Linear track behavioral chamber

A linear track behavioral corridor was constructed for the behavioral recording of animals from two perspectives (bottom-up and side profiles) simultaneously with a single camera. This chamber was designed by Machado et al 2014 and recording was initially completed with a Basler ace camera (acA800-510um)[164]. Lighting for the linear track chamber was done with 4 IR flood lights and 2 supportive IR lights positioned around the chamber. All videos were recorded at 100 frames per second using python script (Github link). Behavioral experiments that did not coincide with intracranial interventions (fiber photometry, cannulation, or optogenetics) were recorded for 15 min in the linear track. The linear track was cleaned with Clidox after every animal was exposed to the chamber and all cleaned with Clidox and then ethanol between every cage. All recordings were completed in the dark with red lights that did not obstruct the IR recordings of the camera.

Machine learning behavioral tracking

Behavioral tracking was performed using the SLEAP tracking algorithm, a convolutional neural network published in Pereira et al 2022[159]. A specialized model was built for linear track behavior with single animal exposure. To develop the model, a subset of 1767 frames from 313 videos were selected to account for a range of sexes (51% male, 49% female), treatment conditions (Vehicle and a dose range of THC), genotypes (WT, VGAT-Cre, VGLUT1-Cre), ages (6 weeks to 6 months), and modified lighting conditions to ensure versatility of the model. Of the 1767 frames, 50% were randomly selected by SLEAP and 50% were hand-picked for difficult/valuable frames to improve model accuracy. Final model precision and recall was 97.15% and 98.74%, respectively (**figure**). All data analyzed were tracked with this model (recorded at 100 frames per second) and exported as .h5 files for further analysis. An analysis package suite was used

to export the positional data and calculate features for respective classification methods described below (Github link).

Supervised Classification

Identification of core behavioral responses within the linear track was performed with an automated supervised ML algorithm to identify frame-by-frame instances of walking, rearing, grooming, and laying on belly. This model was trained on 1.4 million hand-scored frames of naturalistic behavior within the linear track from a dataset of 45 videos consisting of adult (6 week to 6 month) 51% female and 49% male mice. Videos of animals were treated with either vehicle or some drug to expand the model versatility across different behavioral modifications. Model was trained on 1.35 million frames and separated test set revealed a final precision and recall of 98.3% and 97.7%, respectively. Further code was used to isolate behavioral event timestamps from the supervised model to calculate kinematic features or align neural data when applicable.

Kinematic analysis

Analysis of natural behavioral walking kinematics within the linear track was done first by isolating natural walk events across videos with the supervised classification algorithm described above. Walk events were then isolated from the video for batch analysis. Estimated pose points of interest were used to calculate chosen metrics of locomotor kinematics commonly analyzed in previous literature. Metrics were averaged over the course of given walk events and then averaged across all walk events for a given animal. At higher dose THC treatments there were markedly less walk events which did contribute to a higher variability in addition to modified metrics. Due to concerns of multiplicity

significance, kinematic features were analyzed for visualization purposes but only gait widths and dose prediction modelling were used for biological conclusions.

Isolating steps: estimated POIs from the bottom view for the right and left forepaws and hindpaws (4 total) were isolated to identify steps within the walk event. To do this, velocities were measured at every frame and plotted to reveal a wave form-like rate as paws enter and exit a stance phase. Delineation of a “step” within a walk was determined for each paw individually to be within the most recent peak speed (middle of final stride for a given walk, Extended Data). Steps separations were used for some kinematic metrics such as stride length and step number. For kinematics features specific to a given paw, if otherwise not specified to a given paw, metrics were averaged across all four paws.

Dose Prediction Modelling

Identification of a “presented dose” of behavior or neural signal was determined with a random forest regression algorithm. This model type was selected to account for non-linear distributions in effects caused by varying THC dose and allow for the identification of fractional shifts in presented dose. Other regression models such as XGBoost were used and found to be less accurate than random forest regressors. All models were trained on a subset of all WT behavioral C57/bl6 videos recorded in the linear track in which animals were treated with a range of THC 0.1-7 mg/kg. Higher doses (10 and 30 mg/kg) and vehicle videos were removed as it improved the accuracy of the models. All videos for training were 15 min long and retained at that size for consistency and to account for variability in the first few min where activity was heightened. All models were trained with a 70-30 split of training to testing videos split evenly across doses where 70%

of videos were used to train the algorithm and 30% were used to test the accuracy. Accuracy measurements for each model were assessed by mean square error (MSE).

For all models, feature importance was assessed alongside a permutation analysis to assess individual contributions to the model's accuracy (as measured by MSE). Features that contributed to the bottom 25% were removed and the model retrained to assess if model accuracy improved. If it did, the feature was discarded, otherwise it remained for the final model training. All features listed in the following Dose Prediction sub headers are the final selected features found to contribute to model accuracy.

When analyzing a novel video to assess presented dose with a dose prediction model, features for the given video were calculated in respect to the model of interest. Then, the regressor was applied to predict on the calculated features.

Dose Prediction Modeling of General Behaviors

Identification of general naturalistic behavioral signatures to identify THC "presented dose" for each animal was done by utilizing metrics from the previously described supervised algorithm. Core behaviors (walking, rearing, grooming, laying on belly, and other behaviors) were calculated for all training set videos at each frame and smoothed following description above. Then, the following features were calculated on each training video before being used to train a random forest regressor. The final features utilized were as follows: 1) average length of another bout, 2) average length of a walk bout, 3) average length of a rear bout, 4) average length of a groom bout, 5) average length of a lay on belly bout, 6) standard deviation of length of another bout, 7) standard deviation of length of a walk bout, 8) standard deviation of length of a rear bout, 9) standard deviation of length of a groom bout, 10) standard deviation of length of a lay on belly bout, 11)

number of other bouts, 12) number of walk bouts, 13) number of rear bouts, 14) number of groom bouts, 15) number of lay on belly bouts, 16) percent time spent in other behavior, 17) percent time spent in walk behavior, 18) percent time spent in rear behavior, 19) percent time spent in groom behavior, 20) percent time spent in lay on belly behavior, and 21) total number of behavioral transitions.

Dose Prediction Modeling of Kinematic Behaviors

First, walk events across the training dataset were identified using the Supervised algorithm to identify naturalistic walk events. Then, kinematic features were calculated following the description outlined in Kinematic Analysis. All features were calculated solely during walk events and therefore provided a higher within-video confidence at lower dose THC treatments where the animals performed a greater number of walk events. The final features utilized were as follows: 1) back height, 2) belly height, 3) nose height, 4) tail base height, 5) tail tip height, 6) average tail base yaw, 7) average head yaw, 8) average body yaw, 9) average right forepaw yaw, 10) average left forepaw yaw, 11) average right hind paw yaw, 12) average left hind paw yaw, 13) average hind paw gait width, 14) average forepaw gait width, 15) average body angle, 16) average body pitch, 17) average head pitch, 18) average walk bout distance, 19) average walk bout speed, 20) average number of steps, 21) average stride speed, 22) average stride distance, 23) average stride time, 24) average paw speed, 25) maximum walk speed, 26) minimum walk speed, 27) standard deviation of bout distance, 28) standard deviation of bout speed, 29) standard deviation of number of steps, 30) standard deviation of stride speed, 31) standard deviation of stride distance, 32) standard deviation of stride time, 33) standard deviation of right hind paw yaw, 34) standard deviation of left hind paw yaw, 35) standard

deviation of right forepaw yaw, 36) standard deviation of left forepaw yaw, 37) standard deviation of minimum speed, 38) standard deviation of maximum speed, 39) standard deviation of paw speed, 40) standard deviation of head yaw, 41) standard deviation of tail base yaw, 42) standard deviation of body yaw, 43) standard deviation of forepaw gait width, 44) standard deviation of hind paw width, 45) standard deviation of body angle, 46) standard deviation of head pitch, and 47) standard deviation of body pitch. Of the 60 original features selected, 13 were removed after being found to reduce model accuracy.

Unsupervised Classification

Assessment of nuanced naturalistic behaviors was performed on “other” behaviors as identified by our supervised algorithm. These behavioral frames represent all actions performed by the mice that could not be described as walking, rearing, grooming, or laying on belly by the supervised algorithm. These frames across all WT treatments, including vehicle and THC doses 0.1 mg/kg to 30 mg/kg, were isolated and 29 chosen features were selected to represent the animal’s posture in each frame. Certain features were selected to account for temporal dynamics between frames (e.g. velocity and acceleration of POIs). These 29 features, across all videos, were then used in a high dimensional clustering Kmeans algorithm to identify 12 unique clusters of behaviors. The cluster number was iterated on to determine the optimal cluster number by building Kmeans models at varying cluster numbers and recording the downstream accuracy of a dose prediction model (see below).

Within each video, cluster number, frequency and bout length were quantified relative to the total number of “other” frames within each respective video to investigate the dose-dependent effects as displayed in **Figure 4.2**. A random selection of cluster frames was

selected across videos and visualized for a “human-in-the-loop” assessment of model performance and for behavioral identification. These clusters are represented in Extended Data where names have been given to specific clusters such as “sitting”.

Dose Prediction Modeling of Unsupervised Behaviors

Unsupervised clusters of nuanced naturalistic behaviors revealed dose-dependent behavioral expressions that were utilized to construct a dose prediction model. The final features utilized were as follows: 1) Percentage of cluster 1 frames, 2) Percentage of cluster 2 frames, 3) Percentage of cluster 3 frames, 4) Percentage of cluster 4 frames, 5) Percentage of cluster 5 frames, 6) Percentage of cluster 6 frames, 7) Percentage of cluster 7 frames, 8) Percentage of cluster 8 frames, 9) Percentage of cluster 9 frames, 10) Percentage of cluster 10 frames, 11) Percentage of cluster 11 frames, 12) Percentage of Crouching frames, 13) Mean bout length of cluster 1, 14) Mean bout length of cluster 2, 15) Mean bout length of cluster 3, 16) Mean bout length of cluster 4, 17) Mean bout length of cluster 5, 18) Mean bout length of cluster 6, 19) Mean bout length of cluster 7, 20) Mean bout length of cluster 8, 21) Mean bout length of cluster 9, 22) Mean bout length of cluster 10, 23) Mean bout length of cluster 11, 24) Mean bout length of Crouching, 25) Standard Deviation of cluster 1 bout length, 26) Standard Deviation of cluster 2 bout length, 27) Standard Deviation of cluster 3 bout length, 28) Standard Deviation of cluster 4 bout length, 29) Standard Deviation of cluster 5 bout length, 30) Standard Deviation of cluster 6 bout length, 31) Standard Deviation of cluster 7 bout length, 32) Standard Deviation of cluster 8 bout length, 33) Standard Deviation of cluster 9 bout length, 34) Standard Deviation of cluster 10 bout length, 35) Standard Deviation of cluster 11 bout length, 36) Standard Deviation of Crouching bout length.

Combination of Dose Prediction models

Features from the training behavioral set were calculated for all behavioral feature sets as described for the general, kinematic, and unsupervised dose prediction models. For the combined general and kinematic model in **Figure 4.1**, the features used to train the general and kinematic models were combined into a large array. This combined feature array across doses was used to train the combined general-kinematic behavioral model. Similarly, the features were all combined into one large feature set before being used to train a new random forest algorithm to predict dose for total presented dose.

Tissue processing

For all fiber photometry experiments, mice were transcardially perfused with a 4% paraformaldehyde solution in phosphate buffered saline. Heads were subsequently removed and were immediately placed into a same solution bath to set for 24 hours. After this time, fiberoptic implants were removed along with the remainder of the skull, and brains were placed into a cryoprotectant 30% w/v sucrose solution in PBS. Once brains had sunken to the bottom of the tubes (typically around 3-5 days), brains were mounted on cutting blocks using O.C.T. (Sakura Finetek) and sliced in 40μm sections on a Leica CM1900 cryostat at -18°C. Slices were then placed into PBS and either immediately mounted on SuperFrost Plus slides (Fisher) for imaging or stored for up to 1 week. Mice with misplaced fiber optic implants were excluded from the study.

Cell Culture:

Neuro2a cells and HEK 293 cells were grown in DMEM (Gibco, supplemented with 10% fetal bovine serum and 1% penicillin/streptomycin) at 37°C and 5% CO_2. To passage cells for experiments, a confluent 10 cm plate of cells was detached by incubating with 0.25%

Trypsin-EDTA for 2-3 minutes at 37°C, adding 4-5 mls of supplemented DMEM and using gentle pipetting to remove any cells still attached, then added to a new plate with fresh supplemented DMEM. Cells were passaged every 3-4 days, and for no more than 25 passages.

Transfection:

All transfections were done by incubating DNA with the transfection reagent polyethylenimine (PEI, 25K linear, Polysciences) in a 1:3 ratio in serum free DMEM, incubating for 20-30 min. The DNA/PEI mixture was then added to cells in a dropwise fashion (or directly into media in eCB2.0 96 well-plate assay) without changing the growth media. Cells were transfected when they were at least 50% confluent and were incubated for 24 hours after transfection before harvesting or using for $GRAB_{eCB2.0}$ assays.

Live-cell imaging:

Glass bottom cell culture plates (MatTek) were coated with poly-D-lysine (50 ng/ml, Sigma) for 1-2 h at 37°C, after which the poly-D-lysine was removed, and coverslips were washed 3 times with sterile water and one time with DMEM. N2a or HEK 293 cells were detached and resuspended in supplemented DMEM as described above, counted using a hemocytometer, plated (250,000 cells per well) and were transfected after 24 hours with 0.75 µg DNA. 24 hours after transfection, for the N2a cells only, the growth media was exchanged for serum free DMEM and cells were incubated at 37°C and 5% CO_2 for 1-2 hours. To image, the serum free DMEM was exchanged for room temperature phosphate-buffered saline containing 1 mM $CaCl_2$ and 0.55 mM $MgCl_2$. For the HEK 293 cells, the growth media was directly exchanged to phosphate-buffered saline. The plates were transferred to a line-scanning, confocal microscope (Leica SP8X) and cells were imaged

using a 40X oil objective with the following settings: 485 excitation and 525 emission wavelength, 5% laser power, HyD hybrid detector and a scan speed of 200 lines Hz (0.388 frames per second) with bidirectional scanning. All treatments were made in 1 mg/mL BSA in PBS and added directly to buffer for a final concentration of 0.1 mg/ml BSA. For co-culture experiment: HEK 293 cells were plated at a density of 150,000 cells in a 30 mm plate. The next day, the HEK293 cells were transfected with $GRAB_{eCB2.0}$.12 hours after transfection, the media on the cells was exchange for fresh growth media and 200,000 N2a cells were plated in the same plate. 24 hours after plating the N2a cells, the cells were serum starved for 1 hr, the serum free media was then exchanged for imaging buffer and the plate was placed on the confocal microscope. The cells were imaged for 2 min to establish a baseline. Then treatments were added directly into the buffer and the cells were imaged for another 10 min. All treatments formulated in 0.1 mg/ml bovine serum albumin.

96-well Plate Reader $GRAB_{eCB2.0}$ Detection:

Clear-bottom, black 96-well plates (USA Scientific were coated with poly-D-lysine (50 ng/ml, Sigma) for 1-2h at 37°C, after which the poly-D-lysine was removed, and coverslips were washed 3 times with sterile water and one time with DMEM. N2a cells were detached and resuspended in supplemented DMEM as described above, counted using a hemocytometer, then plated (20,000 cells per well) and were transfected after 24h with 0.1 µg DNA and 0.3 µg of PEI in 10 µl of serum free DMEM. 24h after transfection, growth media was initially replaced with serum free DMEM for 1h (with or without ABHD6 and DAGL inhibitors), before replacing with PBS supplemented with 1 mM $CaCl_2$ and 0.55 mM $MgCl_2$. Cells were incubated at room temperature for 20 min then a 1 min baseline

fluorescence reading was obtained using a fluorescent plate reader using 485 excitation and 525 emission filter settings with a 515 nm cutoff, and a speed of 1 reading every 20 sec. Immediately after baseline reading, treatments (made in 1 mg/mL BSA and PBS) were added to buffer in wells. Approximately 2 min after addition of treatment, the plate was read with same filter settings for 30 min. For cells pre-treated with SR1, SR1 made in PBS was added to cells after media had been replaced with PBS and were incubated for 20 min before baseline reading.

Image acquisition and analysis

For histological verification of fiberoptic/ lens placement, images were obtained on a Leica DM6B epifluorescent microscope at 10x or 20x magnification. For RNAscope analysis, images were collected on an Olympus Fluoview 3000 at 20x magnification. Z-stacked images were taken with optical section thickness of 2-3μM. Images were subsequently analyzed using either HALO or QuPath software. For either analysis, brain region boundaries were drawn in accordance with the Allen Brain Institute mouse reference atlas. For HALO, DAPI stained nuclei were used to mark cells, and cell boundaries were set to ~8 μM radius from nucleus center. Thresholds were set for detection in each channel and this threshold was applied to all analyzed images in a given cohort. In order to account for background noise, a neuron had to have >2 transcripts in order to be classified as positive for a specific marker. For QuPath analysis, DAPI was similarly used to define neurons and cell boundaries were set to ~8 μM radius from nucleus center. Individual channels were set via the classifier module, and these classifier settings were held consistent for all images within a cohort. The classifiers were set by individually sorting through each cell automatically registered by the QuPath software and identifying

the first ‘false positive’ neuron, using this as the threshold cut off for subsequent identification of positive neurons.

Stereotaxic surgeries

Mice were anaesthetized in an induction chamber (1-4% isoflurane) and placed into a stereotaxic frame (Kopf Instruments, model 1900) where they were mainlined at 1-1.5% isoflurane. For all viral infections, a Hamilton Neuros Syringe was used, and virus was infused at a rate of 75 nl/minute. For fiber photometry experiments, 500 nl AAV5-DIO-GCaMP6f (Addgene) or 500 nl AAV1-hSyn-GRAB$_{eCB2.0}$ was injected into the PrL of the mPFC of VGAT-Cre, VGLUT1-Cre, VIP-Cre, SST-Cre, or WT mice, with final coordinates of A/P 1.8, D/V -2.0, M/L 0.4. After appropriate infusion of virus, 400uM fiber optic implantation was performed and bonded to the skull with metabond. For CRISPR/ photometry experiments, AAV1-FLEX-sgCNR1-SaCas9 was infused into the PrL at the same coordinates above in VGAT-Cre and VGLUT1-Cre mice. Mice were left for a minimum of 6 weeks to improve viral expression and provide time for recovery before performing a second surgery to inject AAV5-DIO-GCaMP6f and implant a 400uM fiber optic with a stainless-steel ferule (Doric). All implants were secured using Metabond (Parkell). For optogenetics experiments, 500nl of AAV5-DIO-ChR2-eYFP (Addgene) was injected into the PrL of the mPFC of VGAT-Cre, VGLUT1-Cre, VIP-Cre, and SST-Cre mice. After appropriate infusion of virus, ipsilateral 200μM fiberoptics were implanted over the PrL (final coordinates of A/P +1.8, D/V -2.0, M/L + 0.4). The optic fiber was subsequently attached to the skull with Metabond. Intracranial cannulation was performed by drilling bi-lateral holes at the coordinates of A/P +1.8, D/V -2.0, M/L +/- 0.4 whereby a bi-lateral cannula was carefully implanted over the PrL. The cannula was attached to the

skill with metabond. All mice were given at least 4 weeks of recovery time post-surgery before experimentation.

Fiber photometry

Fiber photometry recordings were obtained throughout the duration of all behavioral tests presented in this manuscript. Prior to recordings, a fiberoptic cable was attached to the fiberoptic implant using a plastic or ceramic ferrule sleeve (Doric, ZR2.5). For all photometry recordings, we used a Tucker-Davis Technologies RZ10x processor. A 531-Hz sinusoidal 470 nm LED light (Lx465) was used to excite GCaMP6f or $GRAB_{eCB2.0}$ and evoke Ca2+-dependent emission. A 211-Hz sinusoidal 405 LED (Lx405) light was used as the Ca2+-independent isosbestic control emission. LED intensity was measured at the tip of the cable with a dummy implant attached and adjusted to 30μW before each day of recording. GCaMP6f fluorescence traveled through the same optic fiber before being bandpass filtered (525 ± 25 nm, Doric, FMC4), transduced by a femtowatt silicon photoreceiver (Newport, 2151) and recorded by a real-time processor (TDT, RZ10). The envelopes of the 531-Hz and 211-Hz signals were extracted in real- time by the TDT program Synapse at a sampling rate of 1017.25 Hz. For ChrimsonR stimulation experiments, a 635nm laser was used with a custom filter cube (Doric) at 5-7mW of intensity to deliver 1-20hz pulsed light through the same fiberoptic cable used for photometry recordings.

Photometry analysis

Custom MATLAB scripts were developed for analyzing fiber photometry data in context of mouse behavior and can be accessed via GitHub. The isosbestic 405nm excitation control signal was scaled to the 470nm excitation signal, then this refitted 405nm signal

was subtracted from the 470 nm excitation signal to remove movement artifacts from intracellular Ca^{2+}-dependent GCaMP6f or $GRAB_{eCB2.0}$ signal. Baseline drift was evident in the signal due to slow photobleaching artifacts, particularly during the first several min of each hour-long recording session. A double exponential curve was fitted to the raw trace and subtracted to correct for baseline drift. After baseline correction, $\Delta f/f$ was calculated by subtracting the median baseline subtracted signal from the baseline subtracted signal and dividing by the median raw signal. All photometry data presented at the onset of a behavioral event in this manuscript is Z-scored to a 10-30 second window prior to cue onset.

Dose Prediction Modeling of Photometry Signals

A dose prediction model was developed using photometry trace during and just around identified walk events. For each cell type (VGAT-Cre: GABAergic, VGLUT1-Cre:glutamatergic, SST-Cre:somatostatin, and VIP-Cre:vaso-intestinal peptide) videos of vehicle and THC-treated (1 and 5 mg/kg) were tracked with the supervised algorithm to classify walk events. Within each walk event, features of the Z-score signal were further calculated for model development. The features calculated for random forest regressor were averaged across all walk events within each animal's recording and are: 1) Z-score at walk initiation (time = 0), 2) maximum positive slope before peak signal, 3) time at peak signal level, 4) Z-score at the peak value, 5) maximum negative slope after peak signal, 6) total area under the curve over 3 seconds after walk initiation (time = 0).

Electrophysiology

Coronal brain slices were prepared at 250 μM on a vibrating Leica VT1000S microtome using standard procedures. Mice were anesthetized with Isoflurane, and transcardially

perfused with ice-cold and oxygenated cutting solution consisting of (in mM): 93 N-Methyl-D-glucamine (NMDG), 2.5 KCL, 20 HEPES, 30 NaHCO3, NaH2PO4, 10 MgSO4·7H20, 0.5 CaCl2·2H20, 25 glucose, 3 Na^+-pyruvate, 5 Na^+-ascorbate, and 5 N-acetylcysteine. Following collection of coronal sections, the brain slices were transferred to a 34°C chamber containing oxygenated cutting solution for a 10-minute recovery period. Slices were then transferred to a holding chamber consisting of (in mM) 92 NaCl, 2.5 KCl, 20 HEPES, 2 $MgSO_4$·7H20, 1.2 NaH_2PO_4, 30$NaHCO_3$, 2 $CaCl_2$·2$H_2$0, 25 glucose, 3 Na-pyruvate, 5 Na-ascorbate, 5 N-acetylcysteine and were allowed to recover for ≥ 30 min. For recording, slices were perfused with oxygenated artificial cerebrospinal fluid (ACSF; 31-33°C; 300-303 milliosmols) consisting of (in mM): 113 NaCl, 2.5 KCl, 1.2 $MgSO_4$·7$H_2$0, 2.5 $CaCl_2$·6$H_2$0, 1 NaH_2PO_4, 26 $NaHCO_3$, 20 glucose, 3 Na^+-pyruvate, 1 Na^+-ascorbate, at a flow rate of 2-3ml/min. For recordings of inhibitory currents, 10 μM CNQX was added to the external solution. Stocks of 50mM THC were made in ethanol and diluted 1:5000 in ACSF or HEPES for a final concentration of 10 μM. 0.05% w/v Bovine Serum Albumin (Sigma-Aldrich) was added to ACSF or HEPES to help the drugs from precipitating out of solution. For all drug experiments, slices were incubated in a HEPES bath containing the drugs for >30 min before transferring over to the slice rigs for recording.

mPFC neurons were initially voltage clamped in whole-cell configuration using borosilicate glass pipettes (2-4MΩ). For recordings of excitatory currents, pipettes were filled with internal solution containing (in mM): 125 K^+-gluconate, 4 NaCl, 10 HEPES, 4 MgATP, 0.3 Na-GTP, and 10 Na-phosphocreatine (pH 7.30-7.35). The patch pipette also included 50 μM picrotoxin to block $GABA_A$ currents. For recordings of inhibitory currents, pipettes were filled with 115 $CsCl_2$, 5 NaCl, 10 HEPES, 5 QX-314, 4 Mg-ATP, 0.3 Na-

GTP, and 10 Glucose (pH 7.30-7.35). Following break-in to the cell, we waited ≥ 3 min to allow for exchange of internal solution and stabilization of membrane properties. Neurons with an access resistance of > 30MΩ or that exhibited greater than a 20% change in access resistance during the recording were not included in our datasets. For all voltage clamp experiments, neurons were held at -70mV.

***Ex-vivo* Optogenetics**

To assess how THC treatment modulated eCB regulation of excitatory signaling in the mPFC, VGAT-Cre mice were injected with 550 nL of AAV5-CaMKII-ChR2(H134R)-eYFP into the contralateral mPFC, and 550 nL of DIO-mCherry was injected ipsilaterally to allow us to record from either VGAT+ neurons or putative pyramidal neurons (mCherry negative). To assess how THC treatment modulated eCB regulation of inhibitory signaling in the mPFC, VGAT-Cre mice were injected with 550 nL of AAV5-DIO-ChR2(H134R)-eYFP ipsilaterally and recordings were obtained from putative pyramidal neurons (eYFP negative). 3-5 weeks of viral expression was allowed prior to sacrificing the mice. For all experiments using THC, corresponding vehicle recordings were obtained from the same mice. For optogenetic recordings of input/output curves, we used a Thorlabs LEDD1B T-Cube driver and obtained separate recordings of 470nm wavelength oEPSCs / oIPSCs at 7 output levels corresponding to 5.7, 2.7, 1.6, 1, 0.5, 0.2, and 0.1 mW of LED intensity. PPR recordings of oEPSCs / oIPSCs were obtained in voltage-clamp with an inter-stimulus interval of 50ms. PPR is reported as a ratio between the amplitude of the second oEPSC / oIPSCs divided by the first. Recordings of DSE or DSI were obtained following at 10 s voltage step to +30mV. A baseline of 10 oEPSCs / oIPSCs were taken prior to the depolarizing step, and all data is plotted as an oEPSC / oIPSCs amplitude normalized to

the baseline period. A light exposure time of 2ms was used for all optogenetic experiments.

***In situ* hybridization**

For quantification of mRNA transcripts using RNAscope (ACD Bio), mice were briefly anesthetized using isoflurane and subsequently rapidly decapitated. Brains were immediately removed from the skull and were placed liquid nitrogen for rapid freezing. Then, brains were transferred to a -80°C freezer for long term storage. Prior to sectioning, brains were placed in the cryostat compartment for >30 min to allow them to come up to temperature. Following mounting using O.C.T., brains were slice at 16µm and directly mounted onto SuperFrost Plus slides. Slides were stored at -80°C.

FISH was performed according to the RNAscope 2.0 Fluorescent Multiple Kit User Manual for Fresh Frozen Tissue (Advanced Cell Diagnostics) as previously described. Briefly, slides were fixed in 40% PFA and then serially dehydrated using increasing concentrations of ethanol (50%, 75%, 100% and 100%). Slices were then treated with Protease IV and allowed to incubate in a 40°C hybridization oven for 30 min. Following serial rinses in a wash buffer, slices were incubated with probes directed against a series of probes outlined in given experiments. Samples subsequently went through sequential amplification steps, and lastly application of Opal dyes corresponding to each channel (TSA Vivid Fluorophore 520 (PN 323271), TSA Vivid Fluorophore 570 (PN 323272) and TSA Vivid Fluorophore 650 (PN 323273)). Slides were counterstained with DAPI, and coverslips were mounted with Vectashield Hard Set mounting medium (Vector Laboratories).

Intracranial cannulation

Male and female mice were implanted with bi-lateral guide cannulas with an internal cannula and a cap (RWD: specs) into the Pre-frontal cortex (coordinates). Cannulas were bonded to the skull with metabond and covered in a 5 mM quinine-Cremophor (50:50) solution daily to stop the animals from chewing through the material. Animals were given a 1-week recovery time before experimentation. All animals underwent a vehicle (0.5 : 0.5 : 1 : 17 = DMSO : ethanol : Cremophor : 50mg/ml BSA in saline) test day before any other treatment experiment. For all experimental days, animals were scruffed gently and held in a prone position while the head cap and dummy cannula were removed. An internal infusion cannula was then placed to infuse the desired drug at a rate of 1 uL over 2.5 min, bilaterally. Afterward, animals remained in the scruff for 1 min to allow for diffusion of the treatment before replacing with the dummy cannula and head cap. Then, mice were placed into a home-cage like environment alone for 5 min prior to being placed into the linear track for a 15 min recording. Treatments given included THC at 10 ug (conc), THC at 1ug (conc), DO34, or 20 µg JZL per hemisphere. Due to the high solubility of JZL-184, it had to be administered in 100% DMSO and tubing was changed between every animal.

Mice were placed into the linear track for 15 min to record a baseline for behavior and then were removed to administer the treatment (250 nl over 2.5 min) with 5 min of recovery (~10 min) before being placed back into the linear track for 15 min. Treatment groups were counterbalanced, either receiving a vehicle or a 5 mg THC infusion. After treatment, animals were placed back in their home cage.

Closed-loop optogenetic stimulation

To perform Closed-Loop optogenetic stimulation, two identical cameras (as described above) were setup to face the linear track chamber. One camera was used with the same computer as for all experimentation which recorded at the normal 100 fps for behavioral analysis. The other camera was connected to a second computer. This second computer was equipped with an Arduino controller and subsequent LED with a patch cable for connecting to a prepared mouse. The Arduino code was constructed to set the stimulation frequency (20 Hz), the pulse width (5 ms), the total stimulation time (3 s) and the ramp time (0.5 s) which was written to replicate the ramping in fiber photometry activity seen in **Figures 4.3 and 4.4**. The closed loop script that controlled the camera video capture was written in python and run to capture frames at 30 fps (the fastest possible while performing frame inference without dropping frames). The code batched frames into a sliding window of 15 frames at a time where each frame was passed through a pre-built “pre-walk” Random Forest Classification algorithm which identified behavior as either a 1 (pre-walk), 2 (walking), or 0 (not walk-related). When a threshold of 12 1’s was met within the sliding window, stimulation was triggered. This number of 12 was optimized through trial and error with the efficiency of the algorithm in real time testing. Stimulation was triggered by sending a pulse signal to the Arduino controller which then activated the LED stimulation through the patch cable to the mouse.

Male and female VGLUT1-Cre and VGAT-Cre mice were unilaterally injected with AAV-DIO-eYFP or AAV-DIO-ChR2-eYFP (600 nl) at the mPFC coordinates (AP = 1.8, DV = -2.0, ML = 0.4) before being implanted with an optic fiber. 4 weeks after injection and implantation, mice were habituated to the linear track on two days, 10 min each. On the first test day, animals’ fibers were attached to the LED patch cable and placed in the linear

track. The closed loop script was then run to initialize the Arduino and LEDs while the loop code began. After a manual 15 second delay, the video recording from the original camera began recording for a total 15 min session. After 15 min, the closed loop script was halted and data was exported for further analysis. Due to any potential inaccuracy in the closedloop walk identification, all videos were checked by eye to isolate all walk events where stimulation occurred. The pose estimation data for these walk events was then separated and analyzed for the resulting kinematic dose prediction models.

Pre-walk Random Forest Classification Algorithm

To develop the “pre-walk” classification algorithm, we used the same hand-labeled data as used for the supervised classification algorithm. Instead, we isolated only the events labeled for walking, and then all batches of 30 frames prior to each walk event as a “pre-walk”. Then, we used the same train/split for our data and trained the algorithm to have a final precision and recall for pre-walk (96.4% and 97.2%) and walk (98.8% and 87.6%). Then, the algorithm was uploaded and validated with several animals in the linear track closed loop system described above.

Chrimson stimulation and GRAB$_{eCB2.0}$ fiber photometry

Male and female VGLUT1-Cre and VGAT-Cre mice were uni-laterally injected with a viral mixture of AAV-DIO-Chrimson (450 nl) and AAV-hSyn-GRAB$_{eCB2.0}$ (450 nl) at a rate of 75 nl/min at the mPFC coordinates (AP = 1.8, DV = -2.0, ML = 0.4). Then, immediately after injection, they were implanted with an optic fiber, affixed to the skull with metabond dental cement. Four weeks after injection and implantation, mice were placed in a MedPC behavioral chamber and their optic fiber attached to a TDT stimulation LED stimulation system. Over an 8 min session, animals received 565 nm wavelength stimulation at 1:00,

2:30, 4:00, 5:30, and 7:00 so as to leave 90 s in between stimulations while recording 470 and 405 nm wavelengths. Stimulation in the main figure was performed at 20 Hz frequency with 5 ms pulse width for a total of 10 seconds. Animals were pre-treated 1 hour prior to testing with either vehicle or 5 mg/kg THC and there was always at least 1 week in between tests for each animal. Fiber photometry data was analyzed as described above with the stimulation time points used as epoch references.

Chapter 7.

Appendix

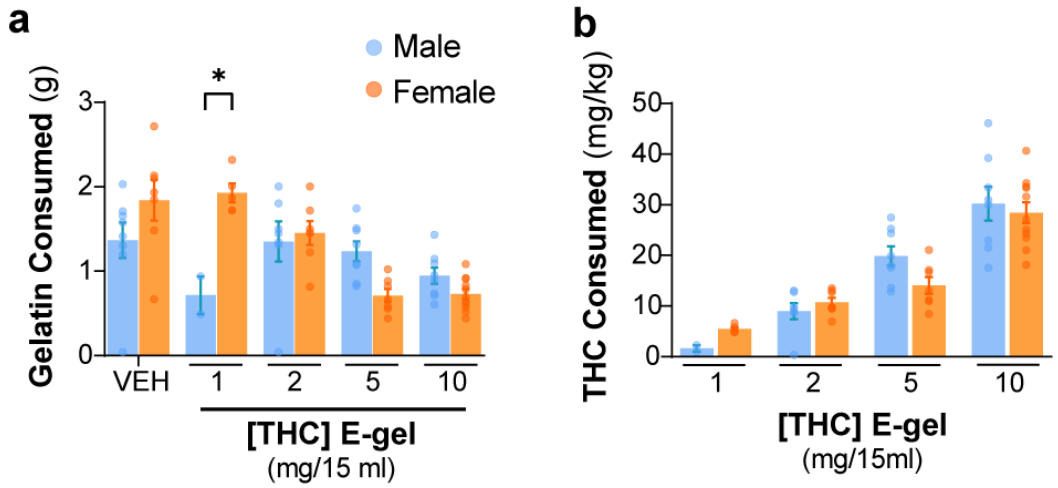

Supplementary Figure S2.1: <u>CTR-gel and E-gel consumption by male and female mice</u>
a) Total E-gel consumed by males (blue) and females (orange) after 2 h *ad libitum* access. **b**) Calculated THC dose based on individual animal weights after E-gel consumption shown in a. No statistical significance due to Sex across doses found from Two-way ANOVA, Sidak's post-hoc, N=2-11. Results are mean ± S.E.M

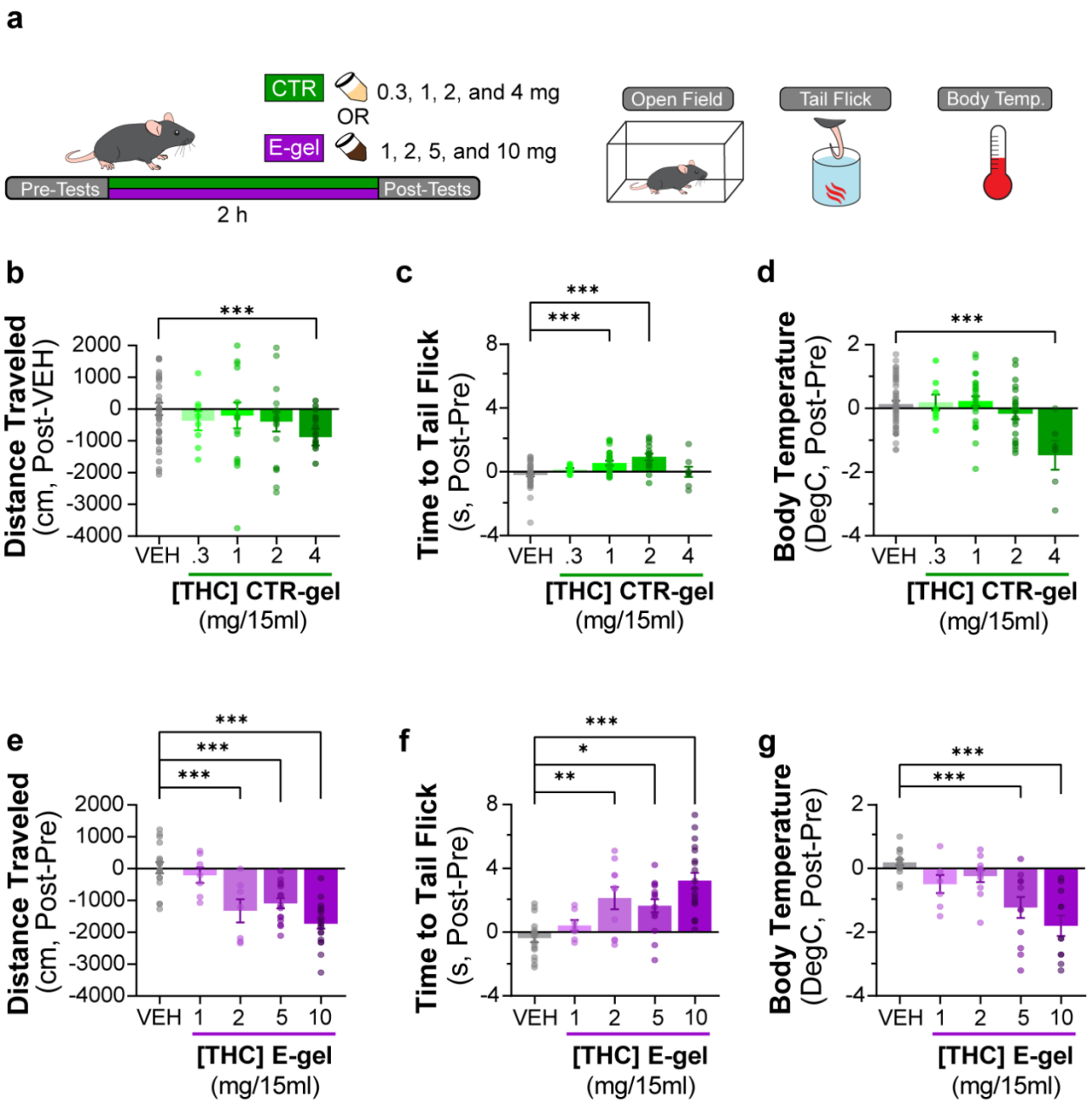

Supplementary Figure S2.2: <u>Triad behavioral responses after CTR-gel and E-gel consumption</u>

a) Diagram outlining 2 h exposure to either CTR-gel (green) or E-gel (purple) preceded and followed by Triad behavioral tests. **b-d**) Behavioral output immediately following CTR-gel administration for the Triad of cannabimimetic behaviors measuring hypolocomotion (**b**), analgesia (**c**), and hypothermia (**d**). In **b**, Distance traveled for CTR-gel was calculated based on averaged VEH consumption. All error expressed as SEM, unpaired Student's T-test (*** p<0.001). **e-g**) Triad of cannabimimetic behaviors following THC E-gel administration measuring hypolocomotion (**e**), analgesia (**f**), and hypothermia (**g**). All error bars expressed as SEM, One-way ANOVA, Sidak's post-hoc (* p<0.05, ** p<0.01, *** p<0.001).

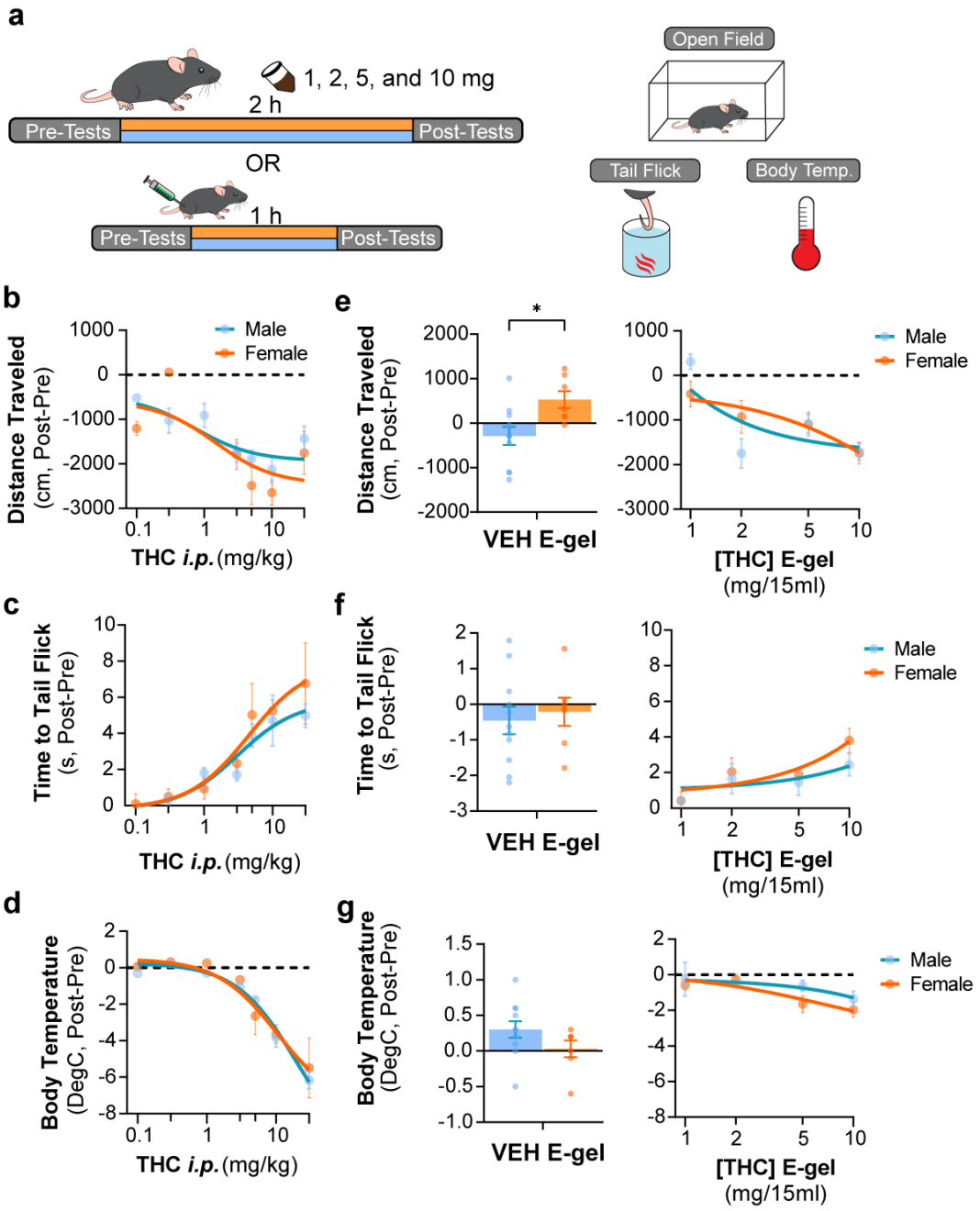

Supplementary Figure S2.3: <u>Triad behavioral responses to THC *i.p.* and E-gel administration by male and female mice</u>

a) Diagram outlining 2 h exposure to either E-gel or *i.p.* for males (cyan) or females (orange) preceded and followed by Triad behavioral tests. **b-d**) Dose-response curves for the Triad of hypolocomotion (**b**), analgesia (**c**), and hypothermia (**d**) cannabimimetic behaviors after *i.p.* THC administration with male responses shown in blue and female responses in orange. **e-g**) Male and female behavioral responses after access to THC E-gel doses for all three triad cannabimimetic behaviors: hypolocomotion (**e**), analgesia (**f**), and hypothermia (**g**). Sex-specific responses to VEH E-gel is separated from concentration-dependent curves. All error bars expressed as SEM, Two-way ANOVA, Sidak's post-hoc, (* $p<0.05$).

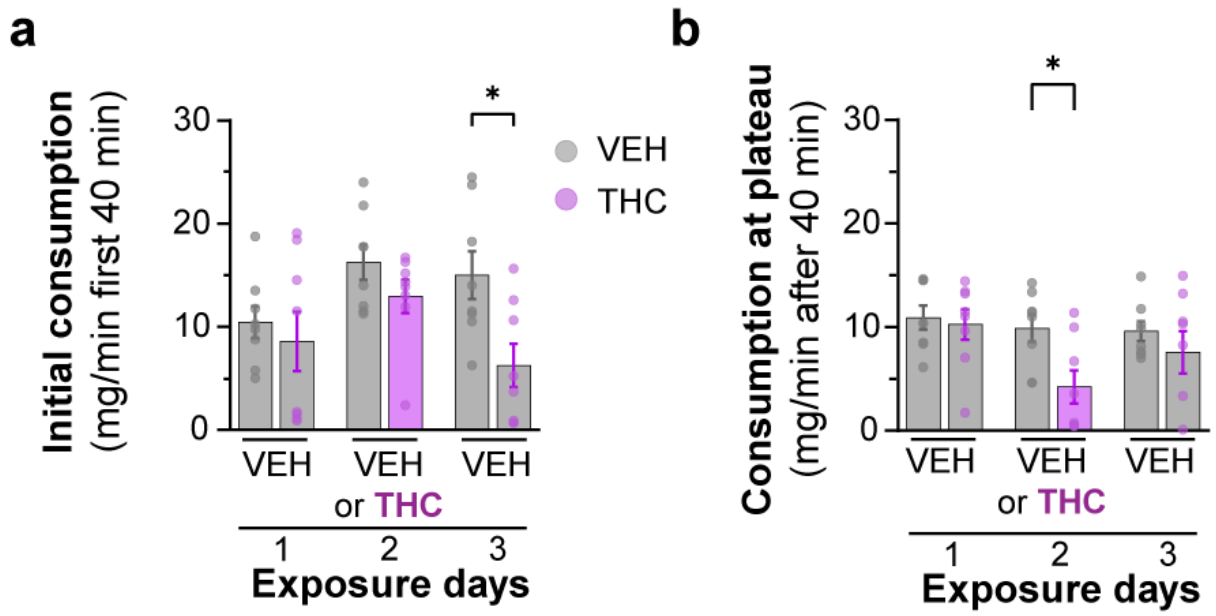

Supplementary Figure S2.4: <u>Analysis of THC-E-gel consumption behavior over 3-day access paradigm</u>

a) Rate of consumption during the first 40 min of 10 mg/15ml THC E-gel access across the three-day paradigm where the THC group received vehicle E-gel on days 1 and 3. Error in S.E.M., unpaired Student's T-test (* $p<0.05$). **b**) Rate of consumption after the first 40 min of E-gel access just as in a. Error in S.E.M., unpaired Student's T-test (*$p<0.05$). **c**) Latency to start consuming gelatin across the same experimental paradigm in a showing a statistical significance between VEH and THC groups but not within experimental days, Two-way ANOVA, Sidak's post-hoc, N=8 (* $p<0.05$).

Brain (pmol/g)						
Compound	Collection time	Sex	Mean	SD	N	Significance
THC	1h	M	557.2	263.2	9	ns
		F	397.7	123.8	7	
	2h	M	661.8	261.2	5	ns
		F	501.6	490.6	5	
	2.5h	M	573.8	303.9	8	ns
		F	289.4	126.9	8	
	26h	M	26.6	15.3	6	ns
		F	67.8	60.6	6	
11-OH-THC	1h	M	367.2	207.5	9	ns
		F	356.2	75.5	7	
	2h	M	406.7	124.7	5	ns
		F	610.6	678.4	4	
	2.5h	M	378.3	253.4	8	ns
		F	268.7	177.3	8	
	26h	M	10.6	16.8	6	ns
		F	69.4	53.3	6	
COOH-THC	1h	M	200.8	227.8	6	ns
		F	188.0	226.4	7	
	2h	M	309.9	313.7	4	ns
		F	371.4	354.4	4	
	2.5h	M	190.0	182.1	8	ns
		F	224.3	258.6	8	
	26h	M	0.0	0.0	6	ns
		F	31.1	52.9	6	

Supplementary Figure S2.5: Brain tissue concentrations of THC and metabolites by sex

Plasma (pmol/ml)						
Compound	Collection time	Sex	Mean	SD	N	Significance
THC	1 h	M	478.5	276.7	8	ns
		F	388.7	240.4	7	
	2 h	M	235.4	122.3	5	ns
		F	51.5	36.5	6	
	2.5 h	M	115.8	75.8	8	ns
		F	70.1	54.9	7	
	26 h	M	3.3	6.2	7	ns
		F	7.6	9.6	6	
11-OH-THC	1h	M	62.4	25.9	7	ns
		F	66.5	28.4	6	
	2h	M	53.9	23.3	5	ns
		F	36.0	6.2	3	
	2.5h	M	58.9	30.3	7	ns
		F	47.2	27.4	5	
	26h	M	0.0	0.0	6	ns
		F	4.6	7.2	6	
COOH-THC	1h	M	167.3	79.4	8	ns
		F	472.4	207.4	7	
	2h	M	116.3	52.9	5	ns
		F	179.3	217.6	7	
	2.5h	M	226.4	172.4	8	ns
		F	194.3	99.5	7	
	26h	M	14.7	24.2	6	ns
		F	90.0	79.6	6	

Supplementary Figure S2.6: Plasma concentrations of THC and metabolites by sex

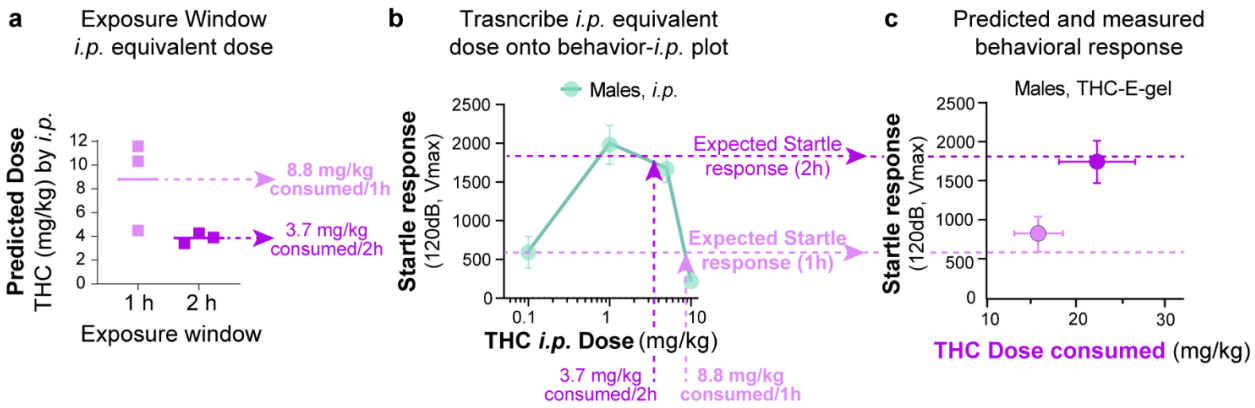

Supplementary Figure S2.7: <u>Methodology for THC-E-gel prediction of a behavioral response</u>

a) *i.p.* equivalent dose calculated from the triad of cannabimimetic behaviors in Figure 4. **b**) Transcribe *i.p.* equivalent doses to the THC-*i.p.* doe response plot for the given behavior to find the predicted behavior after 1 h or 2 h exposure to 10 mg/15 ml THC-E-gel. **c**) Predicted response (dashed line) and measured behavioral responses.

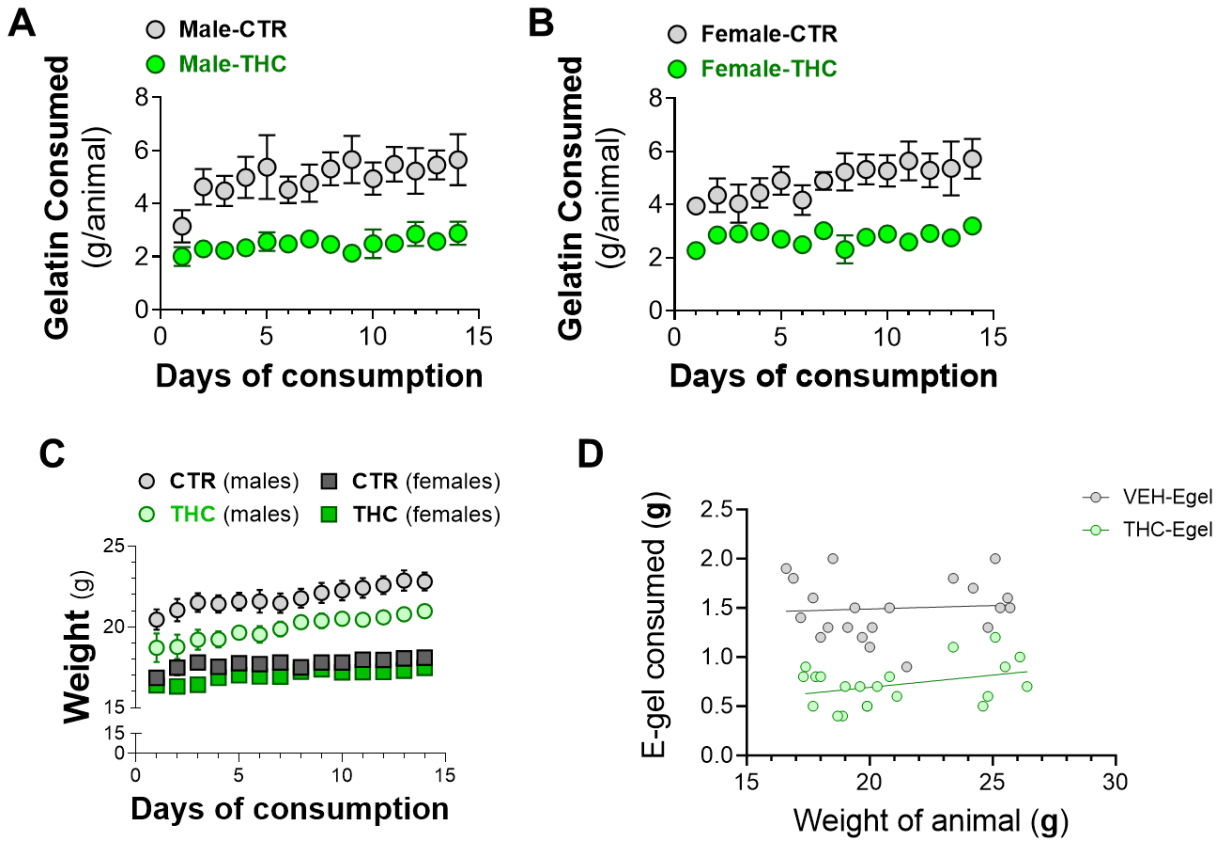

Supplementary Figure S3.1: <u>Adolescent consumption behavior during gelatin exposure.</u>

a) Gelatin consumed by male adolescent mice over the course of the 14 day exposure period to CTR-gelatin or THC-gelatin. **b**) Same as in A but female mice. **c**) Animal weights for male and female mice during adolescent gelatin exposure. **d)** Correlation of E-gel consumed and animal weight.

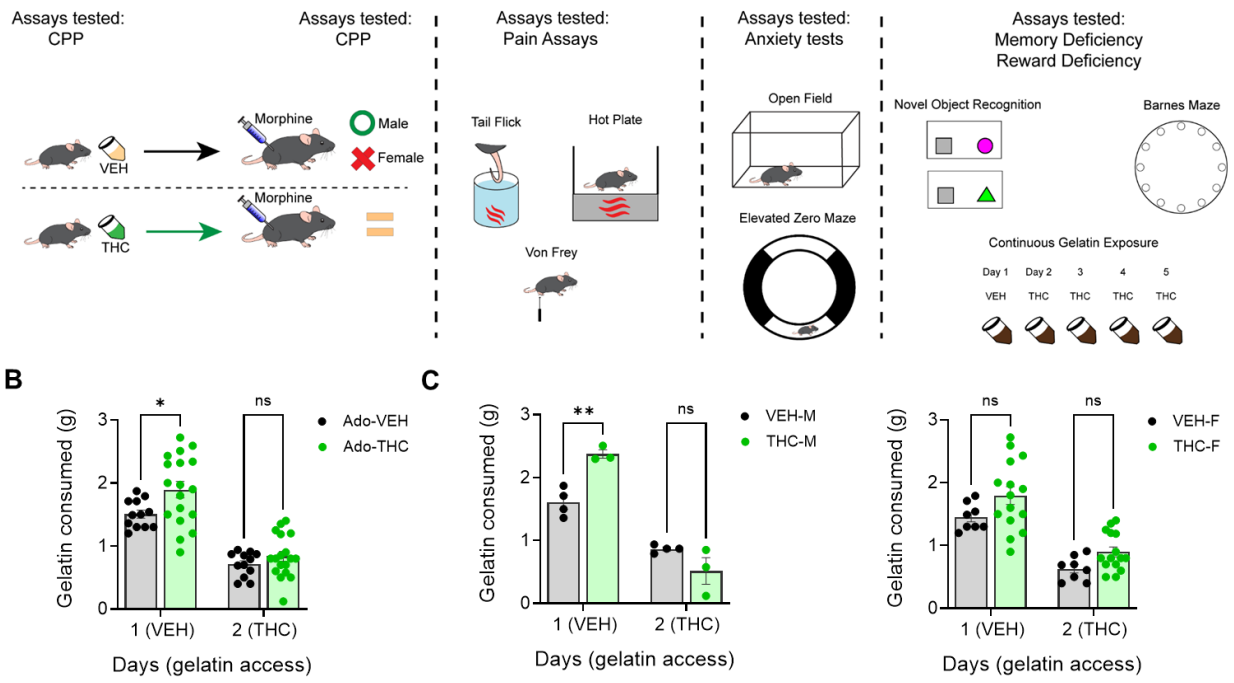

Supplementary Figure S3.2: <u>Adolescent THC exposure enhances acute THC consumption in adulthood</u>

a) Outline of experimental procedures for adolescent exposed mice. **b**) Acute E-gel consumption after adolescent exposure to CTR or THC gelatin during adolescence. **c**) Same as in B except for male and female mice separated out. Student's T-test (*p<0.05, **p<0.01).

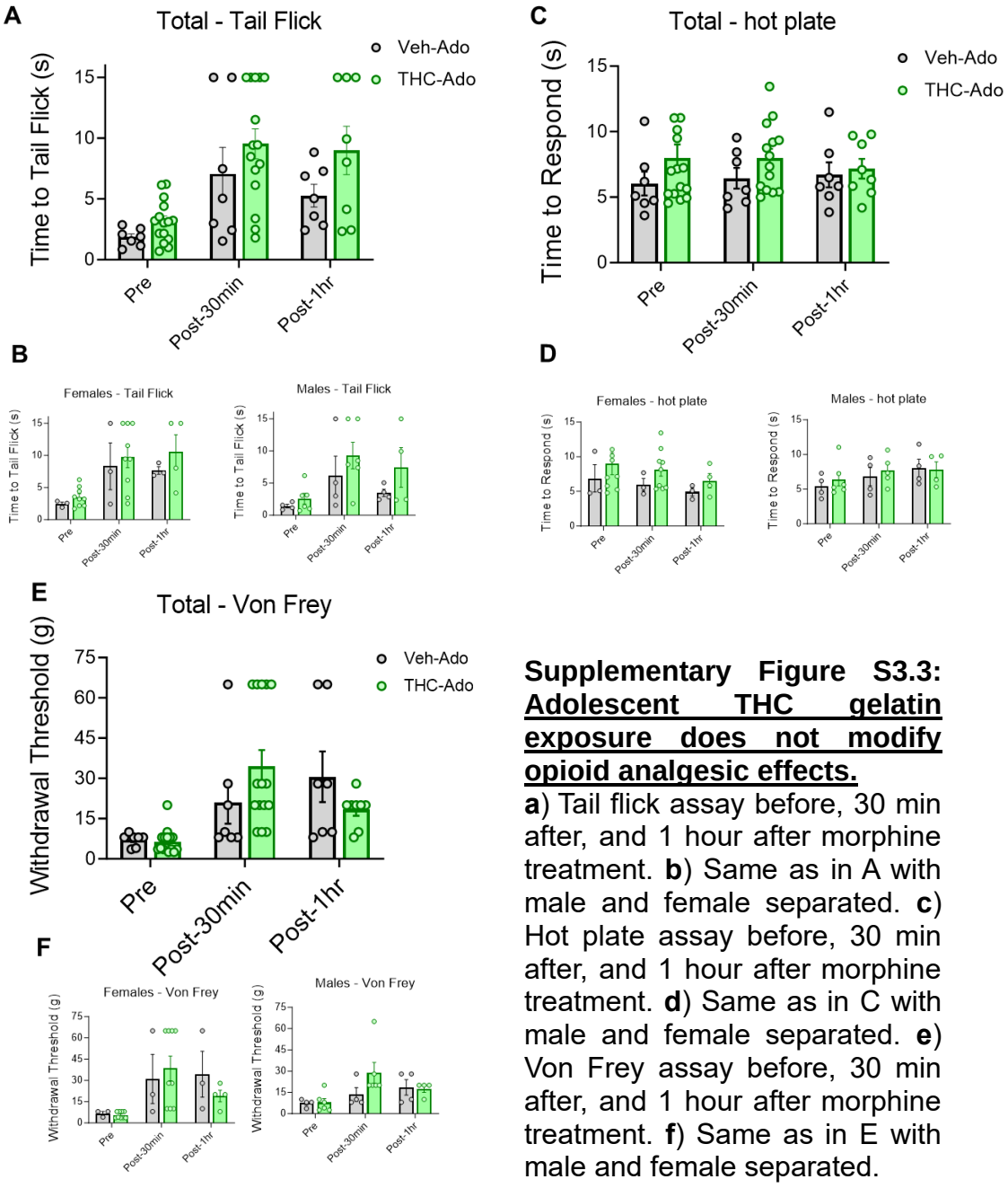

Supplementary Figure S3.3: <u>Adolescent THC gelatin exposure does not modify opioid analgesic effects.</u>
a) Tail flick assay before, 30 min after, and 1 hour after morphine treatment. **b**) Same as in A with male and female separated. **c**) Hot plate assay before, 30 min after, and 1 hour after morphine treatment. **d**) Same as in C with male and female separated. **e**) Von Frey assay before, 30 min after, and 1 hour after morphine treatment. **f**) Same as in E with male and female separated.

Day	1	2	3	4	5	6	7	8	9	10	11	12	13	14	15
E-gel	VEH			VEH	VEH	0.5	1	2			3	4	5	5	5

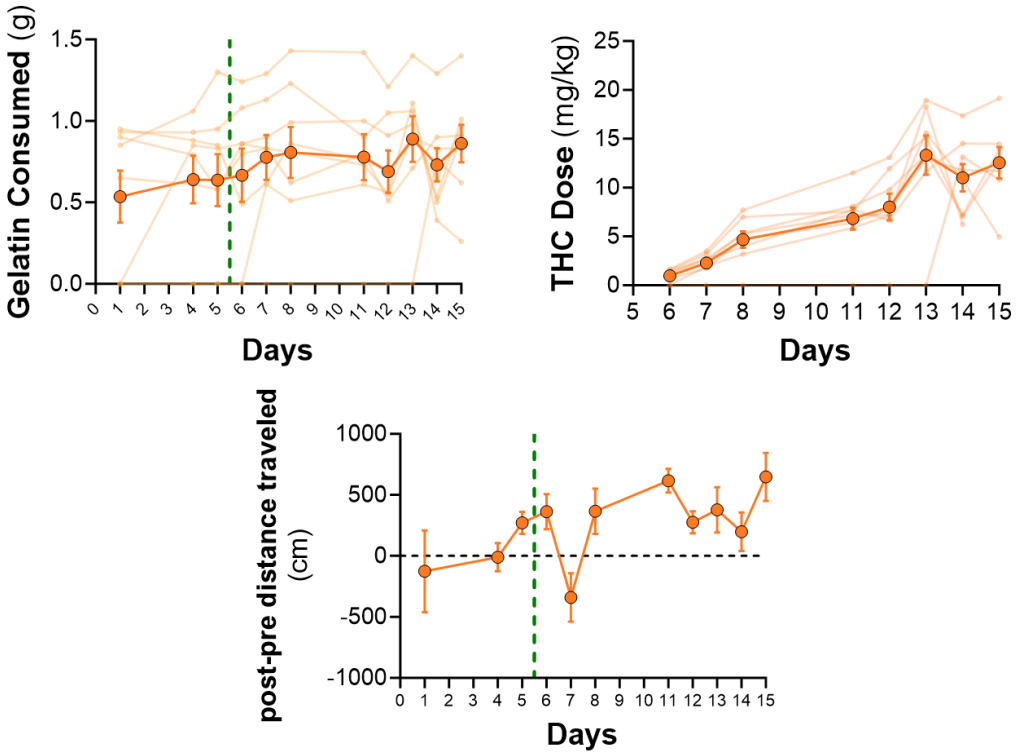

Supplementary Figure 3.4: <u>Alternative THC ramping exposure during adolescence</u>

Gelatin consumption to E-gel over adolescence with increasing THC dose. Gelatin consumed and concentrated THC dose one each day of THC-E-gel exposure. Locomotion pattern on each day measured to assess cannabimimetic response/tolerance over time.

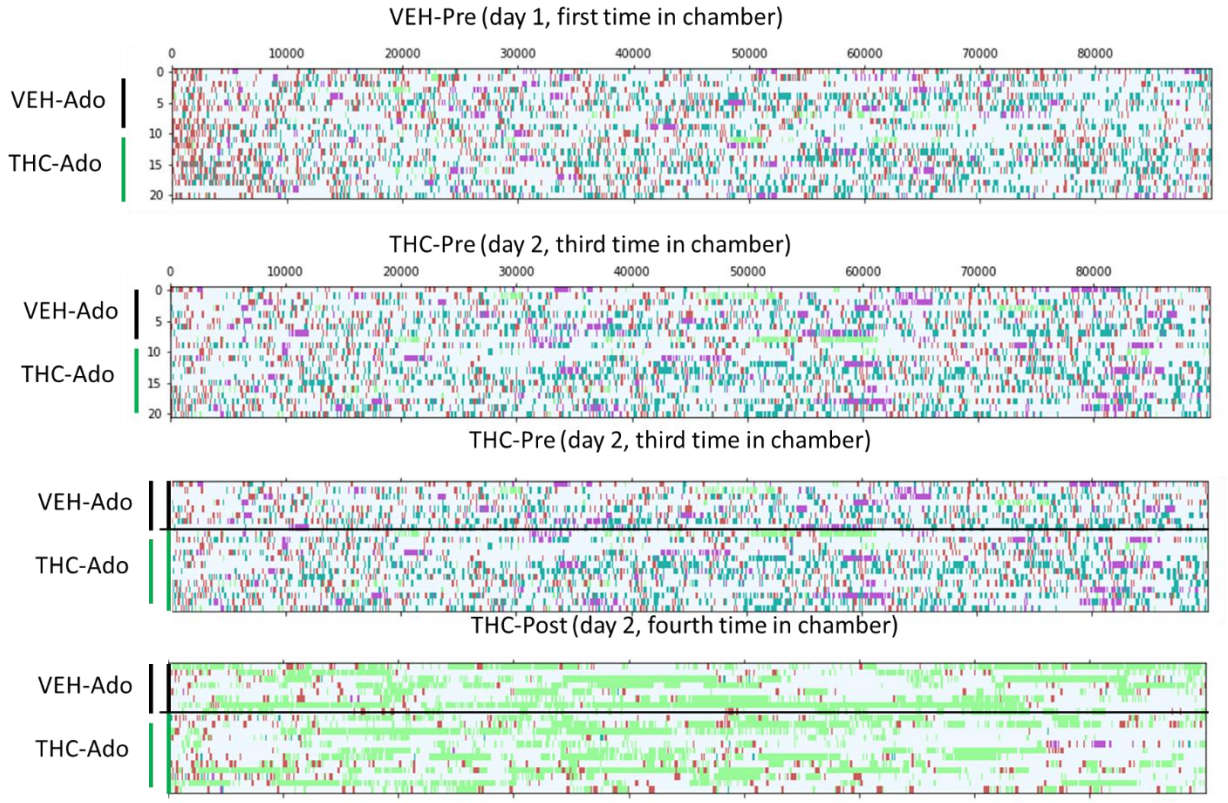

Supplementary Figure S3.5: <u>Linear track behavioral ethogram of mice treated with vehicle or THC during adolescence.</u>
Behavioral ethograms track presence of walking (red), rearing (blue), grooming (purple), laying on belly (green), or other behaviors (white) over the 15 minute sessions.

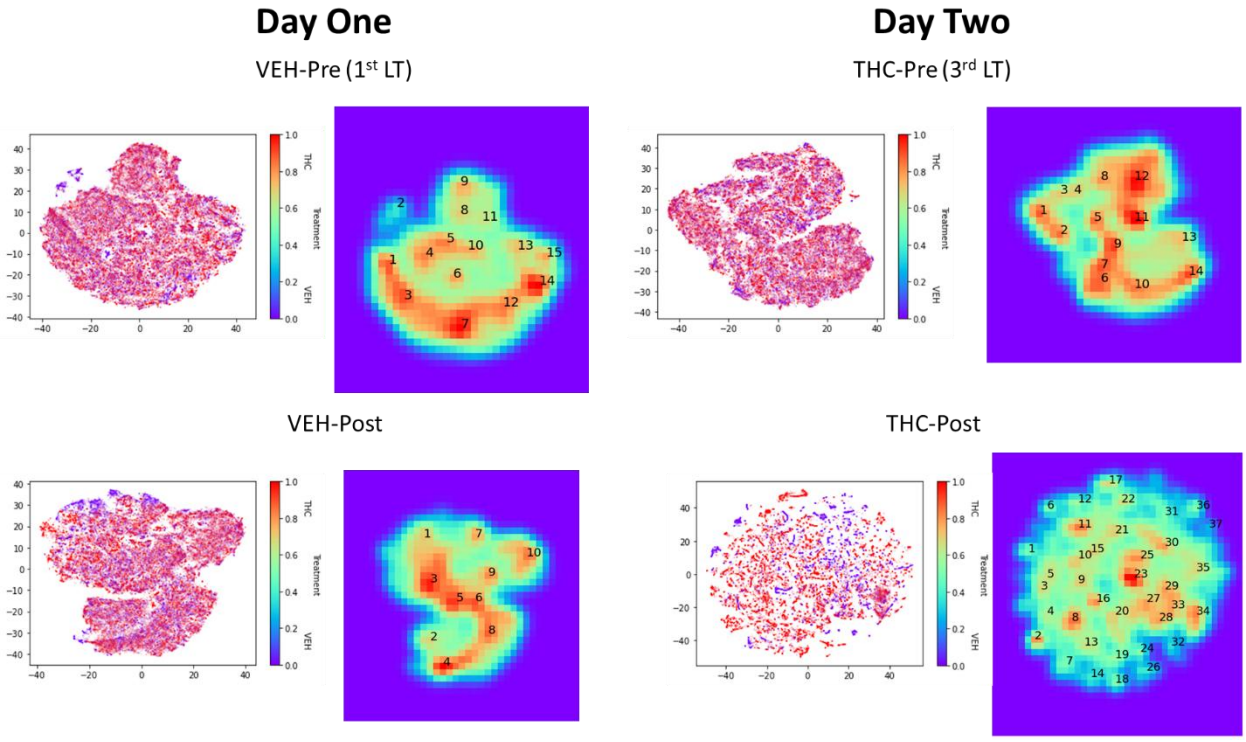

Supplementary Figure S3.6: <u>Unsupervised clustering and segmentation of linear track behavior after vehicle or THC adolescent exposure.</u>
Frames from experimental sessions from Figure S3.5 were fed into dimensionality reduction algorithms (tSNE). Watershed clustering algorithm was applied to assess segmentation trends over time.

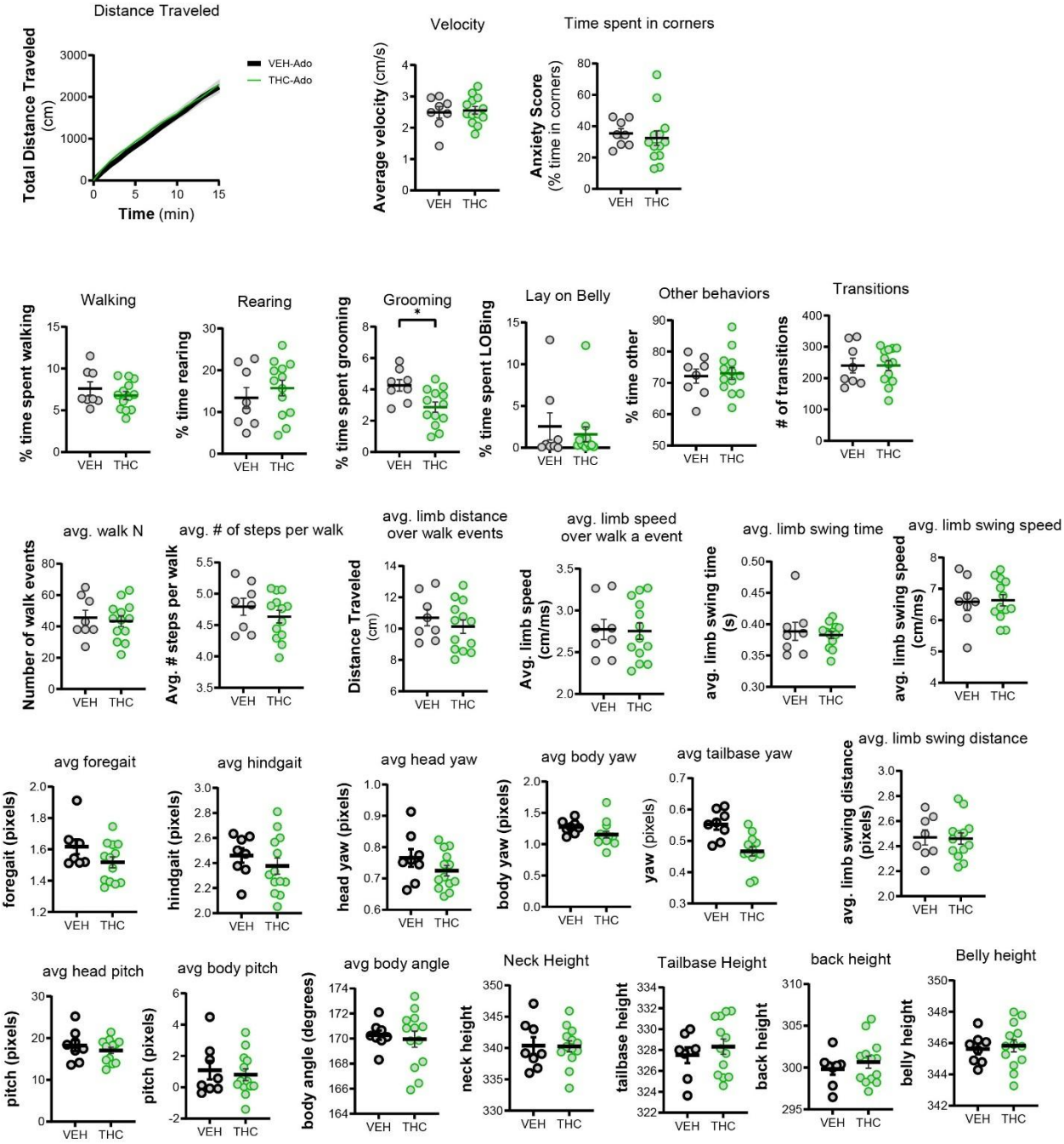
Distance Traveled
Total Distance Traveled (cm)
Time (min)
VEH-Ado
THC-Ado
Velocity
Average velocity (cm/s)
Time spent in corners
Anxiety Score (% time in corners)
Walking
% time spent walking
Rearing
% time rearing
Grooming
% time spent grooming
Lay on Belly
% time spent LOBing
Other behaviors
% time other
Transitions
# of transitions
avg. walk N
Number of walk events
avg. # of steps per walk
Avg. # steps per walk
avg. limb distance over walk events
Distance Traveled (cm)
avg. limb speed over walk a event
Avg. limb speed (cm/ms)
avg. limb swing time
avg. limb swing time (s)
avg. limb swing speed
avg. limb swing speed (cm/ms)
avg foregait
foregait (pixels)
avg hindgait
hindgait (pixels)
avg head yaw
head yaw (pixels)
avg body yaw
body yaw (pixels)
avg tailbase yaw
yaw (pixels)
avg. limb swing distance
avg. limb swing distance (pixels)
avg head pitch
pitch (pixels)
avg body pitch
pitch (pixels)
avg body angle
body angle (degrees)
Neck Height
neck height
Tailbase Height
tailbase height
back height
back height
Belly height
belly height
VEH
THC

Supplementary Figure S3.7: Linear track behavioral quantifications after vehicle or THC adolescent exposure

General metrics such as total distance traveled, average velocity, and anxiety score (measured by time spent in corners) recorded for mice exposed to vehicle or THC gelatin during adolescence. Quantification of percent time spent walking, rearing, grooming, laying on belly, and other behaviors measured over the entire session. Transition frequency between the 5 core behaviors were quantified. Collecitve locomotor kinematics were measured (walk N, average step N, average stride distance, average stride time, average stride speed, average swing distance, average swing time, average swing speed, average forepaw gait width, average hindpaw gait width, average head yaw, average body yaw, average tailbase yaw, average head pitch, average body pitch, average body angle, average neck height, average tailbase height, average back height, and average belly height) averages measured across all walk events of an animal's experimental session.

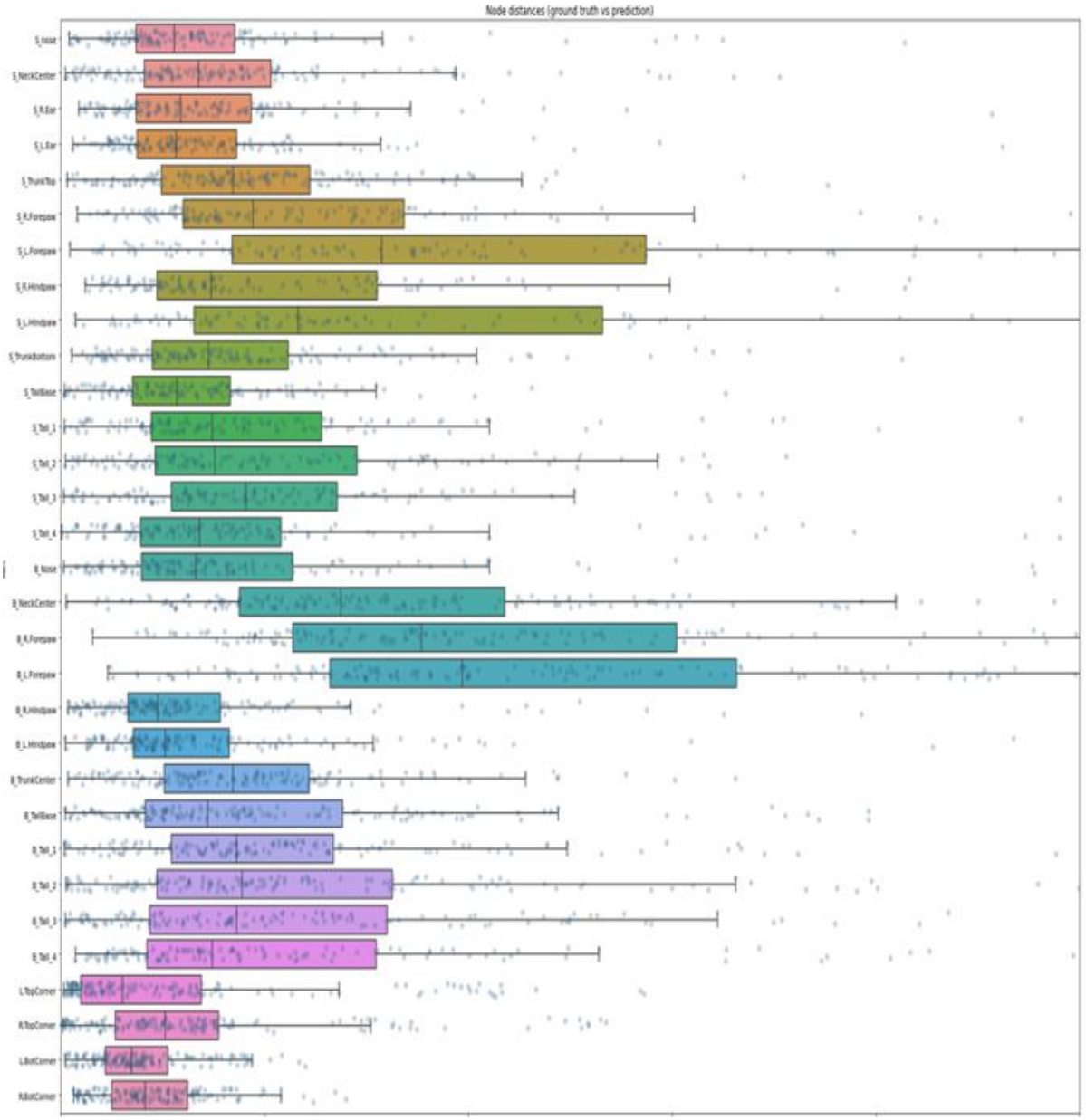

Supplementary Figure S4.1: <u>Pixel error range of individual points of interest from pose estimation.</u>
Individual Key points error from true state hand labels from the hand-labeled dataset were used to calculate pixel range.

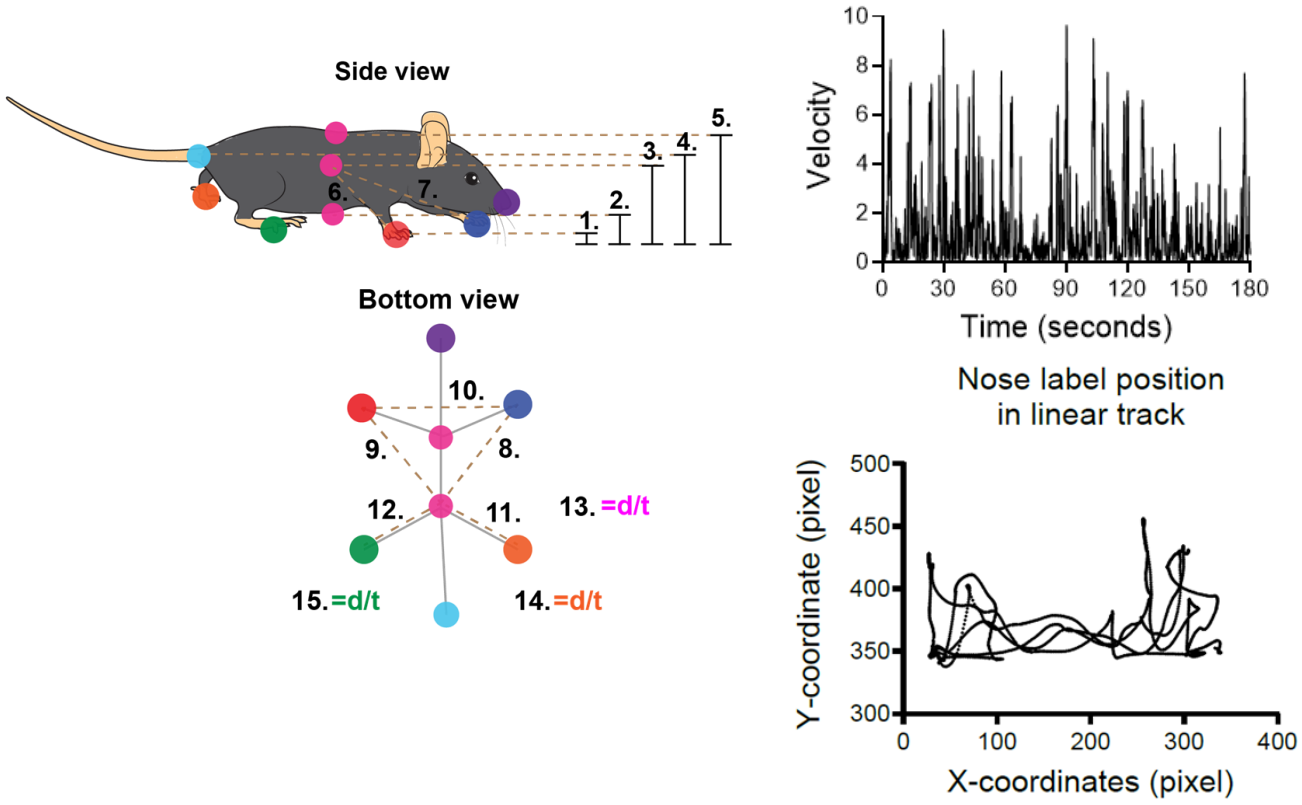

Supplementary Figure S4.2: <u>Pose estimation tracking feature selection</u>
a) Schematic of feature calculations for tSNE representations from side and bottom views within the linear track. **b**) Velocity of nose point throughout a 3 minute session to exemplify walking identification. **c**) Point tracking of nose x and y coordinated over 1 minute session trails trajectory of mouse within linear track.

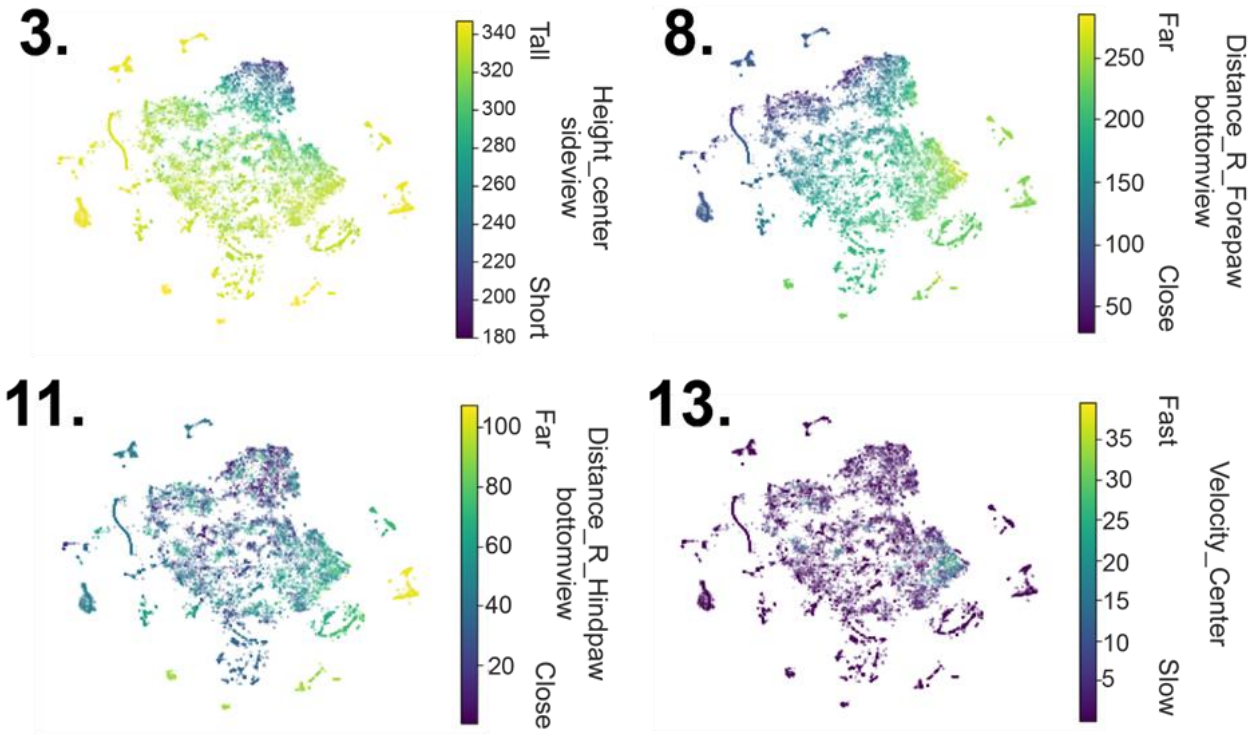

Supplementary Figure S4.3: <u>Feautre contributions to unsupervised clustering approach of lienar track behavior</u>

Features 3, 8, 11, and 13 (center height, right forepaw distance from center, right hindpaw distance from center, and velocity of center, respectively) with relative contributions across a 2D tSNE of mice treated with vehicle and THC.

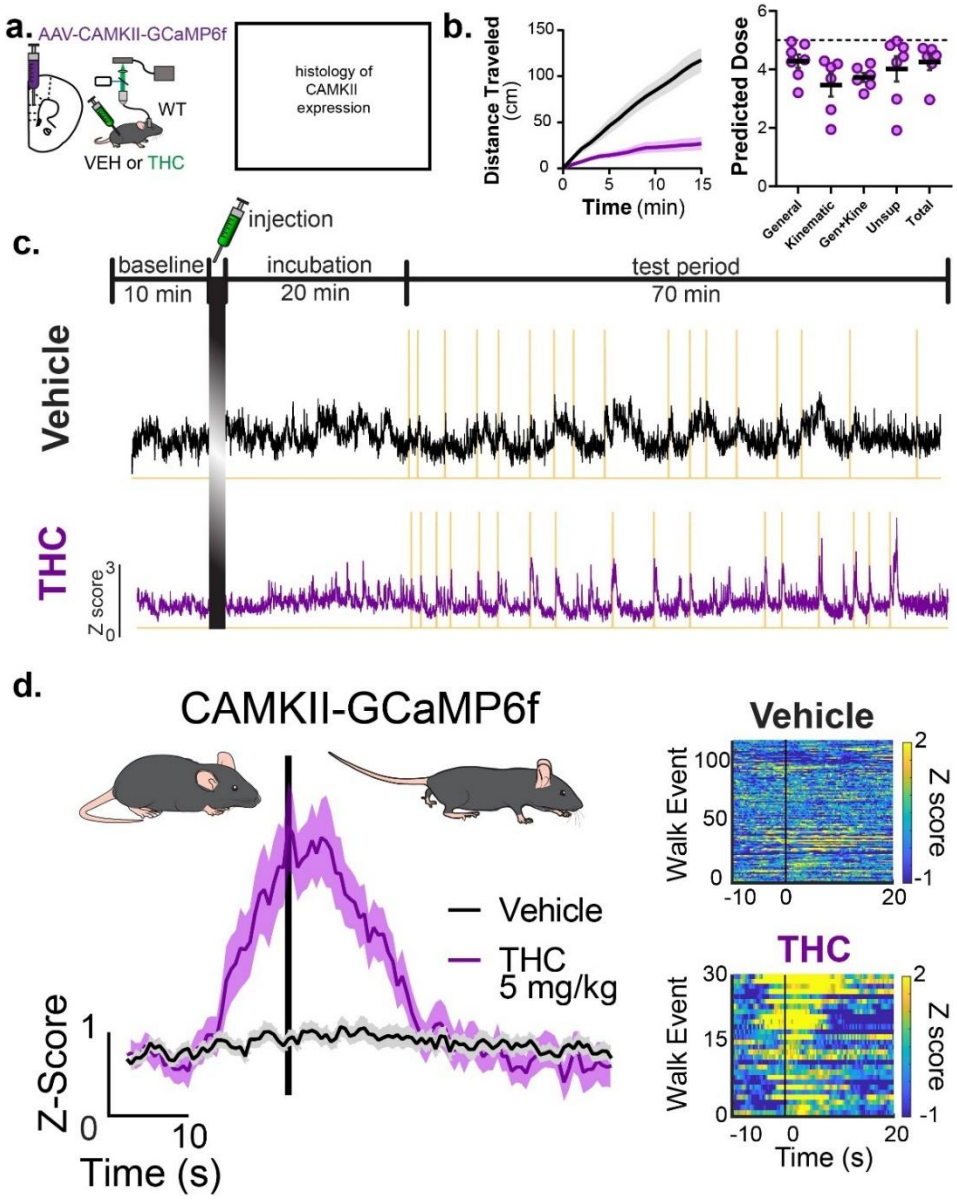

Supplementary Figure S4.4: <u>CAMKII activation during THC impaired behavior</u>

a) CAMKII neurons in the mPFC selected for GCaMP expression and then tested within the linear track. **b**) Total distance traveled and dose prediction shows consistent and robust THC cannabimimetic effects. **c**) Example animal over a 100 minute session with walk events labeled during the 70 min test period. **d)** Neural Z-score trace of vehicle and THC treated mice time-locked to walk initiation.

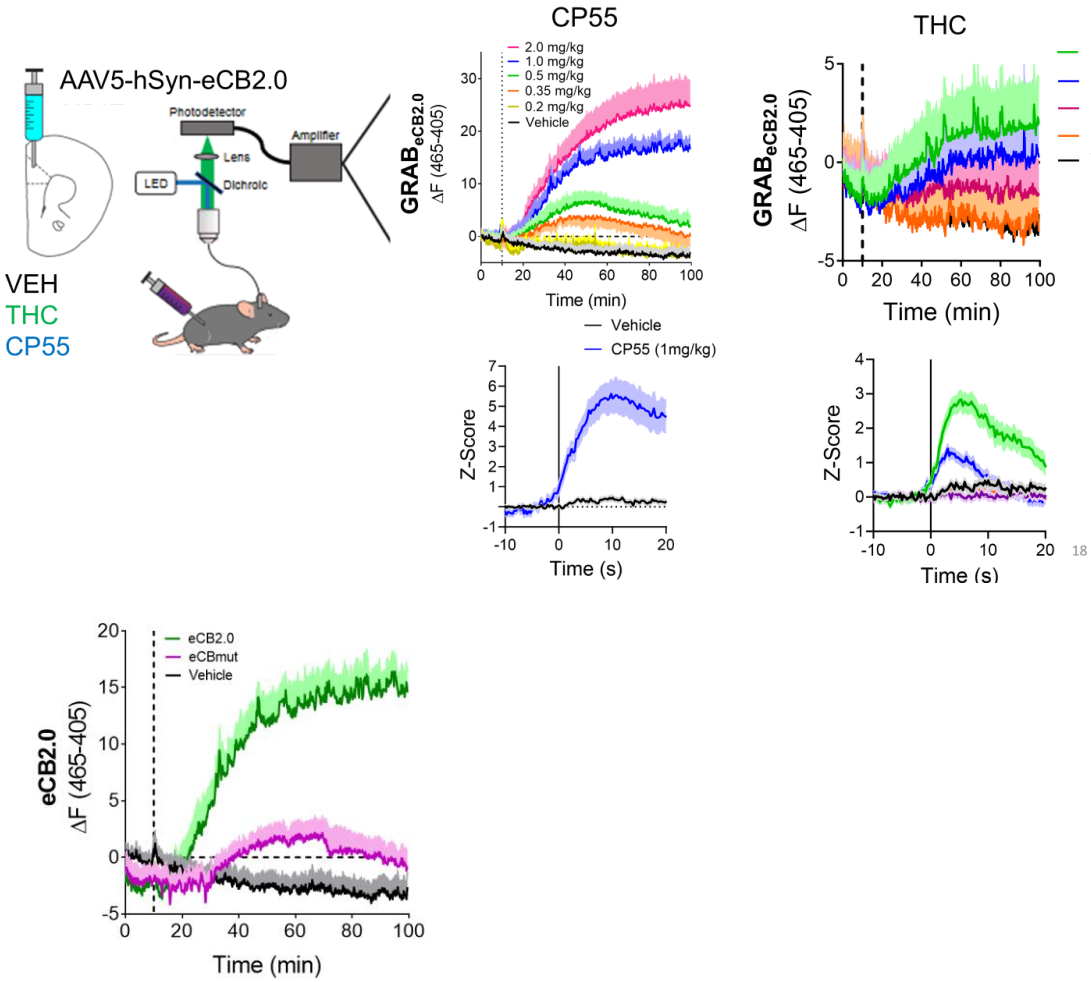

Supplementary Figure S4.5: GRAB$_{eCB2.0}$ validation in vivo

GRAB$_{eCB2.0}$ was virally expressed the mPFC of WT mice and then fiber photometric recordings taken for a 100 minute session with an injection of a pharmacological agent at 10 minutes. Synthetic CB1 agonist CP55 administration produced dose-dependent increases in total signal and an increase in GRAB$_{eCB2.0}$ signal at walk initiation. THC also induced dose-dependent increase over the session with high dose increasing at walk initiation. Mutant GRAB$_{eCB2.0}$ blocked some, but not all, of the GRAB$_{eCB2.0}$ signal by CP55.

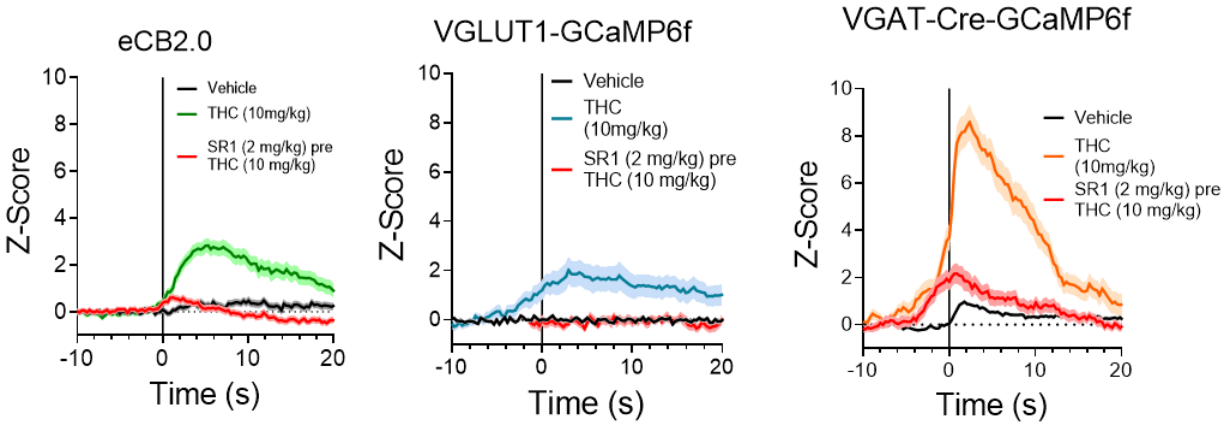

Supplementary Figure S4.6: <u>GRAB$_{eCB2.0}$ blockade by CB1 receprot antagonist SR1</u>

GRAB$_{eCB2.0}$, and GCaMP6f expressed in glutamatergic or GABAergic neurons produce robust signal at walk initiation. SR1 antagonism blocks THC activity to reduce this signal in all cases.

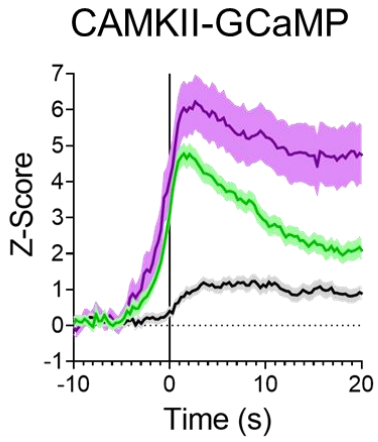

Supplementary Figure S4.7: <u>DAGL inhibition enhances CAMKII signal</u>
DO34 (20 mg/kg) pre-treatment to THC (5 mg/kg) injection blocks 2-AG synthesis leading to enhanced CAMKII-driven GCaMP activity during walk initiation.

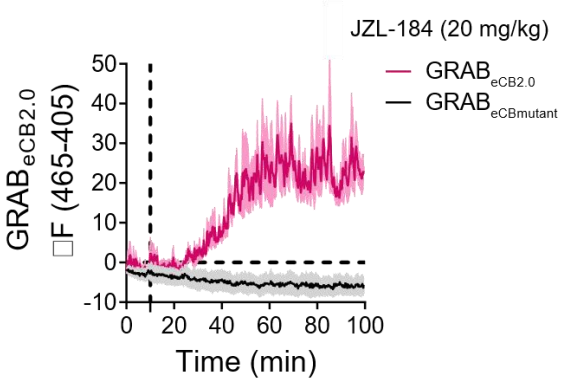

Supplementary Figure S4.8: <u>2-AG accumulation induces robust GRAB$_{eCB2.0}$ signal.</u>
Systemic Injection of 20 mg/kg JZL-184 induces a slow but robust accumulation of endocannabinoids as measured by in vivo mPFC GRAB$_{eCB2.0}$ expression.

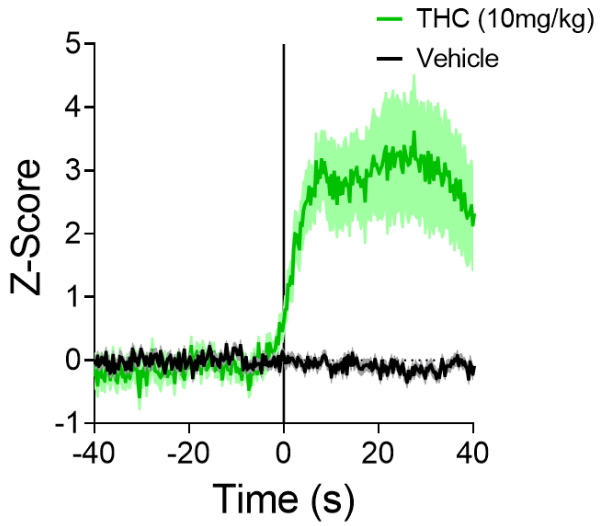

Supplementary Figure S4.9: $GRAB_{eCB2.0}$ expression in the NAc reveals a similar THC impaired locomotor effect.
Expression of $GRAB_{eCB2.0}$ in the NAc reveals a THC-dependent increase in activity at walk initiation that does not diminish as readily as seen in mPFC $GRAB_{eCB2.0}$ THC impairment.

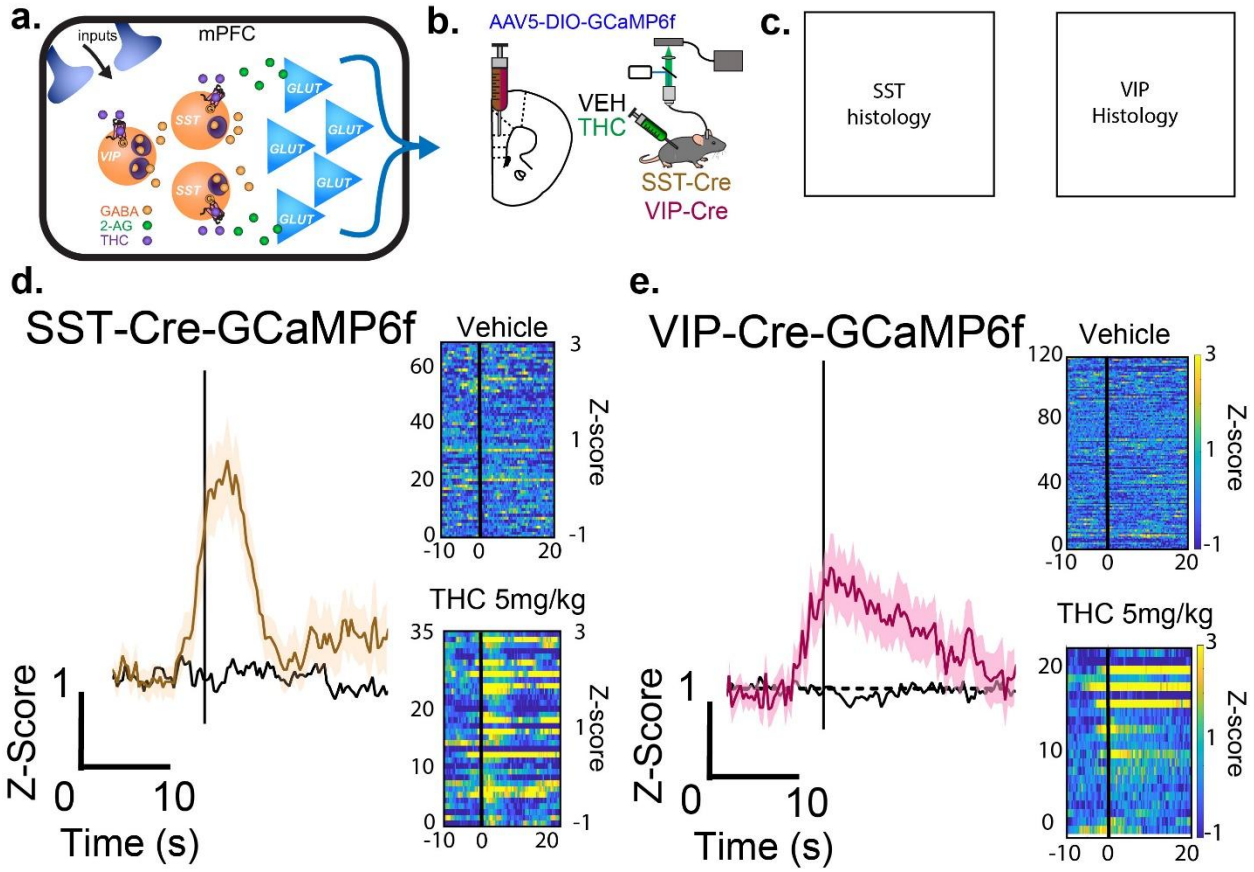

Supplementary Figure S4.10: <u>mPFC GABaergic neuronal subtypes produce differential activities.</u>

a) Circuit diagram displays balances of somatostatin (SST) and vaso-intestinal peptide (VIP) inhibitory neurons involved in disinhibition to modulate the excitatory signal during THC impaired walking. **b-c**) GCaMP6f was virally expressed in the mPFC of SST-Cre and VIP-Cre mice to select for neuronal populations. **d)** Somatostatin GCaMP6f Z-score signal at walk initiation in vehicle and THC 5mg/kg treated mice. **e)** Same as in **d**, except with VIP-Cre-GCaMP6f animals.

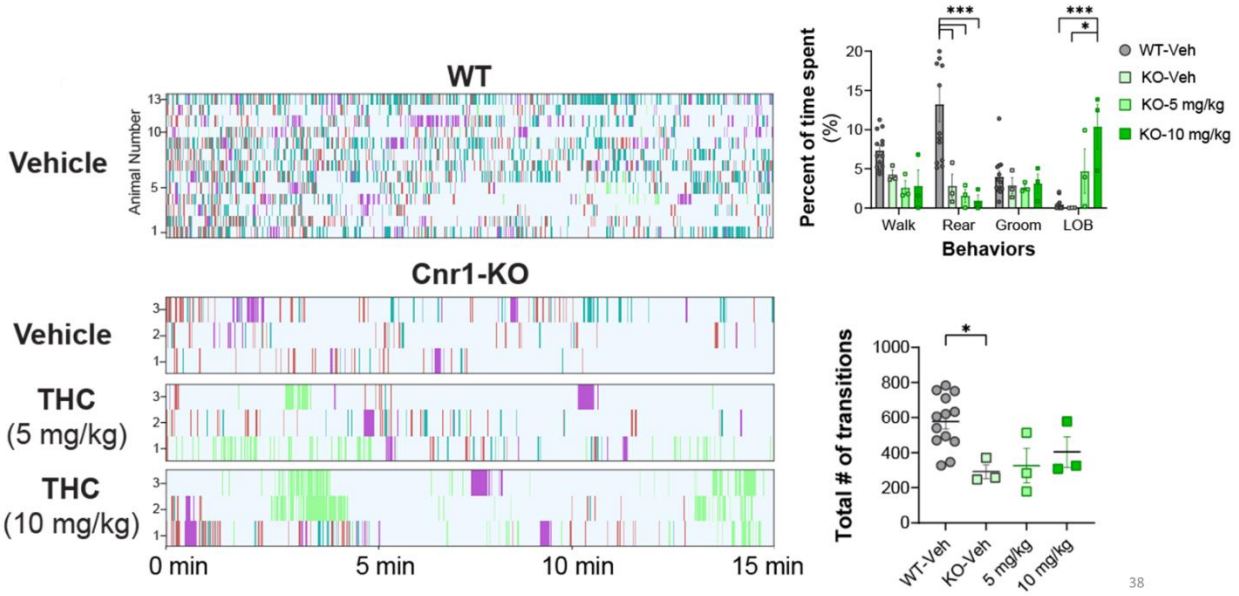

Supplementary Figure S4.11: <u>Linear track pose estimation reveals behavioral differences in Cnr1 knockout mice.</u>
Behavioral ethograms of WT and Cnr1-KO animals treated with vehicle or THC at 5 and 10 mg/kg. Cnr1-KO animals behaved differently in the vehicle condition compared to WT mice and showed little THC dependent effects.

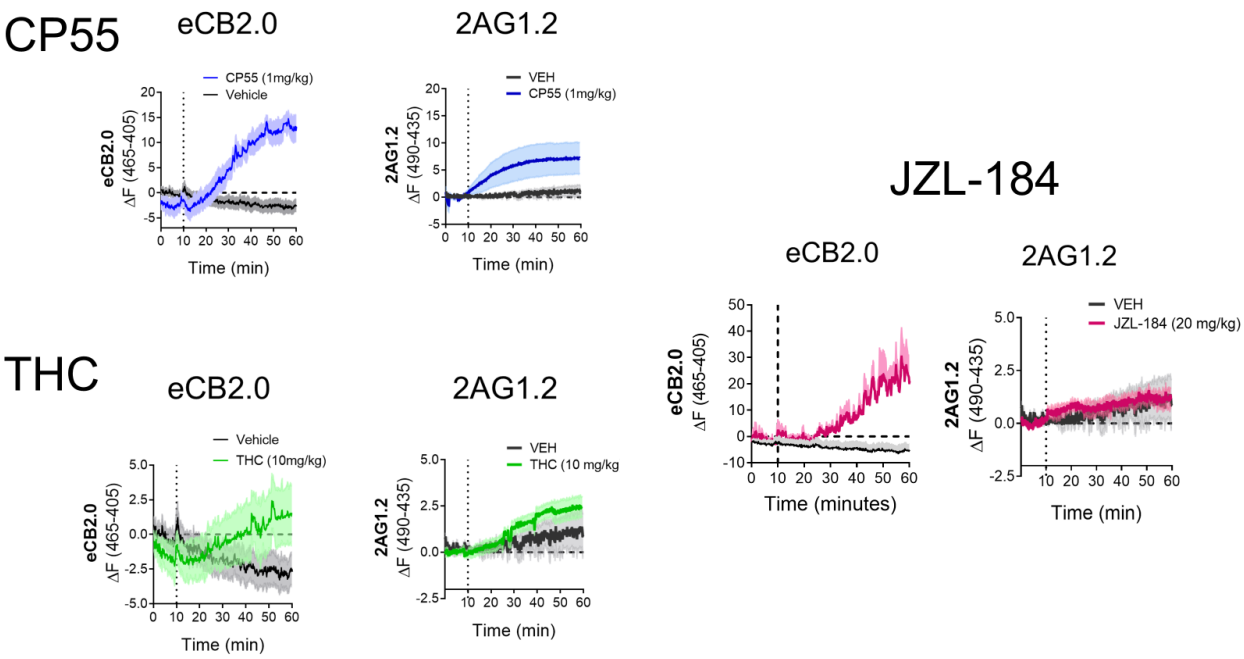

Supplementary Figure S4.12: <u>2-AG specific sensor in vivo struggles to differentiate activity of agonists and eCBs</u>

CP55 and THC produced signal increases at the 2AG1.2 biosensor developed by the Yulong Li lab. Treatment with JZL-184 which should cause accumulation of 2-AG did not produce a robust signal increase.

Supervised Behavioral Classification Model

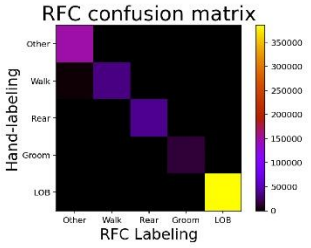

	precision	recall	f1-score
0.0	0.978	0.985	0.981
1.0	0.971	0.951	0.961
2.0	0.978	0.978	0.978
3.0	0.989	0.975	0.982
4.0	0.999	0.999	0.999
accuracy			0.991
macro avg	0.983	0.978	0.980
weighted avg	0.991	0.991	0.991

Supervised Dose Prediction Model

MSE = 0.4816

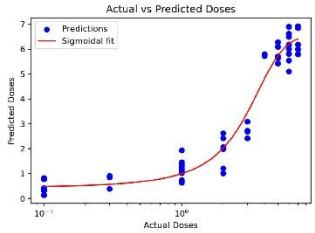

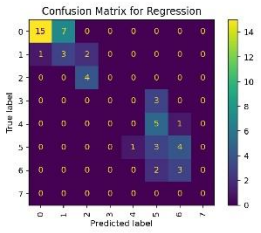

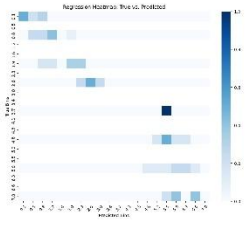

Kinematic Dose Prediction Model

MSE = 0.9235

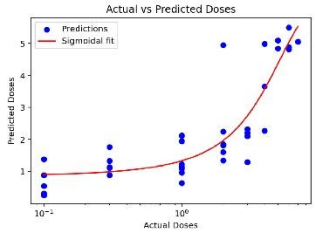

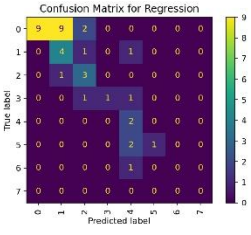

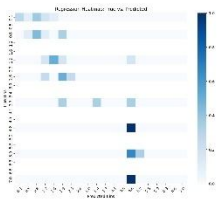

Total Behavioral Dose Prediction Model

MSE = 0.4711

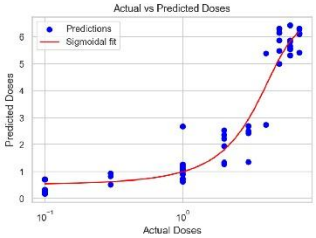

Pre-Walk Classification Model

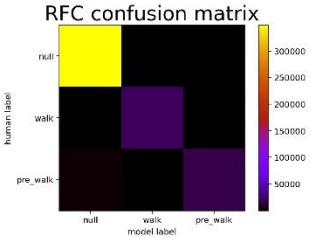

	precision	recall	f1-score
0.0	0.993	0.999	0.996
1.0	0.964	0.972	0.968
2.0	0.988	0.876	0.929
accuracy			0.992
macro avg	0.982	0.949	0.964
weighted avg	0.991	0.992	0.991

Supplementary Figure S4.13: Algorithm metrics for dose prediction and RFC classification algorithms use in chapter 4.
a) Supervised Classification algorithm to identify walking, rearing, grooming, and laying on belly confusion matrix (other behaviors classified as everything else) with their precision and recall scores for each behavior. **b-d)** Supervised (**b**), kinematic (**c**), and general behavior (combined unsupervised and supervised, **d**) dose prediction models built from THC-treated videos. Actual versus predicted dose ranges with confusion matrices for model accuracy. **e**) Supervised Classification algorithm to identify pre-walk, walk, and other behaviors built for closed-loop optogenetic stimulation experiments with a confusion matrix and precision and recall values.

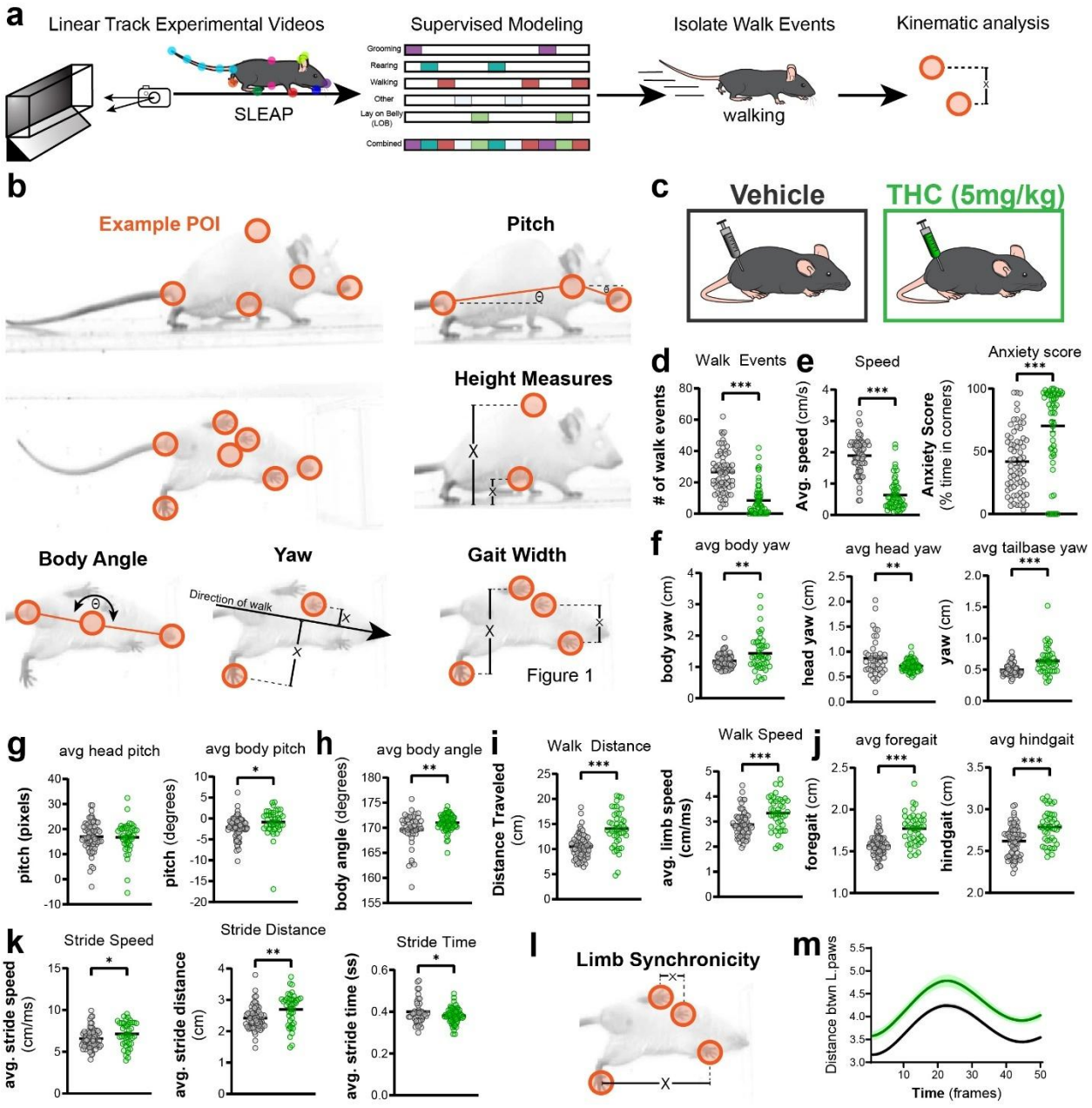
a
Linear Track Experimental Videos
SLEAP
Supervised Modeling
Grooming
Rearing
Walking
Other
Lay on Belly (LOB)
Combined
Isolate Walk Events
walking
Kinematic analysis
b
Example POI
Pitch
Height Measures
Body Angle
Yaw
Direction of walk
Gait Width
Figure 1
c
Vehicle
THC (5mg/kg)
d
Walk Events
# of walk events
e
Speed
Avg. speed (cm/s)
Anxiety score
Anxiety Score (% time in corners)
f
avg body yaw
body yaw (cm)
avg head yaw
head yaw (cm)
avg tailbase yaw
yaw (cm)
g
avg head pitch
pitch (pixels)
avg body pitch
pitch (degrees)
h
avg body angle
body angle (degrees)
i
Walk Distance
Distance Traveled (cm)
Walk Speed
avg. limb speed (cm/ms)
j
avg foregait
foregait (cm)
avg hindgait
hindgait (cm)
k
Stride Speed
avg. stride speed (cm/ms)
Stride Distance
avg. stride distance (cm)
Stride Time
avg. stride time (ss)
l
Limb Synchronicity
m
Distance btwn L paws
Time (frames)

Supplementary Figure S4.14: Kinematic analysis of locomotor behavior in the linear track

a) Schematic of kinematic analysis pipeline for videos recorded in the linear track. **b**) Example outline for key metrics as measured by their changes in key point metrics over the course of walk events. **c**) For these examples, mice treated with either vehicle or THC 5mg/kg (WT mice) were calculated. **d**) total number of walk events during 15 minute session. **e**) Speed and anxiety score metrics. **f**) Lateral displacement metrics (yaw) measured for body center, tailbase, and head during walking. **g**) Average angular pitch in head and body during walking. **h**) average body angle from nose to tail base during body center. **I**) Average walk distance and walk speed. **j**) average forepaw and hindpaw gait width during walking. **k**) stride distance, speed and time. **l**) schematic for tracking synchronicity of limbs. **m**) limb synchronicity after vehicle or THC 5mg/kg treatment. Student's T-test, no multiplicity corrections performed (*p<0.05, **p<0.01, ***p<0.001).

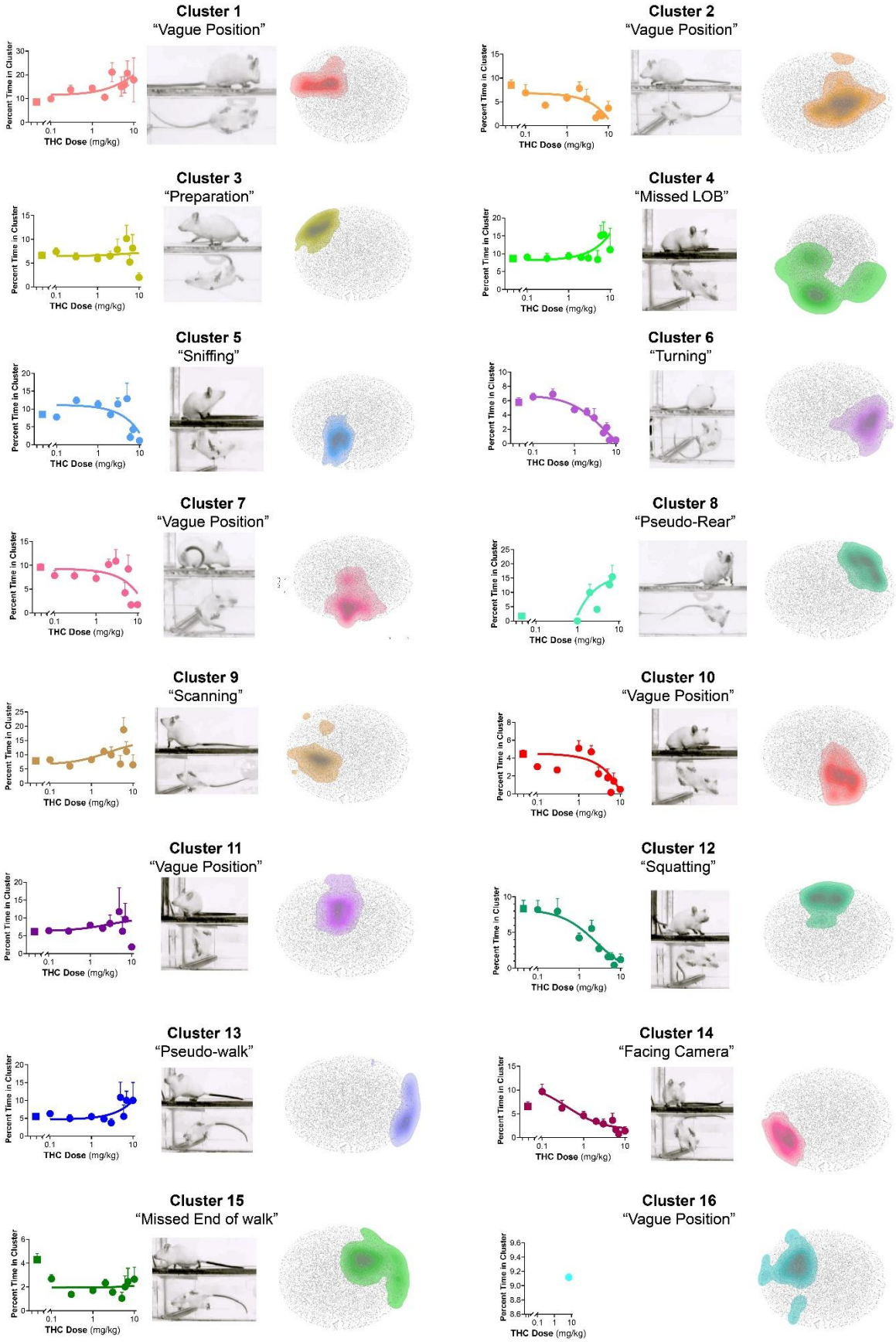
Cluster 1
"Vague Position"
Cluster 2
"Vague Position"
Cluster 3
"Preparation"
Cluster 4
"Missed LOB"
Cluster 5
"Sniffing"
Cluster 6
"Turning"
Cluster 7
"Vague Position"
Cluster 8
"Pseudo-Rear"
Cluster 9
"Scanning"
Cluster 10
"Vague Position"
Cluster 11
"Vague Position"
Cluster 12
"Squatting"
Cluster 13
"Pseudo-walk"
Cluster 14
"Facing Camera"
Cluster 15
"Missed End of walk"
Cluster 16
"Vague Position"
Percent Time in Cluster
THC Dose (mg/kg)

Supplementary Figure S4.15: Unsupervised clusters represent nuanced, THC-dependent effects.
All clustered behaviors have accompanying THC dose response curves plotted in their representative colors, an example screenshot image of the behavior, and a relative density map representation overlaid to a 2D tSNE visualization of the high-dimensional dataset. This was done for Clusters 1 (“Vague Position”), 2 (“Preparation”), 3 (“Vague Position”), 4 (“Missed Lay on BElly”), 5 (“Sniffing”), 6 (“Turning”), 7 (“Vague Position”), 8 (“Pseudo-Rear”), 9 (“Scanning”), 10 (“Vague Position”), 11 (“Vague Position”), 12 (“Squatting”), 13 (“Pseudo-walk”), 14 (“facing camera”), 15 (“Missing end of walk”), 16 (“Vague Position”)

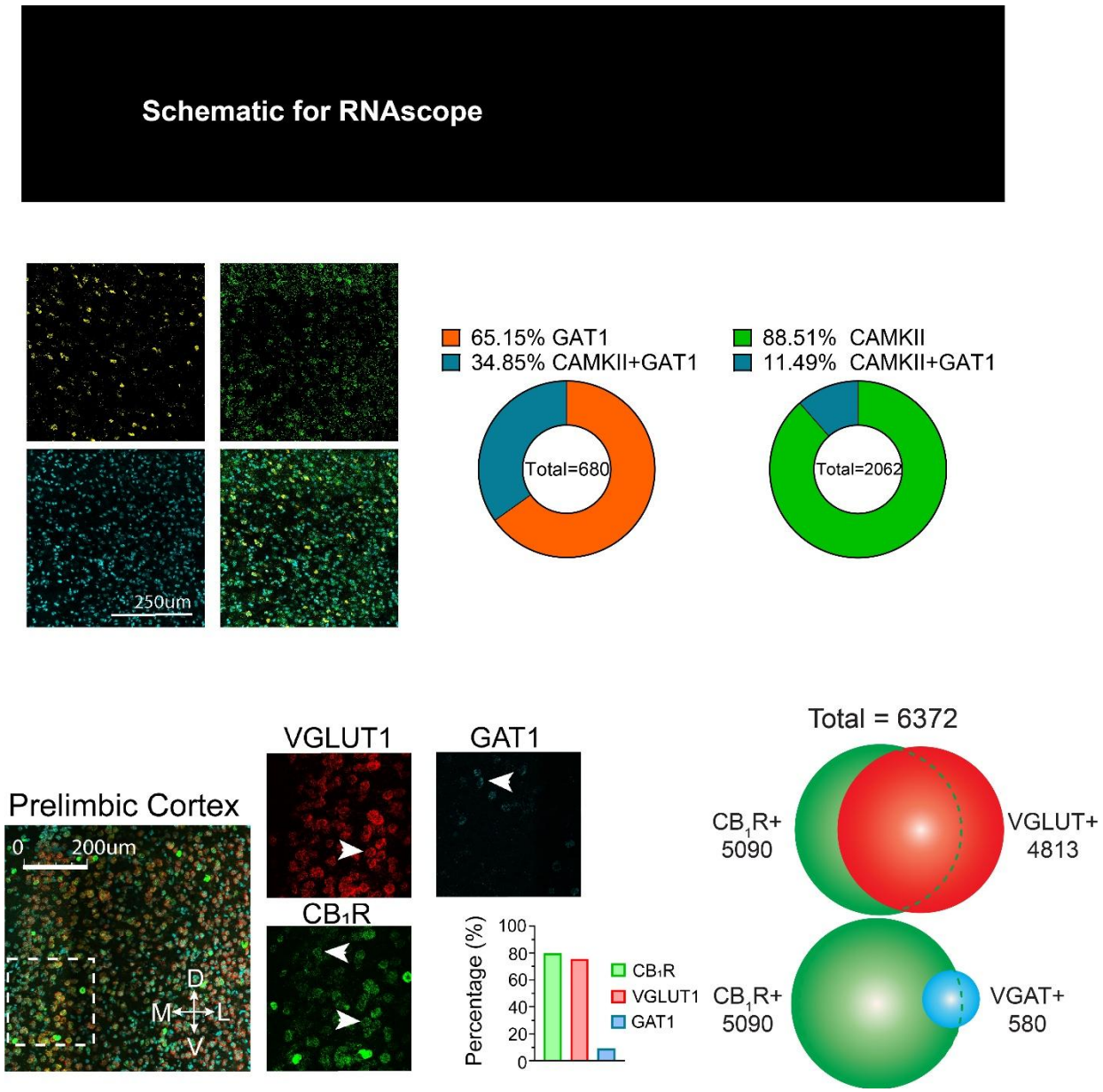

Supplementary Figure S4.16: <u>RNAscope analysis of mPFC CB1R expression.</u> **a**) Schematic for RNAscope in situ hybridization experimentation. **b**) CMKII expression in GABAergic neurons within the mPFC. **c**) mPFC expression of Cnr1 (CB1R gene) in the PrL with RNAscope colocalization of mRNA in glutamatergic and GABAergic labeled neurons.

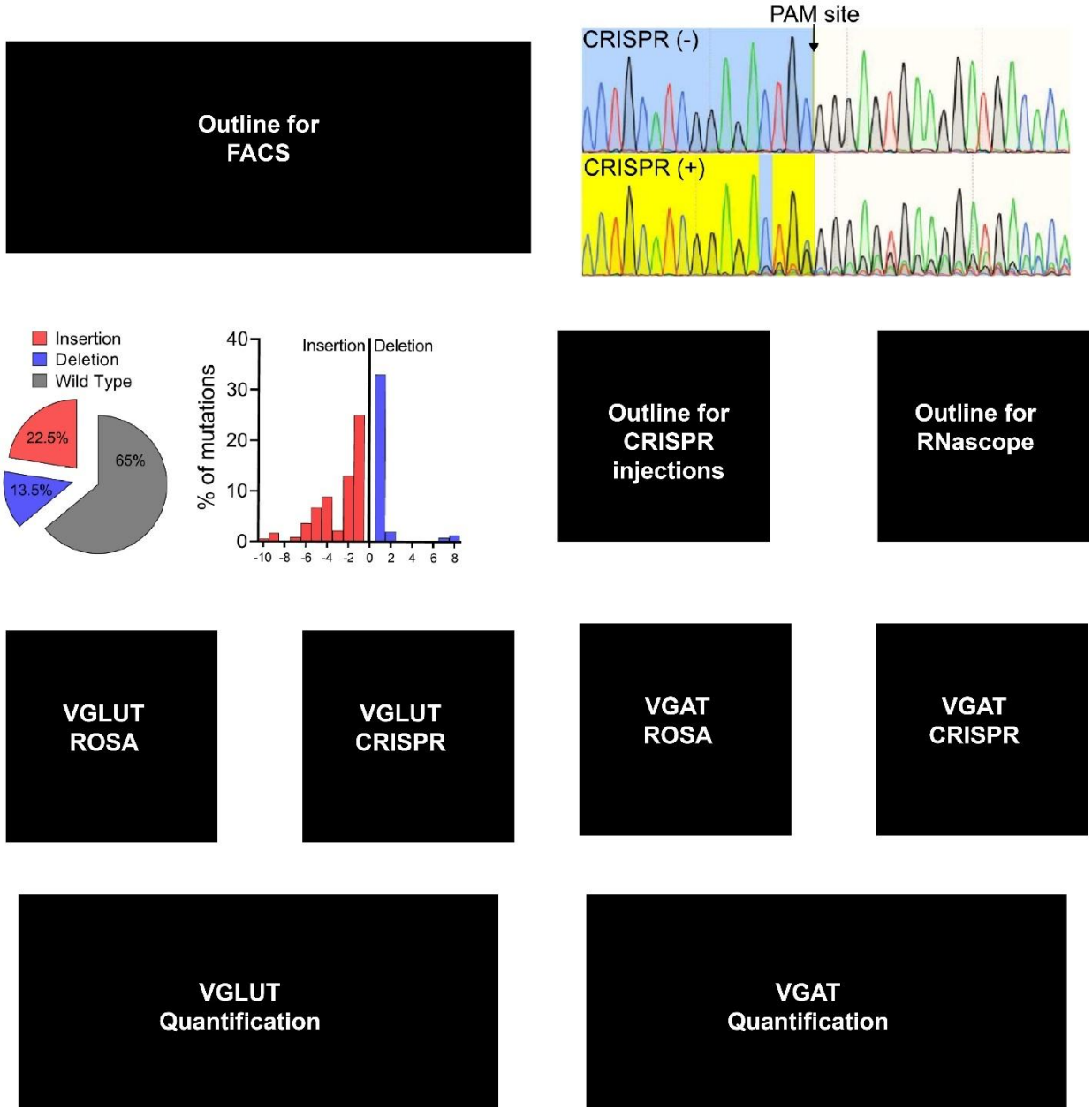

Supplementary Figure S4.17: <u>Cnr1 CRISPR validation reveals knockout of the CB1R gene.</u>

a) Schematic of FACS procedure and the genetic targeting PAM site within the CRISPR gene. **b**) Insertion/deletion frequency of Cnr1 gene of mPFC neurons. **c)** CRISPR validation of knockout in VGAT-Cre and VGLUT1-Cre neurons. **d)** CRISPR validation alongside ROSA control.

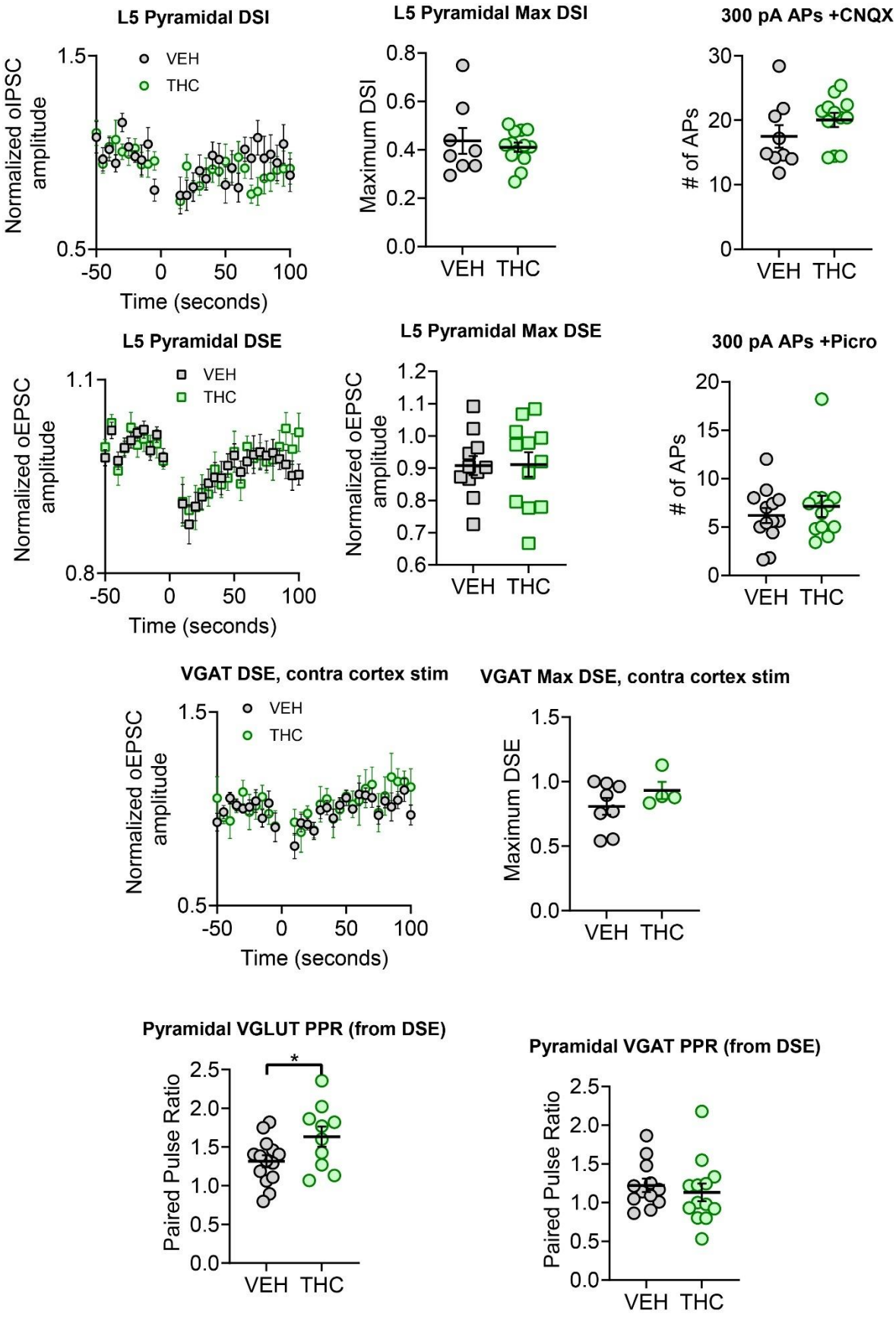
L5 Pyramidal DSI
Normalized oIPSC amplitude
VEH
THC
Time (seconds)
L5 Pyramidal Max DSI
Maximum DSI
VEH THC
300 pA APs +CNQX
# of APs
VEH THC
L5 Pyramidal DSE
Normalized oEPSC amplitude
VEH
THC
Time (seconds)
L5 Pyramidal Max DSE
Normalized oEPSC amplitude
VEH THC
300 pA APs +Picro
# of APs
VEH THC
VGAT DSE, contra cortex stim
Normalized oEPSC amplitude
VEH
THC
Time (seconds)
VGAT Max DSE, contra cortex stim
Maximum DSE
VEH THC
Pyramidal VGLUT PPR (from DSE)
Paired Pulse Ratio
*
VEH THC
Pyramidal VGAT PPR (from DSE)
Paired Pulse Ratio
VEH THC

Supplementary Figure S4.18: Electrophysiological effects of THC on mPFC E/I connectivity.
Depolarized suppression of inhibition after treatment in a vehicle or THC bath. Action potential frequency after CNQX administration. Depolarized suppression of excitation after treatment in a vehicle or THC bath. Action potential frequency after picrotoxin administration. DSE measured after vehicle or THC bath treatment from contralateral pyramidal neurons onto ipsilateral GABAergic neurons. Pyramidal paired pulse ratio measured from the DSE reveals a THC-dependent shift in glutamatergic signaling.

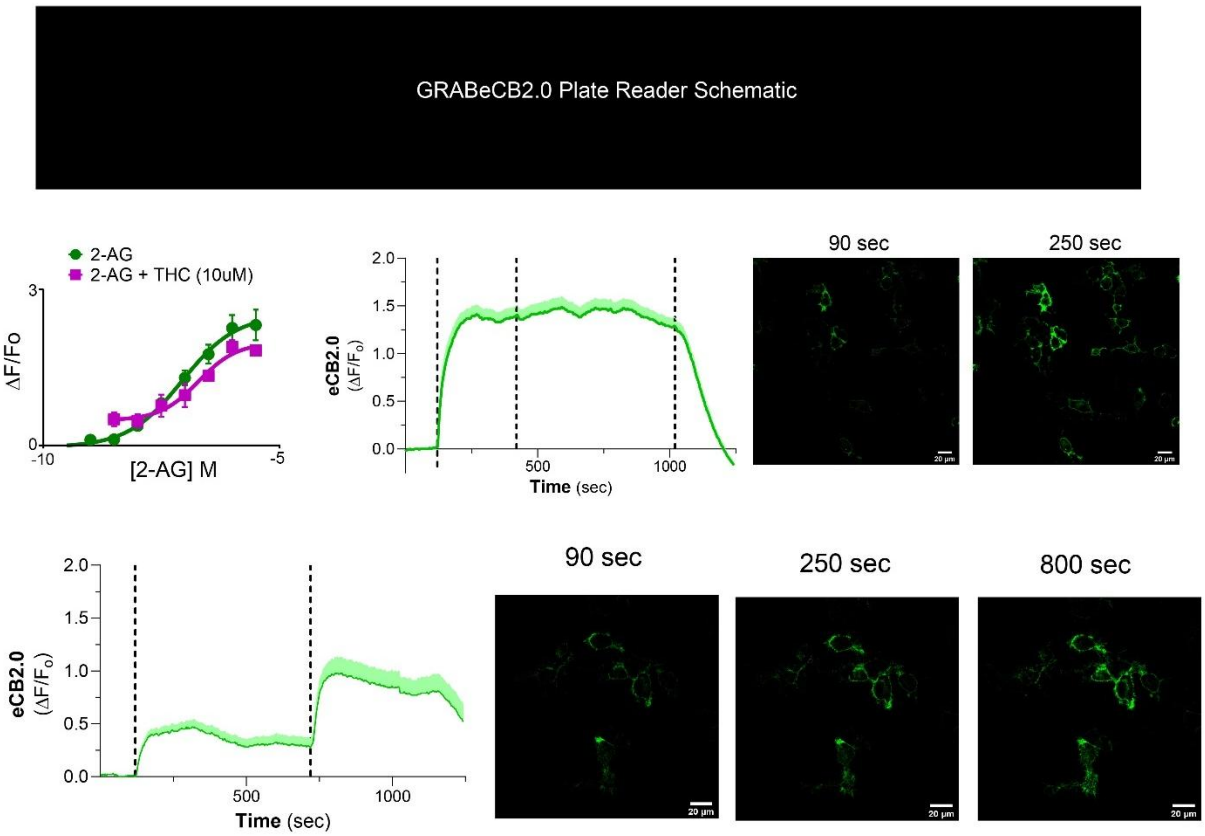

Supplementary Figure S4.19: <u>In vitro plate reader assay reveals THC-dependent activity of THC at the GRAB$_{eCB2.0}$ sensor.</u>
a) Schematic of GRAB$_{eCB2.0}$ plate reader to measure eCB activity in HEK293 cells. **b**) Quantification of 2-AG and 2-AG+THC across a concentration range with a fixed THC concentration. **c**) Live cell imaging after 2-AG administration, then a THC wash, and then a final SR1 blockade. **d)** Plate reader administration with pre-treatment with THC blocks maximal effect of 2-AG at GRAB$_{eCB2.0}$.

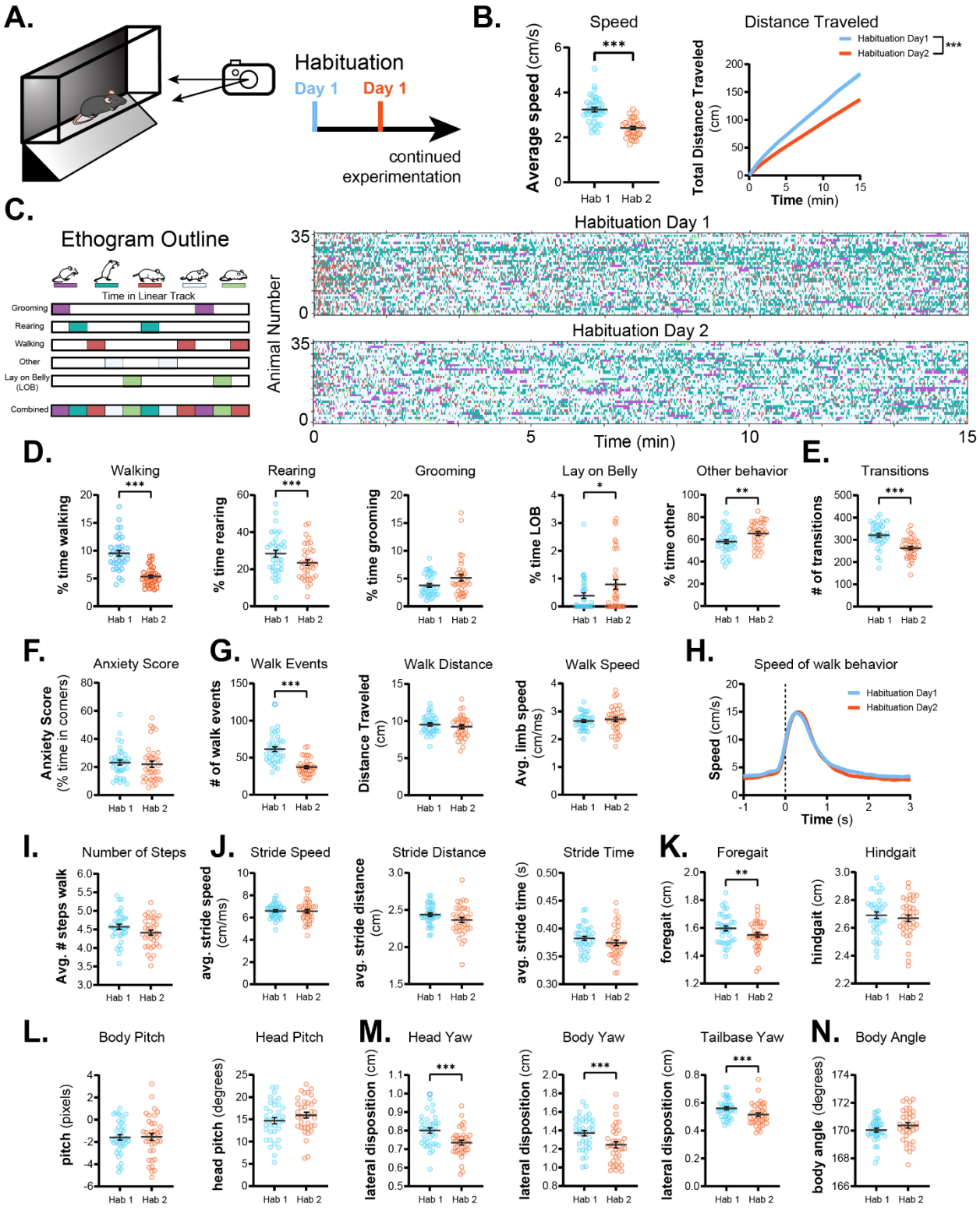
A.
Habituation
Day 1
Day 1
continued
experimentation
B.
Speed
Average speed (cm/s)
***
Hab 1
Hab 2
Distance Traveled
Habituation Day1
Habituation Day2
***
Total Distance Traveled (cm)
Time (min)
C.
Ethogram Outline
Time in Linear Track
Grooming
Rearing
Walking
Other
Lay on Belly (LOB)
Combined
Habituation Day 1
Habituation Day 2
Animal Number
Time (min)
D.
Walking
% time walking
Rearing
% time rearing
Grooming
% time grooming
Lay on Belly
% time LOB
Other behavior
% time other
E.
Transitions
# of transitions
F.
Anxiety Score
Anxiety Score (% time in corners)
G.
Walk Events
# of walk events
Walk Distance
Distance Traveled (cm)
Walk Speed
Avg. limb speed (cm/ms)
H.
Speed of walk behavior
Habituation Day1
Habituation Day2
Speed (cm/s)
Time (s)
I.
Number of Steps
Avg. # steps walk
J.
Stride Speed
avg. stride speed (cm/ms)
Stride Distance
avg. stride distance (cm)
Stride Time
avg. stride time (s)
K.
Foregait
foregait (cm)
Hindgait
hindgait (cm)
L.
Body Pitch
pitch (pixels)
Head Pitch
head pitch (degrees)
M.
Head Yaw
lateral disposition (cm)
Body Yaw
lateral disposition (cm)
Tailbase Yaw
lateral disposition (cm)
N.
Body Angle
body angle (degrees)

Supplementary Figure S4.20: <u>Habituation behavior within the linear track.</u>
a) Schematic for habituation schedule in the linear track experimentation chamber. **b)** distance traveled and speed differences between day 1 and day 2 habituation. **c)** Behavioral ethogram of habituation day 1 and day 2. **d)** Quantification of frequency for walking, rearing, grooming, and laying on belly behavior**. e**) Transition frequency over habituation days. **f**) Anxiety score as measured by time spent in corners of the chamber. **g)** Total walk number, average walk distance and walk speed during habituation days. **h)** Speed of walking trace over habituation days. **i)** Average number of steps per walk event. **j)** Stride speed, distance, and time averages for each habituation day. **k)** forepaw and hindpaw gait width over habituation days. **l)** body and head pitch angle averaged over walk events. **m)** head, body, and tailbase lateral displacement over walk events. **n)** body angles over habituation days. Student's T-test, no post-hoc multiplicity corrections (*$p<0.05$, **$p<0.01$, ***$p<0.001$).

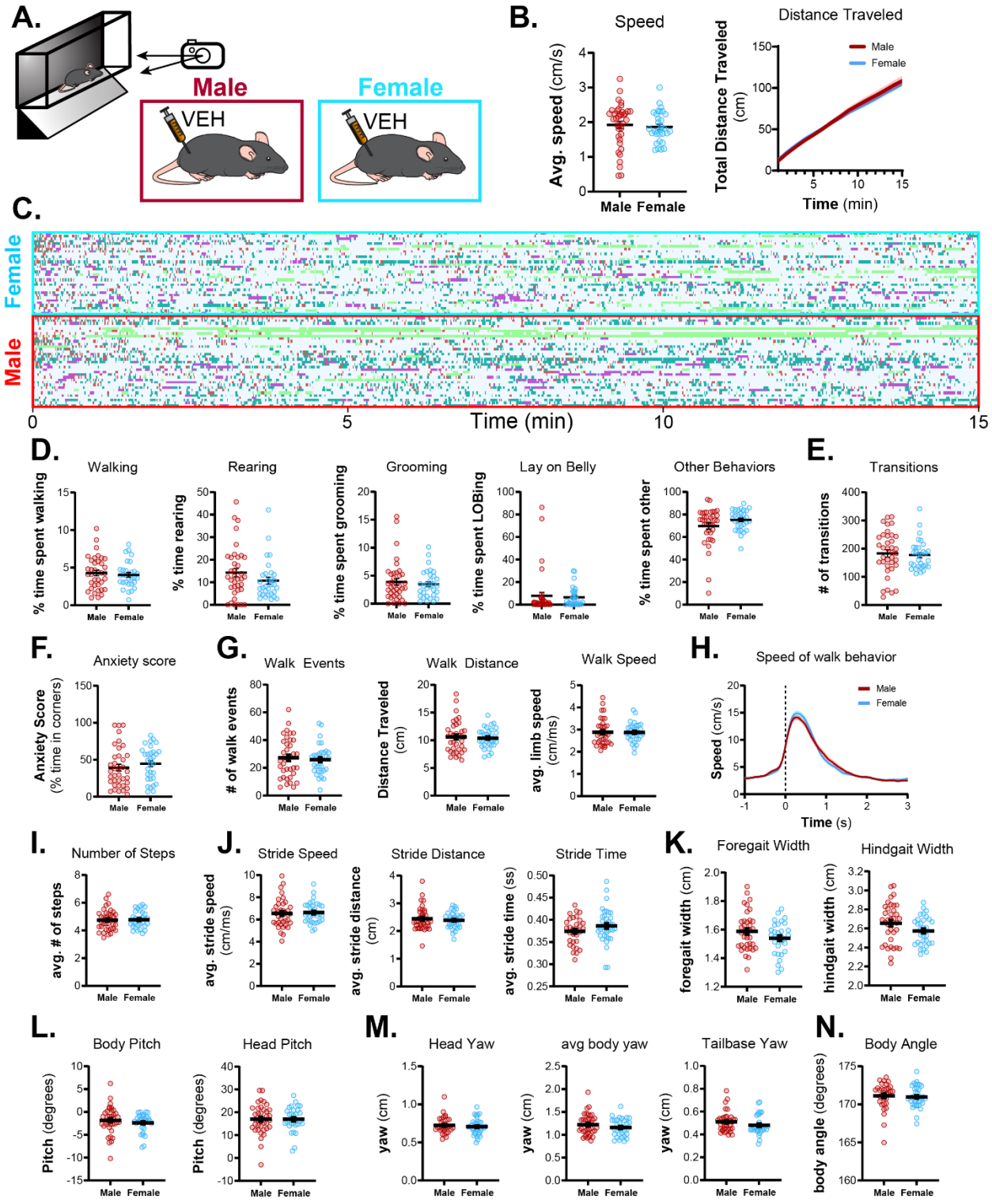
A.
Male
VEH
Female
VEH
B.
Speed
Avg. speed (cm/s)
Male Female
Distance Traveled
Total Distance Traveled (cm)
Male
Female
Time (min)
C.
Female
Male
0
5
Time (min)
10
15
D.
Walking
% time spent walking
Rearing
% time rearing
Grooming
% time spent grooming
Lay on Belly
% time spent LOBing
Other Behaviors
% time spent other
E.
Transitions
# of transitions
F.
Anxiety score
Anxiety Score (% time in corners)
G.
Walk Events
# of walk events
Walk Distance
Distance Traveled (cm)
Walk Speed
avg. limb speed (cm/ms)
H.
Speed of walk behavior
Speed (cm/s)
Time (s)
I.
Number of Steps
avg. # of steps
J.
Stride Speed
avg. stride speed (cm/ms)
Stride Distance
avg. stride distance (cm)
Stride Time
avg. stride time (ss)
K.
Foregait Width
foregait width (cm)
Hindgait Width
hindgait width (cm)
L.
Body Pitch
Pitch (degrees)
Head Pitch
Pitch (degrees)
M.
Head Yaw
yaw (cm)
avg body yaw
yaw (cm)
Tailbase Yaw
yaw (cm)
N.
Body Angle
body angle (degrees)
Male Female

Supplementary Figure S4.21: Linear track behavior of male and female WT mice

a) Schematic for WT vehicle recordings in the linear track separated by male and female subjects. **b)** distance traveled and speed differences for males and females. **c)** Behavioral ethogram of males and females during linear track experimentation. **d)** Quantification of frequency for walking, rearing, grooming, and laying on belly behavior**. e**) Transition frequency for males and female mice. **f**) Anxiety score as measured by time spent in corners of the chamber. **g)** Total walk number, average walk distance and walk speed for males and female mice. **h)** Speed of walking trace for males and female mice. **i)** Average number of steps per walk event. **j)** Stride speed, distance, and time averages for males and female mice. **k)** forepaw and hindpaw gait width for males and female mice. **l)** body and head pitch angle averaged over walk events. **m)** head, body, and tailbase lateral displacement over walk events. **n)** body angles for males and female mice. Student's T-test, no post-hoc multiplicity corrections (*p<0.05, **p<0.01, ***p<0.001).

.

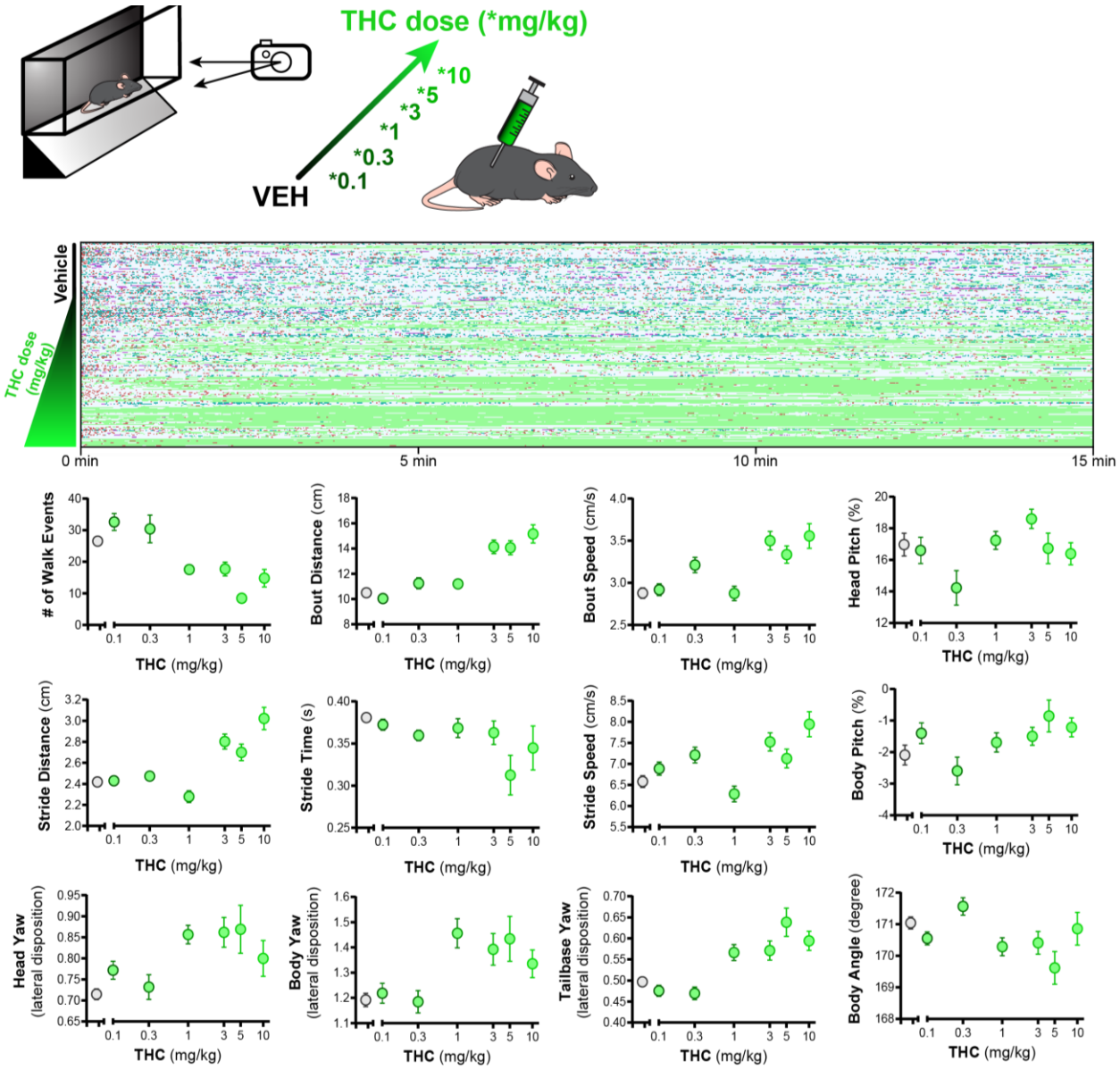

Supplementary Figure S4.22: <u>THC dose-dependent effects across full THC dose range within the linear track.</u>

a) Schematic for THC administration of WT mice for 15 minute exposures in the linear track. Behavioral ethogram of vehicle and THC dosed recordings. Dose response curves for all kinematic metrics measured from walk events in the linear track.

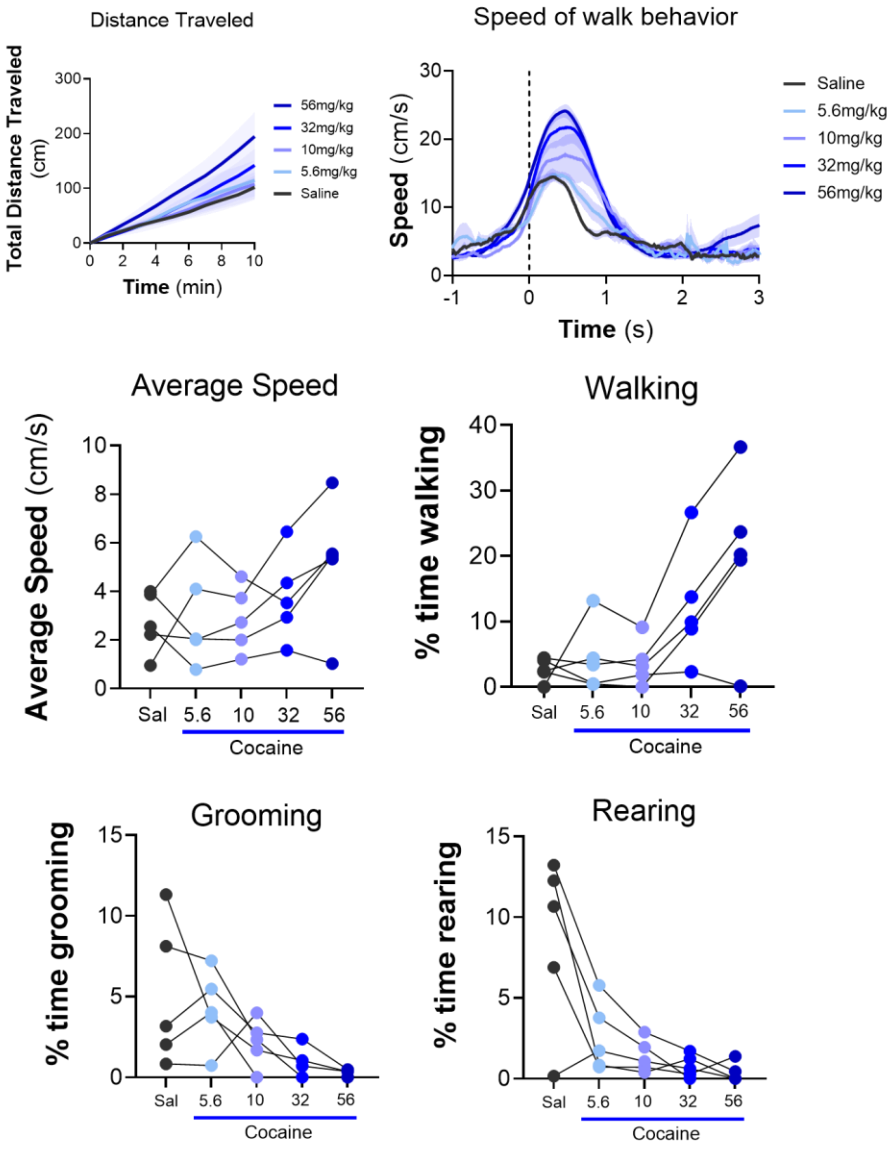

Supplementary Figure S4.23: <u>Cocaine ramping administration in the linear track</u>

Distance Traveled, Speed of walking, average spend, Percent time spent walking, grooming, and rearing for animals treated with saline and then increasing concentrations of cocaine on the same day.

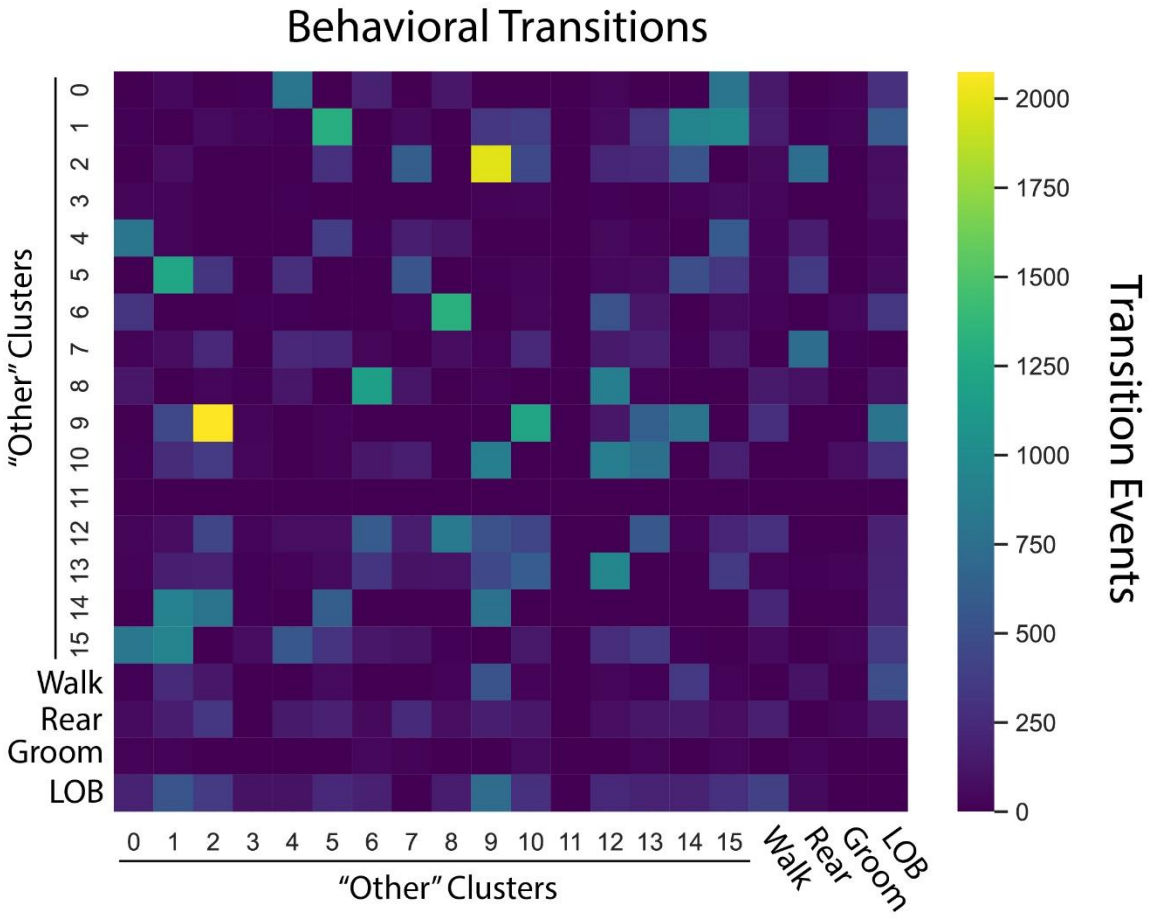

Supplementary Figure S4.24: <u>Transition frequency of supervised and unsupervised behaviors</u>

Vehicle and THC (0.1-10 mg/kg) treated mice videos were assessed for transitions from each behavior (unsupervised or supervised) to each other behavior. Trends in behavior alternate between the matched behaviors, suggesting larger collective behaviors.

BIBLIOGRAPHY

1 Translated by John Andrew Boyle. Manchester, E. M. U. P. Farīd al-Dīn ʻAṭṭār (1976). The 'Ilāhī-nāma [Book of God]. . *UNESCO collection of representative works: Persian heritage series; [no. 29]*.

2 Ryz, N. R., Remillard, D. J. & Russo, E. B. Cannabis roots: a traditional therapy with future potential for treating inflammation and pain. *Cannabis and cannabinoid research* **2**, 210-216 (2017).

3 Wachtel-Galor, S. Y., John; Buswell, John A.; Benzie, Iris F. F. (2011). Benzie, Iris F. F.; Wachtel-Galor, Sissi (eds.). . Ganoderma lucidum (Lingzhi or Reishi): A Medicinal Mushroom. Herbal Medicine: Biomolecular and Clinical Aspects (2nd ed.). . *CRC Press/Taylor & Francis.*

4 Abdel-Salam, O., Galal, A., Elshebiney, S. & Gaafar, A. in *Handbook of Cannabis and Related Pathologies* 110-121 (Elsevier, 2017).

5 Savage-Smith, E. Gleanings from an Arabist's workshop: current trends in the study of medieval Islamic science and medicine. *Isis* **79**, 246-266 (1988).

6 Herodotus. *Herodotus, with an English Translation by AD Godley*. (London,, New York,: W. Heinemann;, GP Putnam's sons, 1931).

7 Russo, E. B. History of cannabis and its preparations in saga, science, and sobriquet. *Chemistry & biodiversity* **4**, 1614-1648 (2007).

8 Aldrich, M. History of therapeutic cannabis. *Cannabis in medical practice. Jefferson, NC: Mc Farland*, 35-55 (1997).

9 Al-Biruni, A. R. al-Biruni. *Alberuni's India* (1989).

10 Shboul, A. M. *Al-Mas' udi with Special Reference to His Treatment of Non-Muslim History and Religions*. (University of London, School of Oriental and African Studies (United Kingdom), 1972).

11 Daftary, F. *Historical dictionary of the Ismailis*. (Scarecrow Press, 2012).

12 Van der Merwe, N. J. Cannabis smoking in 13th-14th century Ethiopia: Chemical evidence. *World anthropology: Cannabis and culture*, 77-80 (1975).

13 U.S. Congress. (2018). Agriculture Improvement Act of 2018, Pub. L. No. 115-334, § 10113, 132 Stat. 4490. .

14 Dewey, L. H. *Fiber production in the western hemisphere*. (US Department of Agriculture, 1943).

15 Iversen, L. L. *The science of marijuana*. (Oxford University Press, 2001).

16 Nahas, G. G. Hashish and drug abuse in Egypt during the 19th and 20th centuries. *Bulletin of the New York Academy of Medicine* **61**, 428 (1985).

17 Guba Jr, D. A. *Taming Cannabis: Drugs and Empire in Nineteenth-Century France*. Vol. 1 (McGill-Queen's Press-MQUP, 2020).

18 Indian Hemp Drugs Commission (1893–1894) ; Young, W. Mackworth (1969). Marijuana: Report of the Indian Hemp Drugs Commission, 1893–1894. Silver Spring, Maryland: Thos. Jefferson Publishing Company. p. 270.

19 Newton, D. E. *Marijuana: a reference handbook*. (Bloomsbury Publishing USA, 2017).

20 Abel, E. L. *Marihuana: the first twelve thousand years*. (Springer Science & Business Media, 2013).

21 Söderbaum, F. & Taylor, I. *Afro-regions: The dynamics of cross-border micro-regionalism in Africa*. (Nordiska Afrikainstitutet, 2008).

22 Zullino, M. G. *Italiana= Italian*, Politecnico di Torino, (2018).

23 Moyston, L. The ganja law of 1913: 100 years of oppressive injustice. *Jamaica Observer* **2** (2013).

24 Lee, M. A. *Smoke signals: A social history of Marijuana-Medical, Recreational and Scientific*. (Simon and Schuster, 2013).

25 Willoughby, W. W. *Opium as an international problem: the Geneva Conferences*. (John Hopkins Press, 1925).

26 Drugs, U. N. C. o. N. *The Question of Cannabis: Cannabis Bibliography*. (United Nations, Economic and Social Council, 1965).

27 U.S. Congress. (1914). Harrison Narcotics Tax Act of 1914, Pub. L. No. 63-223, 38 Stat. 785. https://www.govinfo.gov/content/pkg/STATUTE-38/pdf/STATUTE-38-Pg785.pdf

28 Stensrud, A. *The Racist Roots of International Cannabis Regulation: An analysis of the Second Geneva Opium Conference*, (2022).

29 Manning, P. *Drugs and popular culture*. (Taylor & Francis London, UK, 2013).

30 Porter, B. Empire Ways. (2015).

31 SAORSTÁT EIREANN. STATUTORY RULES AND ORDERS. 1937. No. 40. DANGEROUS DRUGS ACT, 1934 (COMMENCEMENT) ORDER, 1937. https://www.irishstatutebook.ie/eli/1937/sro/40/made/en/print.

32 Filan, K. *The Power of the Poppy: Harnessing Nature's Most Dangerous Plant Ally*. (Simon and Schuster, 2011).

33 Carroll, R. Under the influence: Harry Anslinger's role in shaping America's drug policy. *Federal drug control: The evolution of policy and practice*, 61-99 (2004).

34 Newton, David E. (16 January 2017) [2013]. "4. Profiles Harry J. Anslinger (1892-1975)". Marijuana: A Reference Handbook. Contemporary world issues (2nd ed.). Santa Barbara, California, California, United States of America: ABC-CLIO. p. 183. ISBN 978-1-4408-5051-6. LCCN 2016042067. OCLC 965153723.

35 Gray, M. *Drug crazy: How we got into this mess and how we can get out*. (Routledge, 2013).

36 McWilliams, J. C. *The Protectors: Harry J. Anslinger and the Federal Bureau of Narcotics, 1930-1962*. (University of Delaware Press, 1990).

37 Sloman, L. *Reefer madness: a history of marijuana*. (Macmillan, 1998).

38 Holiday, B. with William Dufty. *Lady Sings the Blues*, 94-95 (1956).

39 Sonneborn, L. *A to Z of American Women in the Performing Arts*. (Infobase Publishing, 2014).

40 Murphy, K. & Studney, D. The history of Reefer Madness. *Reefer-Madness-Movie. com* (2005).

41 ProCon.org. (n.d.). May 4, 1937 - American Medical Association opposes the proposed Marihuana Tax Act and supports research on medical cannabis. Retrieved April 22, 2025, from https://medicalmarijuana.procon.org/timeline-events/may-4-1937-american-medical-association-opposes-the-proposed-marihuana-tax-act-and-supports-research-on-medical-cannabis/.

42 Schaffer Library of Drug Policy. (n.d.). Letter from the American Medical Association - Marihuana Tax Act. Retrieved April 22, 2025, from https://www.druglibrary.org/schaffer/hemp/taxact/t8.htm.

43 Mayor's Committee on Marihuana, City of New York. (1944). The marihuana problem in the city of New York: Sociological, medical, psychological and pharmacological studies (G. B. Wallace & E. V. Cunningham, Eds.). Jaques Cattell Press.

44 Allentuck, S. & Bowman, K. M. The psychiatric aspects of marihuana intoxication. *American Journal of Psychiatry* **99**, 248-251 (1942).

45 Adams, R., Hunt, M. & Clark, J. Structure of cannabidiol, a product isolated from the marihuana extract of Minnesota wild hemp. I. *Journal of the American chemical society* **62**, 196-200 (1940).

46 Gaoni, Y. & Mechoulam, R. Isolation, structure, and partial synthesis of an active constituent of hashish. *Journal of the American chemical society* **86**, 1646-1647 (1964).

47 Mechoulam, R. & Shvo, Y. Hashish? I. *Tetrahedron* **19**, 2073-2078 (1963).

48 Mechoulam, R. & Gaoni, Y. A total synthesis of dl-Δ1-tetrahydrocannabinol, the active constituent of hashish1. *Journal of the American Chemical Society* **87**, 3273-3275 (1965).

49 Isbell, H. & Jasinski, D. R. A comparison of LSD-25 with (−)-Δ 9-trans-tetrahydrocannabinol (THC) and attempted cross tolerance between LSD and THC. *Psychopharmacologia* **14**, 115-123 (1969).

50 Wall, M. E., Sadler, B. M., Brine, D., Taylor, H. & Perez-Reyes, M. Metabolism, disposition, and kinetics of delta-9-tetrahydrocannabinol in men and women. *Clinical Pharmacology & Therapeutics* **34**, 352-363 (1983).

51 Slaughter, J. B. Marijuana Prohibition in the United States: History and analysis of a failed policy. *Colum. JL & Soc. Probs.* **21**, 417 (1987).

52 Act, C. S. Controlled Substances Act. *President Obama's deci* (1970).

53 Blumenthal, S. E. Nixon's marijuana problem: youth politics and 'law and order,'1968–72. *The Sixties* **9**, 26-53 (2016).

54 Rodgers, N. & Aughenbaugh, J. S06, E14: The Shafer Commission. (2021).

55 Devane, W. A. *et al.* Isolation and structure of a brain constituent that binds to the cannabinoid receptor. *Science* **258**, 1946-1949 (1992).

56 Moldrich, G. & Wenger, T. Localization of the CB1 cannabinoid receptor in the rat brain. An immunohistochemical study☆. *Peptides* **21**, 1735-1742 (2000).

57 Thomas, B. F., Compton, D. R. & Martin, B. R. Characterization of the lipophilicity of natural and synthetic analogs of delta 9-tetrahydrocannabinol and its relationship to pharmacological potency. *The Journal of pharmacology and experimental therapeutics* **255**, 624-630 (1990).

58 Mack, F. & Bönisch, H. Dissociation constants and lipophilicity of catecholamines and related compounds. *Naunyn-Schmiedeberg's archives of pharmacology* **310**, 1-9 (1979).

59 Avdeef, A., Barrett, D. A., Shaw, P. N., Knaggs, R. D. & Davis, S. S. Octanol−, chloroform−, and propylene glycol dipelargonat− water partitioning of morphine-6-glucuronide and other related opiates. *Journal of medicinal chemistry* **39**, 4377-4381 (1996).

60 Atwood, B. & CB, K. M. A cannabinoid receptor with an identity crisis., 2010, 160. *DOI: https://doi. org/10.1111/j*, 1476-5381.2010.

61 Zou, S. & Kumar, U. Cannabinoid receptors and the endocannabinoid system: signaling and function in the central nervous system. *International journal of molecular sciences* **19**, 833 (2018).

62 Buczynski, M. W. & Parsons, L. H. Quantification of brain endocannabinoid levels: methods, interpretations and pitfalls. *British journal of pharmacology* **160**, 423-442 (2010).

63 Stella, N., Schweitzer, P. & Piomelli, D. A second endogenous cannabinoid that modulates long-term potentiation. *Nature* **388**, 773-778 (1997).

64 Patilea-Vrana, G. I., Anoshchenko, O. & Unadkat, J. D. Hepatic enzymes relevant to the disposition of (−)-Δ 9-tetrahydrocannabinol (THC) and its psychoactive metabolite, 11-OH-THC. *Drug Metabolism and Disposition* **47**, 249-256 (2019).

65 Huestis, M. A. Human cannabinoid pharmacokinetics. *Chemistry & biodiversity* **4**, 1770 (2007).

66 Meier, M. H. *et al.* Persistent cannabis users show neuropsychological decline from childhood to midlife. *Proceedings of the National Academy of Sciences* **109**, E2657-E2664 (2012).

67 Karschner, E. L. *et al.* Implications of plasma Δ9-tetrahydrocannabinol, 11-hydroxy-THC, and 11-nor-9-carboxy-THC concentrations in chronic cannabis smokers. *Journal of analytical toxicology* **33**, 469-477 (2009).

68 Wong, A. *et al.* Exercise increases plasma THC concentrations in regular cannabis users. *Drug and Alcohol Dependence* **133**, 763-767 (2013).

69 Savinainen, J. R., Järvinen, T., Laine, K. & Laitinen, J. T. Despite substantial degradation, 2-arachidonoylglycerol is a potent full efficacy agonist mediating CB1 receptor-dependent G-protein activation in rat cerebellar membranes. *British journal of pharmacology* **134**, 664-672 (2001).
70 Hempel, B. & Xi, Z.-X. in *Advances in Pharmacology* Vol. 93 275-333 (Elsevier, 2022).
71 Justinová, Z., Yasar, S., Redhi, G. H. & Goldberg, S. R. The endogenous cannabinoid 2-arachidonoylglycerol is intravenously self-administered by squirrel monkeys. *Journal of Neuroscience* **31**, 7043-7048 (2011).
72 Savinainen, J., Saario, S. & Laitinen, J. The serine hydrolases MAGL, ABHD6 and ABHD12 as guardians of 2-arachidonoylglycerol signalling through cannabinoid receptors. *Acta physiologica* **204**, 267-276 (2012).
73 Ogasawara, D. *et al.* Rapid and profound rewiring of brain lipid signaling networks by acute diacylglycerol lipase inhibition. *Proceedings of the National Academy of Sciences* **113**, 26-33 (2016).
74 Keimpema, E. *et al.* Diacylglycerol lipase α manipulation reveals developmental roles for intercellular endocannabinoid signaling. *Scientific reports* **3**, 2093 (2013).
75 Cravatt, B. F. & Lichtman, A. H. Fatty acid amide hydrolase: an emerging therapeutic target in the endocannabinoid system. *Current opinion in chemical biology* **7**, 469-475 (2003).
76 Okamoto, Y., Tsuboi, K. & Ueda, N. Enzymatic formation of anandamide. *Vitamins & Hormones* **81**, 1-24 (2009).
77 Kellogg, R., Mackie, K. & Straiker, A. Cannabinoid CB1 receptor-dependent long-term depression in autaptic excitatory neurons. *Journal of neurophysiology* **102**, 1160-1171 (2009).
78 Jung, K.-M. *et al.* Stimulation of endocannabinoid formation in brain slice cultures through activation of group I metabotropic glutamate receptors. *Molecular pharmacology* **68**, 1196-1202 (2005).
79 Topolnik, L., Azzi, M., Morin, F., Kougioumoutzakis, A. & Lacaille, J. C. mGluR1/5 subtype-specific calcium signalling and induction of long-term potentiation in rat hippocampal oriens/alveus interneurones. *The Journal of physiology* **575**, 115-131 (2006).
80 Kaczocha, M., Vivieca, S., Sun, J., Glaser, S. T. & Deutsch, D. G. Fatty acid-binding proteins transport N-acylethanolamines to nuclear receptors and are targets of endocannabinoid transport inhibitors. *Journal of Biological Chemistry* **287**, 3415-3424 (2012).
81 Katona, I. *et al.* Presynaptically located CB1 cannabinoid receptors regulate GABA release from axon terminals of specific hippocampal interneurons. *Journal of Neuroscience* **19**, 4544-4558 (1999).
82 Tsou, K., Brown, S., Sanudo-Pena, M., Mackie, K. & Walker, J. Immunohistochemical distribution of cannabinoid CB1 receptors in the rat central nervous system. *Neuroscience* **83**, 393-411 (1998).
83 Lu, H.-C. & Mackie, K. Review of the endocannabinoid system. *Biological Psychiatry: Cognitive Neuroscience and Neuroimaging* **6**, 607-615 (2021).
84 Kano, M., Ohno-Shosaku, T., Hashimotodani, Y., Uchigashima, M. & Watanabe, M. Endocannabinoid-mediated control of synaptic transmission. *Physiological reviews* (2009).
85 Nguyen, P. T. *et al.* β-Arrestin2 regulates cannabinoid CB1 receptor signaling and adaptation in a central nervous system region–dependent manner. *Biological psychiatry* **71**, 714-724 (2012).
86 Steindel, F. *et al.* Neuron-type specific cannabinoid-mediated G protein signalling in mouse hippocampus. *Journal of neurochemistry* **124**, 795-807 (2013).

87 Diana, M. A. & Marty, A. Endocannabinoid-mediated short-term synaptic plasticity: depolarization-induced suppression of inhibition (DSI) and depolarization-induced suppression of excitation (DSE). *British journal of pharmacology* **142**, 9-19 (2004).
88 Ohno-Shosaku, T., Maejima, T. & Kano, M. Endogenous cannabinoids mediate retrograde signals from depolarized postsynaptic neurons to presynaptic terminals. *Neuron* **29**, 729-738 (2001).
89 Wilson, R. I. & Nicoll, R. A. Endogenous cannabinoids mediate retrograde signalling at hippocampal synapses. *Nature* **410**, 588-592 (2001).
90 Bara, A., Ferland, J.-M. N., Rompala, G., Szutorisz, H. & Hurd, Y. L. Cannabis and synaptic reprogramming of the developing brain. *Nature Reviews Neuroscience* **22**, 423-438 (2021).
91 Rubino, T. & Parolaro, D. The impact of exposure to cannabinoids in adolescence: insights from animal models. *Biological psychiatry* **79**, 578-585 (2016).
92 Frolli, A. *et al.* Cognitive development and cannabis use in adolescents. *Behavioral Sciences* **11**, 37 (2021).
93 Compagnucci, C. *et al.* Type-1 (CB1) cannabinoid receptor promotes neuronal differentiation and maturation of neural stem cells. *PloS one* **8**, e54271 (2013).
94 Gaffuri, A.-L., Ladarre, D. & Lenkei, Z. Type-1 cannabinoid receptor signaling in neuronal development. *Pharmacology* **90**, 19-39 (2012).
95 Calvigioni, D., Hurd, Y. L., Harkany, T. & Keimpema, E. Neuronal substrates and functional consequences of prenatal cannabis exposure. *European child & adolescent psychiatry* **23**, 931-941 (2014).
96 de Salas-Quiroga, A. *et al.* Prenatal exposure to cannabinoids evokes long-lasting functional alterations by targeting CB1 receptors on developing cortical neurons. *Proceedings of the National Academy of Sciences* **112**, 13693-13698 (2015).
97 Marsicano, G. *et al.* CB1 cannabinoid receptors and on-demand defense against excitotoxicity. *Science* **302**, 84-88 (2003).
98 Rubino, T. *et al.* Changes in hippocampal morphology and neuroplasticity induced by adolescent THC treatment are associated with cognitive impairment in adulthood. *Hippocampus* **19**, 763-772 (2009).
99 Archer, T. Effects of exogenous agents on brain development: stress, abuse and therapeutic compounds. *CNS neuroscience & therapeutics* **17**, 470-489 (2011).
100 Morgunova, A. & Flores, C. in *Seminars in Cell & Developmental Biology.* (Elsevier).
101 Bristot, G., De Bastiani, M. A., Pfaffenseller, B., Kapczinski, F. & Kauer-Sant'Anna, M. Gene Regulatory Network of Dorsolateral Prefrontal Cortex: a Master Regulator Analysis of Major Psychiatric Disorders. *Mol Neurobiol* **57**, 1305-1316, doi:10.1007/s12035-019-01815-2 (2020).
102 Rubino, T. *et al.* Adolescent exposure to THC in female rats disrupts developmental changes in the prefrontal cortex. *Neurobiology of disease* **73**, 60-69 (2015).
103 Renard, J., Norris, C., Rushlow, W. & Laviolette, S. R. Neuronal and molecular effects of cannabidiol on the mesolimbic dopamine system: Implications for novel schizophrenia treatments. *Neuroscience & Biobehavioral Reviews* **75**, 157-165 (2017).
104 Renard, J. *et al.* Adolescent cannabinoid exposure induces a persistent sub-cortical hyper-dopaminergic state and associated molecular adaptations in the prefrontal cortex. *Cerebral Cortex* **27**, 1297-1310 (2017).
105 Renard, J. *et al.* Adolescent THC exposure causes enduring prefrontal cortical disruption of GABAergic inhibition and dysregulation of sub-cortical dopamine function. *Scientific reports* **7**, 1-14 (2017).
106 Monory, K. *et al.* Genetic dissection of behavioural and autonomic effects of Δ9-tetrahydrocannabinol in mice. *PLoS biology* **5**, e269 (2007).

107 Monory, K. *et al.* The endocannabinoid system controls key epileptogenic circuits in the hippocampus. *Neuron* **51**, 455-466 (2006).

108 Kelley, B. G. & Thayer, S. A. Δ9-Tetrahydrocannabinol antagonizes endocannabinoid modulation of synaptic transmission between hippocampal neurons in culture. *Neuropharmacology* **46**, 709-715 (2004).

109 Dong, A. *et al.* A fluorescent sensor for spatiotemporally resolved endocannabinoid dynamics in vitro and in vivo. *bioRxiv*, 2020.2010.2008.329169, doi:10.1101/2020.10.08.329169 (2020).

110 Singh, S. *et al.* Pharmacological characterization of the endocannabinoid sensor GRABeCB2. 0. *Cannabis and Cannabinoid Research* **9**, 1250-1266 (2024).

111 Singh, S. *et al.* P2X7 receptor-dependent increase in endocannabinoid 2-arachidonoyl glycerol production by neuronal cells in culture: Dynamics and mechanism. *British Journal of Pharmacology* **181**, 2459-2477 (2024).

112 Singh, S. *et al.* ABHD6 selectively controls metabotropic-dependent increases in 2-AG production. *bioRxiv*, 2022.2005.2018.492553, doi:10.1101/2022.05.18.492553 (2022).

113 Augustin, S. M., Gracias, A. L., Luo, G., Anumola, R. C. & Lovinger, D. M. Striatonigral direct pathway 2-arachidonoylglycerol contributes to ethanol effects on synaptic transmission and behavior. *Neuropsychopharmacology* **48**, 1941-1951 (2023).

114 Liput, D. J. *et al.* 2-Arachidonoylglycerol mobilization following brief synaptic stimulation in the dorsal lateral striatum requires glutamatergic and cholinergic neurotransmission. *bioRxiv*, 2020.2010.2021.348995, doi:10.1101/2020.10.21.348995 (2020).

115 Straub, V. M. *et al.* The endocannabinoid 2-arachidonoylglycerol is released and transported on demand via extracellular microvesicles. *Proceedings of the National Academy of Sciences* **122**, e2421717122 (2025).

116 Barrus, D. G., Lefever, T. W. & Wiley, J. L. Evaluation of reinforcing and aversive effects of voluntary Δ9-tetrahydrocannabinol ingestion in rats. *Neuropharmacology* **137**, 133-140 (2018).

117 Peters, E. N., Bae, D., Barrington-Trimis, J. L., Jarvis, B. P. & Leventhal, A. M. Prevalence and sociodemographic correlates of adolescent use and polyuse of combustible, vaporized, and edible cannabis products. *JAMA network open* **1**, e182765-e182765 (2018).

118 Hammond, C. J., Chaney, A., Hendrickson, B. & Sharma, P. Cannabis use among US adolescents in the era of marijuana legalization: a review of changing use patterns, comorbidity, and health correlates. *International review of psychiatry* **32**, 221-234 (2020).

119 Knapp, A. A. *et al.* Emerging trends in cannabis administration among adolescent cannabis users. *Journal of Adolescent Health* **64**, 487-493 (2019).

120 Murphy, M. *et al.* Chronic adolescent Δ9-tetrahydrocannabinol treatment of male mice leads to long-term cognitive and behavioral dysfunction, which are prevented by concurrent cannabidiol treatment. *Cannabis and cannabinoid research* **2**, 235-246 (2017).

121 Dow-Edwards, D. & Zhao, N. Oral THC produces minimal behavioral alterations in preadolescent rats. *Neurotoxicology and teratology* **30**, 385-389 (2008).

122 Kruse, L. C., Cao, J. K., Viray, K., Stella, N. & Clark, J. J. Voluntary oral consumption of Δ 9-tetrahydrocannabinol by adolescent rats impairs reward-predictive cue behaviors in adulthood. *Neuropsychopharmacology* **44**, 1406-1414 (2019).

123 Abraham, A. D. *et al.* Orally consumed cannabinoids provide long-lasting relief of allodynia in a mouse model of chronic neuropathic pain. *Neuropsychopharmacology* **45**, 1105-1114 (2020).

124 Smoker, M. P., Hernandez, M., Zhang, Y. & Boehm, S. L., 2nd. Assessment of Acute Motor Effects and Tolerance Following Self-Administration of Alcohol and Edible (9) -Tetrahydrocannabinol in Adolescent Male Mice. *Alcohol Clin Exp Res* **43**, 2446-2457, doi:10.1111/acer.14197 (2019).

125 Manwell, L. A. *et al.* A vapourized Δ9-tetrahydrocannabinol (Δ9-THC) delivery system part I: Development and validation of a pulmonary cannabinoid route of exposure for experimental pharmacology studies in rodents. *Journal of pharmacological and toxicological methods* **70**, 120-127 (2014).
126 Freels, T. G. *et al.* Vaporized cannabis extracts have reinforcing properties and support conditioned drug-seeking behavior in rats. *Journal of Neuroscience* **40**, 1897-1908 (2020).
127 Taffe, M. A., Creehan, K. M., Vandewater, S. A., Kerr, T. M. & Cole, M. Effects of Δ^9-tetrahydrocannabinol (THC) vapor inhalation in Sprague-Dawley and Wistar rats. *Experimental and clinical psychopharmacology* (2020).
128 Bruijnzeel, A. W. *et al.* Behavioral characterization of the effects of cannabis smoke and anandamide in rats. *PloS one* **11**, e0153327 (2016).
129 Huizenga, M. N., Fureman, B. E., Soltesz, I. & Stella, N. Proceedings of the Epilepsy Foundation's 2017 Cannabinoids in Epilepsy Therapy Workshop. *Epilepsy & Behavior* **85**, 237-242 (2018).
130 Brenan, M. Support for legal marijuana inches up to new high of 68%. *Gallup, November* **6**, 2020 (2020).
131 ElSohly, M. A. *et al.* Changes in cannabis potency over the last 2 decades (1995–2014): analysis of current data in the United States. *Biological psychiatry* **79**, 613-619 (2016).
132 Phillips, R. N., Turk, R. F. & Forney, R. B. Acute toxicity of Δ9-tetrahydrocannabinol in rats and mice. *Proceedings of the Society for Experimental Biology and Medicine* **136**, 260-263 (1971).
133 Razban, M., Exadaktylos, A. K., Santa, V. D. & Heymann, E. P. Cannabinoid hyperemesis syndrome and cannabis withdrawal syndrome: a review of the management of cannabis-related syndrome in the emergency department. *International journal of emergency medicine* **15**, 45 (2022).
134 Richards, J. R. Cannabinoid hyperemesis syndrome: pathophysiology and treatment in the emergency department. *The Journal of emergency medicine* **54**, 354-363 (2018).
135 Gajendran, M., Sifuentes, J., Bashashati, M. & McCallum, R. Cannabinoid hyperemesis syndrome: definition, pathophysiology, clinical spectrum, insights into acute and long-term management. *Journal of Investigative Medicine* **68**, 1309-1316 (2020).
136 McCulloch, W. S. & Pitts, W. A logical calculus of the ideas immanent in nervous activity. *The bulletin of mathematical biophysics* **5**, 115-133 (1943).
137 Hebb, D. O. *The organization of behavior: A neuropsychological theory*. (Psychology press, 2005).
138 Rosenblatt, F. The perceptron: a probabilistic model for information storage and organization in the brain. *Psychological review* **65**, 386 (1958).
139 Hopfield, J. J. Neural networks and physical systems with emergent collective computational abilities. *Proceedings of the national academy of sciences* **79**, 2554-2558 (1982).
140 Rumelhart, D. E., Hinton, G. E. & Williams, R. J. Learning representations by back-propagating errors. *nature* **323**, 533-536 (1986).
141 Cortes, C. & Vapnik, V. Support-vector networks. *Machine learning* **20**, 273-297 (1995).
142 Breiman, L. Random forests. *Machine learning* **45**, 5-32 (2001).
143 LeCun, Y., Bottou, L., Bengio, Y. & Haffner, P. Gradient-based learning applied to document recognition. *Proceedings of the IEEE* **86**, 2278-2324 (1998).
144 Krizhevsky, A., Sutskever, I. & Hinton, G. E. Imagenet classification with deep convolutional neural networks. *Advances in neural information processing systems* **25** (2012).
145 Abdel-Hamid, O. *et al.* Convolutional neural networks for speech recognition. *IEEE/ACM Transactions on audio, speech, and language processing* **22**, 1533-1545 (2014).

146 Litjens, G. *et al.* A survey on deep learning in medical image analysis. *Medical image analysis* **42**, 60-88 (2017).

147 Boulent, J., Foucher, S., Théau, J. & St-Charles, P.-L. Convolutional neural networks for the automatic identification of plant diseases. *Frontiers in plant science* **10**, 941 (2019).

148 Yamins, D. L. *et al.* Performance-optimized hierarchical models predict neural responses in higher visual cortex. *Proceedings of the national academy of sciences* **111**, 8619-8624 (2014).

149 Vuyyuru, V. A., Krishna, G. V., Mary, S. S. C., Kayalvili, S. & Alsubayhay, A. M. S. A transformer-CNN hybrid model for cognitive behavioral therapy in psychological assessment and intervention for enhanced diagnostic accuracy and treatment efficiency. *International Journal of Advanced Computer Science and Applications* **14** (2023).

150 Dolensek, N., Gehrlach, D. A., Klein, A. S. & Gogolla, N. Facial expressions of emotion states and their neuronal correlates in mice. *Science* **368**, 89-94 (2020).

151 Li, J. *et al.* in *Adjunct Proceedings of the 2021 ACM International Joint Conference on Pervasive and Ubiquitous Computing and Proceedings of the 2021 ACM International Symposium on Wearable Computers.* 643-648.

152 Choi, H. *et al.* Convolutional neural network based detection of early stage Parkinson's disease using the six minute walk test. *Scientific Reports* **14**, 22648 (2024).

153 Simonyan, K. & Zisserman, A. Very deep convolutional networks for large-scale image recognition. *arXiv preprint arXiv:1409.1556* (2014).

154 Szegedy, C. *et al.* in *Proceedings of the IEEE conference on computer vision and pattern recognition.* 1-9.

155 Huang, G. in *Proc. IEEE Conf. Comput. Vis. Pattern Recognit.(CVPR), Honolulu, HI, USA.* 2261-2269.

156 He, K., Zhang, X., Ren, S. & Sun, J. in *Computer Vision–ECCV 2016: 14th European Conference, Amsterdam, The Netherlands, October 11–14, 2016, Proceedings, Part IV 14.* 630-645 (Springer).

157 Burstein, J., Doran, C. & Solorio, T. in *Proceedings of the 2019 Conference of the North American Chapter of the Association for Computational Linguistics: Human Language Technologies, Volume 1 (Long and Short Papers).*

158 Mathis, A. *et al.* DeepLabCut: markerless pose estimation of user-defined body parts with deep learning. *Nature neuroscience* **21**, 1281-1289 (2018).

159 Pereira, T. D. *et al.* Fast animal pose estimation using deep neural networks. *Nature methods* **16**, 117-125 (2019).

160 Pereira, T. D. *et al.* SLEAP: A deep learning system for multi-animal pose tracking. *Nature methods* **19**, 486-495 (2022).

161 Wiltschko, A. B. *et al.* Mapping sub-second structure in mouse behavior. *Neuron* **88**, 1121-1135 (2015).

162 Weinreb, C. *et al.* Keypoint-MoSeq: parsing behavior by linking point tracking to pose dynamics. *Nature Methods* **21**, 1329-1339 (2024).

163 Chen, Z. *et al.* AlphaTracker: a multi-animal tracking and behavioral analysis tool. *Frontiers in Behavioral Neuroscience* **17**, 1111908 (2023).

164 Machado, A. S., Darmohray, D. M., Fayad, J., Marques, H. G. & Carey, M. R. A quantitative framework for whole-body coordination reveals specific deficits in freely walking ataxic mice. *Elife* **4**, e07892 (2015).

165 Hasin, D. S., Shmulewitz, D. & Sarvet, A. L. Time trends in US cannabis use and cannabis use disorders overall and by sociodemographic subgroups: a narrative review and new findings. *The American journal of drug and alcohol abuse* **45**, 623-643 (2019).

166 Compton, W. M., Han, B., Jones, C. M., Blanco, C. & Hughes, A. Marijuana use and use disorders in adults in the USA, 2002–14: analysis of annual cross-sectional surveys. *The Lancet Psychiatry* **3**, 954-964 (2016).
167 Carlini, B. H. & Schauer, G. L. Cannabis-only use in the USA: prevalence, demographics, use patterns, and health indicators. *Journal of cannabis research* **4**, 1-8 (2022).
168 Martin-Santos, R. *et al.* Acute effects of a single, oral dose of d9-tetrahydrocannabinol (THC) and cannabidiol (CBD) administration in healthy volunteers. *Current pharmaceutical design* **18**, 4966-4979 (2012).
169 Zuurman, L. *et al.* Effect of intrapulmonary tetrahydrocannabinol administration in humans. *Journal of psychopharmacology* **22**, 707-716 (2008).
170 Morgan, C. J. *et al.* Individual and combined effects of acute delta-9-tetrahydrocannabinol and cannabidiol on psychotomimetic symptoms and memory function. *Translational psychiatry* **8**, 1-10 (2018).
171 Hollister, L. E. & Gillespie, H. Delta-8-and delta-9-tetrahydrocannabinol; Comparison in man by oral and intravenous administration. *Clinical Pharmacology & Therapeutics* **14**, 353-357 (1973).
172 Hollister, L. E. Tetrahydrocannabinol isomers and homologues: contrasted effects of smoking. *Nature* **227**, 968-969 (1970).
173 Weinstein, A. *et al.* Brain imaging study of the acute effects of Δ 9-tetrahydrocannabinol (THC) on attention and motor coordination in regular users of marijuana. *Psychopharmacology* **196**, 119-131 (2008).
174 Weinstein, A. *et al.* A study investigating the acute dose—response effects of 13 mg and 17 mg Δ 9-tetrahydrocannabinol on cognitive—motor skills, subjective and autonomic measures in regular users of marijuana. *Journal of psychopharmacology* **22**, 441-451 (2008).
175 Hindley, G. *et al.* Psychiatric symptoms caused by cannabis constituents: a systematic review and meta-analysis. *The Lancet Psychiatry* **7**, 344-353 (2020).
176 Barrett, F. S., Schlienz, N. J., Lembeck, N., Waqas, M. & Vandrey, R. "Hallucinations" following acute cannabis dosing: a case report and comparison to other hallucinogenic drugs. *Cannabis and Cannabinoid Research* **3**, 85-93 (2018).
177 Lira, M. C. *et al.* Trends in cannabis involvement and risk of alcohol involvement in motor vehicle crash fatalities in the United States, 2000–2018. *American journal of public health* **111**, 1976-1985 (2021).
178 Moore, T. H. *et al.* Cannabis use and risk of psychotic or affective mental health outcomes: a systematic review. *The Lancet* **370**, 319-328 (2007).
179 Holtzman, D., Lovell, R. A., Jaffe, J. H. & Freedman, D. X. 1-Δ9-tetrahydrocannabinol: neurochemical and behavioral effects in the mouse. *Science* **163**, 1464-1467 (1969).
180 Beardsley, P. M., Scimeca, J. A. & Martin, B. R. Studies on the agonistic activity of! D9–21-tetrahydrocannabinol in mice, dogs and rhesus monkeys and its interactions with! D–9-tetrahydrocannabinol. *The Journal of Pharmacology and Experimental Therapeutics* (1987).
181 Metna-Laurent, M., Mondésir, M., Grel, A., Vallée, M. & Piazza, P. V. Cannabinoid-induced tetrad in mice. *Current Protocols in Neuroscience* **80**, 9.59. 51-59.59. 10 (2017).
182 Siemens, A. J. & Doyle, O. L. Cross-tolerance between Δ9-tetrahydrocannabinol and ethanol: the role of drug disposition. *Pharmacology Biochemistry and Behavior* **10**, 49-55 (1979).
183 Ruiz, C. *et al.* Pharmacokinetic and pharmacodynamic properties of aerosolized ("vaped") THC in adolescent male and female rats. *Psychopharmacology* **238**, 3595-3605 (2021).
184 Kasten, C. R., Zhang, Y. & Boehm, S. L. Acute cannabinoids produce robust anxiety-like and locomotor effects in mice, but long-term consequences are age-and sex-dependent. *Frontiers in behavioral neuroscience* **13**, 32 (2019).

185 Ibarra-Lecue, I. *et al.* Chronic cannabis promotes pro-hallucinogenic signaling of 5-HT2A receptors through Akt/mTOR pathway. *Neuropsychopharmacology* **43**, 2028-2035 (2018).

186 Long, L. E. *et al.* A behavioural comparison of acute and chronic Δ9-tetrahydrocannabinol and cannabidiol in C57BL/6JArc mice. *International Journal of Neuropsychopharmacology* **13**, 861-876 (2010).

187 Boucher, A. A. *et al.* The schizophrenia susceptibility gene neuregulin 1 modulates tolerance to the effects of cannabinoids. *International Journal of Neuropsychopharmacology* **14**, 631-643 (2011).

188 Hoffman, H. S. & Ison, J. R. Reflex modification in the domain of startle: I. Some empirical findings and their implications for how the nervous system processes sensory input. *Psychological review* **87**, 175 (1980).

189 Burgdorf, C. E. *et al.* Endocannabinoid genetic variation enhances vulnerability to THC reward in adolescent female mice. *Science Advances* **6**, eaay1502 (2020).

190 Lepore, M., Vorel, S. R., Lowinson, J. & Gardner, E. L. Conditioned place preference induced by Δ9-tetrahydrocannabinol: comparison with cocaine, morphine, and food reward. *Life sciences* **56**, 2073-2080 (1995).

191 Kruse, L. C., Cao, J. K., Viray, K., Stella, N. & Clark, J. C. Voluntary oral consumption of Δ9-tetrahydrocannabinol by adolescent rats impairs reward-predictive cue behaviors in adulthood. *Neuropsychopharmacology: official publication of the American College of Neuropsychopharmacology* (2019).

192 Smoker, M. P., Mackie, K., Lapish, C. C. & Boehm II, S. L. Self-administration of edible Δ9-tetrahydrocannabinol and associated behavioral effects in mice. *Drug and alcohol dependence* **199**, 106-115 (2019).

193 Ventura, R., Morrone, C. & Puglisi-Allegra, S. Prefrontal/accumbal catecholamine system determines motivational salience attribution to both reward-and aversion-related stimuli. *Proceedings of the National Academy of Sciences* **104**, 5181-5186 (2007).

194 Barbano, M. F., Castañé, A., Martín-García, E. & Maldonado, R. Delta-9-tetrahydrocannabinol enhances food reinforcement in a mouse operant conflict test. *Psychopharmacology* **205**, 475-487 (2009).

195 Nagai, H. *et al.* Antipsychotics improve Δ9-tetrahydrocannabinol-induced impairment of the prepulse inhibition of the startle reflex in mice. *Pharmacology Biochemistry and Behavior* **84**, 330-336 (2006).

196 Schindler, A. G., Tsutsui, K. T. & Clark, J. J. Chronic alcohol intake during adolescence, but not adulthood, promotes persistent deficits in risk-based decision making. *Alcoholism: clinical and experimental research* **38**, 1622-1629 (2014).

197 Falenski, K. W. *et al.* FAAH−/− mice display differential tolerance, dependence, and cannabinoid receptor adaptation after Δ9-tetrahydrocannabinol and anandamide administration. *Neuropsychopharmacology* **35**, 1775-1787 (2010).

198 Varvel, S. A. *et al.* Δ9-Tetrahydrocannbinol accounts for the antinociceptive, hypothermic, and cataleptic effects of marijuana in mice. *Journal of Pharmacology and Experimental Therapeutics* **314**, 329-337 (2005).

199 Ettaro, R., Laudermilk, L., Clark, S. D. & Maitra, R. Behavioral assessment of rimonabant under acute and chronic conditions. *Behavioural brain research* **390**, 112697 (2020).

200 Wright, F. & Rodgers, R. Low dose naloxone attenuates the pruritic but not anorectic response to rimonabant in male rats. *Psychopharmacology* **226**, 415-431 (2013).

201 Torrens, A. *et al.* Comparative pharmacokinetics of Δ9-tetrahydrocannabinol in adolescent and adult male mice. *Journal of Pharmacology and Experimental Therapeutics* **374**, 151-160 (2020).

202 Vozella, V., Zibardi, C., Ahmed, F. & Piomelli, D. Fast and sensitive quantification of Δ9-tetrahydrocannabinol and its main oxidative metabolites by liquid chromatography/tandem mass spectrometry. *Cannabis and Cannabinoid Research* **4**, 110-123 (2019).
203 Kreuz, D. S. & Axelrod, J. Delta-9-tetrahydrocannabinol: localization in body fat. *Science* **179**, 391-393 (1973).
204 Johansson, E., Norén, K., Sjövall, J. & Halldin, M. M. Determination of Δ1-tetrahydrocannabinol in human fat biopsies from marihuana users by gas chromatography–mass spectrometry. *Biomedical Chromatography* **3**, 35-38 (1989).
205 Pantoni, M. M., Herrera, G. M., Van Alstyne, K. R. & Anagnostaras, S. G. Quantifying the acoustic startle response in mice using standard digital video. *Frontiers in Behavioral Neuroscience* **14**, 83 (2020).
206 Tournier, B. B. & Ginovart, N. Repeated but not acute treatment withΔ 9-tetrahydrocannabinol disrupts prepulse inhibition of the acoustic startle: Reversal by the dopamine D2/3 receptor antagonist haloperidol. *European Neuropsychopharmacology* **24**, 1415-1423 (2014).
207 Deiana, S. *et al.* Plasma and brain pharmacokinetic profile of cannabidiol (CBD), cannabidivarine (CBDV), Δ9-tetrahydrocannabivarin (THCV) and cannabigerol (CBG) in rats and mice following oral and intraperitoneal administration and CBD action on obsessive–compulsive behaviour. *Psychopharmacology* **219**, 859-873 (2012).
208 Dinis-Oliveira, R. J. Metabolomics of Δ9-tetrahydrocannabinol: implications in toxicity. *Drug metabolism reviews* **48**, 80-87 (2016).
209 Cha, Y. M., Jones, K. H., Kuhn, C. M., Wilson, W. A. & Swartzwelder, H. S. Sex differences in the effects of Δ9-tetrahydrocannabinol on spatial learning in adolescent and adult rats. *Behavioural pharmacology* **18**, 563-569 (2007).
210 Harte, L. C. & Dow-Edwards, D. Sexually dimorphic alterations in locomotion and reversal learning after adolescent tetrahydrocannabinol exposure in the rat. *Neurotoxicology and teratology* **32**, 515-524 (2010).
211 Gur, R. C. *et al.* Age group and sex differences in performance on a computerized neurocognitive battery in children age 8− 21. *Neuropsychology* **26**, 251 (2012).
212 Freeman, T. P. *et al.* Changes in delta-9-tetrahydrocannabinol (THC) and cannabidiol (CBD) concentrations in cannabis over time: systematic review and meta-analysis. *Addiction* **116**, 1000-1010 (2021).
213 Smart, R., Caulkins, J. P., Kilmer, B., Davenport, S. & Midgette, G. Variation in cannabis potency and prices in a newly legal market: evidence from 30 million cannabis sales in Washington state. *Addiction* **112**, 2167-2177 (2017).
214 Hurd, Y. L. *et al.* Cannabis and the developing brain: insights into its long-lasting effects. *Journal of Neuroscience* **39**, 8250-8258 (2019).
215 White, F. J. Synaptic regulation of mesocorticolimbic dopamine neurons. *Annual review of neuroscience* **19**, 405-436 (1996).
216 Le Merre, P., Ährlund-Richter, S. & Carlén, M. The mouse prefrontal cortex: Unity in diversity. *Neuron* (2021).
217 Van der Steur, S. J., Batalla, A. & Bossong, M. G. Factors moderating the association between cannabis use and psychosis risk: a systematic review. *Brain sciences* **10**, 97 (2020).
218 Di Forti, M. *et al.* Daily use, especially of high-potency cannabis, drives the earlier onset of psychosis in cannabis users. *Schizophrenia bulletin* **40**, 1509-1517 (2014).
219 Di Forti, M. *et al.* The contribution of cannabis use to variation in the incidence of psychotic disorder across Europe (EU-GEI): a multicentre case-control study. *The Lancet Psychiatry* **6**, 427-436 (2019).

220 Pierre, J. M., Gandal, M. & Son, M. Cannabis-induced psychosis associated with high potency "wax dabs". *Schizophrenia research* **172**, 211-212 (2016).
221 Tart, C. T. Marijuana intoxication: common experiences. *Nature* **226**, 701-704 (1970).
222 Grotenhermen, F., Russo, E. & Zuardi, A. W. Even high doses of oral cannabidiol do not cause THC-like effects in humans: Comment on Merrick et al. Cannabis and Cannabinoid Research 2016; 1 (1): 102–112; DOI: 10.1089/can. 2015.0004. *Cannabis and Cannabinoid Research* **2**, 1-4 (2017).
223 Todd, S. & Arnold, J. Neural correlates of interactions between cannabidiol and Δ9-tetrahydrocannabinol in mice: implications for medical cannabis. *British journal of pharmacology* **173**, 53-65 (2016).
224 Rosenthaler, S. *et al.* Differences in receptor binding affinity of several phytocannabinoids do not explain their effects on neural cell cultures. *Neurotoxicology and teratology* **46**, 49-56 (2014).
225 Turner, S. E., Williams, C. M., Iversen, L. & Whalley, B. J. Molecular pharmacology of phytocannabinoids. *Phytocannabinoids*, 61-101 (2017).
226 Karniol, I. & Carlini, E. The content of (-) Δ9-trans-tetrahydrocannabinol (Δ9-THC) does not explain all biological activity of some Brazilian marihuana samples. *Journal of Pharmacy and Pharmacology* **24**, 833-835 (1972).
227 Sexton, M., Shelton, K., Haley, P. & West, M. Evaluation of cannabinoid and terpenoid content: cannabis flower compared to supercritical CO2 concentrate. *Planta medica* **84**, 234-241 (2018).
228 Russo, E. B. & Marcu, J. Cannabis pharmacology: the usual suspects and a few promising leads. *Advances in pharmacology* **80**, 67-134 (2017).
229 Geithe, C., Noe, F., Kreissl, J. & Krautwurst, D. The broadly tuned odorant receptor OR1A1 is highly selective for 3-methyl-2, 4-nonanedione, a key food odorant in aged wines, tea, and other foods. *Chemical senses* **42**, 181-193 (2017).
230 LaVigne, J. E., Hecksel, R., Keresztes, A. & Streicher, J. M. Cannabis sativa terpenes are cannabimimetic and selectively enhance cannabinoid activity. *Scientific reports* **11**, 1-15 (2021).
231 Sagar, K. A., Lambros, A. M., Dahlgren, M. K., Smith, R. T. & Gruber, S. A. Made from concentrate? A national web survey assessing dab use in the United States. *Drug and alcohol dependence* **190**, 133-142 (2018).
232 Sagar, K. A. & Gruber, S. A. Marijuana matters: reviewing the impact of marijuana on cognition, brain structure and function, & exploring policy implications and barriers to research. *International Review of Psychiatry* **30**, 251-267 (2018).
233 Firth, C. L., Davenport, S., Smart, R. & Dilley, J. A. How high: differences in the developments of cannabis markets in two legalized states. *The International journal on drug policy* **75**, 102611 (2020).
234 Devane, W. A., Dysarz, F. r., Johnson, M. R., Melvin, L. S. & Howlett, A. C. Determination and characterization of a cannabinoid receptor in rat brain. *Molecular pharmacology* **34**, 605-613 (1988).
235 Lutz, B. Neurobiology of cannabinoid receptor signaling. *Dialogues in Clinical Neuroscience* **22**, 207 (2020).
236 Katona, I. & Freund, T. F. Endocannabinoid signaling as a synaptic circuit breaker in neurological disease. *Nature medicine* **14**, 923-930 (2008).
237 Busquets-Garcia, A., Bains, J. & Marsicano, G. CB 1 receptor signaling in the brain: extracting specificity from ubiquity. *Neuropsychopharmacology* **43**, 4-20 (2018).

238 Laprairie, R., Bagher, A., Kelly, M. & Denovan-Wright, E. Cannabidiol is a negative allosteric modulator of the cannabinoid CB1 receptor. *British journal of pharmacology* **172**, 4790-4805 (2015).
239 Bakas, T. *et al.* The direct actions of cannabidiol and 2-arachidonoyl glycerol at GABAA receptors. *Pharmacological research* **119**, 358-370 (2017).
240 Ross, R. A. The enigmatic pharmacology of GPR55. *Trends in pharmacological sciences* **30**, 156-163 (2009).
241 Sharir, H. *et al.* The endocannabinoids anandamide and virodhamine modulate the activity of the candidate cannabinoid receptor GPR55. *Journal of neuroimmune pharmacology* **7**, 856-865 (2012).
242 Iannotti, F. A. *et al.* Nonpsychotropic plant cannabinoids, cannabidivarin (CBDV) and cannabidiol (CBD), activate and desensitize transient receptor potential vanilloid 1 (TRPV1) channels in vitro: potential for the treatment of neuronal hyperexcitability. *ACS chemical neuroscience* **5**, 1131-1141 (2014).
243 Stollenwerk, T. M., Pollock, S. & Hillard, C. J. Contribution of the Adenosine 2A Receptor to Behavioral Effects of Tetrahydrocannabinol, Cannabidiol and PECS-101. *Molecules* **26**, 5354 (2021).
244 Theunissen, E. L. *et al.* Neurocognition and subjective experience following acute doses of the synthetic cannabinoid JWH-018: responders versus nonresponders. *Cannabis and cannabinoid research* **4**, 51-61 (2019).
245 Atwood, B. K., Huffman, J., Straiker, A. & Mackie, K. JWH018, a common constituent of 'Spice'herbal blends, is a potent and efficacious cannabinoid CB1 receptor agonist. *British journal of pharmacology* **160**, 585-593 (2010).
246 Dalton, V. S. & Zavitsanou, K. Cannabinoid effects on CB1 receptor density in the adolescent brain: an autoradiographic study using the synthetic cannabinoid HU210. *Synapse* **64**, 845-854 (2010).
247 Cao, J. K., Kaplan, J. & Stella, N. ABHD6: its place in endocannabinoid signaling and beyond. *Trends in pharmacological sciences* **40**, 267-277 (2019).
248 Stella, N. Cannabinoid and cannabinoid-like receptors in microglia, astrocytes, and astrocytomas. *Glia* **58**, 1017-1030 (2010).
249 Di Marzo, V. *et al.* Formation and inactivation of endogenous cannabinoid anandamide in central neurons. *Nature* **372**, 686-691 (1994).
250 Stella, N. & Piomelli, D. Receptor-dependent formation of endogenous cannabinoids in cortical neurons. *European journal of pharmacology* **425**, 189-196 (2001).
251 Leishman, E., Mackie, K., Luquet, S. & Bradshaw, H. B. Lipidomics profile of a NAPE-PLD KO mouse provides evidence of a broader role of this enzyme in lipid metabolism in the brain. *Biochimica et Biophysica Acta (BBA)-Molecular and Cell Biology of Lipids* **1861**, 491-500 (2016).
252 Gao, Y. *et al.* Loss of retrograde endocannabinoid signaling and reduced adult neurogenesis in diacylglycerol lipase knock-out mice. *Journal of Neuroscience* **30**, 2017-2024 (2010).
253 Bisogno, T. *et al.* Cloning of the first sn1-DAG lipases points to the spatial and temporal regulation of endocannabinoid signaling in the brain. *The Journal of cell biology* **163**, 463-468 (2003).
254 Ohno-Shosaku, T. & Kano, M. Endocannabinoid-mediated retrograde modulation of synaptic transmission. *Current opinion in neurobiology* **29**, 1-8 (2014).
255 Guo, J. & Ikeda, S. R. Endocannabinoids modulate N-type calcium channels and G-protein-coupled inwardly rectifying potassium channels via CB1 cannabinoid receptors heterologously expressed in mammalian neurons. *Molecular pharmacology* **65**, 665-674 (2004).

256 Cravatt, B. F. *et al.* Supersensitivity to anandamide and enhanced endogenous cannabinoid signaling in mice lacking fatty acid amide hydrolase. *Proceedings of the National Academy of Sciences* **98**, 9371-9376 (2001).
257 Fu, J. *et al.* A catalytically silent FAAH-1 variant drives anandamide transport in neurons. *Nature neuroscience* **15**, 64-69 (2012).
258 McKinney, M. K. & Cravatt, B. F. Structure and function of fatty acid amide hydrolase. *Annu. Rev. Biochem.* **74**, 411-432 (2005).
259 Van Sickle, M. D. *et al.* Identification and functional characterization of brainstem cannabinoid CB2 receptors. *Science* **310**, 329-332 (2005).
260 Wu, C. S. *et al.* Requirement of cannabinoid CB1 receptors in cortical pyramidal neurons for appropriate development of corticothalamic and thalamocortical projections. *European Journal of Neuroscience* **32**, 693-706 (2010).
261 Lauckner, J. E. *et al.* GPR55 is a cannabinoid receptor that increases intracellular calcium and inhibits M current. *Proceedings of the national Academy of sciences* **105**, 2699-2704 (2008).
262 Lingerfelt, M. A. *et al.* Identification of crucial amino acid residues involved in agonist signaling at the GPR55 receptor. *Biochemistry* **56**, 473-486 (2017).
263 Foster, S. R. *et al.* Discovery of human signaling systems: pairing peptides to G protein-coupled receptors. *Cell* **179**, 895-908. e821 (2019).
264 Kaplan, J. S., Stella, N., Catterall, W. A. & Westenbroek, R. E. Cannabidiol attenuates seizures and social deficits in a mouse model of Dravet syndrome. *Proceedings of the National Academy of Sciences* **114**, 11229-11234 (2017).
265 Devinsky, O. *et al.* Trial of cannabidiol for drug-resistant seizures in the Dravet syndrome. *New England Journal of Medicine* **376**, 2011-2020 (2017).
266 Sylantyev, S., Jensen, T. P., Ross, R. A. & Rusakov, D. A. Cannabinoid-and lysophosphatidylinositol-sensitive receptor GPR55 boosts neurotransmitter release at central synapses. *Proceedings of the National Academy of Sciences* **110**, 5193-5198 (2013).
267 Chuang, S.-H., Westenbroek, R. E., Stella, N. & Catterall, W. A. Combined Antiseizure Efficacy of Cannabidiol and Clonazepam in a Conditional Mouse Model of Dravet Syndrome. *J Exp Neurol* **2**, 81 (2021).
268 Wu, C.-S., Jew, C. P. & Lu, H.-C. Lasting impacts of prenatal cannabis exposure and the role of endogenous cannabinoids in the developing brain. *Future neurology* **6**, 459-480 (2011).
269 Grant, K. S., Petroff, R., Isoherranen, N., Stella, N. & Burbacher, T. M. Cannabis use during pregnancy: pharmacokinetics and effects on child development. *Pharmacology & therapeutics* **182**, 133-151 (2018).
270 Anavi-Goffer, S. & Mulder, J. The polarised life of the endocannabinoid system in CNS development. *Chembiochem* **10**, 1591-1598 (2009).
271 Harkany, T. *et al.* The emerging functions of endocannabinoid signaling during CNS development. *Trends in pharmacological sciences* **28**, 83-92 (2007).
272 Crews, D. E. Senescence, aging, and disease. *Journal of physiological anthropology* **26**, 365-372 (2007).
273 Aguado, T. *et al.* The endocannabinoid system drives neural progenitor proliferation. *The FASEB journal* **19**, 1704-1706 (2005).
274 Aguado, T. *et al.* The endocannabinoid system promotes astroglial differentiation by acting on neural progenitor cells. *Journal of Neuroscience* **26**, 1551-1561 (2006).
275 Galve-Roperh, I. *et al.* Cannabinoid receptor signaling in progenitor/stem cell proliferation and differentiation. *Progress in lipid research* **52**, 633-650 (2013).

276 Berghuis, P. *et al.* Hardwiring the brain: endocannabinoids shape neuronal connectivity. *Science* **316**, 1212-1216 (2007).
277 Maccarrone, M., Guzmán, M., Mackie, K., Doherty, P. & Harkany, T. Programming of neural cells by (endo) cannabinoids: from physiological rules to emerging therapies. *Nature Reviews Neuroscience* **15**, 786-801 (2014).
278 Tortoriello, G. *et al.* Miswiring the brain: Δ9-tetrahydrocannabinol disrupts cortical development by inducing an SCG 10/stathmin-2 degradation pathway. *The EMBO journal* **33**, 668-685 (2014).
279 Cudaback, E., Marrs, W., Moeller, T. & Stella, N. The expression level of CB1 and CB2 receptors determines their efficacy at inducing apoptosis in astrocytomas. *PLoS One* **5**, e8702 (2010).
280 Priestley, R., Glass, M. & Kendall, D. Functional selectivity at cannabinoid receptors. *Advances in Pharmacology* **80**, 207-221 (2017).
281 Smaers, J. B., Gómez-Robles, A., Parks, A. N. & Sherwood, C. C. Exceptional evolutionary expansion of prefrontal cortex in great apes and humans. *Current Biology* **27**, 714-720 (2017).
282 Passingham, R. E. & Smaers, J. B. Is the prefrontal cortex especially enlarged in the human brain? Allometric relations and remapping factors. *Brain, behavior and evolution* **84**, 156-166 (2014).
283 Kolb, B. *et al.* Experience and the developing prefrontal cortex. *Proceedings of the National Academy of Sciences* **109**, 17186-17193 (2012).
284 Macht, V. A. Neuro-immune interactions across development: a look at glutamate in the prefrontal cortex. *Neuroscience & Biobehavioral Reviews* **71**, 267-280 (2016).
285 Caspi, A. *et al.* Moderation of the effect of adolescent-onset cannabis use on adult psychosis by a functional polymorphism in the catechol-O-methyltransferase gene: longitudinal evidence of a gene X environment interaction. *Biological psychiatry* **57**, 1117-1127 (2005).
286 Bidwell, L. C. *et al.* Association of naturalistic administration of cannabis flower and concentrates with intoxication and impairment. *JAMA psychiatry* **77**, 787-796 (2020).
287 Whitehill, J. M., Dilley, J. A., Brooks-Russell, A., Terpak, L. & Graves, J. M. Edible Cannabis exposures among children: 2017–2019. *Pediatrics* **147** (2021).
288 Davenport, S. Price and product variation in Washington's recreational cannabis market. *International Journal of Drug Policy*, 102547 (2019).
289 Bidwell, L. C., YorkWilliams, S. L., Mueller, R. L., Bryan, A. D. & Hutchison, K. E. Exploring cannabis concentrates on the legal market: User profiles, product strength, and health-related outcomes. *Addictive behaviors reports* **8**, 102-106 (2018).
290 Mennis, J., Stahler, G. J. & McKeon, T. P. Young adult cannabis use disorder treatment admissions declined as past month cannabis use increased in the US: An analysis of states by year, 2008–2017. *Addictive behaviors* **123**, 107049 (2021).
291 Freeman, T. & Winstock, A. Examining the profile of high-potency cannabis and its association with severity of cannabis dependence. *Psychological medicine* **45**, 3181-3189 (2015).
292 Barrington-Trimis, J. L. *et al.* Risk of persistence and progression of use of 5 cannabis products after experimentation among adolescents. *JAMA network open* **3**, e1919792-e1919792 (2020).
293 Arterberry, B. J., Padovano, H. T., Foster, K. T., Zucker, R. A. & Hicks, B. M. Higher average potency across the United States is associated with progression to first cannabis use disorder symptom. *Drug and alcohol dependence* **195**, 186-192 (2019).
294 Gunn, R. L., Aston, E. R., Sokolovsky, A. W., White, H. R. & Jackson, K. M. Complex cannabis use patterns: Associations with cannabis consequences and cannabis use disorder symptomatology. *Addictive behaviors* **105**, 106329 (2020).
295 Kelly, B. C. & Vuolo, M. Cognitive aptitude, peers, and trajectories of marijuana use from adolescence through young adulthood. *PloS one* **14**, e0223152 (2019).

296 Gobbi, G. *et al.* Association of cannabis use in adolescence and risk of depression, anxiety, and suicidality in young adulthood: a systematic review and meta-analysis. *JAMA psychiatry* **76**, 426-434 (2019).
297 Hines, L. A. *et al.* Association of high-potency cannabis use with mental health and substance use in adolescence. *JAMA psychiatry* **77**, 1044-1051 (2020).
298 Gilman, J. M. *et al.* Cannabis use is quantitatively associated with nucleus accumbens and amygdala abnormalities in young adult recreational users. *Journal of Neuroscience* **34**, 5529-5538 (2014).
299 Camchong, J., Lim, K. O. & Kumra, S. Adverse effects of cannabis on adolescent brain development: a longitudinal study. *Cerebral cortex* **27**, 1922-1930 (2017).
300 Albaugh, M. D. *et al.* Association of Cannabis Use During Adolescence With Neurodevelopment. *JAMA psychiatry* (2021).
301 Orr, C. *et al.* Grey matter volume differences associated with extremely low levels of cannabis use in adolescence. *Journal of Neuroscience* **39**, 1817-1827 (2019).
302 Weinstein, J. J. *et al.* PET imaging of dopamine-D2 receptor internalization in schizophrenia. *Molecular psychiatry* **23**, 1506-1511 (2018).
303 Withey, S. L. *et al.* Effects of daily Δ9-Tetrahydrocannabinol (THC) alone or combined with cannabidiol (CBD) on cognition-based behavior and activity in adolescent nonhuman primates. *Drug and alcohol dependence* **221**, 108629 (2021).
304 Freeman, T. P. *et al.* Increasing potency and price of cannabis in Europe, 2006–16. *Addiction* **114**, 1015-1023 (2019).
305 Gabaglio, M., Zamberletti, E., Manenti, C., Parolaro, D. & Rubino, T. Long-Term Consequences of Adolescent Exposure to THC-Rich/CBD-Poor and CBD-Rich/THC-Poor Combinations: A Comparison with Pure THC Treatment in Female Rats. *International Journal of Molecular Sciences* **22**, 8899 (2021).
306 Wiley, J. L. & Burston, J. J. Sex differences in Δ9-tetrahydrocannabinol metabolism and in vivo pharmacology following acute and repeated dosing in adolescent rats. *Neuroscience letters* **576**, 51-55 (2014).
307 Narimatsu, S., Watanabe, K., Yamamoto, I. & Yoshimura, H. Sex difference in the oxidative metabolism of Δ9-tetrahydrocannabinol in the rat. *Biochemical pharmacology* **41**, 1187-1194 (1991).
308 Spiro, A. S., Wong, A., Boucher, A. A. & Arnold, J. C. Enhanced brain disposition and effects of Δ9-tetrahydrocannabinol in P-glycoprotein and breast cancer resistance protein knockout mice. *PloS one* **7**, e35937 (2012).
309 Bonhomme-Faivre, L., Benyamina, A., Reynaud, M., Farinotti, R. & Abbara, C. PRECLINICAL STUDY: Disposition of Δ9 tetrahydrocannabinol in CF1 mice deficient in mdr1a P-glycoprotein. *Addiction biology* **13**, 295-300 (2008).
310 Ruiz, C. M. *et al.* Pharmacokinetic, behavioral, and brain activity effects of Δ 9-tetrahydrocannabinol in adolescent male and female rats. *Neuropsychopharmacology* **46**, 959-969 (2021).
311 Wiley, J. L. & Martin, B. R. Cannabinoid pharmacological properties common to other centrally acting drugs. *European journal of pharmacology* **471**, 185-193 (2003).
312 Dar, M. S. Cerebellar CB1 receptor mediation of Δ9-THC-induced motor incoordination and its potentiation by ethanol and modulation by the cerebellar adenosinergic A1 receptor in the mouse. *Brain research* **864**, 186-194 (2000).

313 Saravia, R. *et al.* Concomitant THC and stress adolescent exposure induces impaired fear extinction and related neurobiological changes in adulthood. *Neuropharmacology* **144**, 345-357 (2019).
314 Calabrese, E. J. & Rubio-Casillas, A. Biphasic effects of THC in memory and cognition. *European journal of clinical investigation* **48**, e12920 (2018).
315 Harkany, T., Keimpema, E., Barabás, K. & Mulder, J. Endocannabinoid functions controlling neuronal specification during brain development. *Molecular and cellular endocrinology* **286**, S84-S90 (2008).
316 Harkany, T., Mackie, K. & Doherty, P. Wiring and firing neuronal networks: endocannabinoids take center stage. *Current opinion in neurobiology* **18**, 338-345 (2008).
317 Alpár, A. *et al.* Endocannabinoids modulate cortical development by configuring Slit2/Robo1 signalling. *Nature communications* **5**, 1-13 (2014).
318 Díaz-Alonso, J. *et al.* The CB1 cannabinoid receptor drives corticospinal motor neuron differentiation through the Ctip2/Satb2 transcriptional regulation axis. *Journal of Neuroscience* **32**, 16651-16665 (2012).
319 Chen, R. *et al.* Δ9-THC-caused synaptic and memory impairments are mediated through COX-2 signaling. *Cell* **155**, 1154-1165 (2013).
320 Ferguson, B. R. & Gao, W.-J. PV interneurons: critical regulators of E/I balance for prefrontal cortex-dependent behavior and psychiatric disorders. *Frontiers in neural circuits* **12**, 37 (2018).
321 De Giacomo, V., Ruehle, S., Lutz, B., Häring, M. & Remmers, F. Cell type-specific genetic reconstitution of CB1 receptor subsets to assess their role in exploratory behaviour, sociability, and memory. *European Journal of Neuroscience* (2020).
322 Fortin, D. A. & Levine, E. S. Differential effects of endocannabinoids on glutamatergic and GABAergic inputs to layer 5 pyramidal neurons. *Cerebral Cortex* **17**, 163-174 (2007).
323 Heng, L., Beverley, J. A., Steiner, H. & Tseng, K. Y. Differential developmental trajectories for CB1 cannabinoid receptor expression in limbic/associative and sensorimotor cortical areas. *Synapse* **65**, 278-286 (2011).
324 Caballero, A., Granberg, R. & Tseng, K. Y. Mechanisms contributing to prefrontal cortex maturation during adolescence. *Neuroscience & Biobehavioral Reviews* **70**, 4-12 (2016).
325 Den Boon, F. S. *et al.* Activation of type-1 cannabinoid receptor shifts the balance between excitation and inhibition towards excitation in layer II/III pyramidal neurons of the rat prelimbic cortex. *Pflügers Archiv-European Journal of Physiology* **467**, 1551-1564 (2015).
326 Poulia, N. *et al.* Detrimental effects of adolescent escalating low-dose Δ9-tetrahydrocannabinol leads to a specific bio-behavioural profile in adult male rats. *British Journal of Pharmacology* **178**, 1722-1736 (2021).
327 Cass, D. K. *et al.* CB1 cannabinoid receptor stimulation during adolescence impairs the maturation of GABA function in the adult rat prefrontal cortex. *Molecular psychiatry* **19**, 536-543 (2014).
328 Pickel, V. M. *et al.* Chronic adolescent exposure toΔ 9-tetrahydrocannabinol decreases NMDA current and extrasynaptic plasmalemmal density of NMDA GluN1 subunits in the prelimbic cortex of adult male mice. *Neuropsychopharmacology* **45**, 374-383 (2020).
329 Ellgren, M. *et al.* Dynamic changes of the endogenous cannabinoid and opioid mesocorticolimbic systems during adolescence: THC effects. *European Neuropsychopharmacology* **18**, 826-834 (2008).
330 Farrell, J. S. *et al.* In vivo endocannabinoid dynamics at the timescale of physiological and pathological neural activity. *Neuron* **109**, 2398-2403. e2394 (2021).

331 Ellgren, M., Spano, S. M. & Hurd, Y. L. Adolescent cannabis exposure alters opiate intake and opioid limbic neuronal populations in adult rats. *Neuropsychopharmacology* **32**, 607-615 (2007).
332 Tomasiewicz, H. C. *et al.* Proenkephalin mediates the enduring effects of adolescent cannabis exposure associated with adult opiate vulnerability. *Biological psychiatry* **72**, 803-810 (2012).
333 Stopponi, S. *et al.* Chronic THC during adolescence increases the vulnerability to stress-induced relapse to heroin seeking in adult rats. *European Neuropsychopharmacology* **24**, 1037-1045 (2014).
334 Lecca, D. *et al.* Adolescent cannabis exposure increases heroin reinforcement in rats genetically vulnerable to addiction. *Neuropharmacology* **166**, 107974 (2020).
335 Higuera-Matas, A. *et al.* Augmented acquisition of cocaine self-administration and altered brain glucose metabolism in adult female but not male rats exposed to a cannabinoid agonist during adolescence. *Neuropsychopharmacology* **33**, 806-813 (2008).
336 Friedman, A. L., Meurice, C. & Jutkiewicz, E. M. Effects of adolescent Δ9-tetrahydrocannabinol exposure on the behavioral effects of cocaine in adult Sprague–Dawley rats. *Experimental and clinical psychopharmacology* **27**, 326 (2019).
337 Gobira, P. *et al.* Adolescent cannabinoid exposure modulates the vulnerability to cocaine-induced conditioned place preference and DNMT3a expression in the prefrontal cortex in Swiss mice. *Psychopharmacology*, 1-12 (2021).
338 Scherma, M. *et al.* Adolescent Δ 9-tetrahydrocannabinol exposure alters WIN55, 212-2 self-administration in adult rats. *Neuropsychopharmacology* **41**, 1416-1426 (2016).
339 Flores, Á., Maldonado, R. & Berrendero, F. THC exposure during adolescence does not modify nicotine reinforcing effects and relapse in adult male mice. *Psychopharmacology* **237**, 801-809 (2020).
340 Dukes, A. J., Fowler, J. P., Lallai, V., Pushkin, A. N. & Fowler, C. D. Adolescent cannabinoid and nicotine exposure differentially alters adult nicotine self-administration in males and females. *Nicotine and Tobacco Research* **22**, 1364-1373 (2020).
341 Hempel, B. J., Wakeford, A. G., Clasen, M. M., Friar, M. A. & Riley, A. L. Delta-9-tetrahydrocannabinol (THC) history fails to affect THC's ability to induce place preferences in rats. *Pharmacology Biochemistry and Behavior* **144**, 1-6 (2016).
342 Tagne, A. M., Fotio, Y., Springs, Z. A., Su, S. & Piomelli, D. Frequent Δ9-tetrahydrocannabinol exposure during adolescence impairs sociability in adult mice exposed to an aversive painful stimulus. *European Neuropsychopharmacology* **53**, 19-24 (2021).
343 Borsoi, M. *et al.* Sex Differences in the Behavioral and Synaptic Consequences of a Single in vivo Exposure to the Synthetic Cannabimimetic WIN55, 212-2 at Puberty and Adulthood. *Frontiers in behavioral neuroscience* **13**, 23 (2019).
344 Jouroukhin, Y. *et al.* Adolescent Δ9-tetrahydrocannabinol exposure and astrocyte-specific genetic vulnerability converge on nuclear factor-κB–cyclooxygenase-2 signaling to impair memory in adulthood. *Biological psychiatry* **85**, 891-903 (2019).
345 Chen, H.-T. & Mackie, K. Adolescent Δ9-Tetrahydrocannabinol Exposure Selectively Impairs Working Memory but Not Several Other mPFC-Mediated Behaviors. *Frontiers in psychiatry* **11** (2020).
346 Iemolo, A. *et al.* Reelin deficiency contributes to long-term behavioral abnormalities induced by chronic adolescent exposure to Δ9-tetrahydrocannabinol in mice. *Neuropharmacology* **187**, 108495 (2021).
347 Klug, M. & van den Buuse, M. Chronic cannabinoid treatment during young adulthood induces sex-specific behavioural deficits in maternally separated rats. *Behavioural brain research* **233**, 305-313 (2012).

348 Mandelbaum, D. E. Cannabidiol in patients with treatment-resistant epilepsy. *The Lancet Neurology* **15**, 544-545 (2016).
349 Small, E. Evolution and classification of Cannabis sativa (marijuana, hemp) in relation to human utilization. *The botanical review* **81**, 189-294 (2015).
350 Hädener, M., Gelmi, T. J., Martin-Fabritius, M., Weinmann, W. & Pfäffli, M. Cannabinoid concentrations in confiscated cannabis samples and in whole blood and urine after smoking CBD-rich cannabis as a "tobacco substitute". *International journal of legal medicine* **133**, 821-832 (2019).
351 Salviato, B. Z. *et al.* Female but not male rats show biphasic effects of low doses of Δ9-tetrahydrocannabinol on anxiety: can cannabidiol interfere with these effects? *Neuropharmacology* **196**, 108684 (2021).
352 Stella, N. THC and CBD: Similarities and differences between siblings. *Neuron* (2023).
353 English, A. *et al.* A preclinical model of THC edibles that produces high-dose cannabimimetic responses. *Elife* **12**, RP89867 (2024).
354 Merz, F. United Nations Office on Drugs and Crime: World Drug Report 2017. 2017. *SIRIUS-Zeitschrift für Strategische Analysen* **2**, 85-86 (2018).
355 Hines, L. A. *et al.* Association of high-potency cannabis use with mental health and substance use in adolescence. *JAMA psychiatry* (2020).
356 Chen, C. Y., Storr, C. L. & Anthony, J. C. Early-onset drug use and risk for drug dependence problems. *Addictive behaviors* **34**, 319-322, doi:10.1016/j.addbeh.2008.10.021 (2009).
357 Grant, B. F. & Dawson, D. A. Age at onset of alcohol use and its association with DSM-IV alcohol abuse and dependence: results from the National Longitudinal Alcohol Epidemiologic Survey. *Journal of substance abuse* **9**, 103-110 (1997).
358 DeWit, D. J., Hance, J., Offord, D. R. & Ogborne, A. The influence of early and frequent use of marijuana on the risk of desistance and of progression to marijuana-related harm. *Preventive medicine* **31**, 455-464, doi:10.1006/pmed.2000.0738 (2000).
359 Walia, P., Ghosh, A., Singh, S. & Dutta, A. Portable Neuroimaging Guided Non-invasive Brain Stimulation of Cortico-cerebello-thalamo-cortical Loop in Substance Use Disorder. (2022).
360 Carliner, H., Brown, Q. L., Sarvet, A. L. & Hasin, D. S. Cannabis use, attitudes, and legal status in the US: a review. *Preventive medicine* **104**, 13-23 (2017).
361 English, A., Land, B. & Stella, N. in *Cannabis and the Developing Brain* 23-58 (Elsevier, 2022).
362 Beale, C. *et al.* Prolonged cannabidiol treatment effects on hippocampal subfield volumes in current cannabis users. *Cannabis and cannabinoid research* **3**, 94-107 (2018).
363 Parmentier-Batteur, S., Jin, K., Xie, L., Mao, X. O. & Greenberg, D. DNA microarray analysis of cannabinoid signaling in mouse brain in vivo. *Molecular Pharmacology* **62**, 828-835 (2002).
364 McKinney, D. L. *et al.* Dose-related differences in the regional pattern of cannabinoid receptor adaptation and in vivo tolerance development to Δ9-tetrahydrocannabinol. *Journal of Pharmacology and Experimental Therapeutics* **324**, 664-673 (2008).
365 Wilson, J., Freeman, T. P. & Mackie, C. J. Effects of increasing cannabis potency on adolescent health. *The Lancet Child & Adolescent Health* (2018).
366 Cao, J. K., Kaplan, J. & Stella, N. ABHD6: Its Place in Endocannabinoid Signaling and Beyond. *Trends in pharmacological sciences* (2019).
367 Bloomfield, M. A., Ashok, A. H., Volkow, N. D. & Howes, O. D. The effects of Delta9-tetrahydrocannabinol on the dopamine system. *Nature* **539**, 369-377, doi:10.1038/nature20153 (2016).
368 Katona, I. & Freund, T. F. Multiple functions of endocannabinoid signaling in the brain. *Annual review of neuroscience* **35**, 529-558, doi:10.1146/annurev-neuro-062111-150420 (2012).

369 Katona, I. & Freund, T. F. Endocannabinoid signaling as a synaptic circuit breaker in neurological disease. *Nat Med* **14**, 923-930, doi:nm.f.1869 [pii]

10.1038/nm.f.1869 (2008).

370 English, A. *et al.* A preclinical model of THC edibles that produces high-dose cannabimimetic responses. *BioRxiv* **10.1101/2022.11.23.517743**, https://doi.org/10.1101/2022.1111.1123.517743 (2022).

371 van den Elsen, G. A. *et al.* Effects of tetrahydrocannabinol on balance and gait in patients with dementia: A randomised controlled crossover trial. *J Psychopharmacol* **31**, 184-191, doi:10.1177/0269881116665357 (2017).

372 Ware, M. A., Wang, T., Shapiro, S. & Collet, J. P. Cannabis for the Management of Pain: Assessment of Safety Study (COMPASS).

373 Ciccarelli, T. M., Leatherdale, S. T., Perlman, C., Thompson, K. & Ferro, M. A. Steering clear: Traffic violations among emerging adults who engage in habitual or casual cannabis use. *Accid Anal Prev* **153**, 106059, doi:10.1016/j.aap.2021.106059 (2021).

374 Füzesi, T., Daviu, N., Wamsteeker Cusulin, J. I., Bonin, R. P. & Bains, J. S. Hypothalamic CRH neurons orchestrate complex behaviours after stress. *Nature communications* **7**, 1-14 (2016).

375 Wiltschko, A. B. *et al.* Revealing the structure of pharmacobehavioral space through motion sequencing. *Nature neuroscience* **23**, 1433-1443 (2020).

376 Hall, W. D. & Lynskey, M. Is cannabis a gateway drug? Testing hypotheses about the relationship between cannabis use and the use of other illicit drugs. *Drug and alcohol review* **24**, 39-48 (2005).

377 Williams, A. R. Cannabis as a gateway drug for opioid use disorder. *The Journal of Law, Medicine & Ethics* **48**, 268-274 (2020).

378 Verweij, K. J. *et al.* Genetic and environmental influences on cannabis use initiation and problematic use: a meta-analysis of twin studies. *Addiction* **105**, 417-430 (2010).

379 Deak, J. D. & Johnson, E. C. Genetics of substance use disorders: a review. *Psychological medicine* **51**, 2189-2200 (2021).

380 Scavone, J., Sterling, R. & Van Bockstaele, E. Cannabinoid and opioid interactions: implications for opiate dependence and withdrawal. *Neuroscience* **248**, 637-654 (2013).

381 Cunningham, C. L. & Shields, C. N. Effects of sex on ethanol conditioned place preference, activity and variability in C57BL/6J and DBA/2J mice. *Pharmacology Biochemistry and Behavior* **173**, 84-89 (2018).

382 Moore, C. F. *et al.* Δ9-Tetrahydrocannabinol vapor exposure produces conditioned place preference in male and female rats. *Cannabis and cannabinoid research* **9**, 111-120 (2024).

383 Torregrossa, M. M., Corlett, P. R. & Taylor, J. R. Aberrant learning and memory in addiction. *Neurobiology of learning and memory* **96**, 609-623 (2011).

384 Bassir Nia, A., Mann, C., Kaur, H. & Ranganathan, M. Cannabis use: neurobiological, behavioral, and sex/gender considerations. *Current behavioral neuroscience reports* **5**, 271-280 (2018).

385 Castelli, V. *et al.* Prenatal THC exposure drives sex-specific alterations in spatial memory and hippocampal excitatory/inhibitory balance in adolescent rats. *Biomedicine & Pharmacotherapy* **181**, 117699 (2024).

386 Pennypacker, S. D., Cunnane, K., Cash, M. C. & Romero-Sandoval, E. A. Potency and therapeutic THC and CBD ratios: US cannabis markets overshoot. *Frontiers in Pharmacology* **13**, 921493 (2022).

387 Asbridge, M., Hayden, J. A. & Cartwright, J. L. Acute cannabis consumption and motor vehicle collision risk: systematic review of observational studies and meta-analysis. *Bmj* **344**, e536 (2012).

388 Pearson-Dennett, V. *et al.* History of cannabis use is associated with altered gait. *Drug and alcohol dependence* **178**, 215-222 (2017).
389 Rosenberg-Katz, K. *et al.* Gray matter atrophy distinguishes between Parkinson disease motor subtypes. *Neurology* **80**, 1476-1484 (2013).
390 Marsicano, G. & Lutz, B. Expression of the cannabinoid receptor CB1 in distinct neuronal subpopulations in the adult mouse forebrain. *European journal of neuroscience* **11**, 4213-4225 (1999).
391 Machado, A. S., Marques, H. G., Duarte, D. F., Darmohray, D. M. & Carey, M. R. Shared and specific signatures of locomotor ataxia in mutant mice. *ELife* **9**, e55356 (2020).
392 Vervoort, G. *et al.* Distal motor deficit contributions to postural instability and gait disorder in Parkinson's disease. *Behavioural brain research* **287**, 1-7 (2015).
393 Willmore, L., Cameron, C., Yang, J., Witten, I. B. & Falkner, A. L. Behavioural and dopaminergic signatures of resilience. *Nature* **611**, 124-132 (2022).
394 Narayanan, N. S. & Laubach, M. Top-down control of motor cortex ensembles by dorsomedial prefrontal cortex. *Neuron* **52**, 921-931 (2006).
395 Risterucci, C., Terramorsi, D., Nieoullon, A. & Amalric, M. Excitotoxic lesions of the prelimbic-infralimbic areas of the rodent prefrontal cortex disrupt motor preparatory processes. *European Journal of Neuroscience* **17**, 1498-1508 (2003).
396 Fogaça, M. V., Daher, F. & Picciotto, M. R. Effects of ketamine on GABAergic and glutamatergic activity in the mPFC: biphasic recruitment of GABA function in antidepressant-like responses. *Neuropsychopharmacology*, 1-12 (2024).
397 Fogaça, M. V. *et al.* Inhibition of GABA interneurons in the mPFC is sufficient and necessary for rapid antidepressant responses. *Molecular psychiatry* **26**, 3277-3291 (2021).
398 Yin, Y.-Y. *et al.* The role of the excitation: inhibition functional balance in the mPFC in the onset of antidepressants. *Neuropharmacology* **191**, 108573 (2021).
399 Chellappa, S. L. *et al.* Circadian dynamics in measures of cortical excitation and inhibition balance. *Scientific reports* **6**, 33661 (2016).
400 Howes, O. D. & Shatalina, E. Integrating the neurodevelopmental and dopamine hypotheses of schizophrenia and the role of cortical excitation-inhibition balance. *Biological psychiatry* **92**, 501-513 (2022).
401 Hunker, A. C. *et al.* Conditional single vector CRISPR/SaCas9 viruses for efficient mutagenesis in the adult mouse nervous system. *Cell reports* **30**, 4303-4316. e4306 (2020).
402 Cela, E. *et al.* An optogenetic kindling model of neocortical epilepsy. *Scientific Reports* **9**, 5236 (2019).
403 Dutta, S., Selvam, B., Das, A. & Shukla, D. Mechanistic origin of partial agonism of tetrahydrocannabinol for cannabinoid receptors. *Journal of Biological Chemistry* **298** (2022).
404 English, A. *et al.* A preclinical model of THC edibles that produces high-dose cannabimimetic responses. *bioRxiv*, 2022.2011.2023.517743, doi:10.1101/2022.11.23.517743 (2022).
405 Wilkerson, J. L. *et al.* Investigation of diacylglycerol lipase alpha inhibition in the mouse lipopolysaccharide inflammatory pain model. *The Journal of pharmacology and experimental therapeutics* **363**, 394-401 (2017).
406 Seillier, A., Aguilar, D. D. & Giuffrida, A. The dual FAAH/MAGL inhibitor JZL195 has enhanced effects on endocannabinoid transmission and motor behavior in rats as compared to those of the MAGL inhibitor JZL184. *Pharmacology Biochemistry and Behavior* **124**, 153-159 (2014).
407 Ignatowska-Jankowska, B. *et al.* Selective monoacylglycerol lipase inhibitors: antinociceptive versus cannabimimetic effects in mice. *The Journal of pharmacology and experimental therapeutics* **353**, 424-432 (2015).

408 Ignatowska-Jankowska, B. *et al.* In vivo characterization of the highly selective monoacylglycerol lipase inhibitor KML 29: Antinociceptive activity without cannabimimetic side effects. *British journal of pharmacology* **171**, 1392-1407 (2014).
409 De Sarkar, N. *et al.* Nucleosome patterns in circulating tumor DNA reveal transcriptional regulation of advanced prostate cancer phenotypes. *Cancer discovery* **13**, 632-653 (2023).
410 Spiller, K. J. *et al.* Cannabinoid CB1 and CB2 receptor mechanisms underlie cannabis reward and aversion in rats. *British journal of pharmacology* **176**, 1268-1281 (2019).
411 Murray, J. E. & Bevins, R. A. Cannabinoid conditioned reward and aversion: behavioral and neural processes. *ACS chemical neuroscience* **1**, 265-278 (2010).
412 Brown, A. P., Dinger, N. & Levine, B. S. Stress produced by gavage administration in the rat. *Journal of the American Association for Laboratory Animal Science* **39**, 17-21 (2000).
413 Hume, C. *et al.* Characterising 'the munchies'; effects of delta-9-tetrahydrocannabinol (THC) vapour inhalation on feeding patterns, satiety, and macronutrient-specific food preference in male and female rats. *bioRxiv*, 2022.2009. 2022.509090 (2022).
414 Boadu, O., Gombolay, G. Y., Caviness, V. S. & El Saleeby, C. M. Intoxication from accidental marijuana ingestion in pediatric patients: what may lie ahead. *Pediatric emergency care* **36**, e349-e354 (2020).
415 Kaufmann, R., Harris Bozer, A., Jotte, A. K. & Aqua, K. Long-term, self-dosing CBD users: Indications, dosage, and self-perceptions on general health/symptoms and drug use. *Medical Cannabis and Cannabinoids* **6**, 77-88 (2023).
416 Secades-Villa, R., Garcia-Rodríguez, O., Jin, C. J., Wang, S. & Blanco, C. Probability and predictors of the cannabis gateway effect: a national study. *International Journal of Drug Policy* **26**, 135-142 (2015).
417 Glimcher, P. W. Understanding dopamine and reinforcement learning: the dopamine reward prediction error hypothesis. *Proceedings of the National Academy of Sciences* **108**, 15647-15654 (2011).
418 Farquhar, C. E. *et al.* Sex, THC, and hormones: Effects on density and sensitivity of CB1 cannabinoid receptors in rats. *Drug and alcohol dependence* **194**, 20-27 (2019).
419 Piantadosi, S. C. *et al.* Holographic stimulation of opposing amygdala ensembles bidirectionally modulates valence-specific behavior via mutual inhibition. *Neuron* **112**, 593-610. e595 (2024).
420 Gremel, C. M. & Costa, R. M. Orbitofrontal and striatal circuits dynamically encode the shift between goal-directed and habitual actions. *Nature communications* **4**, 2264 (2013).
421 Macpherson, T. & Hikida, T. Role of basal ganglia neurocircuitry in the pathology of psychiatric disorders. *Psychiatry and clinical neurosciences* **73**, 289-301 (2019).

VITA

Anthony Edward English earned a Bachelor of Science degree in Pharmaceutical Sciences at The Ohio State University in Columbus, Ohio. Prior to entering graduate school, he worked in multiple academic laboratories, including the Wozniak Lab in the Department of Microbiology and the Yalowich/Elton laboratories in the Pharmacology department at The Ohio State University. As a graduate student at the University of Washington Department of Pharmacology, Anthony worked in the labs of Drs. Nephi Stella and Michael Bruchas where he developed technologies to further his study into the mechanisms of THC-induced impairment.